Measurement and Modelling of Particle Residence Time in a Return-Flow Cyclone

A thesis submitted in fulfilment of the requirements
for the degree of Doctor of Philosophy in
Chemical and Process Engineering
in the University of Canterbury

Thomas Saruchera

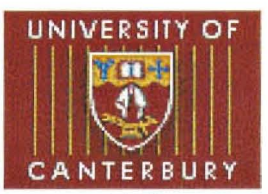

1999

ACKNOWLEDGEMENTS

It is a pleasure to express my gratitude to Dr John Abrahamson for his helpful advice and encouragement throughout the course of this work. His many suggestions and guidance enabled me to forge ahead in constructing the framework of this thesis. I am very appreciative.

Further, I would also like to acknowledge Dr David Frankum and Dr Ian Kemp for their contributions with data and some ideas, some of which are included in this thesis. Through them, I also would like to thank SPS (Separation Process Service, Harwell, UK) for providing the silica gel used in these experiments.

The cooperation of the technical staff in the Department of Chemical Engineering is also greatly appreciated. I want to mention particularly Ron Boyce and Trevor Berry and also Alan Bright (now retired) of Audio Visual Department.

I also wish to thank Dr. Alexander Deev for his help in translating Russian papers.

Numerous other people have helped directly or indirectly in the course of my journey. I can offer here only an inadequate acknowledgment of my appreciation

ABSTRACT

Cyclones find wide applications in industry as drying apparatus or as chemical reactors. For these applications it is necessary to know and predict the residence time of the particles in the reactor for product quality control. In the present study the residence time of granular particles (210 μm < d_p < 850 μm) was measured by the stimuli-response technique using a moving impactor method. The experimental data was analysed by the moments, Laplace transform and the least squares methods. The axially dispersed plug flow model was found to be a valid representation of flow of these particles in the cyclone. The parameters of this diffusion model were the mean particle residence time and the particle Peclet number.

A simple mathematical model based on the particle momentum equation was developed to model the flow of a single particle in the cyclone by the experimentally observed mechanism of bouncing and sliding on the walls. This is the first known bouncing particle model for modelling passage of granular particles through process equipment. The coefficient of restitution and friction for input into the model were obtained from simple bouncing tests. The model was used to predict the residence time of the particles in the cyclone. The experimental results were compared with the model-predicted results. Good agreement between model and experimental results was obtained with regard to trends of residence time with cone angle. However there was deviation with regard to particle size and density, where the model gave opposite trends compared to the experimental results.

The phenomenon of roping was studied with the aid of a high frame rate camera. The incidence of roping was found to increase with increase in cone angle. When the total included cone angle was large > 36° the solids in the rope behaved independently of the gas flow and discharged at a rate controlled by the feed into the cyclone. The discharge of a rope was found to be transient in nature.

TABLE OF CONTENTS

Acknowledgment ii

Abstract iii

Nomenclature xi

Introduction 1-1
1.1. General Background of Cyclones 1-2
1.2. Application of Cyclone as a Chemical Reactor 1-15
1.3. Particle Residence Time Measurements 1-16
1.4. Dynamics of Gas-Solid Flows 1-20
1.4.1. Gas-Particle Interactions 1-20
1.4.2. Particle-Particle Interactions 1-29
1.4.3. Particle Rotations 1-33
1.4.4. Particle-Wall Interactions 1-34
1.4.5. Electrostatic Interactions 1-38
1.5. Modelling in Gas-Particle Systems 1-39
1.5.1. Lagrangian Approach 1-39
1.5.2. Eulerian Continuum Approach 1-40
1.5.3. Equations of Motion 1-41
1.6. Modelling of Particle Flow in a Cyclone 1-42

Experimental 2-1
2.1. Equipment 2.2
2.1.1. Cyclones used 2.2
2.1.2. Solids Conveyor Belt and Tracer Input 2.6
2.1.3. Air Supply 2.7
2.1.4. Photography and Video 2.8
2.2. The Moving Impactor Method 2.8

Analysis of Residence Time Measurements - Data Reduction 3-1
3.1. Residence Time Distributions 3.2
3.2. General Imperfect Tracer Input 3.4
3.3. Moments Analysis 3.5
3.4. Solids Axial Diffusion Model 3.7
3.4.1. Transfer Function 3.8
3.4.2. Least Squares 3.9

Measurement Uncertainties and Analysis 4-1
4.1. Error Types 4.2
4.2. Mean 4.2
4.3. Standard Deviation 4.3
4.4. Standard Deviation of the Mean 4.3
4.5. Error Propagation 4.3

Results 5-1
5.1. Observations 5.2
5.2. Particle Characteristics 5.2
5.3. Particle Velocity into Cyclone 5.6
5.4. Gas Inlet Velocity 5.6
5.5. Solids Hold Up 5.7
5.6. Collection Efficiency 5.10
5.7. Gas Residence Time 5.11
5.8. Particle Distributions and Flow Model 5.11
5.9. Particle Residence Times 5.20
5.9.1. Effect of SGL 5.21
5.9.2. Effect of particle size 5.22
5.9.3. Effect of particle density (and other properties of the particles) 5.23
5.9.4. Effect of gas inlet velocity 5.25
5.9.5. Interaction of gas inlet velocity and SGL 5.26
5.9.6. Effect of particle inlet velocity 5.28
5.9.7. Interaction of gas velocity and particle size 5.29
5.9.8. Effect of cone angle 5.30
5.9.9. Effect of humidity on residence time of silica gel particles 5.32
5.10. Peclet Numbers 5.33
5.11. Effect of surface roughness on Particle Peclet number 5.35
5.12. Observations and Presence of Roping 5.36
5.13. Particle Bouncing Phenomena 5.39

Modelling of Particle Flow 6-1
6.1. Roping Phenomenon along a Wall 6-2
6.3.1. Velocity of rope 6-18
6.2. Sliding Particle Model (SPM) 6-22
6.3. Bouncing Particle Model (BPM) 6-39
6.3.1. Single Particle Approach 6-39
6.3.2. Model Results 6-64
6.3.3. Multiple Particle Approach 6-67

Discussion 7.1
7.1. Measurement uncertainties 7-2
7.2. The Imperfect Tracer Technique 7-6
7.3. Axially Dispersed Plug Flow Model 7-7
7.4. Particle Residence Times 7-7
7.4.1. Effect of moisture content on residence time 7-7
7.4.2. Particle size 7-8
7.4.3. Particle density 7-11
7.4.4. Solid Gas Loading (SGL) 7-12
7.4.5. Gas Inlet Velocity 7-16
7.4.6. Particle Inlet Velocity 7-17
7.4.7. Cyclone Diameter 7-17
7.4.8. Total Height, and Proportion of Cone Height 7-18
7.5. Particle Peclet Numbers 7-20
7.6. Roping 7-24

7.7. Modelling 7-32

Conclusion 8-1

References R-1

Appendices A-1
Appendix 9A - Chemeca 97 Paper A-2
Appendix 9B - International Drying Symposium (IDS'98) A-16
Appendix 9C – Visual Basic Program for BPM A-25
Appendix 9D – Conical Sections A-41
Appendix 9E – Air-Hydraulic Circuit for Moving Shuttles A-45
Appendix 9F – Electric Circuit Diagram for Solenoid Controller A-46
Appendix 9G – Timing Diagram A-47
Appendix 9H - Convolution Theorem A-48
Appendix 9I – Experimental Results A-51
Appendix 9J – Video Recording of Flow in Cyclone A-54
Appendix 9K – Error Analysis A-55

LIST OF FIGURES

Figure 1-1 Schematic diagram of a return-flow cyclone 1-5
Figure 1-2 Trajectory length of particles 1-13
Figure 1-3 Standard Drag Curve 1-24
Figure 1-4 Particle-Particle Interactions 1-32
Figure 1-5 Particle Collision with Cyclone Wall 1-37
Figure 1-6 Agglomerating charged spherical particles 1-39
Figure 1-7 Force balance on a particle in contact with a cyclone wall 1-44
Figure 1-8 Radial variation of gas axial velocity 1-47

Figure 2-1 Photograph of Conical sections showing relative heights of cones 2-3
Figure 2-2 Photo of cyclone with the 36-degree conical section (cyclone E) 2.4
Figure 2-3 Schematic diagram of cyclone 2-5
Figure 2-4 Perspex dust collection hopper 2-6
Figure 2-5 Pulse input 2-7
Figure 2-6 Step input 2-7
Figure 2-7 Aluminium impactors showing the cells 2-8
Figure 2-8 Moving shuttle 2-9

Figure 3.1-1 Ideal pulse and step input and response curves 3-3

Figure 5.2-1 Sand particles [scale x10] 5-4
Figure 5.2-2 Silica gel particles [scale x10] 5-5
Figure 5.2-3 Glass particles [scale x10] 5-5
Figure 5.4-1 Air velocity profile in round entrance tube 5-7
Figure 5.5-1 White and black particles on conveyor belt 5-10
Figure 5.8-1 Number distribution for sand particles on the inlet impactor 5-13
Figure 5.8-2 Number distribution of sand particles in the bin impactor 5-14
Figure 5.8-3 Fraction of sand tracer on inlet and bin impactors 5-15
Figure 5.8-4 Number distribution for a step-input for inlet impactor 5-16
Figure 5.8-5 Number distribution of sand particles for a step input 5-16
Figure 5.8-6 Fraction of sand tracer for a step input for inlet and out 5-17
Figure 5.8-7 Evaluation of parameters [run 86] 5-19
Figure 5.8-8 Experimental tracer distribution and model fitting 5-20
Figure 5.9-1 Effect of SGL on residence time of silica gel particles 5-22
Figure 5.9-2 Fine tracer particles lead the larger tracer particles 5-22
Figure 5.9-3 Effect of particle size on residence time of silica gel particles 5-23
Figure 5.9-4 Effect of density on residence time 5-24
Figure 5.9-5 Effects of particle size and density on residence time 5-25
Figure 5.9-6 Effect of gas inlet velocity on residence time of silica gel particles 5-26
Figure 5.9-7 Effect of gas inlet velocity on residence time of silica gel particles 5-27
Figure 5.9-8 Effect of inlet velocity on particle residence time (Kemp, 1998) ... 5-28
Figure 5.9-9 Effect of particle inlet velocity on residence time 5-29
Figure 5.9-10 Effect of gas velocity, particle size 5-30
Figure 5.9-11 Effect of cone angle on residence time 5-31

Figure 5.9-12 Dimensionless residence time 5-32
Figure 5.10-1 Effect of solids feed rate on Peclet Number 5-34
Figure 5.10-2 Effect of gas inlet velocity on Peclet Number 5-34
Figure 5.10-3 Effect of cone angle and SGL on Peclet Number 5-35
Figure 5.11-1 Effect of wall roughness on Peclet number 5-36
Figure 5.12-1 Particle concentration profile in cyclone conical section 5-37
Figure 5.12-2 Qualitative flow mapping of roping 5-39
Figure 5.13-1 Silica gel particles bouncing from a mild steel plate 5-40
Figure 5.13-2 Bouncing of Silica gel particles from a mild steel surface 5-41
Figure 5.13-3 Silica gel bouncing from a mild steel plate 5-42
Figure 5.13-4 Sand particles bouncing from mild steel plate inclined at 30° 5-42
Figure 5.13-5 Glass beads bouncing from mild steel plate 5-43
Figure 5.13-6 Silica gel bouncing on sand coated mild steel plate 5-44
Figure 5.13-7 Sand particles bouncing off from rough sand coated surface 5-45

Figure 6-1 Sand particle layer remaining in cyclone F 6-3
Figure 6-2 Flow of sand particles in cyclone B (cone angle 14°) 6-5
Figure 6-3 Flow of sand particles in cyclone C (cone angle 20°) 6-5
Figure 6-4 Flow of sand particles in cyclone D (cone angle 28°) 6-6
Figure 6-5 Flow of sand particles in cyclone E (cone angle 36°) 6-6
Figure 6-6 Silica gel particles in a 42°-cone cyclone 6-10
Figure 6-7 Flow of sand in cyclone D; time = 0s 6-12
Figure 6-8 Flow of sand in cyclone D; time = 0.02s 6-12
Figure 6-9 Flow of sand particles in cyclone D; time = 0.05s 6-13
Figure 6-10 Flow of sand particles in cyclone D; time = 0.07s 6-13
Figure 6-11 Flow of sand particles in cyclone D; time = 0.08s 6-14
Figure 6-12 Flow of sand particles in cyclone D; time = 0.1s 6-14
Figure 6-13 Flow of sand particles in cyclone D; time = 0.12s 6-15
Figure 6-14 Flow of sand particles in cyclone D; time = 0.13s 6-15
Figure 6-15 Flow of sand particles in cyclone D; time = 0.15s 6-16
Figure 6-16 Total particle distribution at apex for cyclones B and E 6-16
Figure 6-17 Rope in cyclone D 6-18
Figure 6-18 Rope in cyclone E 6-19
Figure 6-19 Rope in cyclone F (sand 250–500- m) 6-19
Figure 6-20 Rope in cyclone F (sand 150-210- m) 6-20
Figure 6-21 Force acting on a particle 6-22
Figure 6-22 Force balance on rope 6-23
Figure 6-23 Spiral patterns in Cyclone 6-27
Figure 6-24 Set-up for photographs taken at apex of cyclone 6-28
Figure 6-25 Sand particles at the apex of cyclone 6-29
Figure 6-26 Silica gel particles at apex of cyclone 6-30
Figure 6-27 Mechanical and hydrodynamic particle and wall interactions 6-32
Figure 6-28 Impact and lift-off velocities and angles 6-32
Figure 6-29 Impact of a spherical particle on a plane surface 6-34
Figure 6-30 Algorithm for calculating particle initial velocity 6-41
Figure 6-31 Initial impact of particle with wall at entrance 6-42
Figure 6-32 Impact-rebound velocity relationships (plan view) 6-44
Figure 6-33 Impact-rebound velocity components in cylindrical section 6-44

Figure 6-34 Particle axial and radial velocity components in conical..... 6-46
Figure 6-35 Impact and rebound velocities in conical section..... 6-47
Figure 6-36 Impact and rebound velocities in conical section (side view)..... 6-47
Figure 6-37 Diagrammatic representation of velocity components..... 6-50
Figure 6-38 Schematic diagram shown bouncing phenomena in cyclone 6-52
Figure 6-39 Particle trajectory..... 6-53
Figure 6-40 Schematic representation of cyclone 6-56
Figure 6-41 Algorithm for the Bouncing Particle Model (a) 6-58
Figure 6-42 Algorithm for the Bouncing Particle Model (b)..... 6-59
Figure 6-43 Angle of total gas velocity vector at different ports 6-61
Figure 6-44 Angle of total gas velocity vector 6-62
Figure 6-45 Force diagram showing resultant force acting on particle..... 6-63
Figure 6-46 Experimental and model predicted residence time 6-65
Figure 6-47 Experimental and Model predicted residence time..... 6-66
Figure 6-48 Model predicted residence times for sand and silica gel particles... 6-67
Figure 6-49 Flow regime in multi-particle system 6-68
Figure 6-50 Relationship between ΔR and diameter of particle..... 6-70

Figure 7-1 Tracer concentration-time curve for unseived silica gel [run 11].....7-9
Figure 7-2 Tracer concentration-time curve for silica gel 7-9
Figure 7-3 Change in residence time with SGL for cyclones C, D and F 7-12
Figure 7-4 Particle residence time as a function of inverse of mass flow rate 7-15
Figure 7.5 Relative importance of drag and gravitational force 7-27
Figure 7-6 Particle deposition in stratified flow 7-27
Figure 7-7 Cloud of particles discharging into the bin, viewed from the bin. ... 7-30
Figure 7-8 Schematic diagram illustrating velocity profile in rope 7-31
Figure 7-9 Wall boundary layer..... 7-35
Figure 7-10 Different entrance paths for particles into the cyclone..... 7-37
Figure 7-11 Predicted particle residence times with change in approach angle.. 7-38
Figure 7-12 Particle residence time with change in particle inlet velocity..... 7-39

LIST OF TABLES

Table 1.4-1 Data on Sphericity 1-26

Table 2-1 Cyclone dimensions.....2-2

Table 5.2-1 Material size ranges used in investigation.....5-3

Table 5.5-1 Hold up in Cyclone B(14° cone angle) 5-9

Table 5.7-1 Gas residence times in different cyclones..... 5-11

Table 5.9-1 Geometrical properties of conical sections used..... 5-30

Table 6-1 Total velocity of sand particles in ropes..... 6-20

Table 6-2 Post and pre-collision velocities and momentum (silica gel)..... 6-36

Table 6-3 Post and pre-collision velocities and momentum (glass) 6-36

Table 6-4 Post and pre-collision velocities and momentum (sand) 6-37

Table 7-1 Residence times of sand particles in different cyclones 7-18

Table 7-2 Periods of rope discharge and no discharge from cyclone E 7-31

Nomenclature

ΔP	Pressure (Pa)
ΔH	Pressure drop coefficient (-)
Eu	Euler Number (-)
V	tangential velocity (ms^{-1})
W	axial velocity (ms^{-1})
U	radial velocity (ms^{-1})
V_φ	gas tangential velocity in cylindrical coordinates (ms^{-1})
V_z	gas axial velocity in cylindrical coordinates (ms^{-1})
V_r	gas radial velocity in cylindrical coordinates (ms^{-1})
W_φ	particle tangential velocity in cylindrical coordinates (ms^{-1})
W_z	particle axial velocity in cylindrical coordinates (ms^{-1})
W_r	particle radial velocity in cylindrical coordinates (ms^{-1})
H	height of cyclone (m)
h	height of cylindrical section (m)
D_c	diameter of cylindrical section (m)
D_e	diameter of vortex finder (m)
r	radius of cyclone (m)
a	width of entrance section (m)
b	height of entrance section (m)
d_p	diameter of particle (m)
g	gravitational acceleration (ms^{-2})
t	time (s)
f	coefficient of friction (-)
M	mass (kg)
M_f	mass flow rate (kgs^{-1})
m	mass (kg)
V_c	volume of cyclone (m^3)
Q	gas volumetric flowrate (m^3s^{-1})
Re_p	Reynolds number (-)
Pe	Peclet number (-)
F_D	drag force (N)
F_f	frictional force (N)
F_g	gravitational force (N)
F_m	Magnus force (N)
F_B	buoyancy force (N)
F_E	electrostatic force (N)
F_c	inter-particle contact force (N)
C_D	drag coefficient (-)
A	surface area (m^2)

Greek symbols

ν	gas kinematic viscosity (m^2s^{-1})
α	cone half angle (degrees)
ρ	density (kg m^{-3})
μ	kg solids/ kg gas (-)
ε	coefficient of restitution
τ	particle relaxation time (s)

Subscripts

g	gas
p	particle
w	wall
t	tangential

Introduction

1

1.1. General Background of Cyclones 1-2

1.2. Application of Cyclone as a Chemical Reactor 1-15

1.3. Particle Residence Time Measurements 1-16

1.4. Dynamics of Gas-Solid Flows 1-20
1.4.1. Gas-Particle Interactions 1-20
1.4.2. Particle-Particle Interactions 1-29
1.4.3. Particle Rotations 1-33
1.4.4. Particle-Wall Interactions 1-34
1.4.5. Electrostatic Interactions 1-38

1.5. Modelling in Gas-Particle Systems 1-39
1.5.1. Lagrangian Approach 1-39
1.5.2. Eulerian Continuum Approach 1-40
1.5.3. Equations of Motion 1-41

1.6. Modelling of Particle Flow in a Cyclone 1-42

1.1. General Background of Cyclones

The first cyclone was patented about a century ago. Although its basic design has remained largely unchanged a number of design variations have emerged to meet new performance targets in specific applications. A return-flow cyclone in its simplest form consists of a cylindrical section with a concentric vortex finder extending to just below the tangential inlet duct. The cylindrical section is connected to a conical section. A tangential rectangular inlet tube is attached at the top of the cylindrical tube. A schematic diagram is shown in Figure 1-1.

The separation power of cyclones relies on the effect of centrifugal forces. The feed stream is pumped through the tangential inlet pipe creating a rotating flow when it enters the cyclone. This creates a vortex about the centre and this vortex action causes the solids or dense phases to migrate to the wall. Secondary wall flows cause these solids material to move in spirals where they are eventually collected and the gas exits through the central vortex finder tube.

Cyclones have no moving parts and therefore have very low maintenance costs. Because of their simple design, low capital cost and simplicity of operation these devices have proved to be very attractive for dust cleaning operations. Cyclones have high operational efficiency especially at high throughput. Another advantage is their ability to operate at high temperature. When lined with special refractories, operating temperatures can exceed 800°C and can be limited only by the integrity of the refractories. This is desirable for high temperature applications like power generation where they are useful in collecting boiler fly ash and in other pyrometallurgical process industries. Cyclones are the only devices of technical relevance for separation of particles at high temperature (Mothes and Löffler, 1985). Patterson and Munz (1996) reported that particle collection efficiencies were lower for high temperature applications of cyclones. Cyclones are capable of

handling particle sizes ranging from 5 to 2000 μm although their efficiency decreases in the lower particle size ranges.

Given their versatility, a variety of industrial processes utilise the separation ability of cyclones at various stages. Generally, cyclones are utilised in most process stages were dust is generated or particulate material is handled, where the primary purpose is air cleaning and product recovery. Cyclones are an integral part of pneumatic conveying systems where they are preferred units for separation of the solids from the conveying gas.

The field of application of cyclones is ever expanding. General applications include pulp and paper, mineral and metallurgical processes, power generation, oil industry, cement and food industries. The mineral industry can actually be regarded as one of the traditional fields of application of cyclones after gas cleaning where cyclones were first used and for which the first patent was registered. In the mineral industry, cyclones are used primarily for classification, separation of dense material from materials of lighter density and dewatering. When used in wet streams cyclones are referred to as hydrocyclones. Hydrocyclones are extensively used in the pulp and paper industry and are capable of classifying pulp suspensions according to fibre size for specialty papers. The other type of cyclone is the gas cyclone and it is this one which has the widest range of applications. Of this type the reverse flow cyclone with tangential inlet is the most common.

The design of cyclones is mostly characterised by dimensions expressed as a number of diameters of the cylindrical barrel. Although a number of commercial proprietary designs exist nevertheless the design procedure is in most cases empirical in nature. The lack of a fundamental approach has lead to diverse claims and generalisations cannot be made. Nevertheless the design objective has been

primarily to limit pressure drop and increase collection efficiency at a given throughput.

In spite of the simplicity of operation of cyclones the fluid dynamics in these chambers is extremely complex. One of the main disadvantages of cyclones is their high pressure drops and low collection efficiency especially for particle sizes lower than 5μm. The collection efficiency is mostly expressed in terms of a cut diameter d_{50}, the particle size for which collection efficiency is 50 per cent.

In fact the major operating expense for cyclones is energy cost due to pressure drop. The pressure drop impacts directly on the pumping requirements as the pressure drop is a measure of the back pressure which the blower has to overcome. Indeed the performance of cyclones is primarily evaluated in terms of pressure drop and collection efficiency. Most research effort has therefore of necessity been directed at understanding the fundamentals of the flow field and various parameters and factors which impact on pressure drop and collection efficiency.

Literature on the investigation of pressure drop in cyclones is vast. As the focus of this study is not on these aspects, it will not be possible in this context to cover it all but notable pioneers are Sheppard and Lapple (1939) and ter Linden (1949). Sheppard and Lapple (1939) conducted an experimental study of flow pattern and pressure drop in a model cyclone constructed partly from glass to enable flow visualisation. They used an adjustable inlet vane and varied the vortex diameter and height in the cyclone. From their results Sheppard and Lapple (1939) found that the pressure losses were proportional to the square of the inlet velocity. The relationship between pressure loss and the inlet velocity is given by the following equation

$$\Delta P = C\frac{1}{2}\rho_g V_g^2 \tag{1-1}$$

where C is an empirical coefficient of pressure drop sometimes also referred to as the Euler number (Eu), ρ_g is density of fluid medium and V_g is the inlet velocity.

The coefficient of pressure drop C is constant for a given cyclone design and is not dependent on the size of the cyclone.

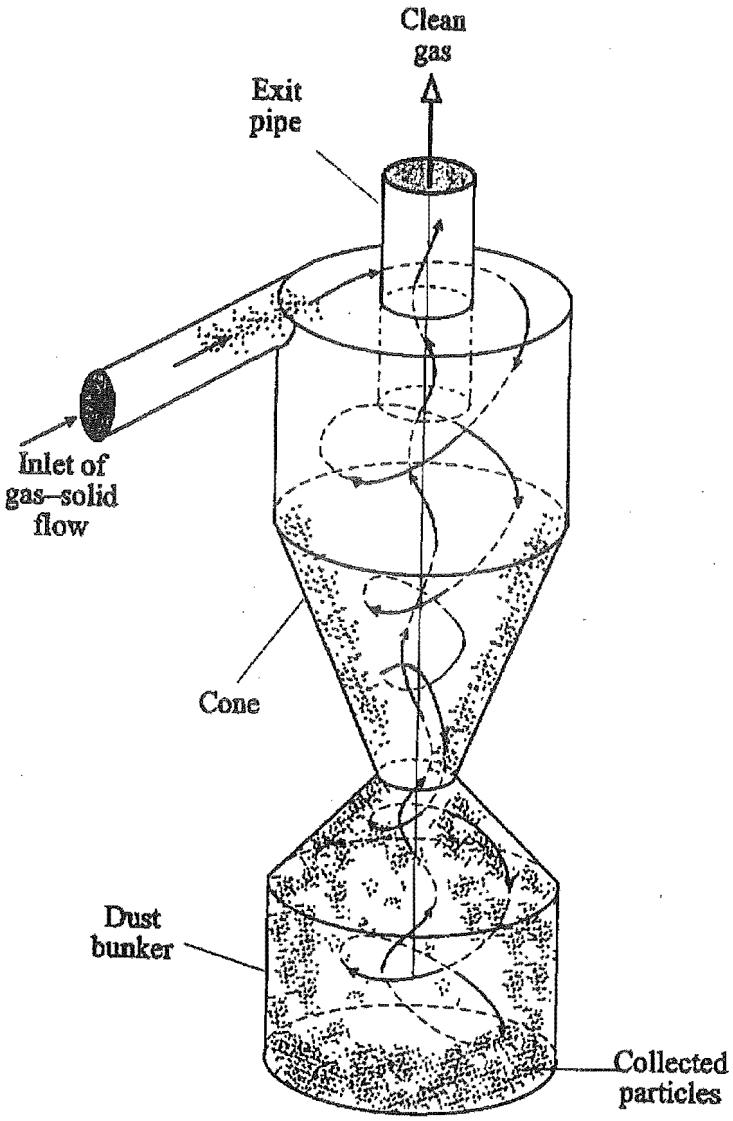

Figure 1-1 Schematic diagram of a return-flow cyclone (Liang-Shih et al., 1997)

The pressure drop in a cyclone is usually expressed as the number of gas inlet velocity heads, ΔH, which is equivalent to Eu and is a constant for any cyclone configuration with similar geometric proportions and same gas entrance velocity. The expression for ΔH by Sheppard and Lapple (1940) is:

$$\Delta H = \frac{16ab}{D_e^2} \qquad (1\text{-}2)$$

where D_e is diameter of vortex finder, a is the height and b is width of the rectangular entrance section.

The pressure loss falls as the square of the diameter of vortex finder for a given air flow. However the efficiency of the cyclones drops with increase in diameter of vortex finder. It is said there is a general rule of cyclones (Gregory, 1984) which says, ".... every measure which increases resistance to flow improves separation efficiency and vice versa". The lengthening of the cyclone however decreases pressure drop without loss of efficiency as shown below in Equation 1.3.

Numerous other expressions for ΔH exist in literature. First (1950) proposed an expression as discussed by Kang et al. (1989) which considered the effects of the dimensions such as overall height H, or diameter of cylinder D_c:

$$\Delta H = \frac{24ab}{D_e^2}\left[\frac{D_c}{h(H-h)}\right]^{1/3} \qquad (1\text{-}3)$$

where h is the height of the cylinder

Bohnet (1983) resolved the pressure drop into two components. The first component represented inlet losses and the second component losses through the outlet pipe. The pressure drop was said to occur across the gas outlet tube, in which the gas must be accelerated to very high axial velocities (Bohnet, 1983).

Straightening vanes inserted in the exit duct were found to reduce the pressure drop by as much as 50% (Sheppard and Lapple, 1939). However as these devices have the effect of reducing the vortex, the pressure drop reduction is accompanied by a loss in collection efficiency as the vortex is essential for the mechanism of dust collection. These findings were supported by ter Linden (1949) who observed that damping of the rotating gases had an unfavourable effect on the collection efficiency.

The presence of dust was also found to reduce pressure drop (Sheppard and Lapple). Yuu et al. (1978) reported that the reduction of pressure drop in the presence of dust was a result of a reduction in the tangential velocity. Beeckmans and Morin (1987) supported these findings in a separate study.

ter Linden (1949) measured the efficiency of a number of cyclone models with varying dimensions and recommended a gradual entry of the gas into the cyclone to achieve reasonable collection efficiency. Dietz (1981) divided the cyclone into three regions. Region 1 being the outer annulus region around the exhaust tube (inlet region) and region 2 the region below it (down flow region), and region 3 the core of the cyclone where the gas is essentially moving upwards (up flow region). Dietz solved the equations of conservation of particles in each of the three regions. However Dietz's model did not account for particle bouncing and re-entrainment which adversely affects collection efficiency. For further details on the model the reference can be consulted (Dietz, 1981). Numerous other workers have carried out investigations on collection efficiency. Beeckmans and Kim (1977), Kim and Lee (1997), Mori et al. (1968) are amongst some of the workers in this field. It is worth mentioning that most of these studies are dealing with very dilute systems and these models will generally be invalid for heavy loaded flows.

Sheppard and Lapple (1952) reported the double vortex theory. They observed that the primary flow pattern consisted of an outer downward spiral and an inner upward spiral. The average angle with the horizontal for the outer spiral was found to be about 10°. Kelsall (1952) also measured the particle track angle at the wall in a hydrocyclone at different radial positions for given operating conditions. From these results the angle was also a constant and about 15°. Kelsall reported a slight decrease in particle track angle with decreases in feed pressure for particles initially having higher axial velocity components. However these changes could not be quantified because of accuracy limitations of his equipment. The spirals in the central vortex were also found to prescribe a fixed angle. In the outer vortex flow, the gas has a radially inward velocity component. These observations were supported by measurements by ter Linden (1949), which revealed a highly turbulent low-pressure core extending over the entire length of the cyclone.

ter Linden (1949) experimentally measured the three gas velocity components, axial (W), radial (U) and tangential (V). Of the three components, the tangential velocity component was found to be predominant, with the total velocity almost equal to the tangential velocity. The tangential velocity was also found to deviate slightly from the tangential inlet velocity. The tangential velocity was found to increase from the wall attaining a maximum at a radial distance of 65 per cent from the wall and given by the following expression (ter Linden, 1949)

$$V_g = V_w \left(\frac{r}{r_i} \right)^n \qquad (1\text{-}4)$$

where V_w is the tangential velocity at the wall, r is radius of the cyclone, r_i is current radius and n is an exponent ($n = 0.52$). The exponent n considers the friction losses. Typical values of n lie between 0.5 and 0.8 (Bohnet et al., 1996).

Kelsall (1952) also measured tangential velocities V_g in a hydrocyclone and calculated the axial velocity W_g from the measured tangential velocity and track angle θ by the following equation

$$W_g = V_g \tan\theta \tag{1-5}$$

The axial component of the velocity (W_g) is directed downwards along the wall (in the barrel) and vertically upwards towards the centre while the radial velocity component of the gas (U_g) is directed radially inwards at the wall.

Kelsall observed that tangential velocity was the same at a given radial distance from the axis of the cyclone, independent of axial position. Loci of constant tangential velocities could be drawn in this "free vortex" region.

For purposes of understanding and hence application of a fundamental method to cyclone design or performance assessment, considerable theoretical work has been undertaken at modelling the internal flow field in cyclones. Given the turbulent nature of flow in cyclones and presence of recirculation, momentum and mass conservation principles are used in the formulation of these problems. The fluid flow is then represented by the Navier-Stokes and continuity equations. A major constraint of this approach is the accurate determination of the appropriate Reynolds stresses.

Most of this theoretical work has been geared towards pressure drop prediction and collection efficiency and ultimately a fundamentally based design method. Given the geometry of the cyclone the preferred coordinate systems have been spherical polar coordinates R, θ, ϕ or cylindrical polar coordinates z, r and θ. The work of Bloor and Ingham (1973) was one of the first theoretical investigations on the fluid dynamics of cyclones. Bloor and Ingham's theoretical predictions agreed with the experimental results of Kelsall (1952). Boysan et al. (1982) presented a mathematic model of the gas flow patterns in a cyclone. In their analysis Boysan et al. (1982) considered the momentum coupling between gas and solid to be absent. As the work of Bloor and Ingham (1973) and Boysan et al. (1982) was concerned with

collection efficiency, the particle trajectories were only considered up to the point the particle reached the wall. For the simple efficiency models a particle was considered collected once it struck the wall. The slip velocity between the gas and solid was assumed to be negligible. This assumption was not unreasonable considering the fact the size of the particles considered was no larger than 50 μm.

The strong momentum coupling between gas and solid phases in cyclone flow was reported by Parida and Chand (1980). Parida and Chand (1980) used the two-phase Navier Stokes equations to evaluate the tangential velocity components of the gas and solid phases. The governing equations in cylindrical coordinates are presented below

Continuity equation

$$\frac{\partial W_g}{\partial z} + \frac{1}{r}\frac{\partial (U_g r)}{\partial r} = 0 \tag{1-6}$$

For the radial, tangential and axial components of the gas phase respectively

$$\rho_g\left(U_g\frac{\partial U_g}{\partial r} - \frac{V_g^2}{r} + W_g\frac{\partial U_g}{\partial z}\right) = -\frac{\rho_p(U_g - U_p)}{\tau} - \frac{\partial p}{\partial r} + \mu_{eff}\left(\nabla^2 U_g - \frac{U_g}{r^2}\right) \tag{1-7}$$

$$\rho_g\left(U_g\frac{\partial V_g}{\partial r} + \frac{U_g V_g}{r} W_g\frac{\partial V_g}{\partial z}\right) = -\rho_p\frac{(V_g - V_p)}{\tau} + \mu_{eff}\left(\nabla^2 V_g - \frac{V_g}{r^2}\right) \tag{1-8}$$

$$\rho_g\left(U_g\frac{\partial W_g}{\partial r} + W_g\frac{\partial V_g}{\partial z}\right) = -\rho_p\left(\frac{W_g - W_p}{\tau}\right) - \frac{\partial p}{\partial z} + \mu_{eff}\nabla^2 W_g \tag{1-9}$$

For the particle phase

$$\rho_p\left(U_p\frac{\partial U_p}{\partial r}-\frac{V_p^2}{r}+W_p\frac{\partial U_p}{\partial z}\right)=-\frac{\rho_p\left(U_g-U_p\right)}{\tau} \tag{1-10}$$

$$\rho_p\left(U_p\frac{\partial V_p}{\partial r}+\frac{U_pV_p}{r}W_p\frac{\partial V_g}{\partial z}\right)=-\rho_p\frac{\left(V_g-V_p\right)}{\tau} \tag{1-11}$$

$$\rho_p\left(U_p\frac{\partial W_p}{\partial r}+W_p\frac{\partial V_p}{\partial z}\right)=-\rho_p\left(\frac{W_g-W_p}{\tau}\right) \tag{1-12}$$

where U, W, V are the radial, axial and tangential velocity components respectively and τ is the particle relaxation time, assuming a laminar type drag interaction.

Parida and Chand (1980) assumed the particle concentration in the cyclone to be uniformly distributed. This assumption is an over simplification as particles are immediately thrown to the wall region of the cyclone on entry. Particle-particle interactions and the interactions between particle and wall are also assumed negligible. The particles considered by Parida and Chand are also of the order of a few microns. Their results (Parida and Chand) showed that the tangential velocity was significantly affected even by particles of this size.

In their study of pressure drop reduction in a cyclone due to the presence of solids, Yuu et al. (1978) reported that the character of the gas flow was influenced by the concentration of the solid phase. They observed that some of the particles moved as a thin layer on the wall of the cyclone. These particles on the wall were said to increase the friction factor and in turn lowered the tangential velocity. They experimentally observed that the amount of particles travelling on the wall increased with increase in inlet velocity up to a maximum of 10 ms^{-1}. In their investigations on the aerodynamics of two-phase streams in cyclones Kiselnikov et al. (1971) reported that when particles travel through a cyclone they can travel in a *ordered* manner or in *chaotic* fashion. The *ordered* nature of the particle flow was called

roping and any non-rope travel was said to be *chaotic*. The experiments were carried out in a cyclone with a cone half angle of 15°. According to Kiselnikov et al. (1971) the particles moving in ropes have mutual interactions while the particles moving freely or in the dispersed phase have little interactions with each other with only the interactions between particles and wall being of significance. Kiselnikov et al. (1971) suggested that the formation of these ropes was influenced by particle rotations and was dependent on material properties as they found silica gel to move in a *chaotic* manner for concentration below 2 *kg/kg air* compared to the resin SG-1 which formed ropes. The velocities for these conditions are however not specified. In their paper Kiselnikov et al. investigated the nature and conditions leading to the formation of these ropes. The trajectory of the particles were said to be influenced by a number of factors, which are listed below:

Gas velocity (V_g)

Velocity of the particles (V_p)

Particle and gas densities (ρ_p and ρ_g)

Viscosity of the gas (υ)

Diameter of particles (d_p)

Weight concentration of the particles (μ)

Gravitational acceleration (g)

Cyclone dimensions, diameter (D_c), height (H) and angle of cone.

Kiselnikov et al. (1971) introduced dimensionless quantities to empirically describe the length of the rope through the cyclone as shown below

$$\frac{l}{H} = f\left(Ar, Fr_c, \mathrm{Re}_g, \mu, \frac{d_p}{D_c}, \frac{\rho_p}{\rho_g}\right) \qquad (1\text{-}13)$$

where $\frac{l}{H}$ is the ratio of length of particle trajectory to height of apparatus,

Ar, Fr$_c$ and *Re* are the dimensionless numbers Archemedes, Froude and Reynolds numbers respectively.

The trajectory length of the particles was found to decrease with increase in the mass flow ratio μ (solids/gas) as shown in Figure 1-2 by moving directly to the discharge side.

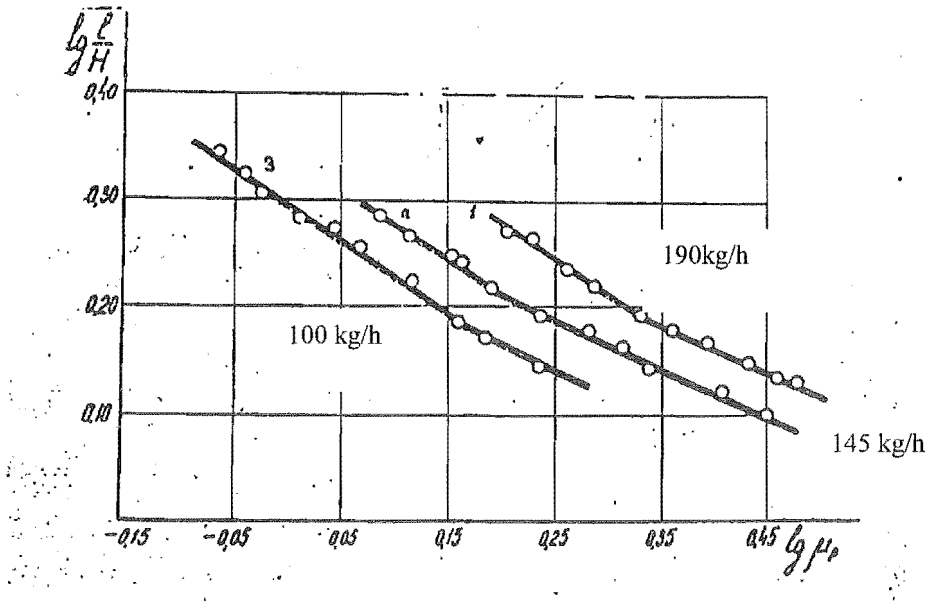

Figure 1-2 Function $\frac{l}{H} = f(\mu)$ for granulated urea at different feedrates

Diameter = 1 mm, 1. 190 kg/h; 2. 145 kg/h; 3. 100 kg/h (Kiselnikov et al. (1971)

The points of inflection on the graph were said to indicate the onset of roping. The region before the point of inflection (lower μ) was said to be the region of unstable rope formation while stable ropes formed after the point of inflection. This would suggest that for a given solid feed rate (e.g. 190 kg/h) a stable rope forms when the airflow is decreased (ie. the region of higher solid concentration) and vice versa

unstable ropes would form for high airflows (low solid concentration). This would seem to contradict the observations of Yuu et al. (1978) where the proportion of particles on the wall would increase with increase in airflow. Although the feed is increased at regular intervals, there seems to be a discrepancy, which is not explained in the point of inflection in moving from the high feed ratio to the low feed ratio. Kiselnikov et al. (1971) suggested two empirical equations for the flow in the region of stable rope formation and the unstable rope region.

The equation describing the rope path for the stable rope region is:

$$\frac{l}{H} = 0.275 \mathrm{Re}_g^{0.11} Fr_c^{0.24} Ar^{0.03} \mu^{-0.1} \tag{1-14}$$

and for the unstable region is:

$$\frac{l}{H} = 0.275 \mathrm{Re}_g^{0.11} Fr_c^{0.18} Ar^{0.02} \mu^{-0.18} \tag{1-15}$$

The separated particles in the cyclone form strands (ropes) on the cyclone wall and these boundary layer strands were found to decelerate in their descent towards the dust hopper (Muschelknautz and Trefz, 1993). The existence of dust strands (ropes) at high particle concentration was also reported by Rajendra & Abrahamson (1994) who experimented with sand particles of size range 150–210 μm in a 225 mm diameter Stairmand (1951) design cyclone. In their paper Rajendra & Abrahamson (1994) stated that particles moved in rope fashion and some of the particles in the dispersed phase. The movement of the ropes is reported by Kiselnikov et al. (1971) to be continuous. However this fact is at variance with the observations of Rajendra and Abrahamson who observed that the ropes where in some cases intermittent i.e. discharged at irregular intervals. In their interpretation of this intermittent phenomenon, Rajendra and Abrahamson suggested that the cyclone held a permanent inventory of solids at equilibrium and that rope discharges were a result of imbalances or disturbances in the feed stream. In their model (Rajendra and Abrahamson) the discharge of a rope represented the excess solids probably

triggered by disturbances in the feed rate. From their observations of flow patterns of particles they reported that a proportion of dust particles travelled in thin strands and a smaller proportion travelled freely in a dispersed phase. Rajendra and Abrahamson (1994) measured the residence time of the sand particles in their cyclone and from their results they reported two characteristic residence times, short and long. They attributed and associated the short residence time to a discharge of a rope and the long residence time to particles travelling in dispersed phase.

1.2. Application of Cyclones as Chemical Reactors

Gas flow in a cyclone is highly turbulent and there is good contact between gas and solids. It is common knowledge that turbulent flows enhance heat and mass transfer. Given these favourable gas-particle hydrodynamics the use of cyclones is being extended beyond their conventional use as dust separators as reviewed previously (§ 1.1). Cyclones are now being used in a variety of chemical processes. Examples are as drying chambers for granular materials, combustion of solid fuel and in pyrometallurgical processes like "flash smelting". Lédé et al. (1996) presented an experimental and theoretical study on fast sublimation of solid particles in a cyclone. The experiments were carried out with isocynanic acid, which reached 99% efficiency of phase change in less than 1 s under their experimental conditions. In a separate study Lede et al (1986) reported the continuous flash pyrolysis of wood sawdust in a cyclone reactor with wall temperatures between 893 and 1330K. In their study (Lede et al.) they reported the wood particles to be mainly heated by radiation and solid convection and reacted in less that 1 s. In their set-up the gas was found to be only weakly heated by the wall and had a residence time of the order of 0.05 s. The cyclone was found to be very efficient for carrying out reactions of the solid $\rightarrow$ fluid type. Although the results were satisfactory they (Lede et al.) emphasized the need for a more accurate determination of process parameters such as gas and solid residence times and heat transfer efficiencies for a better understanding of this novel reactor.

Lebedev et al. (1971) reported the application of cyclone chambers for drying of dispersed material. From their results the cyclone proved to be effective in drying, especially for removal of surface water. Because of the short residence times of the material in the cyclone the process must be carried out at higher temperatures and relatively fast. A significant advantage of the cyclone is its ability to carry out two processes in a single stage, ie. drying of the wet material and product separation from the process gas. The residence time is an important parameter for control of any chemical process. It is therefore important to measure or predict the material residence time in a cyclone reactor.

1.3. Particle Residence Time Measurements

There are few studies in the literature on measurement of residence time of particulate materials in a cyclone chamber. The work of Szekely and Carr (1966) was one of the first experimental measurements of particle residence time in cyclones. In their technique Szekely and Carr measured the solids mass flow rate and the solids hold-up in a cyclone chamber with an overall height of 330 mm. The solids hold up was measured by simultaneously isolating the cyclone from the inlet and exit ducts and weighing the amount of solids trapped. A mean particle residence time was obtained by dividing the solids hold-up by the solids flow rate

$$t_p = \frac{M}{M_f} \qquad (3\text{-}1)$$

In their cyclone (Szekely & Carr, 1966) the values of the solids residence time ranged from 0.86 to 1.05 s.

Lédé et al. (1989) used different methods to measure the solids residence time in a cyclone considered as a high temperature chemical reactor. In the first method they used a photosensitive particle with detectors at the inlet and outlet. The residence time was calculated by the time difference between the inlet and outlet signals. By repeat of this action they deduced *a residence time distribution* by statistical means. In the second method they utilised the piezo electric properties of the particles also

with detectors at the inlet and outlet. The third method was based on high-speed photography.

Lede et al. (1989) made an attempt to model the solids residence time as a function of the Reynolds number with a free fall terminal settling velocity as a parameter, ignoring the centrifugal forces and contact forces between particles and wall. It is known that the centrifugal acceleration can be many times that of gravity and therefore it is questionable whether centrifugal acceleration can be ignored and consideration given only to gravity. The model of Lede et al. suggested the following empirical equation

$$t_p = t_\infty + 4x10^{-5}\,\mathrm{Re}_o^{1.09} \qquad (3\text{-}2)$$

$(400 < Re_o < 250000)$

where t_p is the particle residence time and t_∞ is the residence time calculated from the terminal velocity of the particle and Re_o is the particle Reynolds number, based on the terminal velocity.

The fourth method was based on solid hold-up as was done by Szekely and Carr (1966). In the first method the mean solid residence time was determined by timing by hand when the particles passed through the entrance section to the time it exited. There are a lot of uncertainties with this technique and given the order of the magnitude of particle residence in the cyclone a large error will be involved in timing.

As for the hold up method, the results cannot be generalised, as it can be applicable only to particular process equipment. It does not account for change in particle trajectories when certain parameters are changed. It is doubtful whether the residence time obtained by this method can be representative as different material properties will result in different hold ups in the cyclone in addition to change in trajectories. Economies of use dictate that concentrated solid streams will of

necessity be encountered in cyclone chambers used in drying or in general as a chemical reactor.

Kang et al. (1989) also carried out measurements of solids residence time in a cyclone using KCl coated tracer particles. Kang et al. used charcoal and glass of size range 141-211 μm with a range of gas inlet velocities from 6-17 m s^{-1}. In their set-up they replaced the solids collection hopper at the dust outlet with a sampling tube of ID 10 mm. The column of sampled solids was then sectioned into small slices. The tracer particles in each slice were then dissolved in water for an hour and the tracer concentration determined by measuring the electrical conductivity of the solution. In this way, a time trace of concentration was obtained. The replacement of the normal collection hopper with a narrow collection tube will likely give a non-representative residence time and in addition the method is cumbersome. From the results of Kang et al. the average solid residence time was found to increase with increase in gas inlet velocity but decreased with particle size. Kang et al. also reported decrease of particle residence time with increase in density of particles. Kang et al. proposed a correlation for calculating particle residence time

$$\frac{\bar{t}_p}{\bar{t}_g} = 0.032\,\mathrm{Re}_p^{0.43}\left(\frac{u_g - u_t}{u_t}\right)^{0.70}\left(\frac{\rho_p - \rho_g}{\rho_g}\right)^{0.42}\left(\frac{H}{H-h}\right)^{-1.76.} \qquad (3\text{-}3)$$

where Re_p is the particle Reynolds number, t_g is the average gas residence time, H is the height of cyclone and h is the height of the cylindrical section.

The average gas residence time given is

$$t_g = \frac{V_c}{Q} \qquad (3\text{-}4)$$

where Q is volumetric flow rate of gas, V_c is effective volume of the cyclone.

Kang et al. used the Peclet number to represent the backmixing in the cyclone. The solids Peclet number was found to decrease with increase in gas velocity indicating an increase in dispersion.

Godoy et al. (1993) also did some measurements using the technique used by Szekely and Carr where the cyclone volume was isolated and the contents weighed. Godoy et al. (1993) used particles of size range 0.8-2.6 mm with gas inlet velocity from 6.2 to 11.5 m/s. Because of the large size difference between the particles used by Godoy et al. compared to Kang et al., a meaningful comparison of their results is not possible. Godoy et al. reported a decrease in solids residence time with increase in solids concentration. From their results the residence time decreased with increase in air velocity. A strong correlation of residence time with particle diameter and density was reported.

Pasley and Kemp (1993), using a photographic method also reported a decrease in particle residence time with increase in solids concentration. The particles used were silica gel and glass ballotini of size range 0.1-0.8 mm. The residence time of glass ballotini with a density about 2.5 times that of silica gel was higher than that of silica gel. An increase in residence time with increase in gas velocity was reported.

Rajendra and Abrahamson (1994) described a tracer technique to measure particle residence time in a cyclone by the moving impactor method. In their method Rajendra and Abrahamson (1994) introduced the pulse input by superposition on a steady feed stream. The introduction of the pulse input by this superposition on the steady feed introduced some unwanted disturbance to the flow. Another difficulty encountered was that sharp tracer changes could not be attained because of mixing upstream of the detection point. This mixing arose along the channel of a vibratory feeder used to feed the solids. As the residence times were evaluated by time difference between the peaks the task was made difficult when the tracer concentration curves were spread over long time intervals.

Saruchera and Abrahamson (1997) reported that they obtained sharp tracer inputs by replacement of the vibratory feed mechanism with a conveyor belt. Quantitative

techniques were also used to analyse the results from the moving impactor method. Two parameters, the mean residence time and the Peclet number were obtained from which the residence time distribution was deduced. The full paper is appended (Appendix 9A). The measurement of particle residence time in this PhD study is as described by Saruchera and Abrahamson and is based on the method of Rajendra and Abrahamson. A complete description of this method is given in the experimental section of this thesis (§ 2) and the Appendices 9E, 9F, and 9G can also be consulted.

In the present study the residence time of granular materials in a cyclone was measured by the stimulus-response technique. The influence of operating parameters, design variables, material properties and size distribution on the residence time of these particles in the cyclone are identified. The data from the experimentally measured particle residence times are analysed by various techniques to yield a mean residence time and the merits and demerits of the different methods of analysis are discussed (Saruchera and Abrahmson, 1997). A likely flow model to represent the flow of these particles in the cyclone is proposed and the validity of the model is checked with the experimental data. A theoretical approach to model the flow of these particles in the cyclone is also adopted. Several correlations are reported in literature with conflicting experimental results. These correlations are in most cases of little use besides applying to the particular set of results and experimental conditions. A more fundamental approach will therefore permit generalisations.

1.4. Dynamics of Gas-Solid Flows

1.4.1. *Gas-Particle Interactions*

The hydrodynamics of multi-particle systems are of interest in many fields of engineering. Most process engineering operations involve gas-solid interactions. The mutual interactions between the gas and solid phases govern the nature of flow in these systems. Common examples are drying, calcination, fluidised bed

systems, flows in cyclones and pneumatic conveying. The importance of gas-solid systems has led to extensive research, especially in pneumatic conveying. A lot of progress has been made over the years and the accumulated knowledge in this area will be utilised for our understanding of the flow of particles in cyclones bearing in mind the centrifugal force effects.

In two phase flows there are two general classifications based on particle size; fine particles and course particles (Tsuji et al., 1982). Particles with diameters above 100 microns are regarded as course particles and those below as fine particles (Cabrejos and Klinzing, 1994, Matsumoto et al., 1970). For very fine particles Stokes law is generally applicable but for course particles the flow condition lies beyond the Stokes region (Tsuji et al., 1981).

Gas-solid flows are characterised by the coupling between the solid and the gas phases. Coupling can be *two way* or *one way*. In *two way* coupling the gas flow field affects the particle motion and at the same time the particle phase has an effect on the gas flow field. This coupling comprises strong mutual interactions, which have the effect of modulating the turbulent structure of the gas flow field and altering particle trajectories. In *one way* coupling the particle phase is assumed to not have any effect on the gas flow field and this is generally valid for very lean phase suspensions. This coupling can in general either restrict or promote the flow of particles. Coupling can be expressed in terms of mass, momentum and thermal energy. Mass coupling is encountered in drying where the particle loses mass by for example evaporation to the gas phase. In momentum coupling, the interaction is by aerodynamic drag forces while in thermal coupling there is transfer of heat resulting in temperature changes in the phases.

In pneumatic conveying or cyclone flow, gas particle flows are normally characterised by the mass loading ratio (SGL) which is defined as the ratio of the

mass flow of the dispersed phase to the mass flow of the conveying gas. Crowe (1982) distinguished two types of flow regimes, dilute and dense phase flow. Dilute gas-particle flow is defined as flow in which the particle motion is controlled by local aerodynamic forces while in dense phase flow particle motion is governed by particle-particle interactions. For dilute systems the fluid dynamic force on a suspended particle can be assumed to be the same as that on a single particle without the interaction (Tsuji et. al., 1981). A quantitative distinction between these flow regimes is made by a ratio of aerodynamic response time or particle relaxation time τ_a to the time between collisions τ_c. For a ratio of $\tau_a / \tau_c < 1$, a particle has enough time to respond to the gas flow field before a collision and therefore the motion of the particle is said to be dominated by aerodynamic forces and the flow is referred to as dilute flow. On the other hand for $\tau_a / \tau_c > 1$ the particle will not have sufficient time to respond to the aerodynamic forces before collision with another particle and therefore the particle motion is collision controlled and the flow is described as dense phase. The loading ratio, particle size distribution and gas velocity gradient governs the nature of the flow (Tsuji et al., 1981).

The phenomenon of fluid resistance is extremely complex, and measurements of fluid drag, or particle motion have often been confusing and sometimes even contradictory (Clift and Gauvin, 1971). Given the complexity of these systems the general approach has been to start with the dynamics of single spherical particle and extend the theory to multi-particle systems. Because of the experimental approach in the study of these systems the results are generally in form of empirical correlations. The variety of random geometric structures and surface characteristics adds the complexity of these systems (Torobin and Gauvin, 1960a).

Two types of flow regimes are normally encountered. They are flows in which viscous forces predominate and flows in which inertial forces are predominant. A dimensionless criterion is universally used to differentiate these flow regimes. The

dimensionless criterion is the Reynolds number (Re_P) defined by the following expression for the particle Reynolds number:

$$\mathrm{Re}_p = \frac{\rho_g (V_g - V_p) d_p}{\mu} \qquad (4\text{-}1)$$

where ρ_g is the fluid density and V_g is gas velocity, V_P is particle velocity, d_P is particle diameter and μ is viscosity of the conveying fluid (gas).

For low Reynolds numbers ($Re_P < 1$) viscous forces are predominant and for higher Reynolds numbers ($1 < Re_P < 100$) inertia effects increase. These limits are temperature dependent and decrease with an increase in temperature. The flow regimes encountered in the process industry are generally restricted to Reynolds numbers $Re_P \leq 10^5$ (Molerus, 1993). The force exerted by the fluid on a particle is referred to as the drag force. Stoke's law gives the drag force in the viscous flow regime:

$$F_D = 3\pi d_p \mu (V_g - V_p) \qquad (4\text{-}2)$$

where F_D is drag force, d_P is particle diameter, μ is kinematic viscosity, V_g is gas velocity and V_P is particle velocity.

In general drag force is given by

$$F_D = 0.5 C_D \rho_g (V_g - V_p)^2 A \qquad (4\text{-}3)$$

where C_D is a drag coefficient and A ($= \frac{\pi d^2}{4}$ for a spherical particle) is projected area normal to flow. In the viscous flow regime C_D is

$$C_D = \frac{24}{\mathrm{Re}_p} \qquad (4\text{-}4)$$

$C_{D\infty}$ denotes the drag coefficient for a single particle in an unbounded fluid with a voidage of 1. The drag coefficient is a function of the Reynolds number.

The relationship between the drag coefficient and Reynolds number under these ideal conditions is the standard drag curve (Figure 1-3)

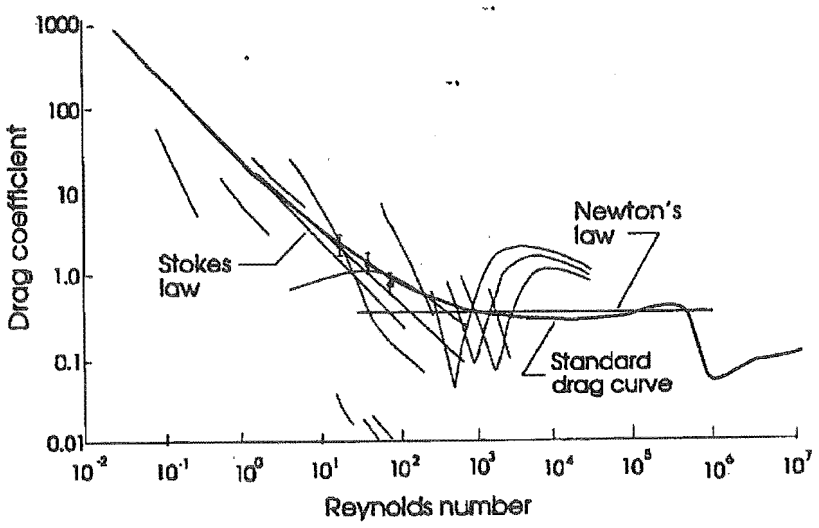

Figure 1-3 Standard Drag Curve (Crowe et al. 1998)

The standard drag curve can be divided into four regions namely

Stokes law regime with $Re_p < 2$ where $C_{D\infty} = \frac{24}{\mathrm{Re}_p}$

Intermediate region $0.5 < Re_p < 500$ where $C_{D\infty} = 18.5\mathrm{Re}_p^{-0.6}$

Fully developed turbulence regime (Newton's law region) $500 < Re_p < 2 \times 10^5$ where $C_{D\infty} = 0.44$

Turbulent boundary layer region $Re_p > 2 \times 10^5$ where $C_{D\infty} \approx 0.1$

Reynolds numbers outside this range shown in Figure 1-3 are normally not encountered when considering flow in cyclones.

There are a lot of other factors which increase the complexity of these systems. Conditions of non-ideality alter the flow pattern. However, ideal conditions are rarely if ever encountered in practical situations. In situations of practical interest particles have irregular shapes and the surfaces are not smooth. The resistance to motion of a particle or its drag coefficient was found to decrease with surface roughness. This reduction in drag coefficient has been attributed to an early transition of the boundary layer flow so that it was turbulent at relatively lower Reynolds numbers (Torobin and Gauvin, 1960). The effect of surface irregularities is reported to be dependent on the turbulence intensity of the fluid with high relative intensities causing the roughness effects to become effective at lower Reynolds numbers. Torobin and Gauvin (1960) point out the difficulty of quantitatively describing the roughness effect in the absence of an adequate system to define roughness. A particle is generally assumed to be smooth if the irregularities are confined to within the boundary layer. A more practical approach would be to consider particle shape rather than particle roughness. The shape characteristics of a particle can exert a profound influence on its ability to absorb momentum from a moving fluid (Torobin and Gauvin, 1960). Non-spherical particles can be characterised by a shape factor. A common shape factor used is the sphericity ψ defined by:

$$\psi = \frac{surface\ area\ of\ sphere\ with\ same\ volume\ as\ particle}{surface\ area\ of\ particle} \qquad (4\text{-}5)$$

where $\psi = 1$ for a spherical particle and $0 < \psi < 1$ for a non spherical particle.

Some data on sphericity of certain particulate materials are taken from Klinzing et al. (1997) and are shown in Table 4.1-1.

Table 4.1 Data on Sphericity (Klinzing et al. 1997)

Material	ψ
Sand	0.534-0.861
Iron catalyst	0.578
Bituminous coal	0.625
Pulverized coal	0.696
Celite cylinders	0.861
Broken solids	0.63
Silica	0.554-0.628

An alternative measure used to characterise shape of a particle is the circularity C_{cir}. The circularity is defined by the ratio of square of perimeter to projected area:

$$Circularity = \frac{(\pi D)^2}{\left(\frac{\pi D^2}{4}\right)} \qquad (4\text{-}6)$$

where D is the diameter of an equivalent sphere

The drag force on a particle is affected by a number of factors including surface roughness, proximity of a wall, particle shape and rotation, particle - particle interactions and in some cases electrostatic effects. The main effect of roughness is a decrease of the critical Reynolds number (Clift and Gauvin, 1971). The degree of particle–particle interactions is a function of the voidage. Void fraction ε_g, is defined as the fraction of volume between the particles in a given volume element.

$$\varepsilon_g = 1 - \frac{\rho_{df}}{\rho_p} \qquad (4\text{-}7)$$

where ρ_{df} is density of dispersed phase (mass of particles per unit volume) and ρ_p is density of particle. If the density of the gas is ignored then $\rho_{df} = \rho_{bulk}$ (bulk density).

The relationship between the voidage ε_g and the volume occupied by the solids ε_s is the following equation

$$\varepsilon_g + \varepsilon_s = 1 \tag{4-8}$$

Clift, Grace and Weber (1978) defined a measure of the effect of bounding wall on drag. A drag factor can be defined for the same particle at the same fluid velocity and is given by

$$K_f = \frac{drag\ in\ bounded\ fluid}{drag\ in\ infinite\ fluid} = \frac{F_D}{F_{D_\infty}} \tag{4-9}$$

The factor K_f can be determined experimentally.

In a cyclone there are two distinct flow regions, the central core region in which $\varepsilon \approx 1$ and the periphery region in which $\varepsilon < 1$. The width of this periphery region is dependent on particle properties and gas velocity.

In the periphery region, where many particles exist, the drag coefficient on a particle is influenced by the presence of other particles. The drag force for interacting particles at high Reynolds number cannot be determined analytically. The only multiparticle system for which the drag force can be rigorously determined analytically is a two-particle system (Zhu, et al. 1994). An empirical equation relating the drag force of an interactive particle with the drag force on a single particle was given by Zhu et al. (1994).

$$F_D = F_{D0}\left(1 - (1 - A)\exp\left(B\frac{l}{d_p}\right)\right) \tag{4-10}$$

where F_D is the drag force for an interactive particle, F_{D0} is the drag force for a single particle, l is the distance between the particles and d_p is particle diameter. Coefficients A and B are functions of the Reynolds number.

The drag coefficient can be assumed to depend only on voidage yielding a new drag coefficient C_{Ds} where (Wen and Galli, 1985)

$$C_{Ds} = C_{D\infty}\varepsilon^{-4.7} \tag{4-11}$$

There are numerous empirical relationships in literature relating the drag coefficient to the Reynolds number (Haider and Levenspiel, 1989). The modified drag coefficient C_{Ds} can be related to the Reynolds number by (Rowe and Henwood, 1961)

$$C_{Ds} = \frac{24}{\mathrm{Re}_p}\left(1 + 0.15\mathrm{Re}^{0.687}\right) \tag{4-12}$$

for $Re_p < 1000$

The drag force F_D per unit volume of particles between the gas and particles in the laminar regime is given by

$$F_D = \frac{\rho_g \left|\mathrm{V_g} - \mathrm{V}_p\right| (\psi d_p)}{\mu} \tag{4-13}$$

where $\left|\mathrm{V_g} - \mathrm{V}_p\right| = \left[\left(\mathrm{V}_g - \mathrm{V}_p\right)^2 + \left(\mathrm{W_g} - \mathrm{W}_p\right)^2 + \left(\mathrm{U_g} - \mathrm{U}_p\right)^2\right]^{0.5}$ and

V_g and V_p are the gas and particle tangential (swirl) velocity components,

W_g and W_p are the gas and particle axial velocity components

U_g and U_p are the gas and particle radial velocity components

ψ is a shape factor, ρ_g is density and μ is viscosity

The motion of a solid particle in a cyclone is almost entirely due to the gas drag force and the particle trajectory is approximately in the direction of gas flow. The velocity of the gas consists of a mean and fluctuating component. Particle presence

in the flow stream will result in a damping effect on the fluctuating component of the velocity. This strong interaction between the solid particle and the gas has important implications on both the solid particle and gas residence time inside the cyclone.

Inertial effects are important for large diameter and dense particles (where $\rho_p >> \rho_f$) and for low viscosity fluids. Inertia is generally used to describe the reduction in the fluctuating component of the particle velocity. A common term used in dynamics of gas particle flows to characterise inertial effects is the particle *relaxation time or response* τ. The particle relaxation time is defined as the rate of response of particle acceleration to the relative velocity between the particle and the carrier fluid (Shirolkar et al., 1996). It characterizes the time it takes for a particle to return to steady motion after a disturbance. The mathematical formulation of the relaxation time is:

$$\tau = \frac{4\rho_p d_p^{\,2}}{3\mu C_D \,\mathrm{Re}_p} \qquad (4\text{-}14)$$

A large dense particle with a higher relaxation time will on average be influenced less by the gas flow.

1.4.2. *Particle-Particle Interactions*

Two modes of transport for the hydrodynamic flow of granular materials can be distinguished. The first one is one in which the concentration of the particles is low and the particles behave more or less independently. In this regime the particle-wall interactions are more important. Collisions between particles are possible but they are likely to be infrequent. The second one is obtained at higher particle concentrations. In this regime particle-particle interactions increase. Particle-particle contacts can be subdivided into two classes according to the duration of contact, long and short. The long contacts can be treated as semi-permanent

frictional contacts and the short contacts can be treated as inelastic collisions of short duration. With the long class, contacts between particles are semi-permanent with the normal reaction forces and associated tangential frictional forces at these sliding contacts more dominant (Johnson and Jackson 1987). Lun, Savage and Jeffrey (1984) and other workers have used statistical methods analogous to those used in the kinetic theory of gases to model particle-particle interactions in pneumatic conveying systems. In the kinetic theory of gases collisions are assumed to be elastic. However this idealised situation is unlikely to be representative of actual flow situations as the collisions are likely to be damped in most cases and therefore highly inelastic. For flow in cyclones at high particle concentrations a layer of particles will form on the wall of the cyclone (Trefz and Muschelknautz, 1993). Particles in contact with the wall are no longer free to escape and incident particles are more likely to strike at an existing particle layer on the walls. For particles further away from the wall it is possible for them to escape and be re-entrained.

When particles enter a cyclone their inertia is regarded as a centrifugal force. This force induces a radial migration of the particles to the wall of the cyclone (Schmidt, 1993). The time a particle takes to reach the wall boundary layer is referred to as the migration time. This is the time normally used in collection efficiency models where a particle is assumed collected when it reaches the wall. The migration time of solid particles in a cyclone is very small compared to the residence time in the cyclone and can be estimated by a balance of forces in the radial direction (Hsieh and Rajamani, 1991). For practical purposes all the particles are assumed collected on the wall immediately on entering the wall boundary layer. This pattern of flow results in a locally high concentration of particles on the wall. Particle-particle interactions are strong and increase with increase in solids loading (Soo, 1989). The motion of a particle in a stream of other particles is thus constrained by the movement of its neighbouring particles. Therefore a particle undergoes a series of random collisions with other particles as it travels through the cyclone. The random velocity fluctuations in the gas flow field also induce analogous flow behaviour in the particle phase ie. velocity fluctuations. Thus the interactions between particles

can be largely due to velocity differences. The inter-particle collisions can be a means of transfer of kinetic energy from the faster moving particles to the slower moving particles. Particle-particle collisions are a mechanism by which particle fluctuating kinetic energy associated with one direction is redistributed in all directions and dissipated by inelastic collisions (Senior and Grace, 1998). It is expected a velocity gradient would exist in the particle boundary layer on the wall with particles further away from the wall influenced more by the gas drag and particles closer to the wall retarded by wall friction.

Arastoopuor (1986) proposed that particle-particle interaction forces are a combination of collision and drag effects. For purely drag related interaction force the density of the particle is not a factor and on the other hand for the collision type, particle-particle interactions are a function of the density of the particles. Drag related interactions are likely to be important at higher relative velocity for particles with low relaxation time. Under these circumstances a particle is driven by the gas phase to strike at another particle. When the relative velocity is low the momentum of the gas is not enough to drive the particles and particle density and gravity effects will cause the collisions. In cyclones the particle-particle interactions are likely to be a mixture of the drag related and collision type particle-particle interactions.

Although the collisions are multiple, for dispersed phases only binary collisions are normally considered for simplicity and the results can be generalised for multiple collisions by summation of all the contact forces. For dense layers the assumption of only binary collisions is no longer valid. Under these conditions collisions are more frequent and semi-permanent. In the extreme case of close packing shear flow will result.

There are generally two approaches to the modelling of inter-particle collisions, the hard sphere model and the soft sphere model. The physical model shown in Figure 1-4 can represent the hard sphere binary particle-particle interactions (Tsuji et al., 1998).

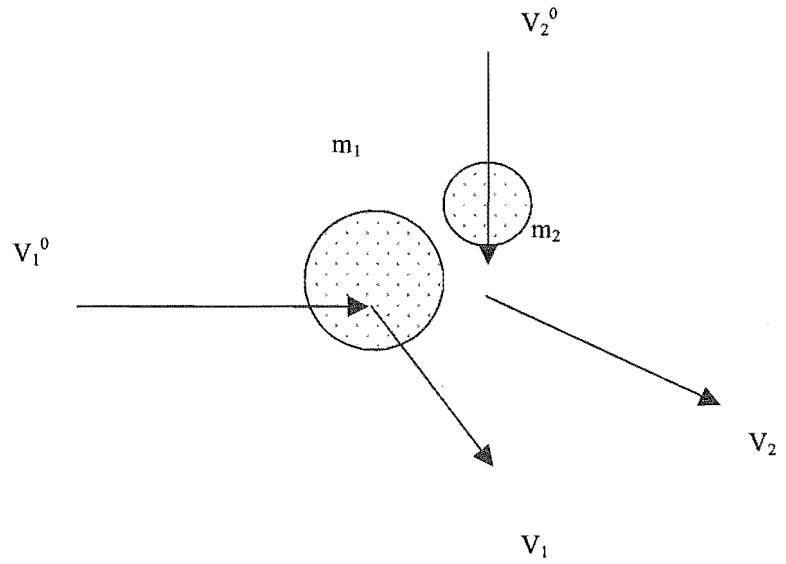

Figure 1-4. Particle-Particle Interactions

The two particles are of mass m_1 and m_2. The velocities before collision are V_1^0 and V_2^0 while the velocities after collision are V_1 and V_2 respectively.

The hard particle approach assumes that the interaction forces are impulsive and that momentum exchange is achieved only during these collisions. Assuming particle rotations are absent and particles do not undergo any deformation, the conservation of linear momentum for a frictionless contact can be expressed by the impulse equations

$$J = m_1(V_1 - V_1^0) \tag{4-15}$$

$$J' = -m_2(V_2 - V_2^0) \tag{4-16}$$

The relationship between the normal initial velocity difference and final velocity difference is the coefficient of restitution e_p for binary particle collisions. For elastic collisions the coefficient $e_p = 1$ and $e_p = 0$ for plastic collisions.

The coefficient of restitution generally decreases with increase in impact velocity. The kinetic energy of the colliding particles is transformed into vibrations of the particles and in some case breakage.

The kinetic theory of gases can be extended to model the inter-particle collisions in multi-particle systems. In this model it is assumed that the collision of particles is the only mechanism by which mass, momentum and energy are transported (Tsuji et al., 1998).

1.4.3. *Particle Rotations*

A phenomenon that is associated with particle rotation is the *Magnus effect* and is due to velocity gradients in shear flow or the result of collision with other particles or a wall boundary (Liang-Shih Fan and Chao Zhu, 1997). The Magnus effect is insignificant generally for particles below the size of 100 μm. The Magnus force is small when the particle diameter is small compared to the characteristic length of the turbulent eddies of the gas (Soo and Tien, 1960). The effect of the Magnus force is to cause a lift force on the particle in the direction of higher gas velocity. Torobin and Gauvin (1960) made a detailed review of the effect of particle rotations on the motion of particles in gas-solid suspensions. Particle rotation was attributed to velocity gradients in the flow and collisions with solid boundaries. Fluid entrainment effectively adds velocity to the side of the sphere where the rotation and fluid velocity direction are the same, and conversely retards the fluid velocity on the opposite side (White, 1986). The Magnus effect can thus be associated with energy dissipation around the rotating particle. Torobin and Gauvin noted that particle rotation appeared to have little effect on the drag coefficient at low Reynolds numbers but was found to influence the linearity of the motion of the particles. Thus a consequence of this phenomena is that rotation due to shape irregularity of a particle could influences particle trajectories and hence residence time in a reactor. Spin rates up to the order of thousands of revolutions per second have been reported for particles in high-speed compressible flows. The spinning of the particles is also

associated with a vortex behind the particle where the air velocity in the vortex is relatively low.

1.4.4. *Particle-Wall Interactions*

Experimental studies by Soo and Tien (1960) revealed that the presence of a wall and the distribution of the turbulent intensity of the stream near the wall affected the motion of large solid particles in gas-solid suspensions. In some cases the turbulent intensity of particle motion was found to exceed the fluid intensity by a factor as much as three. Soo and Tien (1960) attributed this to the increase of stream intensity toward the wall. These findings would seem to contradict the theory that particles are carried through by gas drag and their energy can therefore not exceed that of the carrier gas. In addition the stream intensity is moderated by the presence of the wall. Torobin and Gauvin (1961) sought to interpret these particle velocity fluctuations as reported by Soo and Tien (1960) in terms of electrostatic forces or some unsymmetrical drag force over and above the Stokesian drag force. Puzzled by Soo's findings Min (1967) conducted experimental tests and found that the electrostatic charge did not have any effect on the particle flow and therefore Soo and Tien's results could not be explained in terms of electrostatic charges. Although evidence from Min (1967) suggested the effect of electrostatic forces to be insignificant, it should be pointed out however that the effect of electrostatic forces is complex and can depend on a lot of factors including humidity, particle properties and confining wall properties. Torobin and Gauvin (1961) examined particle trajectories photographically and found that particle velocities differed considerably from one particle to another and came to the conclusion that Soo and Tien erred in their interpretation. They suggested that what Soo and Tien (1960) interpreted as turbulent intensity was instead the variation of particle velocity from the general flow and this deviation in velocities from the general was due to particle-wall collisions. The effect of particle wall collisions especially for large particles is therefore significant.

Louge, Mastorakos and Kenkins (1991) supported the explanations of Min (1967) that although the drag force exerted by the mean gas flow suspended particles, particle velocity fluctuations are the result of inter-particle collisions and collisions with the wall.

As was mentioned previously in the treatment of particle-particle interactions (§ 1.4-2), particles often travel on the walls or in close proximity to the walls of the cyclone. In view of the above findings, particle-wall interactions have to be considered in any modelling of flow of particles in a cyclone. Particle-wall interactions can be of two forms, particle bouncing from a wall and sliding of particles along the wall. In pneumatic conveying, irregular particle bounce has long been considered as the mechanism of suspension of particles (Matsumoto and Saito, 1970). Mori et al. (1986) observed that for large particles the irregularity of bouncing is one of the main mechanisms of particle back-mixing against gravitational or the centrifugal separating force in ducts. This back mixing due to irregular bouncing of particles was said to affect the collection efficiency of large particles in cyclone separators. Such irregular bounces can be due to particle shape irregularities and wall surface imperfections. The collision of a single particle with a surface randomly composed of similar particles is highly inelastic (White, 1986). In cyclones particles entering the chamber quickly migrate to the walls. When solids loading is high the probability of an incident particle striking at another particle on the wall is high.

In their work on mechanics of particle bounce from a surface Ranz et al. (1960) reported that when particles strike at a surface they bounce at an angle with a probabilistic distribution about the average angle of reflection. In addition to the energy interchange between the particle and the wall there is also interchange between the rotational and translational energies of the particle. Ranz et al (1960) used irregularly shaped ping-pong balls to demonstrate the bounce characteristics of irregularly shaped particles. They impacted five representative shapes of ping-pong

balls at a constant incidence angle and measured the distribution of the angle of reflection. The angle of incidence and reflections were measured from the normal to the particle velocity vector before and after collision respectively. Later the incident angles were varied and the process repeated. Their results revealed that there was a probability of a particle striking at a low angle and bouncing off at a high angle. For an angle of incidence of α', the reflected angle was α''. The velocity after impact is a function of the elasticity of the bounce, the irregularity of the particle, and the friction encountered with the wall (Ranz et. al, 1960).

A simple diagram can represent the collisions of the particles with the walls of the cyclone in 2D as shown in Figure 1-5. In practice the wall has a curvature but for a point contact it can be assumed to be linear. Although the wall appears as plane and smooth in reality the wall has surface imperfections and for high dust loadings a layer of particles can compose the wall surface.

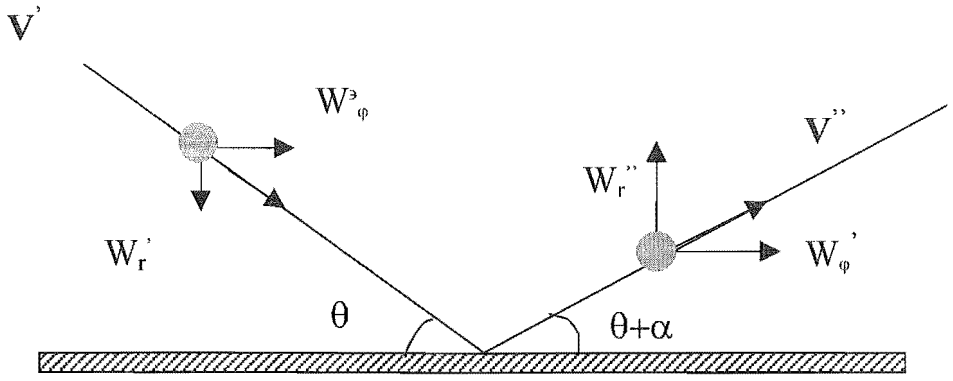

Figure 1-5 Particle Collision with Cyclone Wall

The plane of particle travel (assumed to be in the same plane after the collision) is the plane of the paper. Thus the axis of the cyclone (z coordinate in cylindrical

coordinates) is almost perpendicular to the paper. The coefficient of restitution is given by

$$W_r'' = \varepsilon W_r' \tag{4-17}$$

where W_r' is the velocity component in the radial direction and W_φ is in the tangential direction. α' and α" are the incident and reflected angles respectively.

As shown in Equation 4-17 above, W_r" is directly proportional to the coefficient of restitution and will increase with an increase in the coefficient of restitution. In a cyclone the magnitude of the radial component of the particle velocity is related to the magnitude of its centrifugal force or acceleration. The magnitude of W_r" affects the trajectory of the particle. If that component of the particle velocity is high there will be a loss of gas momentum in the tangential direction, as the particle will have to be reaccelerated by the gas drag.

The incident and reflected angles can be expressed as

$$\alpha' = \tan^{-1}\left(\frac{W_r'}{W_\varphi'}\right) \qquad \text{and} \qquad \alpha'' = \tan^{-1}\left(\frac{W_r''}{W_\varphi''}\right)$$

The incident angle α' is small where the component of velocity in the radial direction is small relative to the tangential direction. In this case the particle trajectory will be dominated by the gas drag and therefore the approach angle to the wall will be narrow. A decrease in the magnitude of W_r' will result in a slight increase in the coefficient of restitution (Senior and Grace, 1998). For a particle whose collision with the wall is highly inelastic the reflected velocity in the radial direction will be reduced. A low reflected angle would also result and the particle would stay close to the wall. This can also be extended to multiple of particles and two cases can be considered. The first case is for elastic collision where the coefficient of restitution is close to one. In this case the particles will be scattered away from the wall where they are acted on by the gas drag. In the second case the

particle-wall collisions are inelastic. Under this situation the particles are reflected with a low angle of reflection and tend to stay close to the wall. As the wall bounds the particles, the particles will tend to interact with each other even more and are likely to form strands. It is important to note that the incident and reflected angles are also influenced by the particle shape factor. On the point of contact of the particle with the wall a frictional force will also act in the tangential direction.

1.4.5. *Electrostatic Interactions*

Electrostatics is the term given to the study of the interactions between electrically charged bodies (Cross, 1987). The force between two equally charged bodies can be described by the following equation

$$F_E \propto \frac{q^2}{r^2} \tag{4-1}$$

where q is the charge on each body and r is the distance separating them.

When two particles come in contact and are quickly separated charge transfer can occur. After the separation of the contact area the electric charge is conserved on the particle and its value is determined by the electric strength of the gaseous environment (Kuczynski et al., 1981). For non-conducting particles this particle-particle interaction can result in a redistribution of surface charge and an electrostatic charge build up. In process industries handling granular material this charge build-up may be undesirable and has been linked to dust explosions. However, in some case charge build up may be desirable and aid in agglomeration processes as illustrated below (Figure 1-6)

Electrostatic forces can produce particle clusters and thus alter the drag force acting on these particles. Electrostatic effects should therefore be considered not only for safety but maybe helpful in interpreting flow phenomenon of particulate material

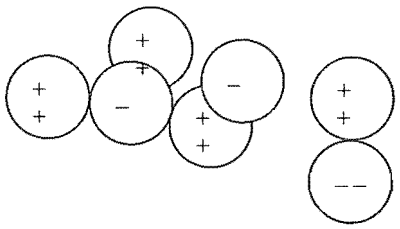

Figure 1-6 Agglomerating charged spherical particles

1.5. Modelling in Gas-Particle Systems

The principles of momentum, mass and energy balances are applied to the dynamics of gas-solid flows. There are two basic approaches in modelling of multiphase flows, the Lagrangian trajectory tracking and the Eulerian continuum approach.

1.5.1. *Lagrangian Approach*

The Lagrangian coordinate reference is the most convenient and straightforward approach for modelling dilute systems where interactions between particles are negligible. In this approach the trajectory of a single particle is described. The Lagrangian model can be broken down into two basic models - the *deterministic* trajectory model and the *stochastic* trajectory model. The *deterministic* trajectory model is applicable for steady and dilute flow while the *stochastic* trajectory model is applicable for unsteady or dense flows. In the *deterministic* model the averaged momentum equation of the particles is solved using a previously determined average fluid velocity field. The instantaneous position of the particle can thus be considered as a function of the location from where the particle originated and the time elapsed (Shirolkar et al, 1996). Therefore the problem reduces to the solution of the particle momentum equation. The stochastic approach involves the so-called Monte Carlo method where the particle behaviour is determined by solving the instantaneous momentum equation in Lagrangian coordinates. The Monte Carlo approach requires considerable amount of computing power as a large number of particle trajectories have to be calculated to yield statistical averages with reasonable

accuracy. Particles with similar properties e.g. particle size and velocity are grouped into "parcels". The trajectories of these representative parcels are then tracked by the Lagrangian approach. The stochastic approach is sometimes knows as the discrete element model (DEM) (Cundal et al., 1979). A special technique for modelling particle motion with inter-particle collisions is the direct simulation Monte Carlo method (DSMC) (Tsuji, et al. 1998). A disadvantage of the Lagrangian approach is that particles also experience a dispersion effect, which cannot easily be handled by this method.

1.5.2. *Eulerian Continuum Approach*

The Eulerian approach treats the gas and solid phases as an interpenetrating continuous phase with a fixed reference frame (Shirolkar et al, 1996). Solution of the continuity equation and the set of Navier-Stokes equations in an appropriate coordinate system obtains the flow field. The effect of the particle phase is taken into account by the introduction of appropriate source terms in the gas conservation equations.

Careful consideration must be given on the choice of the two methods. Generally the Eulerian approach is suitable for mono-sized uniformly distributed heavily loaded suspensions. The complication of this approach is that since the particles are treated as a pseudo-fluid the rheological behaviour is in most cases unknown which compounds the problem of satisfactorily describing the stress components. On the other hand the Lagrangian model is most suitable for low solid loadings with the assumption that the coupling between the phases is one way gas to particle. Given the fairly course nature of the particles considered for cyclone processing, the solids and gas phases can hardly be considered as a continuum and particle inertia effects will be strong after particle-particle and particle-wall interactions.

1.5.3. *Equations of Motion*

The Lagrangian approach is the most appropriate for modelling of particle phases in the cyclone where large particles are involved. Applying the law of conservation of momentum per unit volume which states that for a particle for phase i,

[rate of momentum accumulation]$_i$ = [rate in of momentum by convection]$_i$ – [rate out of momentum by convection]$_i$ + [sum of external forces]$_i$ + [sum of internal forces]$_I$

In the above equation viscous forces are ignored if the particle phase is treated as a discrete phase. Although the possible interaction forces (fluid-particle, particle-particle and particle-wall) can be qualitatively described it is not feasible to accurately quantify these forces, as they are not only dependent on immediate neighbours but also particles in the vicinity due to propagation of force disturbances.

The general equation of motion is expressed by

$$\frac{dV_p}{dt} = \frac{\sum F_i}{m_p} \qquad (5\text{-}1)$$

where $\sum F_i$ is the summation of all external forces acting on the particle assuming they are additive, m_p is the mass of particle and V_p is the velocity.

The various external forces of significance, which can be acting on a particle, are

F_D - gas aerodynamic drag force

F_M - Magnus force

F_g - gravity force

F_B - buoyancy force

F_f - wall friction force

F_p - inter-particle contact force

F_E - electrostatic force

In dilute flows the aerodynamic drag force and the gravitational force are the most important forces. The Magnus force is negligible where no shear flow exists and the buoyancy force is neglected where particle density is much greater than the carrier gas density ie. $\rho_p >> \rho_g$. In particular cases electrostatic forces can be neglected.

The generalised equation of motion (Equation 5.1) reduces to

$$m\frac{dV}{dt} = F_D + F_g + F_f + F_c \qquad (5\text{-}2)$$

1.6. Modelling of Particle Flow in a Cyclone

There have been few attempts to model particle residence time in a cyclone. Most of the models were empirical (Szekely & Carr, 1966, Kang et al, 1989, Lede et al., 1989). The disadvantage of empirical models is that they are valid for a limited range of parameters and in most cases cannot be extended to other experimental conditions. The results cannot be generalised or independently verified. A few empirical models are reviewed in Section 1.3.

The external forces influencing the trajectory of a particle in a cyclone were qualitatively described by Kiselnikov et al. (1971). Lebedev et al. (1979) analysed the aerodynamics of two-phase streams on the wall in a two-stage combined cyclone drier by application of the conservation laws. This work (Lebedev et al. 1979) constitutes the earliest known attempt at application of the momentum balance to the modelling of particle trajectories in a cyclone. A force balance diagram shown in Figure 1-7 can represent the model of forces acting on a particle in contact with the wall. A complete representation of all the various forces is not possible owing to

inadequate knowledge and understanding and only those forces which can easily be described are considered to be significant and are shown (Lebedev et al., 1979)

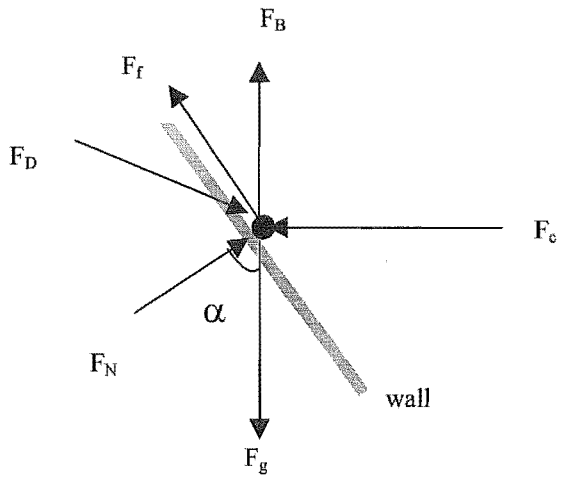

Figure 1-7 Force balance on a particle in contact with a cyclone wall (Lebedev et al., 1979)

The equations of motion in polar cylindrical coordinates for a particle on the wall of a cyclone are (Lebedev et al., 1979)

$$\frac{dW_z}{dt}=\left(1-\frac{\rho_g}{\rho_p}\right)g+\left(\frac{\rho_g}{\rho_p}-1\right)g\cdot Sin^2\alpha+\frac{W_\varphi^2}{R}Sin\alpha\cdot Cos\alpha+\frac{3}{4}\frac{\psi\nu}{d_p^2\rho_p}(V_z-W_z)-$$
$$f\left[\left(\frac{\rho_g}{\rho_p}-1\right)g\cdot Sin\alpha+\frac{W_\varphi^2}{R}Cos\alpha\right]\frac{W_z}{\sqrt{W_z^2+W_r^2+W_\varphi^2}}$$

(6-1)

$$\frac{dW_r}{dt}=\frac{W_\varphi^2}{R}-\left[\left(\frac{\rho_g}{\rho_p}-1\right)g\cdot Sin\alpha+\frac{W_\varphi^2}{R}Cos\alpha\right]Cos\alpha-$$
$$f\left[\left(\frac{\rho_g}{\rho_p}-1\right)g\cdot Sin\alpha+\frac{W_\varphi^2}{R}Cos\alpha\right]\frac{W_r}{\sqrt{W_r^2+W_z^2+W_\varphi^2}}+\frac{3}{4}\frac{\psi\nu\rho_g}{d_p^2\rho_p}(V_r-W_r))\quad(6\text{-}2)$$

$$\frac{dW_\varphi}{dt} = -2W_r\frac{W_\varphi}{R} + \frac{3}{4}\frac{\psi\nu\rho_g}{d_p^2\rho_p}\left(W_\varphi - V_\varphi\right) -$$
$$f\left[\left(\frac{\rho_g}{\rho_p} - 1\right)g\cdot Sin\alpha + \frac{W_\varphi^2}{R}Cos\alpha\right]\frac{W_\varphi}{\sqrt{W_z^2 + W_r^2 + W_\varphi^2}} \qquad (6\text{-}3)$$

where V_r, V_φ and V_z are the radial, tangential and axial velocity components of the gas. W_r, W_φ and W_z are the radial, tangential and axial velocity components of the particles. d_p is the particle diameter and ρ_g and ρ_p are the gas and particle densities respectively. f is the frictional coefficient between particle and wall, ψ is the drag coefficient, ν is the gas kinematic viscosity, R is the current radius, g is the gravitational constant and α is the angle of the cone, which has an axis aligned with g.

For drying purposes the energy exchange between the gas and particle controls the process. A complete knowledge of the gas velocity flow field is also necessary for the drying process to be accurately modelled. The gas can be treated as a continuum and the velocity flow field can be modelled by the solution of the Navier Stokes equations. Major drawbacks with the procedure are that the Reynolds stresses cannot be obtained analytically and therefore have to be determined empirically.

The double vortex theory in cyclones is well documented. There exists a "free vortex" in the outer regions and a forced central vortex. The central vortex behaves like a solid body rotating at a constant angular velocity (ω)

$$V_\varphi = R\omega \quad 0 \le R \le R_c \qquad (6\text{-}4)$$

The free vortex gas tangential velocity can be modelled by the following equation (ter Linden , 1949)

$$V_{\varphi}(R) = V_{\varphi}^{a}\left(\frac{R_a}{R}\right)^{n} \qquad (6\text{-}5)$$

where V_{φ}^{a} is the gas tangential velocity at the wall (neglecting the boundary layer), R is the current radius at which $V_{\varphi}(R)$ is evaluated and $n < 1$ for gas cyclones. The tangential velocity at the circumference does not deviate much from the gas tangential velocity at the entrance into the cyclone (ter Linden, 1949). The presence of solids in the air streams was found to reduce the intensity of the swirl velocity (Sheppard and Lapple, 1949, Yuu et al., 1978, Smirnov et al. 1991). According to Smirnov et al. (1991) when the solid-gas flow ratio is less the 0.004 $\frac{kg\ solids}{kg\ air}$ the influence of the solids phase can be considered negligible. Such low solid loading ratios are encountered in air cleaning using cyclones.

Zhou and Soo (1990) modelled the radial distribution of the gas tangential velocity by the following equation

$$V_{\varphi}(r) = \frac{K}{r}\left[1 - \exp\left(\frac{-r^2}{R_c^2}\right)\right] \qquad (6\text{-}6)$$

where K is the maximum vorticity, R_c is the radius of the central vortex and r is current radius at which the velocity is evaluated.

The mean gas axial velocity can be modelled by the following equation (Smirnov et al., 1991)

$$V_z = \frac{Q}{\pi\left(R_a^2 - R_e^2\right)} \qquad (6\text{-}7)$$

where Q is the gas volumetric flow rate into the cyclone, R_a is the outer radius and R_e is the radius of the central vortex. Smirnov et al., (1991) assumed this radius to be conical and coincided with the radius of the vortex finder (exit tube) at the top.

Equation 6-7 does not however take into account the radial inflow of gas into the inner vortex with increase in distance along the cyclone height to the bottom exit.

The radial profile of the axial velocity was modelled (Smirnov et al., 1991) by a second order polynomial

$$V_z(R) = \begin{cases} -V_{z,p}\left[1-\left(\dfrac{R}{R_c}\right)^2\right] \; for \; 0 \le R < R_c \\ V_{z,r}\left[1-\left(\dfrac{R-R_a}{R_c-R_a}\right)^2\right] \; for \; R_c \le R < R_a \end{cases} \qquad (6\text{-}8)$$

where $R_a = R_a(z)$ and $R_c = R_c(z)$ are current radii of the apparatus and of the inner vortex respectively.

$V_{z,r}$ and $V_{z,p}$ are the current peak axial velocities in the free vortex and forced vortex as illustrated in Figure 1-8

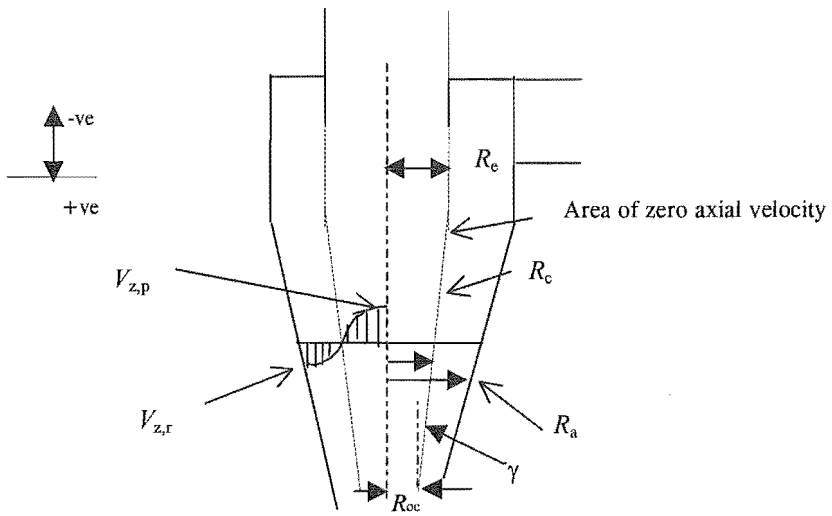

Figure 1-8 Radial variation of gas axial velocity, as assumed by Smirnov et al. 1991

A simplified model of the radial gas velocity is obtained by assuming that the radial flow is constant over the boundary between the inner vortex and the outer vortex (Smirnov et al., 1991)

$$V_r(R_c) = \frac{Q(1-\eta)\cos\gamma}{\pi(R_e - R_{oc})\sqrt{(R_c - R_{oc})^2 + H_c^2}} \qquad (6\text{-}9)$$

where $V_r(R_c)$ is gas radial velocity over boundary R_c and η is the fraction of total gas flow recirculating through the bin, H_c is the height of the cone.

The variation of the forces acting on a 300 μm and 100 μm particle down the wall of the cyclone and the Reynolds number and drag coefficient were given by Smirnov et al. (1991). Of the forces considered, the Archimedes force is the lowest and is about 0.1 per cent for the 300-μm particle compared to the aerodynamic drag force, centrifugal force and gravitational force.

Silva and Nebra (1994) modelled the particle flow in the cyclone as a continuum. An effective eddy viscosity allowed for changing mean particle concentration. The Navier-Stokes equations were written in cylindrical coordinates with the discretized equations solved by the SIMPLE algorithm (Patankar, 1980). Their numerical results when compared to experimental results demonstrated the difficulty of determining the effective eddy viscosity. Nevertheless the influence of the particle phase viscosity was clearly evident. From their results (Silva and Nebra, 1994) it appears the discrepancy between the numerical and experimental results of the tangential velocity profile increased as the radial distance was decreased. There is close agreement close to the wall. Close to the wall at a solid gas loading of as high as 0.04 $\frac{kg\ solids}{kg\ air}$ both the experimental and numerical results of Silva and Nebra (1994) suggested insignificant changes in the tangential gas velocity profile because of the presence of solids. Smirmov et al. (1991) suggested the influence of the

solids on the gas velocity profile is significant about solid gas loadings of 0.004 $\frac{kg\ solids}{kg\ air}$, one tenth of the value reported by Silva and Nebra (1994).

Cremasco et al. (1996) presented a model for the flow of air and particles in a cyclone. In their model Cremasco et al. divided the cyclone into two regions, a central region with no particles and a peripheral region where the particles are concentrated. The friction between the air and the particles on the wall was modelled by the following equation

$$\frac{1}{\sqrt{f}} = -2\log\left[0.27\frac{l}{D} + \left(\frac{6.81}{\mathrm{Re}_p}\right)^{0.9}\right] \qquad (6\text{-}10)$$

for $Re_p > 10^3$

The approach of Cremasco et al. is based on the work of Lebedev et al. (1979). Lebedev et al. (1979) assumed the particles travelled in ropes on the wall of the cyclone.

In the periphery region the air velocity was obtained by the following equations assuming steady state conditions (Cremasco, et al. 1996).

The continuity equation in the axial direction

$$\frac{d}{dz}(\varepsilon W_z) = 0 \qquad (6\text{-}11)$$

In the tangential direction

$$\frac{\partial}{\partial z}(\varepsilon W_\varphi \psi) = \frac{1}{r}\frac{\partial}{\partial r}\left(\varepsilon r \nu_{ef}\frac{\partial \psi}{\partial r}\right) - F(\psi - \psi_p) - \varepsilon f\frac{\|V\|\psi}{2D(z)} \qquad (6\text{-}12)$$

In the axial direction

$$\frac{\partial}{\partial z}(\varepsilon W_z W_z) = \frac{1}{r}\frac{\partial}{\partial r}\left(\varepsilon r \nu_{ef}\frac{\partial W_z}{\partial r}\right) + \varepsilon g - F(V_z - W_z) - \varepsilon f\frac{\|V\|W_z}{2D(z)} - \frac{1}{\rho}\frac{\partial P}{\partial z} \qquad (6\text{-}13)$$

where $\psi = rV$, f is the friction coefficient between gas and particles and ε is the porosity or voidage fraction, of the particle stream (rope) and ν_{ef} is the effective kinematic viscosity of the gas (Cremasco et al., 1996)

$$\nu_{ef} = (1-n)c^2\psi \qquad (6\text{-}14)$$

Cremasco et al. (1996) reported an excellent fit for the gas tangential velocity profile between the experimental and numerical results. The results for the axial velocity were good in the periphery region. The residence time of glass and plastic particles was modelled by adjustment of the porosity function to match the model results with the experimental results.

Experimental

Equipment and Procedure

2

2.1. Equipment ... 2.2

2.1.1. Cyclones used ... 2.2
2.1.2. Solids Conveyor Belt and Tracer Input ... 2.6
2.1.3. Air Supply ... 2.7
2.1.4. Photography and Video ... 2.8

2.2. The Moving Impactor Method ... 2.8

2.1. Equipment

2.1.1. Cyclones used

Six different conical geometrical shapes were used. The barrel of the cyclone was kept constant and had a diameter of 225 mm with a height of 230 mm. The cyclone construction was modular and therefore the conical sections could be interchanged. Letters as shown in Table 2.1 denoted the combination of each conical section with the barrel of fixed dimensions.

Table 2-1 Cyclone Dimensions

Cyclone	Cone Angle (deg) (Total included)	Cone Height (m)	Total Height (m)
A	10	0.790	1.020
B	14	0.560	0.790
C	20	0.397	0.627
D	28	0.280	0.510
E	35	0.222	0.452
F	42	0.190	0.420

The cyclones were fabricated from a mild steel sheet metal material.

A photograph showing the relative sizes of some of the conical sections used is shown in Figure 2.1. Drawings are shown in Appendix 9D.

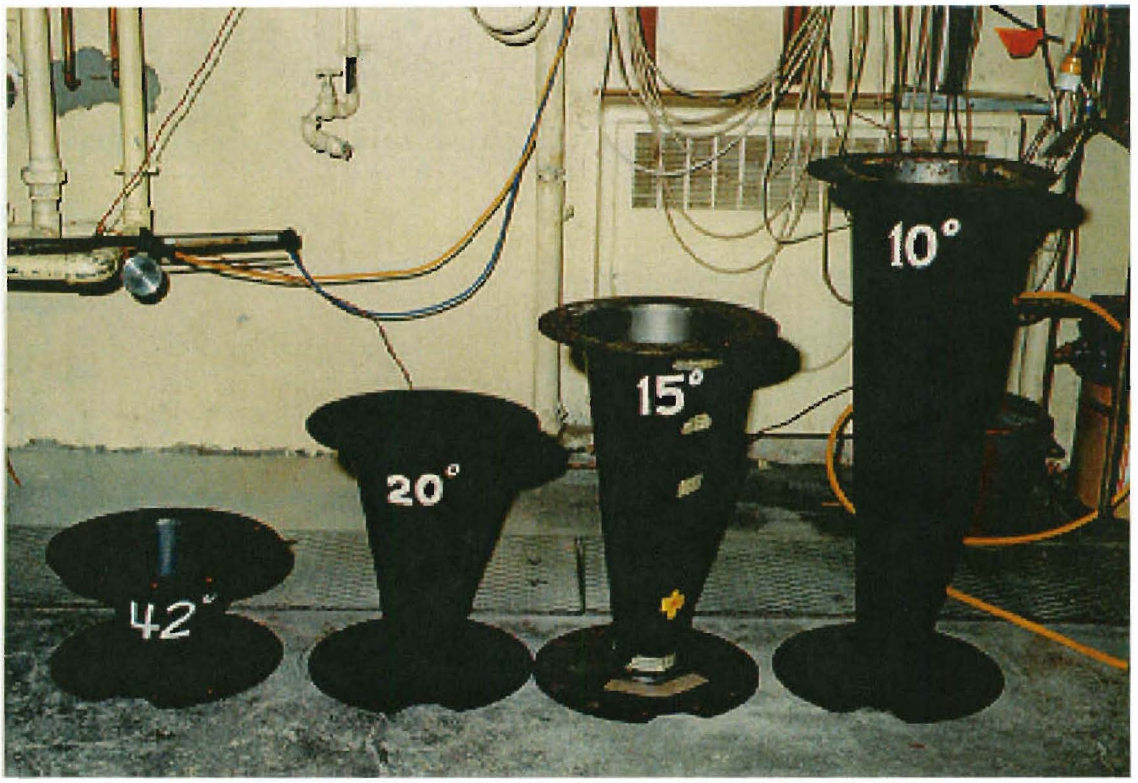

Figure 2-1 Photograph of Conical sections showing relative heights of cones

There are distortions in Figure 2-1 caused by shadows when the photographs were taken.

Figure 2.2 shows a picture of the cyclone with the 36-degree cone attached.

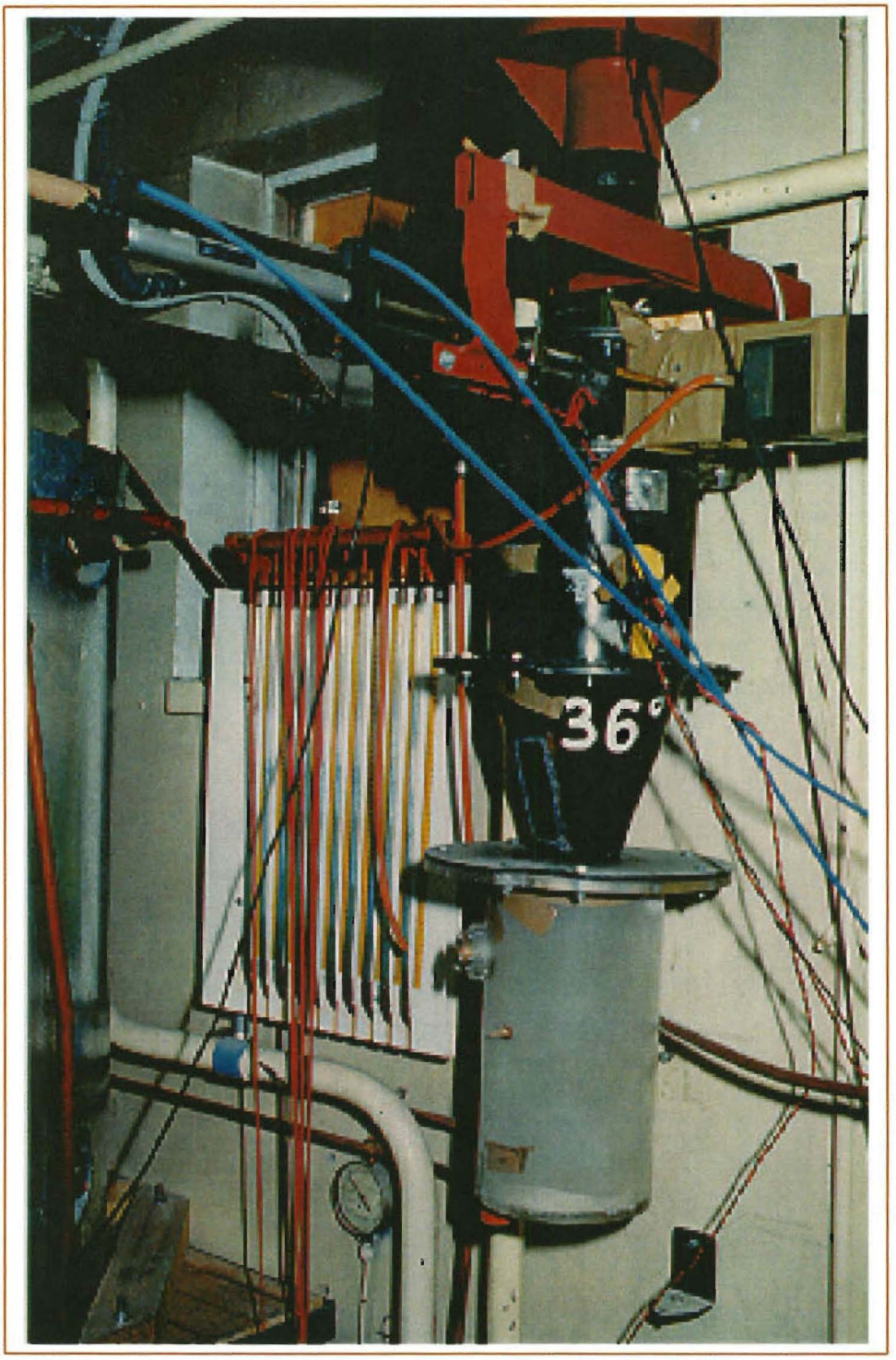

Figure 2-2 Photo of cyclone with the 36-degree conical section (cyclone E).

A schematic diagram of the cyclone is given in Figure 2-3 showing relative dimensions and impactor position.

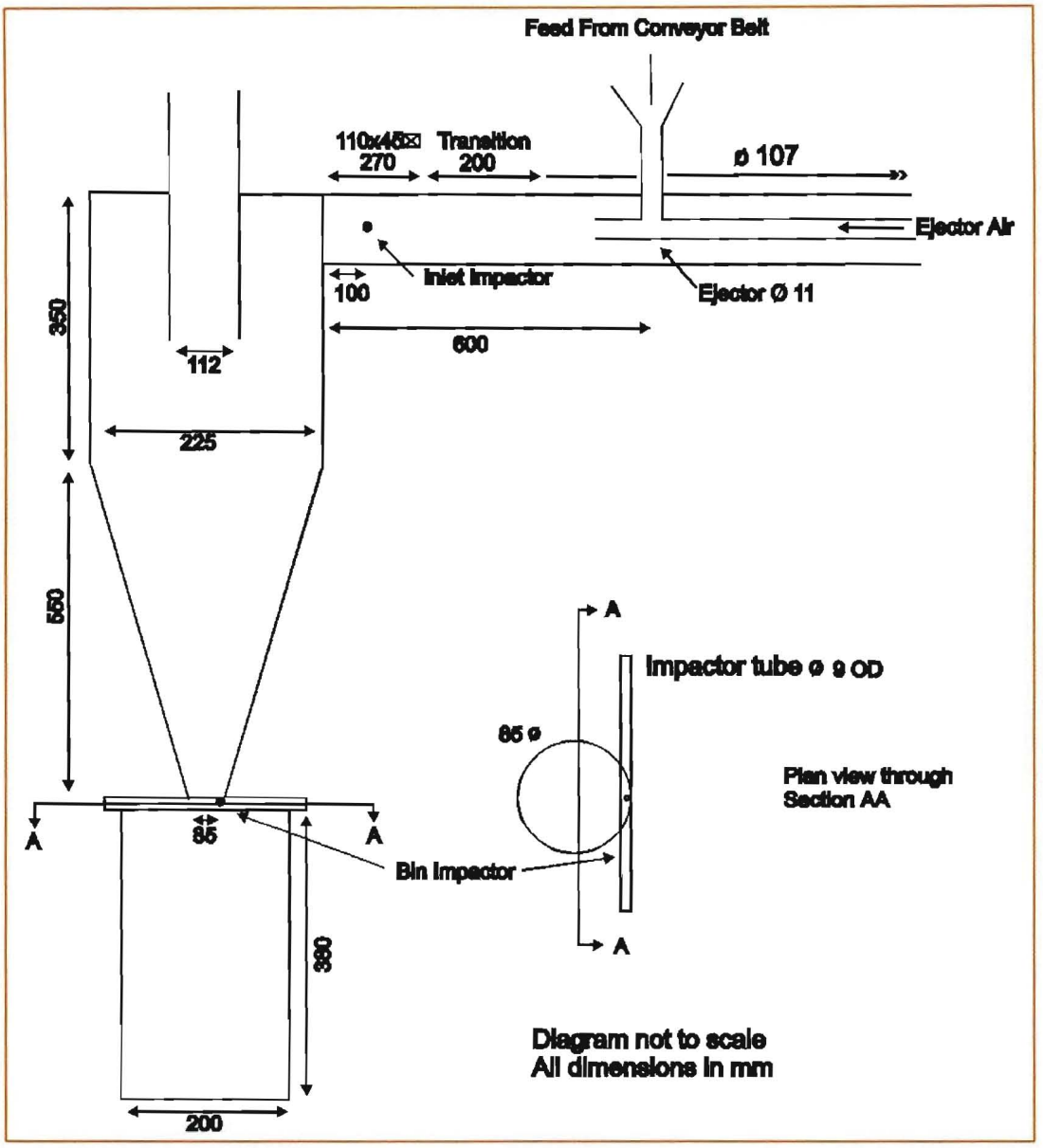

Figure 2-3 Schematic diagram of cyclone

Both conical sections and the barrel had glass openings to enable flow visualisations. In addition the top end of the barrel had glass windows along the circumference of the cyclone barrel on either side of the vortex finder with widths of about 50 mm. The particle collection hopper was made of perspex material. The base of the particle collection hopper was modified as shown in Figure 2-4 to enable photographing the particle discharge end of the cyclone. An opening, which could be plugged, was also made for easy emptying of the hopper. A 300 W projector lamp was fitted inside the cyclone, positioned at the end of the vortex finder.

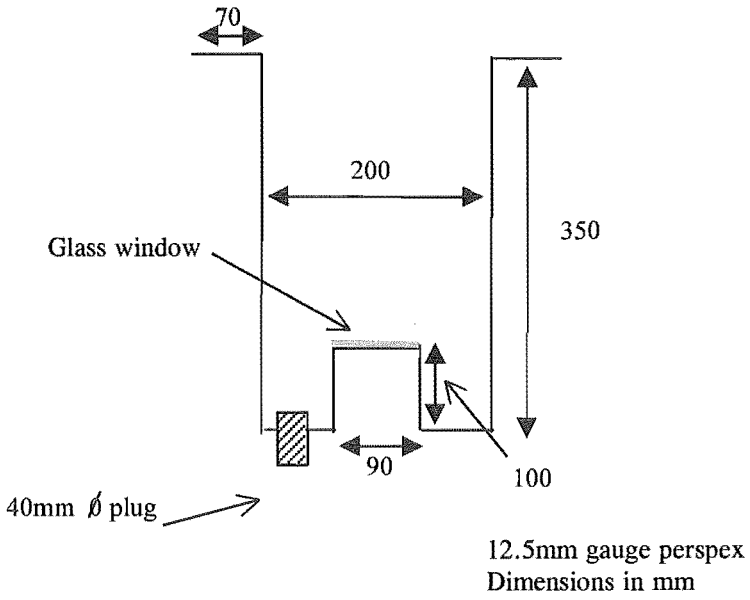

Figure 2-4 Perspex dust collection hopper

2.1.2. Solids Conveyor Belt and Tracer Input

The solids feed to the cyclone was via a 0.55 m conveyor belt. The conveyor belt was driven by a 1370 RPM, 0.18 kW electric motor through a gear with a reduction ratio of 40:1. A variable speed controller with short ramp acceleration time controlled the motor. For extended run periods with a single colour feed the conveyor belt was fed by a vibratory feeder. The solids from the conveyor belt then dropped through a funnel into an air ejector driven by compressed air at about 5 bar gauge in the centre of the main PVC air duct to the cyclone.

For the stimulus-response experiments the feed arrangement was as shown in Figure 2.5 and Figure 2.6 for the pulse and step input respectively. The black band illustrates the tracer particles and was about 25 mm long. The tracer particles were coloured by black ink and dried in an oven at a temperature of 100°C. Silica gel and sand particles were used for the feed material. The particles were sieved into close size ranges.

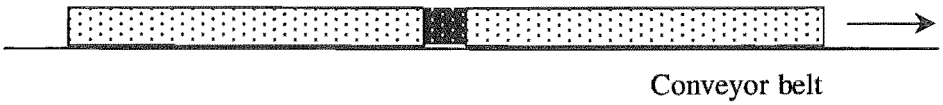

Figure 2-5 Pulse input

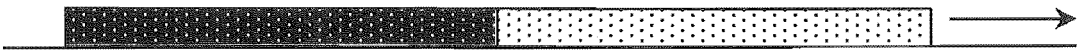

Figure 2-6 Step input

The particle piles illustrated in Figures 2-5 and 2-6 had a cross-sectional area of about 8 mm by 25 mm and a cut out piece of wood with the said dimensions was used to place the particles on the conveyor belt.

2.1.3. Air Supply

An 8 kW rotary lobe Rootes blower drove air into the cyclone via a 107 mm diameter PVC tube. The gas flow rate into the cyclone was controlled by a gate valve and measured by a Pitot tube with an MP Series 4 Neotronics Digital Micromanometer.

2.1.4. Photography and Video

For still photography 150 W halogen floodlights were used where continuous lighting was required. A Pulse Photonics Argon Jet Stabilised Spark equipped with a triple flash timer was used when flash photography was necessary.

A JC Lab HSC 250 high frame rate video camera capable of recording up to 200 frames per second with an HSR high speed recording VCR were used for analysis

of solids flow in the cyclones. The video recordings were time coded and played via a personal computer using the Optimus® image grabbing software.

2.2. *The Moving Impactor Method*

The moving impactor method as described and used by Rajendra (1995) was used in this study. An aluminium impactor of overall dimensions 155 mm x 4 mm as shown in Figure 2-7 was coated with a very thin film of grease. The thin film prevented particles from rebounding from the impactor surface. Hexane was used as the solvent for the Vaseline™ grease. The impactor had cells machined 2.5 mm in length with chamfered partitioning walls of 1mm thickness and 2 mm in height. Thus the effective impact area was divided into pockets of 2.5x4 mm, with one pocket every 2.5-mm of the length.

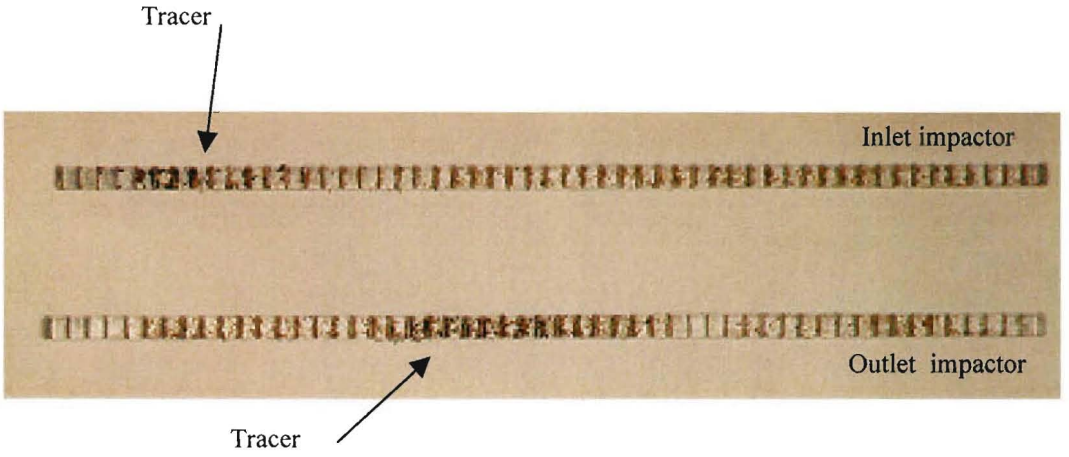

Figure 2-7 Aluminium impactors showing the cells

The impactors were mounted inside brass protective tubes with sampling nozzles onto two synchronised constant velocity hydraulically driven moving shuttles driven by hydraulic rams. One was placed at the entrance to measure the disturbance and the other positioned at the discharge end to measure the response. The velocity of the moving shuttles was controlled by needle valves on the air and oil lines. The movement of the shuttles was recorded on a chart recorder via a spring-loaded thread and pulley on a multi-turn potentiometer transducer. Under test conditions the hydraulic ram and therefore the moving impactor travelled a distance of 181

mm. The velocity of the impactor was calculated by the time taken to travel this distance (8 s).

$$V = \frac{181}{8} = 22.62\ mm s^{-1} \qquad (2\text{-}1)$$

A moving shuttle is shown in Figure 2-8.

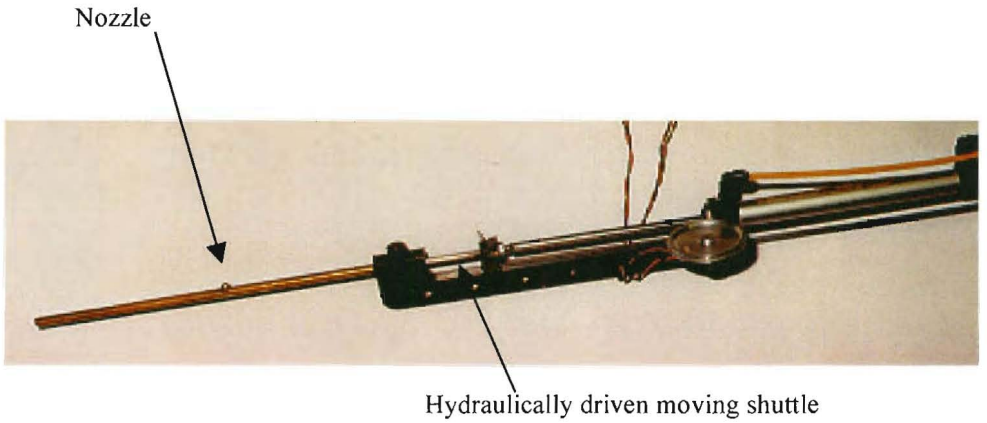

Figure 2-8 Moving shuttle

A schematic diagram of the moving shuttle with the impactor is shown in Figure 2-8. The moving shuttle has a sampling nozzle and as the moving impactor travels past this nozzle succeeding cells of moving surface are exposed to the flowing suspension flow. The air/hydraulic line and circuit diagrams are shown in Appendix 9E. Installing a pressure gauge for the airline modified this circuit used by Rajendra (1995). The pressure gauge was necessary to eliminate the pressure variations in the airline and was maintained at a pressure of 5 bar.

The particles collected in each cell were counted (both tracer and non-tracer) and the tracer expressed as a fraction of the total in each cell. The methods of data reduction are outlined in Chapter 3.

Analysis of Residence Time Measurements – Data Reduction

3

3.1. Residence Time Distributions 3.2

3.2. General Imperfect Tracer Input 3.4

3.3. Moments Analysis 3.5

3.4. Solids Axial Diffusion Model 3.7
3.4.1. Transfer Function 3.8
3.4.2. Least Squares 3.9

3.1. Residence Time Distributions

The residence time of a particle in a reactor is the amount of time the particle spends in that reactor. The trajectories of particles in a cyclone or any reactor are different because of the different particle properties or reactor geometry, which impacts on the fluid flow field. The different trajectories of particles give rise to a distribution of residence times for the particles flowing through the reactor. Danckwerts (1953) first introduced the concept of residence time distributions (RTD) to predict the non-ideal behaviour of reactors. Ideal flow in a reactor can either be plug flow or perfect mixing. In practice flow in reactors is non-ideal. In the analysis of reactors or performance prediction, in most cases it is sufficient to know only the residence time distributions (RTD) and thus the degree of mixing. For first order reactions, the mean residence time only can be used in predicting conversion of reactants to products.

Residence time distribution is commonly measured by the stimulus-response technique. In this method tracer is injected at time t= 0 in the feed stream and its response or concentration with time in the exit stream is measured. The tracer should be indistinguishable in its flow or physical properties compared to the normal flow, other than being identifiable as tracer. For particulate flow analysis a tracer particle is marked with a distinct colour or coated with a radioactive material or any other material with properties that can easily be detected. Kang et al. (1989) used KCl coated particles and used titration methods to measure tracer concentration. Radioactive tracer coating was precluded in favour of colour coating because of the inherent generation of dust in cyclones.

The most common and simplest of tracer injection techniques are pulse or step input. Any periodic function can also be used for input. In pulse input a finite amount of tracer is injected in a short time interval. Typical concentration curves are given in Figure 3.1-1. For a step input at time t = 0, the feed material is switched to the tracer feed. Typical concentration curves are also shown in Figure 3.1-1

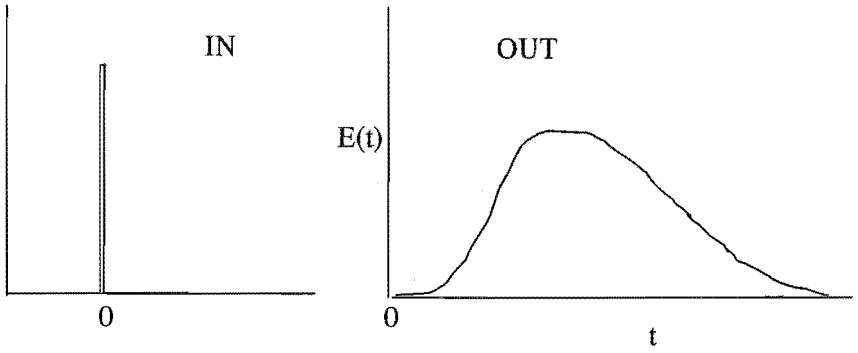

(a) Pulse input and response

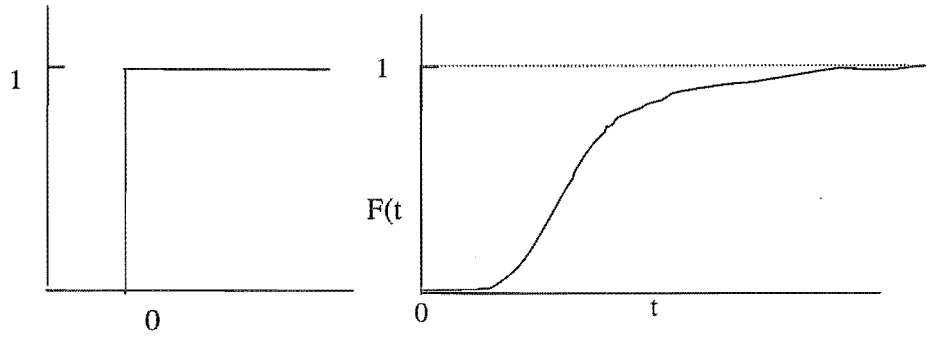

(b) Step input and response

Figure 3.1-1 Ideal pulse and step input and response curves

When the responses are normalised the response curve for the pulse input is *E(t)* - the residence time distribution function and for the step input is *F(t)*

The residence time distribution function is given by

$$E(t) = \frac{C(t)}{\int_0^\infty C(t)dt} \qquad (3.1\text{-}1)$$

where *C(t)* is concentration of the tracer particles at time t or in a cell

$$C(t) = \frac{number\ of\ tracer\ particles\ in\ cell\ i}{total\ number\ of\ partices\ in\ cell\ i} \qquad (3.1\text{-}2)$$

The total number of particles in each cell will be different. However the residence time distribution will not change when there is uniform particle concentration distributions in the particle streams

The relationship between $F(t)$ and $E(t)$ is

$$F(t) = \int_0^t E(t)dt \qquad (3.1\text{-}3)$$

and

$$\int_0^\infty E(t)dt = 1 \qquad (3.1\text{-}4)$$

In practice it is impossible to achieve perfect tracer inputs as shown in Figure 3.1-1.

3.2. *General Imperfect Tracer Input*

Aris (1959) stated that no great effort needed to be expended on devising an injection system if the concentration, as a function of time was measured at two points. The imperfect tracer pulse is a powerful technique for experimental analysis of chemical engineering flow systems (Ostergaard and Michelsen, 1969). An imperfect pulse is injected at the upstream of the first measurement point and the response is measured at the second measuring point. Ostergaard and Michelsen (1969) used the imperfect pulse technique to analyse hold-up and mixing in gas-liquid fluidised beds. The methods of data reduction from these experiments are discussed. Saruchera and Abrahamson (1997) used both the imperfect pulse and step input to analyse particle residence times in a cyclone (Appendix 9A). With the imperfect trace input, the residence time is given by the difference in means between

the two measuring points and the difference in variance is a measure of the effective diffusion coefficient. The imperfect tracer input data can be analysed by the simple method of moments or a diffusion model can be used.

3.3. Moments Analysis

The moment analysis is the simplest method of analysis of data reduction from these experiments. When tracer measurements are made at two measuring points (1 and 2) at the inlet and outlet, the first moment for the first measuring point is μ_1

$$\mu_1 = \frac{\sum_{i=1}^{N} C_{1i} t_i}{\sum_{i=1}^{N} C_{1i}} \qquad (3.3\text{-}1)$$

and the first moment for the second point μ_2 is given by

$$\mu_2 = \frac{\sum_{i=1}^{N} C_{2i} t_i}{\sum_{i=1}^{N} C_{2i}} \qquad (3.3\text{-}2)$$

The mean residence time is the difference between the first moments at the two measuring points (1 and 2)

$$\tau = \mu_2 - \mu_1 \qquad (3.3\text{-}3)$$

The second moment for the first measuring point is the variance for the distribution σ_1^2

$$\sigma_1^2 = \frac{\sum_{i=1}^{N} C_{1i} t^2}{\sum_{i=1}^{N} C_{1i}} - \mu_1^2 \qquad (3.3\text{-}4)$$

The second moment for the second measuring point σ_2^2 is

$$\sigma_2^2 = \frac{\sum_{i=1}^{N} C_{2i} t^2}{\sum_{i=1}^{N} C_{2i}} - \mu_2^2 \qquad (3.3\text{-}5)$$

The difference between the second moments for the measuring points is

$$\Delta\sigma^2 = \sigma_2^2 - \sigma_1^2 \qquad (3.3\text{-}6)$$

The particle Peclet number is a dimensionless quantity, which is the ratio of transport by convection to transport by diffusion

$$Pe_p = \frac{u_p L}{D_p} \qquad (3.3\text{-}7)$$

where L is the path length between the measuring points, u_p is mean particle velocity and D_p is the particle dispersion coefficient in the path direction.

The variance from the measured experimental curve is used to calculate the Peclet number when a diffusion model is assumed. For fairly large values of Pe and when end effects are ignored the Peclet number is given by

$$Pe = \frac{2\tau^2}{\Delta\sigma^2} \qquad (3.3\text{-}8)$$

In equation 3.3-8, the Peclet number Pe characterizes the dispersion in the stream direction of particle flow. A significant drawback of the moments method is that the variances at the two measuring points can be quite large. Tailing of data is often accompanied by a lot of uncertainty in measurements. Since the "tail" of a tracer response curve is the least precisely-recorded portion, due to the small values of c involved, the computed moments can be seriously in error (Clements, 1969). The Peclet numbers calculated by this procedure are likely to be unreliable because of the large uncertainties in the variances. In their measurement of hold-up and axial mixing, Ostergaard and Michelsen (1969) concluded that the straightforward moments method was unreliable for determination of liquid phase Peclet numbers. When the moments method was used to calculate particle Peclet numbers is a cyclone (Saruchera and Abrahamson, 1997) the Peclet numbers were found to vary

by as much as 465 per cent. To overcome the tailing problem a modified moments method was proposed (Ostergaard and Michelsen, 1969 and Anderssen and White, 1971). The modified moments method gives a lesser emphasis to the tail of the signal by a weighting factor s

$$w_k(t) = t^k \cdot e^{-st} \tag{3.3-9}$$

where k = 0, 1 and 2 for the zeroth moment, first moment and second moment respectively.

3.4. *Solids Axial Diffusion Model*

The hydrodynamic diffusion model, based on Fickian molecular diffusion is the most widely used general model for non-ideal flow in many industrial flow systems. The simplest case is the one-dimensional model, which has been found useful even in many cases where the flow is not strictly one-dimensional (Clements, 1969). However, where warranted, consideration has been given to the three-dimensional diffusion model. Ostergaard and Michelsen (1969) used the axially dispersed plug flow model for flow analysis in gas-liquid fluidized beds. Maybe because the hydrodynamic diffusion model was based on the molecular scale Fickian diffusion, most of the original work was based on gas-liquid or liquid-liquid or gas systems (Birschoff and Levenspiel, (1962), Parimi, and Harris, (1975), Keey and Pham, (1977), Kehinde et al. (1983)). There was reluctance or maybe scepticism towards application of this hydrodynamic dispersion model beyond these traditionally established systems to gas-solid suspensions. Yang and Kojima (1995) investigated the lateral mixing of coarse particles in fluidized beds. From their results they concluded that the one-dimensional dispersion model could represent the lateral flow and mixing of particles in these systems. The axially dispersed plug flow model was found to be valid for representation of flow of particles through a cyclone (Saruchera and Abrahamson, 1997). Werther and Hirschberg, 1997, reported that the axial dispersion model was a simple way to represent the measured profiles of solids residence time distributions (RTD) in circulating fluidized beds (CFB).

The plug flow model with axial dispersion can be represented by the following one dimensional partial differential equation of conservation of mass species as a function of concentration c

$$\tau\frac{\partial c}{\partial t}+\frac{\partial c}{\partial x}-\frac{1}{Pe}\frac{\partial^2 c}{\partial x^2}=0 \qquad (3.4\text{-}1)$$

with boundary conditions

$c = c(t)$ at $x = 0$, $t \geq 0$ and $c = 0$, $0 < x < \infty$ at $t = 0$

where τ is the mean residence time, Pe is the particle Peclet number, c is the concentration of tracer particles. The Peclet number is a measure of the dispersion in the direction of flow. A constant velocity across the section of flow, and with advance along the path, is assumed.

3.4.1. Transfer Function

This method based on the Laplace transform of the concentration was proposed by Ostergaard and Michelsen (1969). In general any linear system can be represented by a transfer function. In the stimuli-response technique the relationship between the input and the response functions in the Laplace transform domain is the transfer function.

$$C_2(s) = F(s)C_1(s) \qquad (3.4\text{-}2)$$

where $C_1(s)$ and $C_2(s)$ are the tracer particle concentrations for the input and response in the Laplace transform domain respectively. $F(s)$ is the system transfer function.

The system transfer function is therefore by definition a linear operator, which transforms the input function to yield a response function. When the tracer particle concentration for the input and output are known at discrete time intervals, the system transfer function is

$$F(s) = \frac{\left[\sum_{i=1}^{N} c_{2i} e^{-st_i} \Delta t\right] / \left[\sum_{i=1}^{N} c_{2i} \Delta t\right]}{\left[\sum_{i=1}^{N} c_{1i} e^{-st_i}\right] / \left[\sum_{i=1}^{N} c_{1i} \Delta t\right]} \qquad (3.4\text{-}3)$$

When the Laplace transform of Equation 3.4-1 with the appropriate boundary conditions is taken the transfer functions is given by

$$F(s) = \exp\left\{\frac{Pe}{2}\left(1 - \left(1 + \frac{4s\tau}{Pe}\right)^{1/2}\right)\right\} \qquad (3.4\text{-}4)$$

Equation 3.4-4 can be algebraically manipulated to yield the equation of the form

$$\left(\ln\frac{1}{F(s)}\right)^{-1} = \tau s\left[\ln\left(\frac{1}{F(s)}\right)\right]^{-2} - \frac{1}{Pe} \qquad (3.4\text{-}5)$$

Equation 3.4-5 is the general equation of a straight line with gradient m and intercept c

$$y = mx + c \qquad (3.4\text{-}6)$$

The validity of the one-dimensional axially dispersed plug flow model is checked by plotting the left-hand side of Equation 3.4-5, $\ln\left(\frac{1}{F(s)}\right)^{-1}$ against $s\left(\ln\left(\frac{1}{F(s)}\right)\right)^{-1}$. If the graph is linear, the model is a valid representation of the flow and the mean residence time τ is the slope and the intercept is $-\frac{1}{Pe}$.

3.4.2. Least Squares

The least squares method is one of the most common data smoothing techniques. Associated with any physical measurements are random errors, which are generally regarded as unwanted noise. The basis of this method is fitting a function to a set of measured data points, for example fitting a function *f(x)* to data points y_i for conditions of x_i

$$f(x) = a_2x^2 + a_1x + a_0 \tag{3.4-7}$$

The constants a_i's are selected so that the sum of squares of residuals is a minimum. The sum of squares of residuals or deviations is a form of global error.

The residuals is given by

$$Error = \frac{\sum_{i=1}^{N}[f(x)_i - y_i]^2}{N-n} \tag{3.4-8}$$

where $f(x)_i$ is obtained by substitution of the independent variable (time) for each point and y_i is the experimental measured quantity, n is the number of parameters a_i in Equation 3.4-7

The *convolution* theorem of the Laplace transform is a theorem of significant practical importance. In its general form the *convolution* theorem can be expressed by the following equation

$$L^{-1}\{f(s)g(s)\} = \int_0^t F(u)G(t-u)du \tag{3.4-9}$$

where L^{-1} is the inverse Laplace transform and $f(s)$ and $g(s)$ have inverses $F(t)$ and $G(t)$ and u is time.

Equation 3.4-4 can be expressed into the following form

$$C_2(s) = C_1(s)\exp\left[a\left(1-(1+bs)^{1/2}\right)\right] \tag{3.4-10}$$

where $a = \frac{Pe}{2}$ and $b = \frac{4\tau}{Pe}$

If Equation 3.4-10 is inverted by the means of the *convolution* theorem of the Laplace transform (Appendix 9H), the output tracer concentration in the time domain $C_2(t)$ is given by

$$C_2(t) = \int_0^t C_1(u)\frac{1}{2\sqrt{\pi}}\sqrt{\frac{Pe\tau}{(t-u)^3}}\exp\frac{\left(Pe(\tau-t+u)^2\right)}{4(t-u)\tau}du \tag{3.4-11}$$

When the tracer particle concentration distribution for the input and response are known then parameters *Pe* and τ can be estimated by the least squares method using the Solver tool in Excel.

Measurement Uncertainties and Analysis

4

4.1. Error Types 4.2

4.2. Mean 4.2

4.3. Standard Deviation 4.3

4.4. Standard Deviation of the Mean 4.3

4.5. Error Propagation 4.3

4.1. Error Types

Every measured quantity has some uncertainties or errors associated with it. Error is the difference between the measurement and the *true value* (Dieck, 1995). Quite often the *true value* of the measured quantity is not known. Nevertheless the uncertainties in the measured quantity should be quantified systematically for a proper understanding and interpretation of the results.

Errors fall into two main categories, random or precision errors and systematic or bias errors. Each of these errors at every stage affects the final result. Random errors are usually not correlated and are for example due to some imprecision in estimating a fraction of a division in a scale. These errors can either be positive or negative with equal probability. Systematic errors arise from causes, which act consistently for the duration of the experiment thereby giving a bias in the results. Systematic errors can either be positive or negative for a given set of experimental conditions. As a general rule if an error source causes scatter in the test result, it is a precision (or random) error. All other error sources are bias (or systematic) errors (Dieck, 1995). Analysis of errors can be either deterministic or based on statistical means. The deterministic approach is not robust but simpler and quite often focuses on the worst scenario case.

4.2. Mean

The mean of sample of n data measurements X_i is defined by

$$\overline{X} = \frac{\sum_{i=1}^{n} X_i}{n} \qquad (4.2\text{-}1)$$

4.3. Standard Deviation

For a sample of n data points the standard deviation is characterized by the following equation

$$S_X = \sqrt{\frac{\sum_{i=1}^{N}\left(X_i - \overline{X}\right)^2}{n-1}} \qquad (4.3\text{-}1)$$

where X_i is the ith value in the sample, $\overline{X}$ is the mean and *(n-1)* is the degrees of freedom

When the degrees of freedom are > 30, the multiplier is usually taken as u, the Normal distribution variate, ie. uS_x. When the degrees of freedom are less than 30 a multiplier is used on the standard deviation for the confidence intervals, the multiplier is the Student's t statistic, eg. tSx

4.4. Standard Deviation of the Mean

The Central Limit Theorem can be used to characterise the scatter in the calculated average

$$S_{\bar{X}} = \frac{S_X}{\sqrt{N}} \qquad (4.4\text{-}1)$$

where N is number of X_i , and the distribution of $\bar{X}$ tends to Normal as N increases, whatever the distribution of X.

4.5. Error Propagation

Error propagation is the combined effect of the individual error contributions in the final calculated result. In other words the errors in the final result are inherited

from the individual error sources. One of the methods of error propagation is Taylor's series approximation.

If a function y is defined by

$$y = f(x_1, x_2) \qquad (4.5\text{-}1)$$

It is assumed that the error sources in x_1 and x_2 are independent.

The Taylor series approximation normally used for systematic error is

$$\Delta y = \left(\frac{\partial f}{\partial x_1}\right)\Delta x_1 + \left(\frac{\partial f}{\partial x_2}\right)\Delta x_2 \qquad (4.5\text{-}2)$$

where

Δy = is the error in y which can be either systematic or random

Δx_1 = is the error in the measured quantity x_1 (systematic or random)

Δx_2 = is the error in the measured quantity y_1 (systematic or random)

$\frac{\partial f}{\partial x_i}$ = is the influence coefficient which expresses the influence of a change in x_1

on the y at the defined interval, or the *sensitivity* of y at x_i

The following approximation is normally used for random error

$$\Delta y^2 = \left(\frac{\partial f}{\partial x_1}\right)\Delta x_1^2 + \left(\frac{\partial f}{\partial x_2}\right)\Delta x_2^2 + ... \qquad (4.5\text{-}3)$$

where $\Delta X_1 = tS_{X_1}$ etc

Results

5

5.1. Observations 5.2

5.2. Particle Characteristics 5.2

5.3 Particle Velocity into Cyclone 5.6

5.4. Gas Inlet Velocity 5.6

5.5. Solids Hold Up 5.7

5.6. Collection Efficiency 5.10

5.7. Gas Residence Time 5.11

5.8. Particle Distributions and Flow Model 5.11

5.9. Particle Residence Times 5.20

5.10. Peclet Numbers 5.33

5.11. Effect of Surface Roughness on Particle Peclet number 5.35

5.12. Observations and Presence of Roping 5.36

5.13. Particle Bouncing Phenomena 5.39

5.1. Observations

Two rectangular slots measuring about 80 mm by 100 mm were cut from the front and back of the rectangular entrance duct and replaced by glass. These windows enabled flow visualisation and measurement of particle velocity in the entrance duct. For observation of flow inside the cyclone the top of the cylindrical section also had two glass windows on opposite sides of the vortex finder. In addition glass windows measuring about 50 mm by 100 mm were also cut in the conical and cylindrical sections of the cyclone. A physically small 300W projector bulb (diameter $\approx$ 15 mm) was also positioned at the end of the vortex finder to illuminate the inside of the cyclone. The positioning was chosen in such a manner as to minimise flow disturbance. The glass windows were also fitted flush with the wall to have minimal effect on the flow field. A stroboscope was used to observe the particles through the entrance tube window. The particles were observed to enter the cyclone in a dispersed state from the ejector with no settling at the bottom of the pipe. In industrial practice however, particle velocities are usually lower and settling at the bottom of the pipe usually occurs. The velocity of the particles was made deliberately high to minimise mixing upstream of the first measurement point in the stimulus-response experiments.

A video camera connected to a TV monitor was also used for observation and recording of the particle flow field inside the cyclone through the glass windows. Still photography was also used to capture some images of particle flow. Less than 1 per cent of the total solids into the cyclone was converted to fines through attrition and subsequently lost with the gas through the vortex finder.

5.2. Particle Characteristics

The particles used in this investigation were silica gel and sand particles. The density of the silica gel was 1200 kgm^{-3} while that for the sand used was 2600 kgm^{-3}.

The existence of a wide particle size range increases the complexity of the system and makes it difficult to observe trends in measured quantities, as each particle size will act as a different phase. To mitigate this constraint, the material in the case of silica gel was crushed and sieved into narrow particle size ranges. The sand used was crushed quartz and it was also sieved into different size ranges. Seven different size ranges were used and these are tabulated in Table 5.2-1.

Table 5.2-1 Material size ranges used in investigation

Size Range(μm)	Silica Gel	Sand
150-210	✔	✔
210-295	✔	✔
212-425	✔	✘
250-500	✔	✔
295-500	✔	✔
500-700	✔	✘
700-850	✔	✘

Residence time measurements with glass ballotini were also performed at SPS.

Silica gel and sand represent an array of different properties. By observation silica gel particles were more angular in shape compared to the sand particles which were more rounded. The circularity was used to characterise the shape factor of these particles. The circularity (for a sphere) of a particle is defined as the ratio of square of perimeter to projected area

$$Circularity = \frac{(\pi D)^2}{\left(\frac{\pi D^2}{4}\right)} \qquad (5.2\text{-}1)$$

The circularity has a value of 4π (ie. 12.6) for a circle. The circularity of the particles used was determined using the image analysis package Optimas® version 5. The average circularity for a sample of sand particles was about 19.4 while that for silica gel was 26.2. Figure 5.2-1 shows a photograph of sand particles.

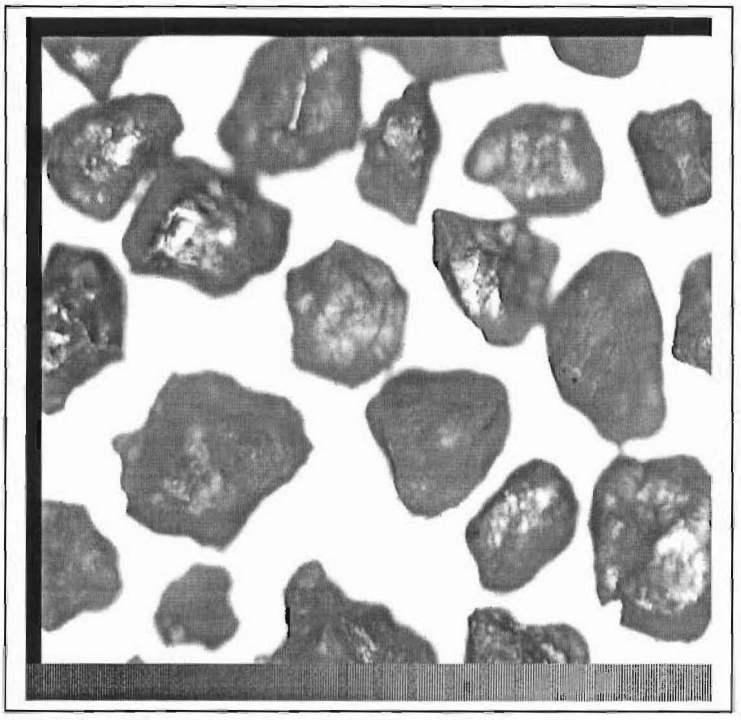

Figure 5.2-1 Sand particles [scale x10]

A photograph of silica gel particles is shown in Figure 5.2-2 and glass particles are shown in Figure 4.2-3.

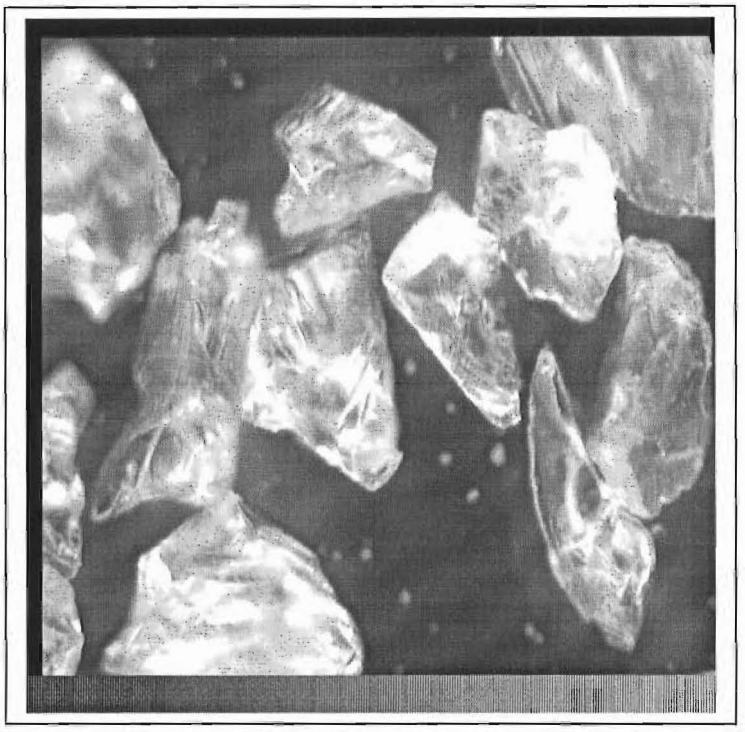

Figure 5.2-2 Silica gel particles [scale x10]

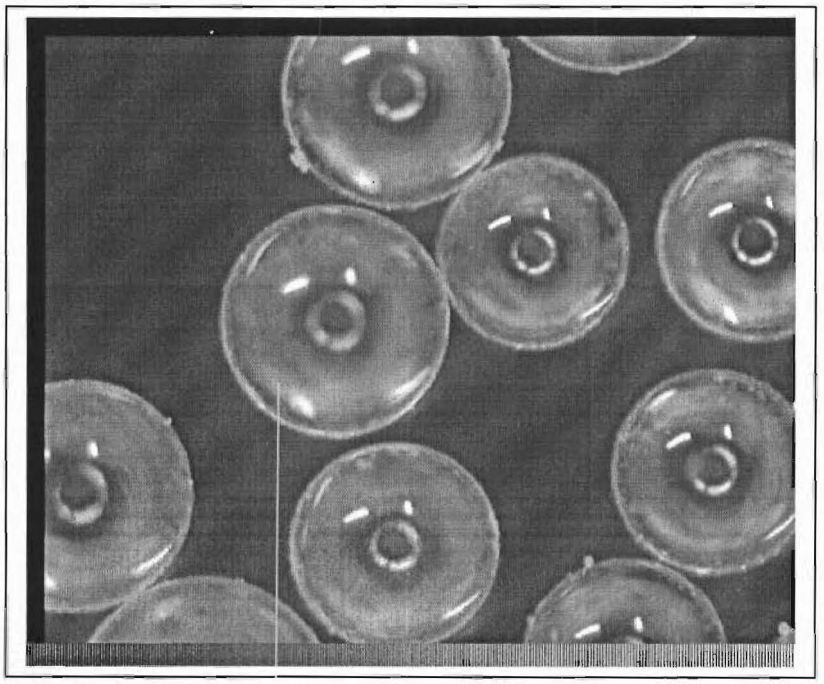

Figure 5.2-3 Glass particles [scale x10]

5.3. Particle Velocity into Cyclone

Particle entrance velocity into the cyclone was measured through a glass window 350 mm upstream from the cyclone entrance by photography. The particles were ejected from an 11 mm-diameter ejector tube 270 mm upstream from the particle velocity measurement point. All particle velocity measurements were at a gas velocity of 20 ms^{-1} in the rectangular entrance section. The velocity of gas in the ejector tube was about 25 ms^{-1}. Under these conditions the velocity of both sand and silica gel particles was found to be about 15 ms^{-1}. When the ejector gas velocity was increased to about 75 ms^{-1} the velocity of silica gel particles of size range 700-850 μm was found to be about 49 ms^{-1}. Thus when the gas velocity was increased three fold the particle velocity also increased by the same factor.

5.4. Gas Inlet Velocity

An 8kW rotary lobe Rootes blower with a maximum throughput of 0.315 m^3s^{-1} drove air through the cyclone via a 107 mm diameter PVC pipe. A gate valve controlled the flow of the gas into the cyclone. A Pitot tube with a digital micromanometer as detailed before measured the gas flow into the cyclone. The gas velocity profile in the round entrance tube to the cyclone as a function of the radial pipe distance is shown in Figure 5.4-1.

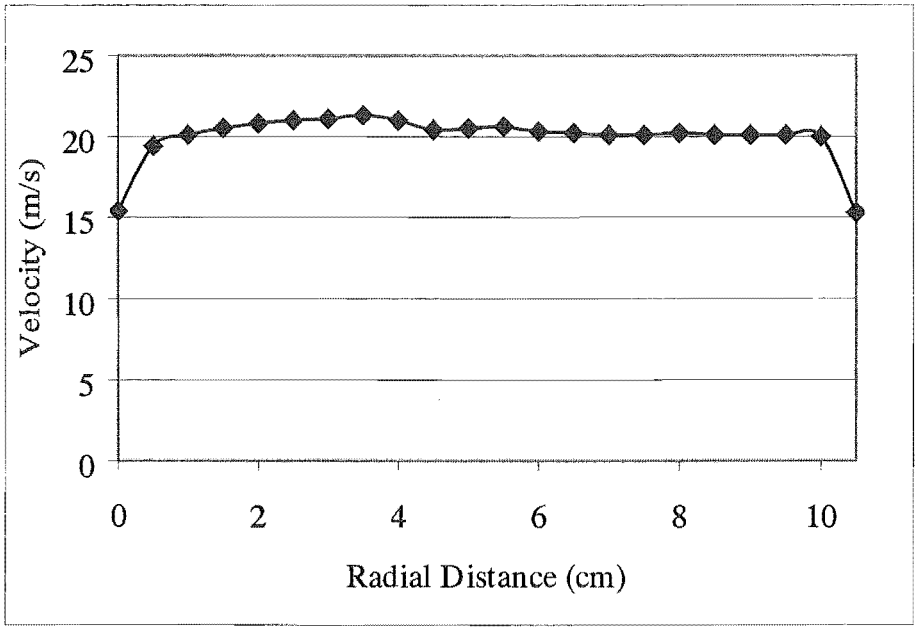

Figure 5.4-1 Air velocity profile in round entrance tube

As the gas velocity profile (Figure 5.4-1) was fairly flat, the gas velocity was measured at a point in the centre of the round entrance tube and the gas flow rate was calculated from this average velocity value. To cross check these measurements gas velocity was also measured in the rectangular entrance section and the calculated gas flow rate was in agreement with the measurement in the round entrance tube. Making independent measurements with an inclined liquid manometer checked the reliability of the digital instrument. The two independent pressure or velocity measurements agreed to within 4%.

5.5. Solids Hold Up

The total mass of solids or material held up in the reactor under steady feed conditions can be obtained by simultaneously cutting off the feed and outlet streams and measuring the mass of material trapped. The present set up of the equipment did not permit this procedure. Instead, solids hold up in the present sense refers to the amount of solids circulating in the cyclone after feed is stopped but airflow

maintained. In general this hold up is a transient quantity as losses are expected gradually due to abrasion and leakage into the dust collection hopper.

In general the amount of hold up was found to increase with an increase in the particle size fractions. For instance the hold up for silica gel particles of size range +850 μm in cyclone B (14° cone angle) was found to be about 2.0 g while that for particles of size range 295-500 μm was 1.5 g. The particles were observed to be largely circulating in the cylindrical barrel of the cyclone. These amounts are insignificant compared to solids feed rate of about 13 g s^{-1} prior to cutting off the feed. The hold up was also observed to increase with increase in the cone angle of the cyclone. When the feed of sand particles was stopped but air flow maintained, large amounts of solids in ropes were observed circulating in the conical section of cyclones with cone angles larger than 28°. However for cyclones tested with cone angles of 20° and below no solids were observed circulating in the conical section. With silica gel particles no solids were observed circulating in the conical section with cyclones with cone angles of 28° and larger after solids feed had been stopped.

According to Trefz and Muschelknautz (1993) "when the carrying capacity of the gas is exceeded" solids settle out to form ropes. This concept appears to originate from air conveying experience. Silica gel has a lower density than that of sand so the carrying capacity of air for silica gel, according to the theory of Trefz and Muschelknaut is much higher compared to that for sand. The fact that no ropes were observed where ropes formed with sand for similar conditions seems to support this theory of Trefz and Muschelknautz. However, density alone will be a part explanation as sand and silica gel have different frictional and coefficient of restitution properties.

The wide-angle conical sections have higher gas tangential velocity components because of the decreased radius with axial height. From pneumatic conveying experience this therefore should result in an increase in the carrying capacity of the gas for given solids feed rate as the radius considered on the cone is decreased. It

therefore appears the formation of ropes cannot be explained simply by the gas carrying capacity theory of Trefz and Muschelknautz. The phenomenon of roping is discussed in more detail (§ 6.1).

The amount of hold up for silica gel particles of size range 700-850 μm was measured by doing a series of runs whereby the mass fed over 2 minutes was gradually increased while maintaining the air flow at 0.099 $m^3 s^{-1}$. For each run when the solids had all been fed into the cyclone the bin was drained while keeping the airflow going. After that the airflow was stopped and the solids circulating were collected. The mass of material initially collected in the dust collection hopper and also that circulating in the cyclone was measured. The results are shown in Table 5.5-1. The hold up in Table 5.5-1 is the hold up after stopping solids flow.

Table 5.5-1 Hold up in Cyclone B(14° cone angle) for run time of 2 minutes

Mass fed in (g)	Mass collected in hopper (g)	Hold up in cyclone
3	0.9	1.1
10	7	2
20	17.2	1.9
40	37.3	1.9

There is a finite amount of solids of about 2g held up in a cyclone as shown in Table 5.5-1 above. Any solids in excess of this amount are drained into the dust collection hopper. The amount of solids could be said to be the carrying capacity of the gas for these silica gel particles. The total "hold up" during particle feed will be the 2g in addition to the particles flowing through. For the highest mass of solids feed in (40 g in Table 5.5-1) the hold up was only about 5 per cent of the total feed.

A band of white particles was fed into the cyclone followed by a step change from white to black particles as shown in Figure 5.5-1.

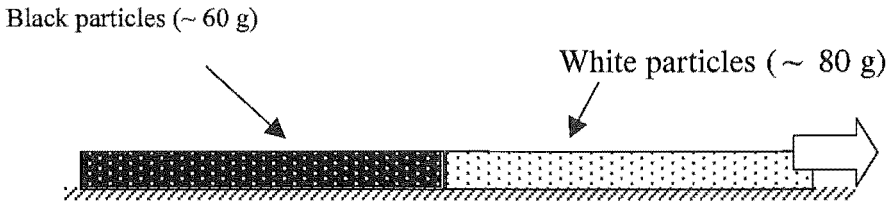

Figure 5.5-1 White and black particles on conveyor belt

The percentage of black particles in the hold-up was 70 percent while the balance of 30 percent were white particles. This suggests a significant amount of mixing and recirculation in the cyclone.

5.6. Collection Efficiency

The collection efficiency is defined as the amount of solids recovered in the underflow expressed as a percentage of the total feed into the cyclone. Studies on collection efficiency were mainly confined to the fine particle size ranges (Beeckmans and Kim, 1977, Dietz, 1981). The collection efficiency of coarse particles was studied by Mori et al. (1968). The fine particles used by Mori et al. (1968) were in the interval 150-200 on the Tyler mesh screen size, which means the largest particle in micrometers, were less than 75 μm. The smallest particles used in this study were in the size interval of 150-210 μm. Mori et al. (1968) found the collection efficiency of sand particles in the size interval 20-40 mesh in a 0.24m diameter cyclone to be about 99%. The collection efficiency of particles used in this study was found to be about 99%. Losses were incurred mainly through attrition especially in the case of silica gel particles. When particles stayed long in the cyclone they became rounder and smaller. For practical purposes the losses are negligible and collection efficiency will not be dealt with in this study.

5.7. Gas Residence Time

The residence time of gas in the different cyclone geometries was calculated by the following equation

$$t_g = \frac{V}{Q} \qquad (5.7\text{-}1)$$

where V is the total volume of the cyclone between the ceiling and the cone discharge, including the vortex finder and Q is the volumetric flow rate of gas into the cyclone. The calculated gas residence times in the different cyclone geometries for a gas volumetric flow rate of 0.099 m^3s^{-1} are tabulated in Table 5.7-1

Table 5.7-1 Gas residence times in different cyclones for Q = 0.099 m^3 s^{-1}

Cone angle (degrees)	Cyclone	Gas residence time (s) t_g
10	A	0.30
14	B	0.26
20	C	0.22
28	D	0.20
26	E	0.18
42	F	0.17

As the volumetric capacity of the cyclone is decreased there is a corresponding decrease in the gas residence time.

5.8. Particle Distributions and Flow Model

The stimulus-response technique is a powerful experimental technique used to analyse non-ideal flow behaviour in reactors. The stimulus could be a pulse, step or any other periodic input into the system and the response is measured at the outlet. In practice it is difficult to achieve a perfect of pulse or step input. Recognising the difficulty of achieving perfect pulse or step input, Aris (1959) proposed the

imperfect pulse method that was later used by Ostergaard & Michelsen (1969). Ostergaard & Michelsen (1969) analysed the mixing in gas-liquid fluidised beds. Rajendra & Abrahamson (1994) used the same experimental technique as used in this PhD to measure residence time of granular material in a cyclone. Saruchera & Abrahamson (1997) analysed the experimental data on flow of these materials by the method of Ostergaard & Michelsen. A detailed background of the stimulus-response technique is provided by Levenspiel (1972) and also by Fogler (1992). A review of the technique and data analysis from these experiments is given in this work in Chapter 3.

Tracer particles were coated by black ink and dried in an oven at 100 °C. Sample particles (both tracer and non-tracer) were collected in cells on impactors placed at the inlet and outlet of the cyclone. The number of tracer and non-tracer particles in each cell for the inlet and outlet impactors were counted using a travelling microscope with a camera mounted on it and connected to a video monitor.

Representative number distributions of white and black (tracer) particles on the inlet impactor as a function of distance along the impactor is shown in Figure 5.8-1 for a pulse input. Each point on the graph represents the numbers counted on the impactor in each cell. The particles were sand particles of size range 250-500 μm.

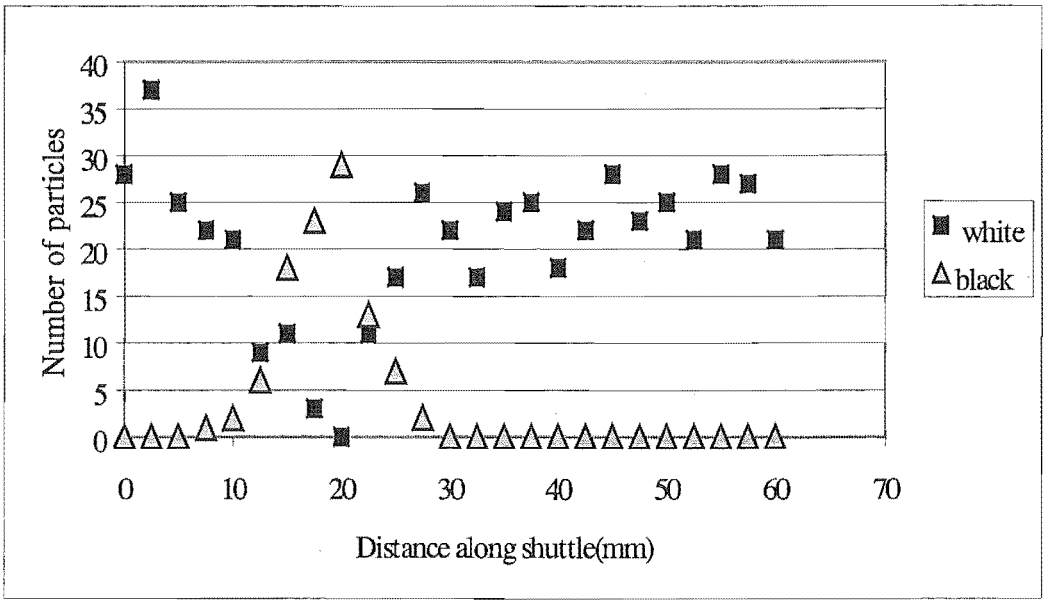

Figure 5.8-1 Number distribution for sand particles on the inlet impactor [run 96]

Gas inlet velocity: 20 ms^{-1}; cyclone B; particle size range; 250-500 μm

The number distribution of particles on the (outlet) bin impactor is shown in Figure 5.8-2.

The number distributions of particles for the inlet shuttle do not fluctuate appreciably compared to those on the bin impactor. The total number of particles fluctuates up to about 40 percent for the inlet impactor and up to over 100 for the bin impactor. The particles are uniformly distributed over the entrance section. Therefore any random fluctuation in the particles collected is mostly due to the probability of a particle going through the sampling nozzle. The probability of a particle rebounding after impactor is almost zero. This latter conclusion was arrived at after examination under the microscope of the thin layer of grease in each the cells which showed absence of any marks which would have been left by a rebounding particle. The high local concentrations of particles, which appear as peaks in Figure 5.8-2 as will be shown later, are caused by the phenomenon of roping. Roping is the collection of particles flowing down on the wall of the cyclone, and more or less particles are sampled as the rope moves over and away from the sampling position. The rope(s) itself is/are also transitory.

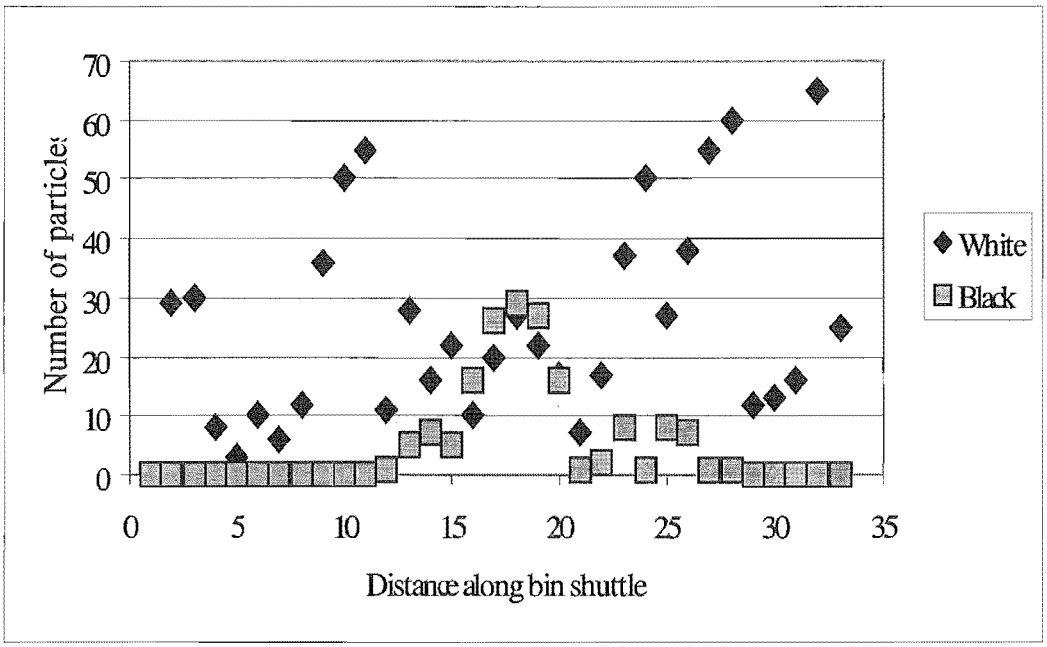

Figure 5.8-2 Number distribution of sand particles in the bin impactor [run96]

It can be assumed that the fraction of tracer particles in each cell can be used to represent the fraction over the whole stream, i.e., uniform distribution. The concentration of tracer particles in each cell is given by the following expression

$$c_i = \frac{number\ of\ tracer\ particles}{total\ number\ of\ particles} \qquad (5.8\text{-}1)$$

The concentration of tracer as a function of time is plotted in Figure 5.8-3. This concentration is a number concentration, within the solid phase. Most runs were done with particles of similar size, so the concentration is also approximately a volume concentration within the solid phase. Although the number distribution of particles (Figure 5.8-2) is erratic, when expressed as a concentration (Figure 5.8-3) instead of number of particles the curves are fairly smooth. This is evidence of good mixing across the stream in the cyclone, as although the numbers of particles fluctuate, the fraction or distribution of tracer particles is uniform in the various streams. The bimodal nature of the outlet concentration curve towards the tail end is

probably due to the erratic nature of the flow resulting in only a few particles being collected.

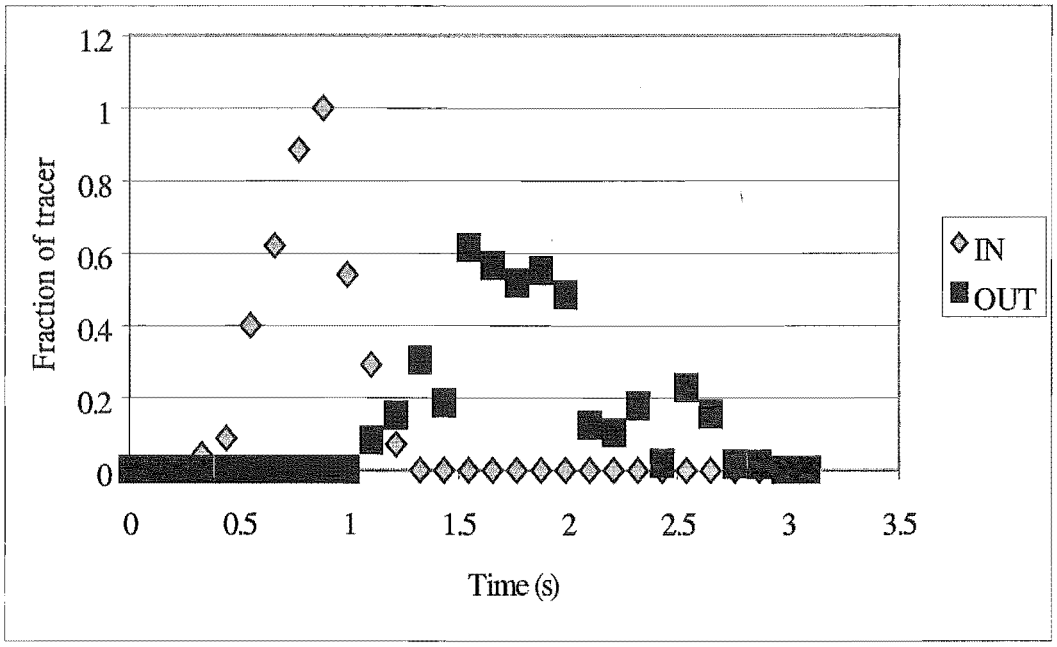

Figure 5.8-3 Fraction of sand tracer on inlet and bin impactors [run 96]

One measurement of particle residence time is given by the time difference between the inlet and outlet concentration peaks.

Similar number distributions can also be obtained for the step-input experiment. In this case the feed is instantaneously switched from the regular to the coloured tracer particles. The numbers of tracer and non-tracer particles in each cell are also counted. A representative numbers distribution of particles for a step input experiment for the inlet is shown in Figure 5.8-4 and for the outlet in Figure 5.8-5.

The fraction of tracer for the inlet and outlet impactors for step input is shown in Figure 5.8-6. A mean residence time can also be evaluated using the time difference for a 50 percent change in tracer concentration for the inlet and outlet impactors.

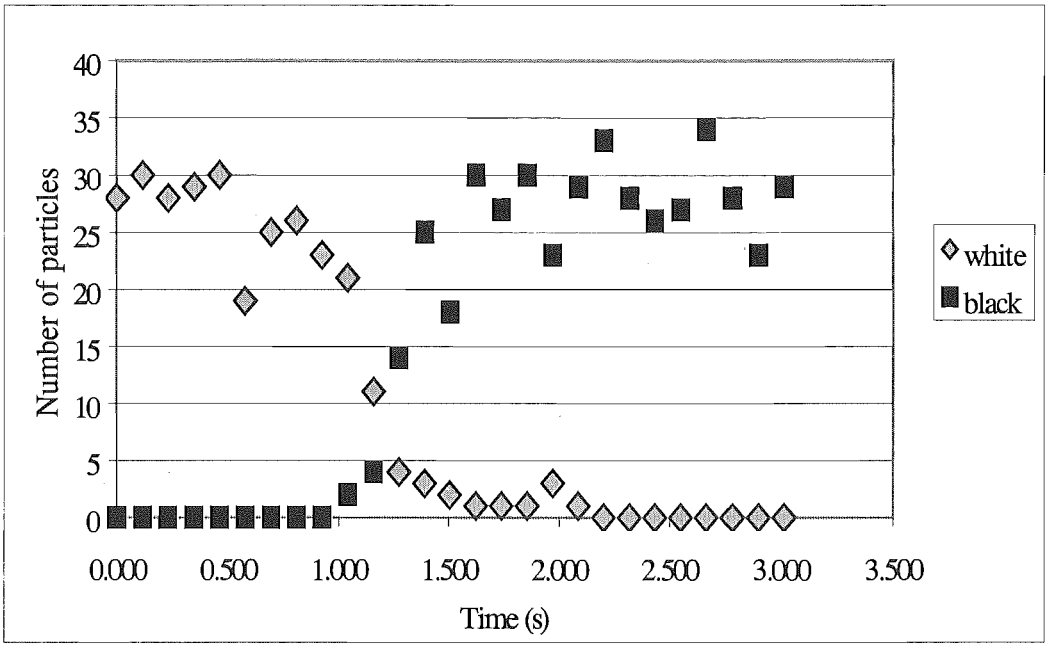

Figure 5.8-4 Number distribution for a step-input for inlet impactor [run 86]

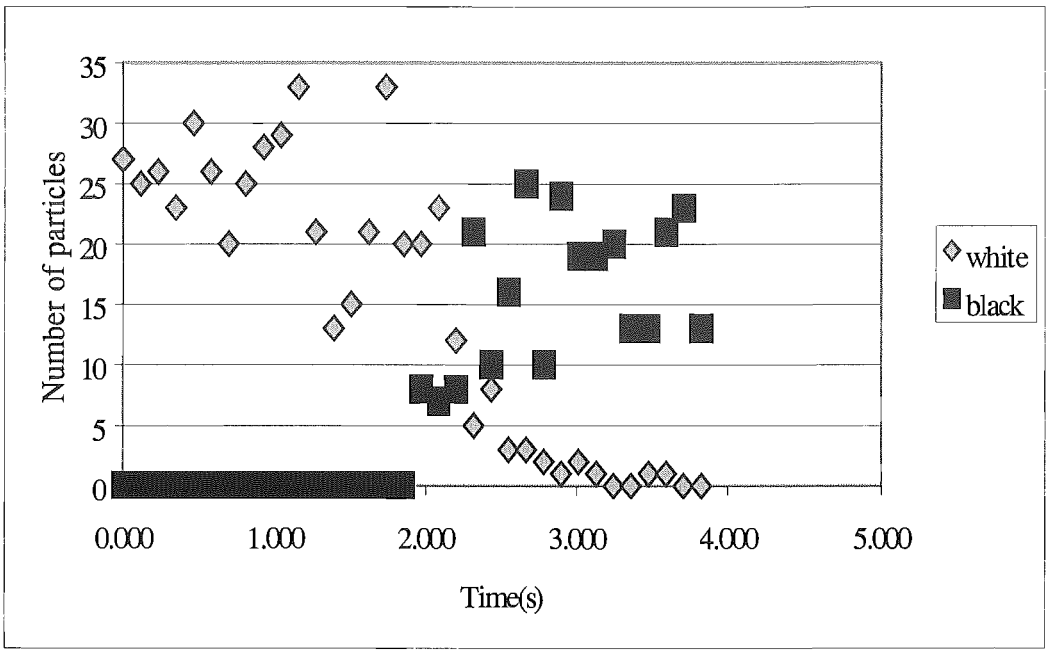

Figure 5.8-5 Number distribution of sand particles for a step input for bin impactor [run 86]

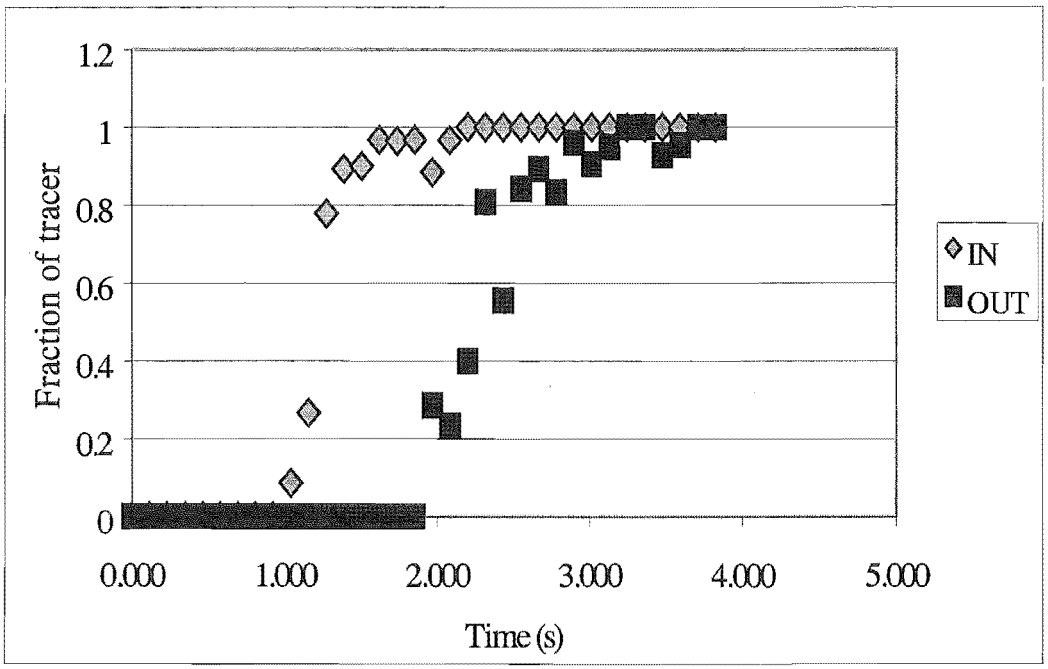

Figure 5.8-6 Fraction of sand tracer for a step input for inlet and out impactors [run 86]

The method of moments, transfer function and least squares methods was used to analyse the stimuli-response experimental data (Saruchera and Abrahamson, 1997). When the concentration C_i is known at discrete time intervals the mean for the input $\bar{t}_1$ or for the output tracer curves $\bar{t}_2$ is given by

$$\bar{t}_1 = \frac{\sum_{i=1}^{n} t_i C_i}{\sum_{i=1}^{n} C_i} \qquad (5.8\text{-}2)$$

The spread in variance for the input and output curves are σ_1^2 and σ_2^2 respectively, where σ_1^2 is given by

$$\sigma_1^2 = \frac{\sum_{i=1}^{n} C_i t_i^2}{\sum_{i=1}^{n} C_i} - \bar{t}_1^2 \qquad (5.8\text{-}3)$$

The Peclet number for large *Pe* can then be obtained by the following expression (Levenspiel, 1972)

$$Pe = \frac{2(\bar{t}_2 - \bar{t}_1)^2}{\sigma_1^2 - \sigma_1^2} \qquad (5.8\text{-}4)$$

The axially dispersed plug flow model was found to be valid for representation of the flow of granular particles in a cyclone (Saruchera and Abrahamson, 1997). The mathematical representation of the model is the following partial differential equation

$$\bar{t}\frac{\partial c}{\partial t} + \frac{\partial c}{\partial x} - \frac{1}{Pe}\frac{\partial^2 c}{dx^2} = 0 \qquad (5.8\text{-}5)$$

where c is tracer concentration, $\bar{t}$ is the mean residence time and Peclet number

$$Pe = \frac{uL}{D_p} \qquad (5.8\text{-}6)$$

where D_p is the particle hydrodynamic dispersion coefficient, u is the particle velocity in the direction of particle flow, and L is the axial path length of solids through the vessel or reactor.

In this model there is bulk flow of particles in the particle streamline direction. Superimposed on this bulk flow is a spread of particle velocities in the direction of the bulk flow. This distribution in particle velocities can be due to particle size distribution, particle-particle interactions, particle-wall friction and particle bouncing on the wall.

In the method of Ostergaard and Michelsen (1969) the transfer function analysis was used to obtain $\bar{t}$ and Pe. The transfer function is by definition the ratio of the Laplace transform of the output over the Laplace transform of the input tracer concentration

$$F(s) = \frac{C_2(s)}{C_1(s)} \qquad (5.8\text{-}7)$$

Equation 3.4-4 can be algebraically manipulated to yield the following equation (Ostergaard and Michelsen (1969)

$$\left(\ln\frac{1}{F(s)}\right)^{-1} = \bar{t}\,s\left(\ln\left(\frac{1}{F(s)}\right)\right)^{-2} - \frac{1}{Pe} \qquad (5.8\text{-}8)$$

A graph of Equation 5.8-8 with $\left(\ln\left(\frac{1}{F(s)}\right)\right)^{-1}$ against $s\left(\ln\left(\frac{1}{F(s)}\right)\right)^{-2}$ is linear with slope of $\bar{t}$ and intercept $-\frac{1}{Pe}$.

A sample plot is shown in Figure 5.8-7. From Figure 5.8-7 the particle residence time is 0.99 s and the Peclet number is 63.3.

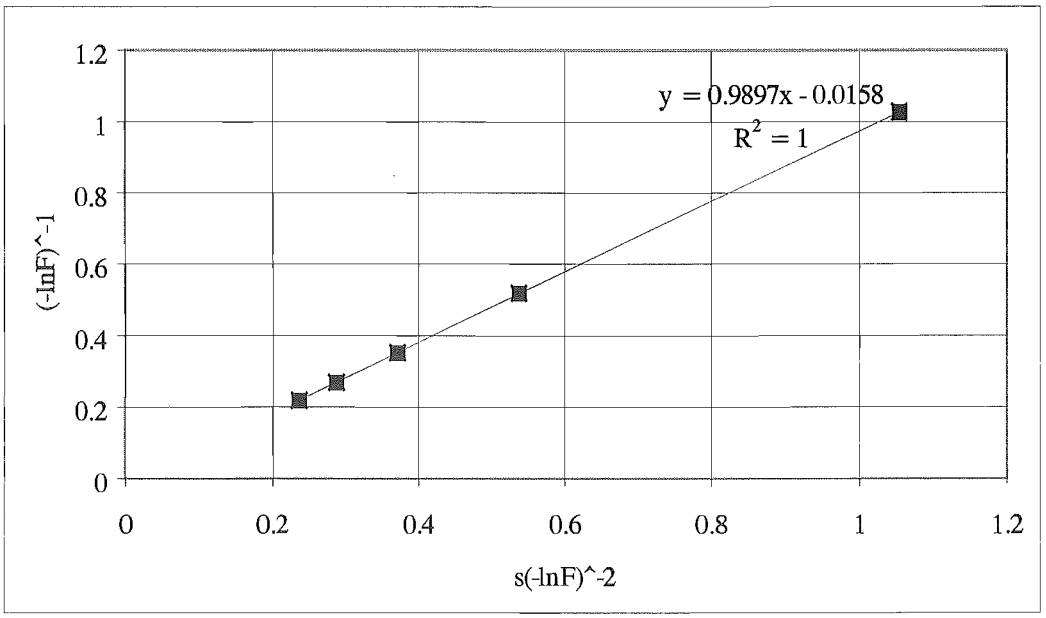

Figure 5.8-7 Evaluation of parameters [run 86]

The output tracer response curve can be given by the following equation (Appendix 9H)

$$C_2(t) = \int_0^t Ci(u)\frac{1}{2\sqrt{\pi}}\sqrt{\frac{Pe\,\bar{t}}{\left(\bar{t}-u\right)^3}}\exp\frac{\left[Pe\left(t-\bar{t}+u\right)^2\right]}{4\left(\bar{t}-u\right)\bar{t}}du \qquad (5.8\text{-}9)$$

The calculated values of $\bar{t}$ and Pe can be substituted into Equation 5.8-9 and Pe adjusted accordingly to match the model response curve to the experimental output curve.

The Solver tool in Excel was used to evaluate $\bar{t}$ and *Pe* by minimisation of the sum of square of residuals (Saruchera and Abrahamson, 1997). This method was found to be more stable especially for calculation of Peclet numbers. The following results were calculated by this procedure. A typical result of this procedure is shown in Figure 5.8-8. Figure 5.8-8 shows a good fit between the model and experimental curve.

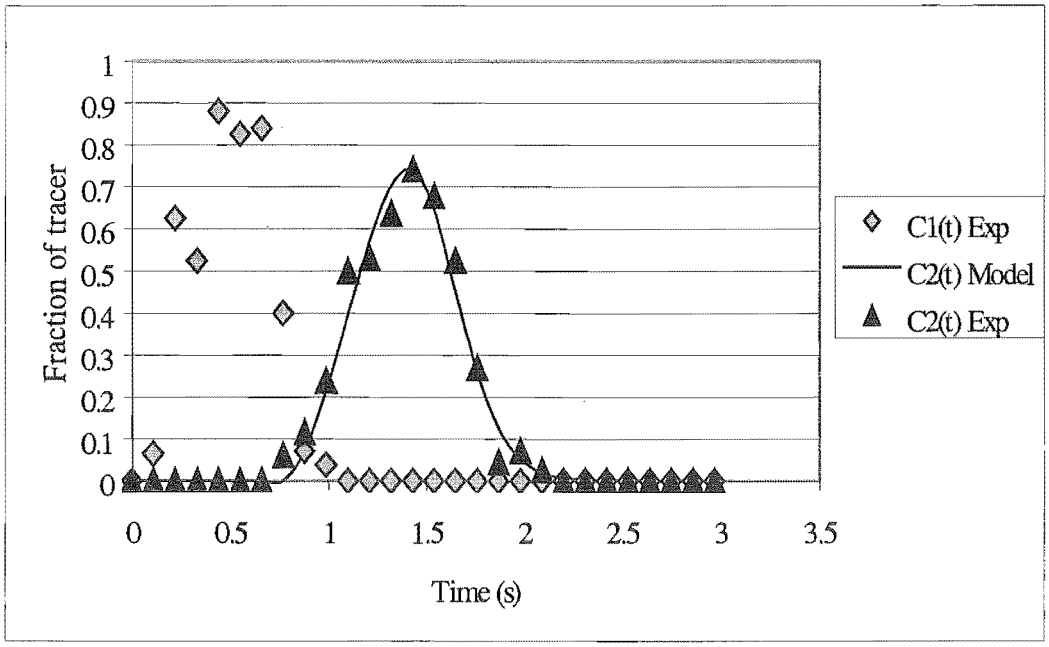

Figure 5.8-8 Experimental tracer distribution and model fitting [run 88]

5.9. Particle Residence Times

For applications of cyclones as chemical reactors, e.g. for drying, the residence time of the particle is an important parameter in the design of these equipment. A distribution of particle sizes is expected in feed streams. This distribution of size of particles will result in a distribution of residence times and consequently a difference in residual moisture contents for the different particles. For close product control it is imperative to control this distribution in residence times.

In the present study a series of experiments were carried out to determine the effect of several variables on the residence time of particles in a cyclone. The effect of the following variables was investigated

1. Air flow into cyclone
2. Particle inlet velocity
3. Particle diameter
4. Particle type (initially attributed to density)
5. Solids-gas mass flow ratio (SGL)
6. Geometry of conical section of cyclone
7. Cyclone size
8. Moisture content of particles

The average residence times of these particles in different cyclones was determined from the response curves using the Solver Tool in the Excel spreadsheet package by minimisation of the sum of square of residuals (Saruchera and Abrahamson, 1997). The results of these measurements are presented in graphical form.

5.9.1. Effect of SGL

The solids gas loading (SGL) is defined by the following equation

$$SGL = \frac{kg\ solids\ per\ unit\ time}{kg\ gas\ per\ unit\ time} \qquad (5.9\text{-}1)$$

The variation of particle residence time with increase in SGL is shown in Figure 5.9-1. It is evident that for the range of SGL investigated (0.04 to about 0.12) there is a slight decrease in the particle residence time as the SGL is increased.

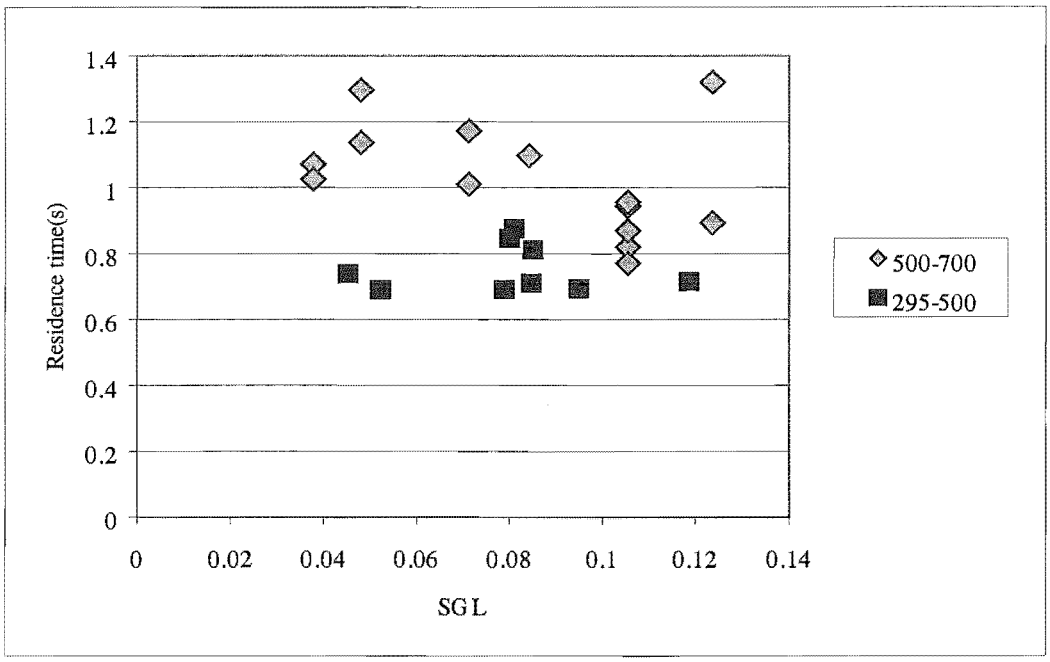

Figure 5.9-1 Effect of SGL on residence time of silica gel particles

Cyclone B; Gas inlet velocity: 20ms^{-1}
Particle size ranges: 295-500 μm and 500-700 μm

5.9.2. Effect of particle size

The effect of particle size on particle residence time is shown in Figure 5.9-1 and Figure 5.9-3. Particle residence time decreases with decrease in particle size. Also when counting the number of particles collected on the impactor it was found that very fine tracer particles were leading one or two cells ahead of the general particle flow (Figure 5.9-2). This supports the finding that smaller particles have lower residence times under the same conditions in a cyclone.

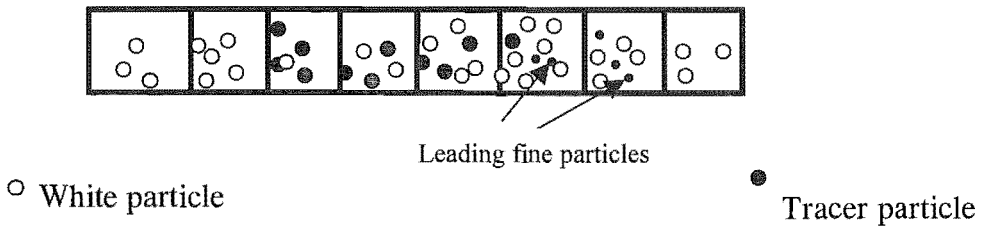

Figure 5.9-2 Fine tracer particles lead the larger tracer particles

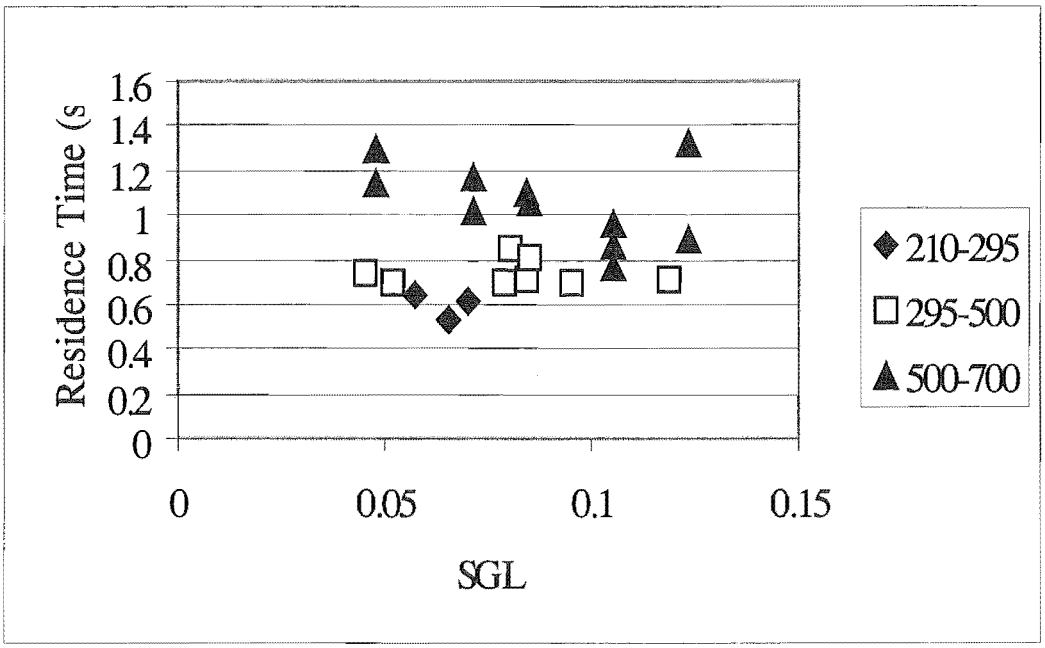

Figure 5.9-3 Effect of particle size on residence time of silica gel particles

Cyclone: B; Gas inlet velocity: $20ms^{-1}$

The scatter in mean particle residence times could in part be due to the range in particle sizes

5.9.3. Effect of particle density (and other properties of the particles)

The residence time of silica gel and sand particles is shown in Figure 5.9-4. Silica gel has a density of 1200 kgm^{-3} and the type of sand used has a density of 2600 kgm^{-3}. The particles size range of these particles was 250-500 μm. The residence time of the silica gel particles was about twice that for the sand particles.

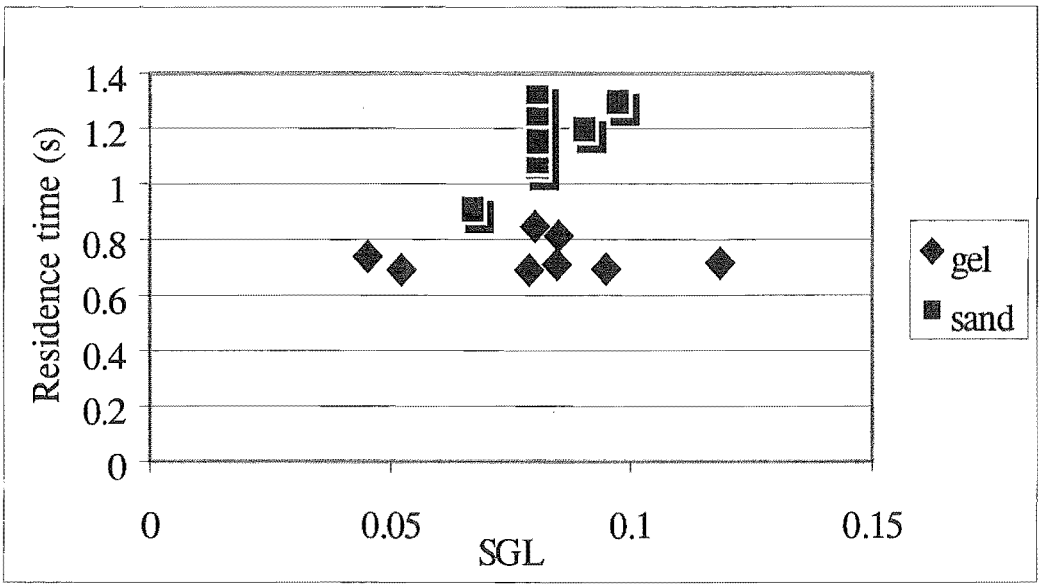

Figure 5.9-4 Effect of density on residence time

Silica gel particle density: 1200 kgm^{-3} Sand density: 2600 kgm^{-3}
Gas inlet velocity: 20 ms^{-1}
Cyclone: B

In a separate study Kemp et al. (1998) using identical impactors to those in this study measured the residence time of silica gel and glass particles. The density of glass is two fold that of silica gel. The residence time of glass was found to be about twice that for silica gel particles of the same size (Figure 5.9-5). The effect of particle size is also shown in Figure 5.9-5. Silica gel particles of size range 212-425 μm are compared to particles of size range > 425 μm. The measured mean particle residence times in Figure 5.9-5 are almost double those shown in Figure 5.9-4. The diameter of cyclone B was 225 mm and this can be compared to the SPS cyclone of diameter of 350 mm. An increase in the diameter of the cyclone by a factor of two also increased the mean particle residence time by the same factor. The total included cone angle of cyclone B was 14 degrees compared to that of Kemp et al. (1998) which had an angle of 10.7 degrees.

The weak dependence of mean particle residence time on SGL as exhibited in Figure 5.9-1 are in agreement with those obtained by Kemp et al. (Figure 5.9-5).

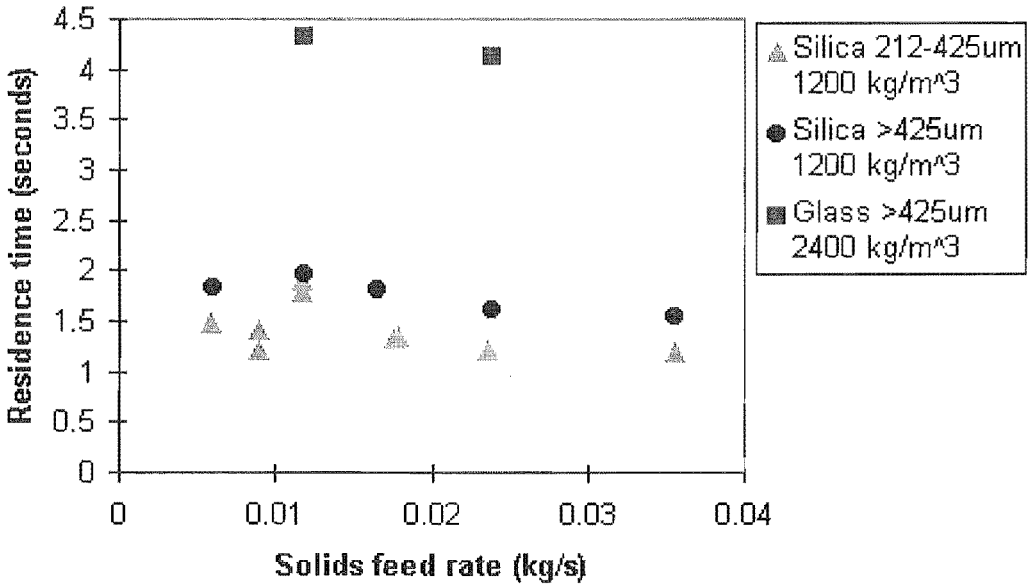

Figure 5.9-5 Effects of particle size and density on residence time

(Kemp et al., 1998)

Silica: Silica gel

The upper bounds of the particle sizes in Figure 5.9-5 are not specified, but must be smaller than the sampling nozzle diameter of 3 mm. Therefore in addition to the variability in density, Figure 5.9-5 is also likely to exhibit the effect of a range of particle size especially for silica gel since glass particles normally come in close size ranges.

5.9.4. Effect of gas inlet velocity

The mean residence time of silica gel particles was measured for a range of gas inlet velocity from 10 to 30 ms^{-1} at an SGL of 0.08 as shown in Figure 5.9-6. The mean residence time significantly decreases with increase in gas tangential velocity and can be modelled by a third order polynomial of the form

$$t_p = aV^3 + bV^2 + cV + d \qquad (5.9\text{-}2)$$

where t_p is the mean particle residence time (s) , V is gas tangential inlet velocity (m/s)

For cyclone B the constants a, b, c and d take the following values

a = 0.0001 0

b = -0.00540

c = 0.03640

d = 1.69820

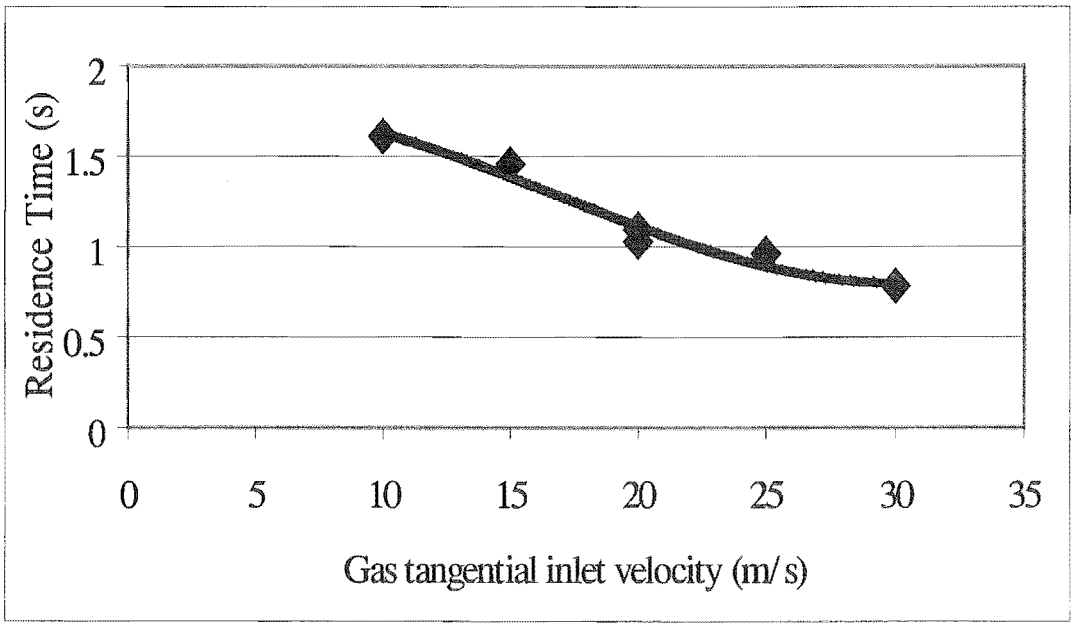

Figure 5.9-6 Effect of gas inlet velocity on residence time of silica gel particles

Size range: 700-850 μm SGL = 0.08 Cyclone B

The gas inlet velocity is a very important variable in controlling the particle residence time.

5.9.5. Interaction of gas inlet velocity and SGL

The residence times of silica gel particles of size range 500-700 μm in cyclone B is shown in Figure 5.9-7 with both inlet velocity and SGL varied. The measurements were at gas inlet velocities of 15 and 20 m s^{-1}. There is a gradual decrease in

particle residence time with increase in SGL with the residence time higher for a gas inlet velocity of 15 m s^{-1}. The rate of decrease of particle residence time with increase in SGL is also lower for gas entrance velocity of 15 m s^{-1}.

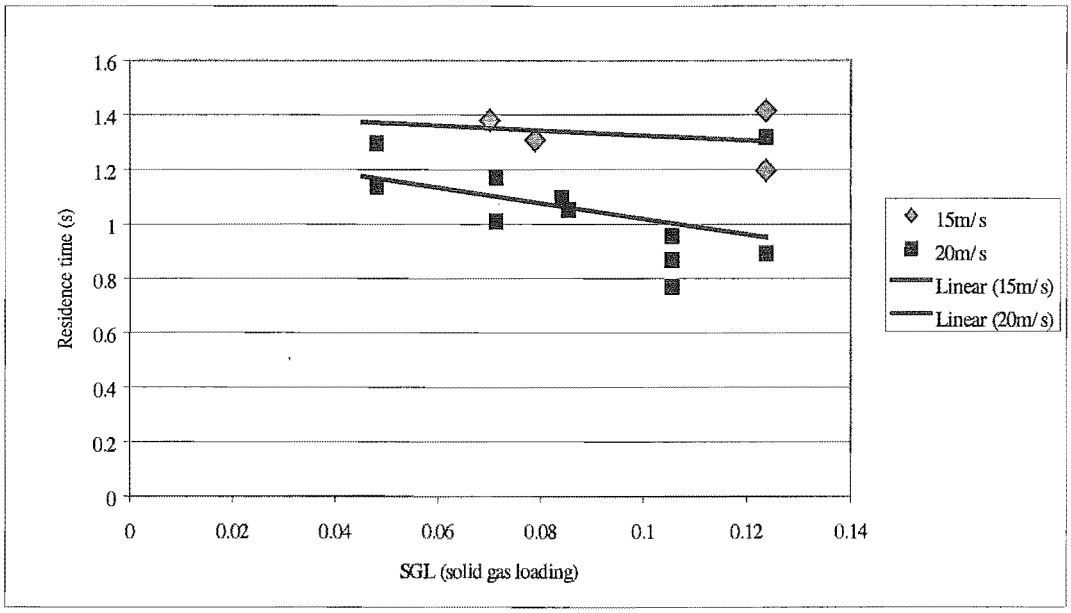

Figure 5.9-7 Effect of gas inlet velocity on residence time of silica gel particles

Cyclone B, Particle size range 500-700 μm

Kemp et al. (1998) made similar measurements in their cyclone but over a narrower range of gas tangential inlet velocity from 10 to 18 m s^{-1}. Their results also show a general decrease in particle residence time with increase in gas tangential inlet velocity.

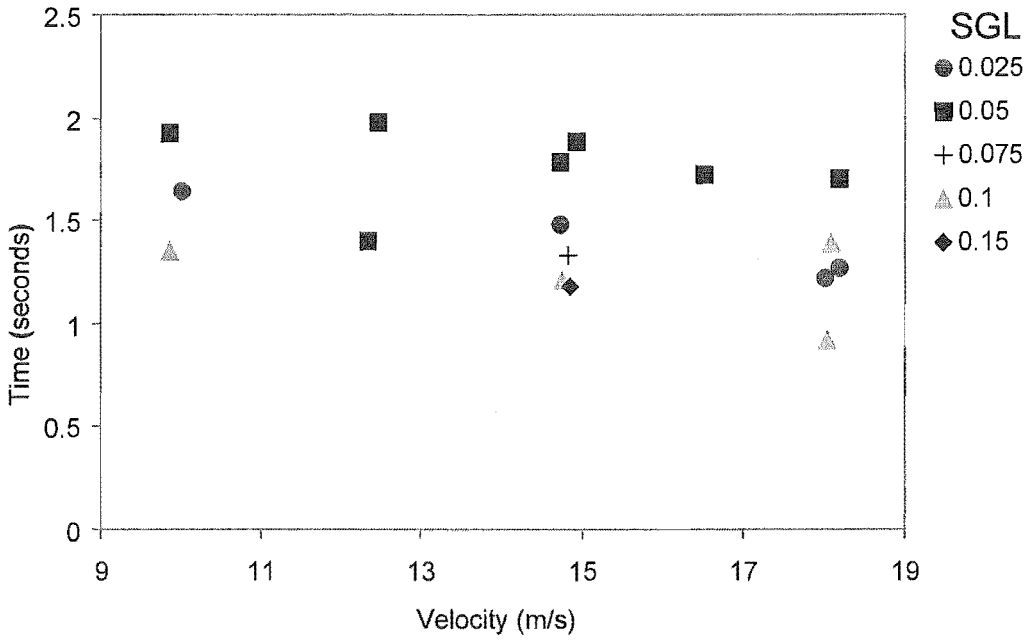

Figure 5.9-8 Effect of inlet velocity on particle residence time (Kemp, 1998)

5.9.6. Effect of particle inlet velocity

When the gas velocity in the ejector tube was at a flow rate of 0.00236 m^3s^{-1} (5 SCFM) particle velocity was measured at about 15 m^3 s^{-1}. However when the gas flow rate was increased three fold to 0.007 m^3 s^{-1} (15 SCFM) measured particle velocity was about 49 m s^{-1}. The residence time of silica gel particles of size range 295-500 μm was measured when the gas flow rate in the ejector tube was set at 0.00236, 0.00330 and 0.007 m^3 s^{-1}. The results are shown in Figure 5.9-9. It appears the particle inlet velocity does not influence the residence time of the particle in the cyclone. This suggests that equilibrium between the conveying gas and the particle from the ejector is attained early in its path through the cyclone. The particle probably loses most of its initial energy when it first interacts with the wall. The gas then resuspends the particle and subsequently its trajectory is dependent only on the gas velocity flow field and not the velocity at which it comes out of the ejector. In industrial practice particle velocities will be much lower. The important result is that these measured mean particle residence time results when particles are ejected at high velocity from the ejector are not expected to deviate from results under

conditions of normal industrial practice. The ejector velocity was made deliberately high to achieve sharp tracer changes for the stimuli-response experiments.

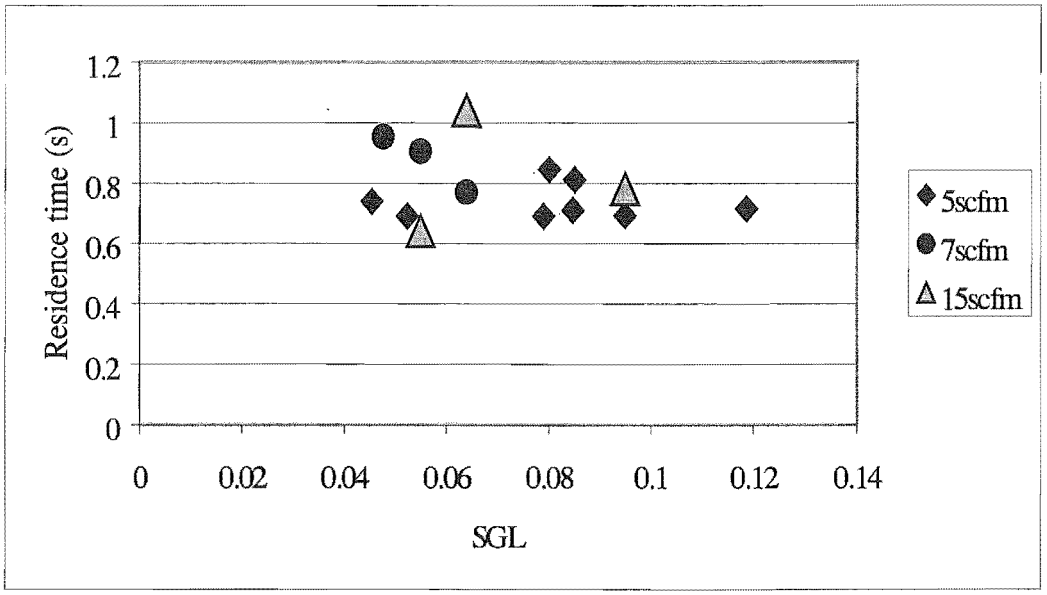

Figure 5.9-9 Effect of particle inlet velocity* on residence time

*Ejector gas flow rate (SCFM: standard cubic feet per minute)

5.9.7. Interaction of gas velocity and particle size

Experiments were done with cyclone A where the residence time of smaller particles was measured at lower velocity and compared to the residence time of larger particles at higher velocity. Figure 5.9-3 showed that the residence time of particles increased with increase in particle size at a given gas tangential inlet velocity. Figure 5.9-10 shows that the interaction of the gas is more dominant than the particle size in determining the flow of these particles. From the results shown in Figure 5.9-10 when the gas tangential inlet velocity is held constant, silica gel particles of the smaller size range (212-425 μm) are expected to have a lower residence time compared to the larger size range particles. However as shown in Figure 5.9-10, the influence of gas velocity change is much stronger than the effect of the small change

in size. These results illustrate the strong influence of the gas velocity on particle residence time.

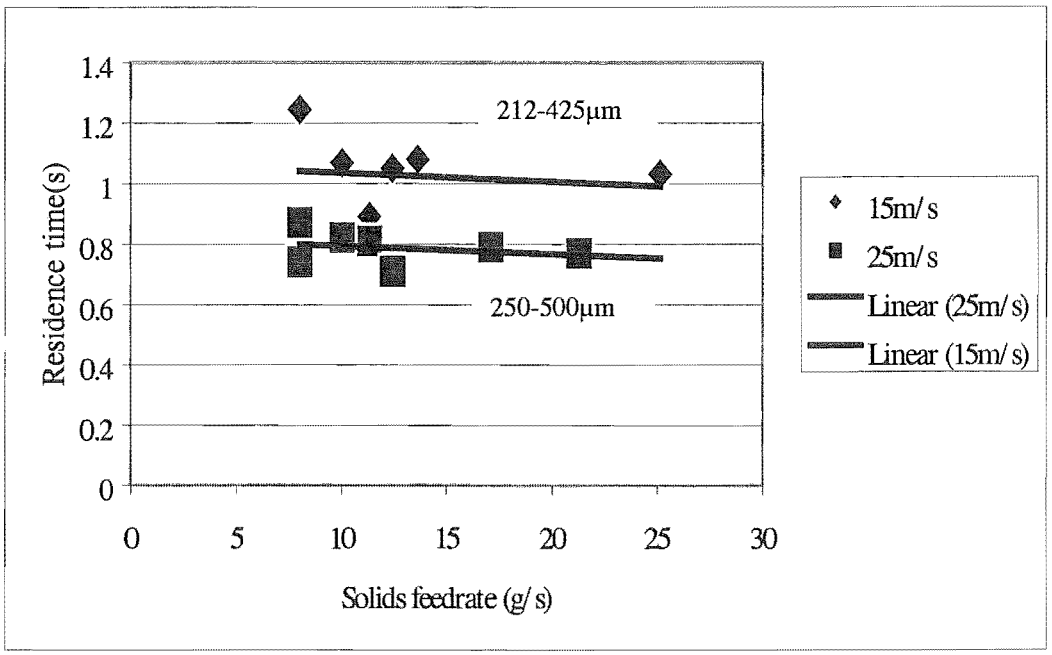

Figure 5.9-10 Effect of gas velocity, particle size and solids feedrate on residence time

Silica gel
Cyclone: A

5.9.8. Effect of cone angle

Six different conical geometrical shapes were used and the properties are shown in Table 5.9-1. All these conical sections are connected to a cylindrical barrel of inside diameter 225 mm and of height 230 mm. All discharge openings at the bottom of the cones were the same size (85 mm).

Table 5.9-1 Geometrical properties of conical sections used

Cone	Total angle (degrees)	Height of cone (mm)	Total Height of Cyclone (mm)
A	10	790	1020
B	14	560	790
C	20	397	627
D	28	280	510
E	36	222	452
F	42	190	420

The total height of the cyclone increases by about 143 percent from cyclone F to cyclone A. This same trend is not reflected in the mean residence time of particles in these different cyclones as shown in Figure 5.9-11.

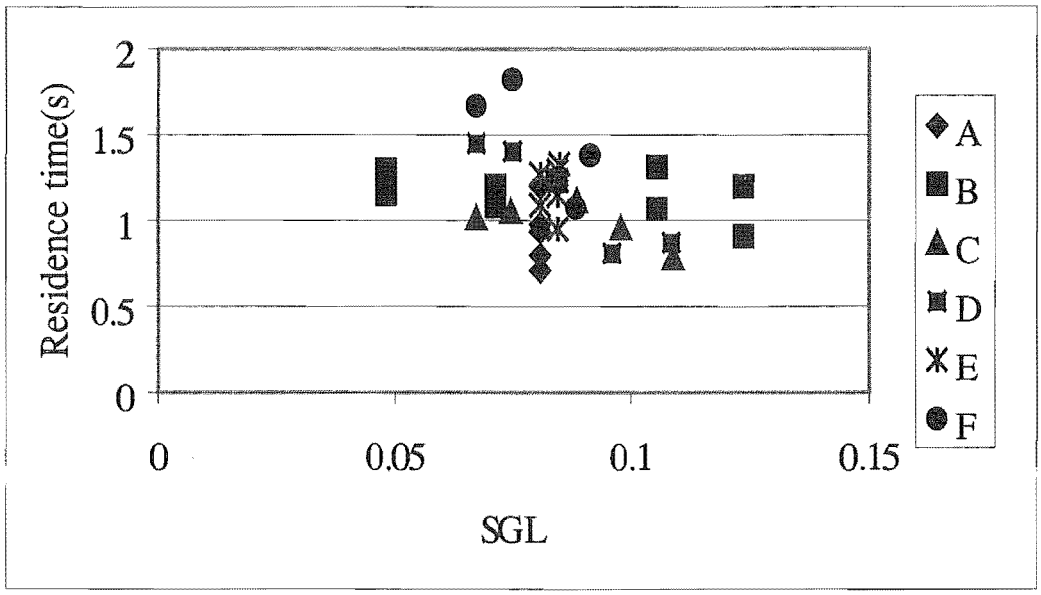

Figure 5.9-11 Effect of cone angle on residence time

Sand particles: 250-500 μm,; inlet gas velocity 20 m/s

The dimensionless residence time t_s/t_g is plotted as a function of the dimensionless quantity SGL in Figure 5.9-12.

A coefficient of slip $(\frac{t_s}{t_g})$ can be estimated from Figure 5.9-12 and is equal to about 0.11 for particles in cyclone F and 0.33 for particles in cyclone A. The "total velocity" of particles can be expressed in terms of the coefficient of slip and total gas velocity

$V_s = 0.11V_g \quad (cyclone\ F)$

$V_s = 0.33V_g \quad (cyclone\ A)$

on the basis that the paths are identical for gas and particles.

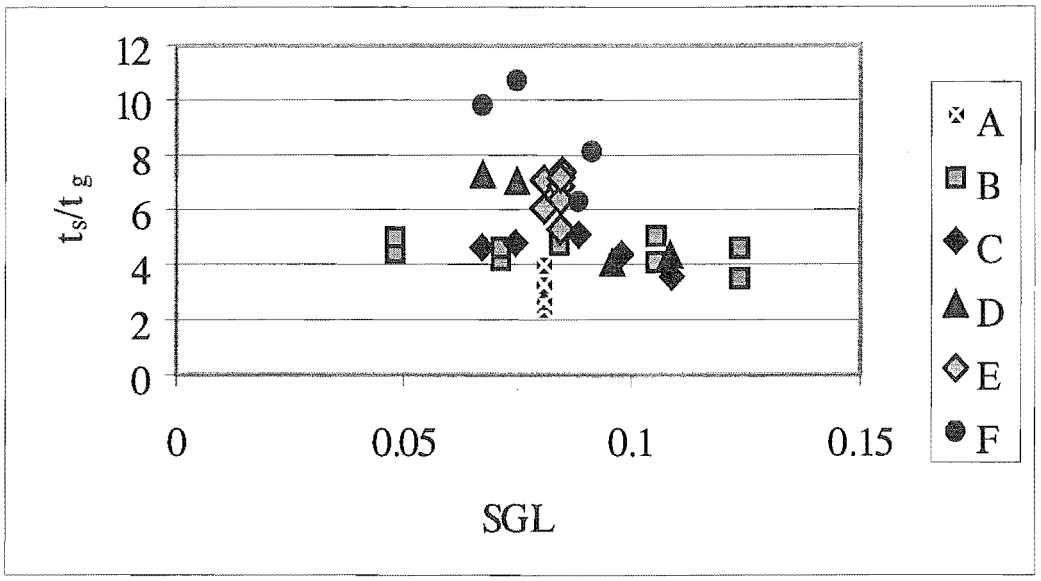

Figure 5.9-12 Dimensionless residence time as function of SGL for different cone geometrises

The gas tangential velocity is approximately equal to the total velocity (ter Linden, 1949, Kelsal, 1952). For a gas tangential velocity of 20 m s^{-1} the total velocity of the particle could be estimated from this coefficient of slip. In cyclone F the particle velocity was approximately equal to 2.2 m s^{-1} and about 6.6 m s^{-1} in cyclone A. The velocity of particles in cyclone F was approximately 30% that of particles in cyclone A. These results suggest a general and gradual decrease in particle velocity with increase in cone angle (Figure 5.9-11). The difference in mean particle residence time with cone angle for the same inlet conditions indicate different flow phenomenon in the different cyclones.

5.9.9. Effect of humidity on residence time of silica gel particles

Silica gel is hygroscopic and a substance for studies on drying of particulate materials. The impact of relative humidity and hence moisture content in the particles on residence time was investigated. Silica gel particles were exposed on a

screen to an atmosphere with a relative humidity (%RM) of about 85 per cent for a period of about 1 hour. The residence time of these particles in a cyclone was then measured. For these particles a mean value of residence time of 1.05 s was obtained compared to a mean value of 1.13 s for particles exposed to a normal environment with a relative humidity of about 24 per cent.

5.10. Peclet Numbers

The Peclet number is a dimensionless quantity obtained by the following expression

$$Pe = \frac{transport\ rate\ by\ convection}{transport\ rate\ by\ diffusion} = \frac{uL}{D} \qquad (5.10\text{-}1)$$

where u is convection velocity, L is a characteristic dimension of the apparatus and D is the hydrodynamic dispersion coefficient D.

The inverse of the Peclet number (1/Pe) is plotted against the feed rate as shown in Figure 5.10-1. Figure 5.10-1 shows an increase in Peclet number with increase in feed rate. In this interpretation the outlying data point (Run 39) was ignored because of few particles collected (sometimes only two in each cell). These few number of particles would thus lead to erroneous number concentration of particles.

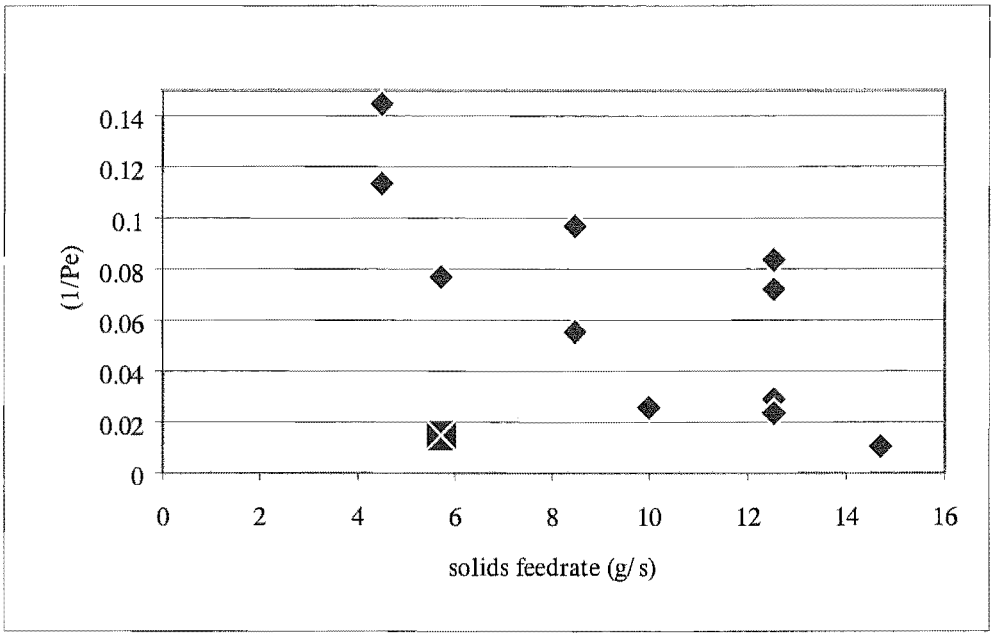

Figure 5.10-1 Effect of solids feed rate on Peclet Number

Silica gel: Size range: 500-700 μm; Cyclone: B; Gas inlet velocity: 20 ms^{-1}

The effect of gas inlet velocity on the Peclet number is shown in Figure 5.10-2. In Figure 5.10-2 the inverse of the Peclet number is plotted against the gas inlet velocity. The Peclet number decreases with increase in the gas inlet velocity.

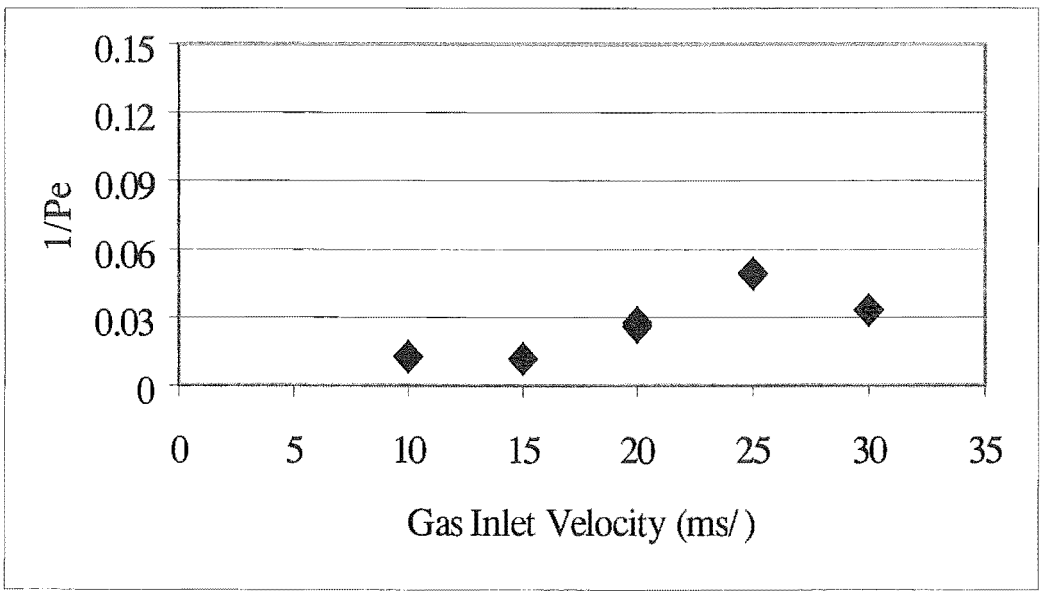

Figure 5.10-2 Effect of gas inlet velocity on Peclet Number

Silica gel
Size range: 700-850 mm; Cyclone: B; SGL: 0.075

A plot of the inverse of the Peclet numbers for different cone geometries is shown in Figure 5.10-3. The Peclet number increases with increase in the total included angle of the cone. The incidence of roping was found to increase with increase in cone angle. The increase in particle-wall interactions appears to result in a strong increase in the effective dispersion coefficient.

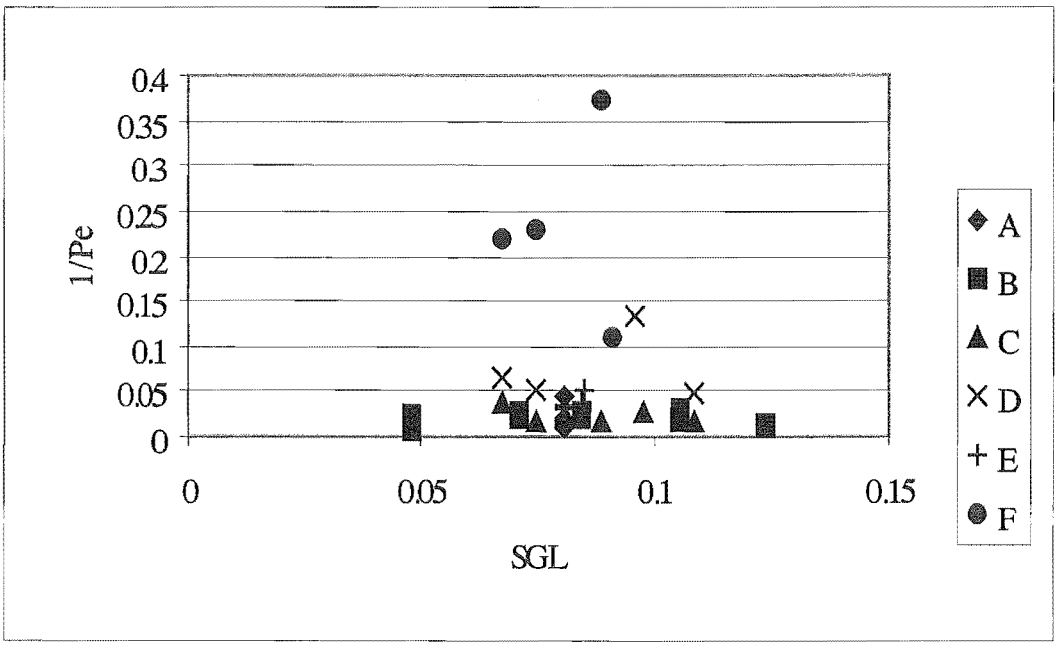

Figure 5.10-3 Effect of cone angle and SGL on Peclet Number

Sand: Size range: 250-500 μm; Gas inlet velocity: 20 ms^{-1}

5.11. Effect of surface roughness on Particle Peclet number

The conical section of a 20-degree cyclone (cyclone C) was coated with a monolayer of sand particles of size range 250-500 μm. The residence time and Peclet numbers of sand particles were measured in this cyclone. The Peclet number of sand particles in a plain steel cyclone and a sand-coated cyclone are shown in Figure 5.11-1. The Peclet number is higher for a plane mild steel wall compared to that for sand coated surface. It was also observed that ropes disappeared when the wall was coated with the sand.

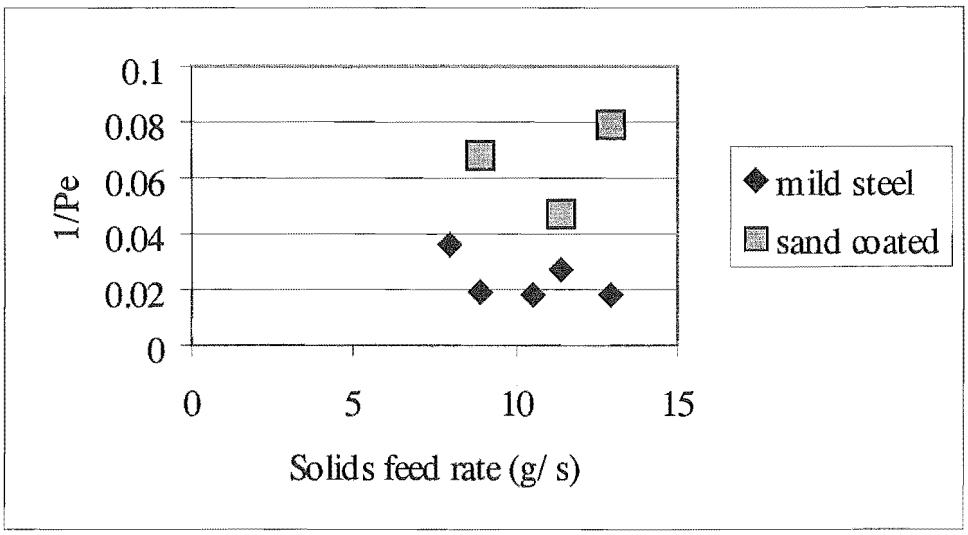

Figure 5.11-1 Effect of wall roughness on Peclet number

5.12. Observations and Presence of Roping

Roping is characterised as flow in which particles travel collectively in thin strands in the wall region. The presence of roping was found to be a combination of various factors and variables. The variables, which were observed in the present study to be necessary for the formation of these ropes, are listed below

(a) air inlet velocity

(b) particle characteristics (size and mechanical properties)

(c) cone angle

(d) feed rate or solids-gas mass flow ratio (SGL)

(e) coefficient of friction with the wall

Detailed analysis of the phenomenon of roping is given elsewhere (§ 6-1). In the present section the general principles thought to be underlying the formation of these ropes and qualitative observations are presented.

Wall flows of particles at high particle concentrations were experimentally observed to consist of ropes together with some particles travelling in dispersed state. There was no observed rope formation in the cylindrical section of the cyclone under all

experimental conditions of the present study. Observations through windows inserted in the conical sections by high speed video revealed that there was a particle concentration variation along the circumference of the cone. There was a high concentration of particles forming a rope, followed by very dispersed particles. This particle concentration profile is illustrated in Figure 5.12-1.

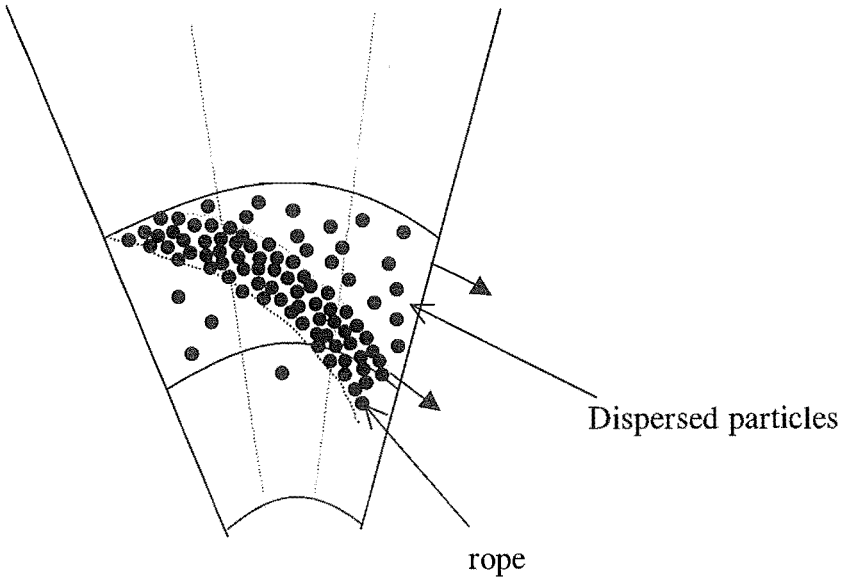

Figure 5.12-1 Particle concentration profile in cyclone conical section

The high concentration particle phase constitutes the rope and the light concentration regions are the particles travelling in the dispersed state. The direction of gas flow is from left to right.

In cyclones A to C particles travelled predominantly in a dispersed state although cyclone C with the 20 degree cone angle appeared to mark the boundary for roping-non roping flow. In these cyclones faint ropes formed only at or towards the discharge end where particle concentrations became higher. Where ropes were quite distinct, especially for cyclones with cone angels above 20 degrees (cyclones D, E and F) when the air velocity was less than 10-m s^{-1} the ropes were disrupted. It should be pointed out that the reduction in air velocity corresponded to reduction in the volumetric flow rate of the gas. For a given mass flow of solids, the net effect

was an increase in the solids-gas mass flow ratio (SGL). These observations were with sand particles of size range 150-210 and 250-500 μm. No roping was observed with silica gel particles under the same experimental conditions.

The gas inlet velocity controlled both the formation and flow of the rope. In cyclone E (36 degree cone angle) the rope could be observed through a window under continuous feeding conditions. However, when the feed into the cyclone was stopped the rope disappeared from the window. The rope was made to reappear against the window by increasing the gas inlet velocity to about 23-m s^{-1}. Thus the gas velocity controlled the movement of the rope up and down the cyclone conical wall.

Particles travelling in cyclone F formed ropes while there was absence of roping in cyclone A with a flow transition in between. Given the strong interaction between the particles in the rope it is likely that the velocity of a rope could be less than the velocity of particles travelling independently in a dispersed state. However the paths could be different in the two states, as discussed later.

A qualitative flow mapping of rope-no rope flows is given in Figure 5.12-2. The region of no roping is extended to the right past 20° for silica gel particles and larger size sand particles in general. Conversely there would be a movement of the roping region to the left for small particle sizes for a given material. An increase in the SGL would also shift the roping region to the left.

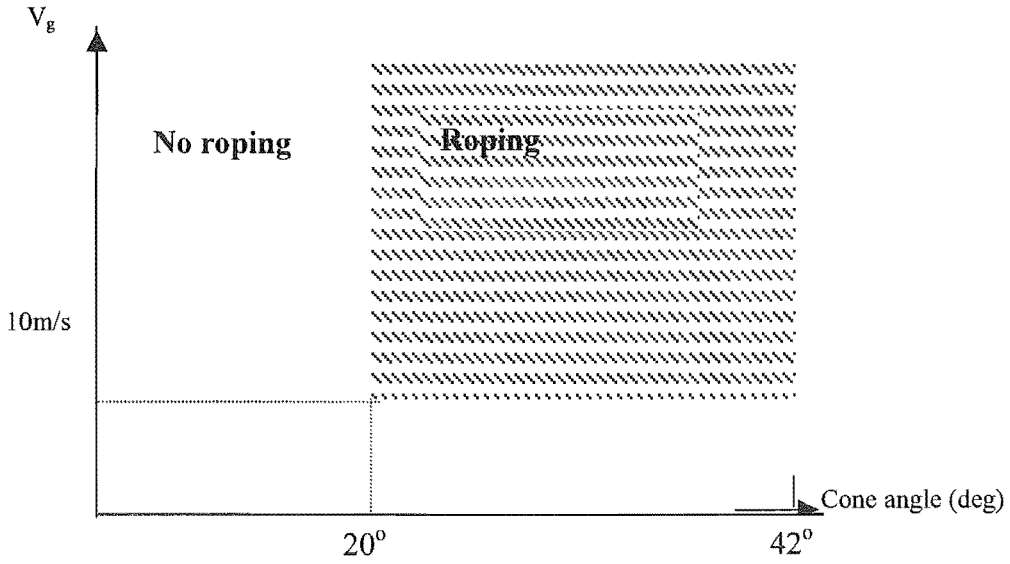

Figure 5.12-2 Qualitative flow mapping of roping with change in cone angle and gas velocity; sand: size range 250-500 mm; feed rate 9 g s^{-1}

5.13. Particle Bouncing Phenomena

The nature of interaction of a particle with a wall is a function of the mechanical and surface properties of both the particle and the wall. These interactions govern the post collision transport processes of these particles in the gas phase. The collision forces at impact thus affect the motion of the particles.

The behaviour of particles when they bounce off from a plain mild steel surface or a rough wall was investigated in this study. The particulate materials used in this case were sand, glass and silica gel particles. Particles were dropped freely from a height of about 40 cm to strike a 1.5 mm thick smooth plane mild steel plate inclined at an angle of about 35° to the horizontal. The material was the same as that used in the construction of the cyclones. The action was recorded by a Sony Hi-8 camcorder at a shutter speed of $\frac{1}{215}s$. At this shutter speed the particles appeared as streaks enabling the velocities to be determined. Later the recording was replayed and images captured using the Optimas® image grabbing software. Figure 5.13-1 shows

the bouncing of silica gel particles of size range 700-850 μm and illustration of this phenomenon is shown in Figure 5.13-2. The average velocity of a particle just before impact was about 2.15 m s^{-1}. These particles are reflected with an average velocity of 1.13 m s^{-1}. Although all the particles impact from a vertical plane with a uniform velocity and angle of incidence there is a wide scatter in the reflected angle. The angles of the reflected particles range from 87° to about 17° with an average of 47° measured from the normal to the plate. The incident angle of the particles is at an angle of about 35° from the normal. The scatter in velocity is probably due to irregularity of shape of particles and surface roughness on the steel plate.

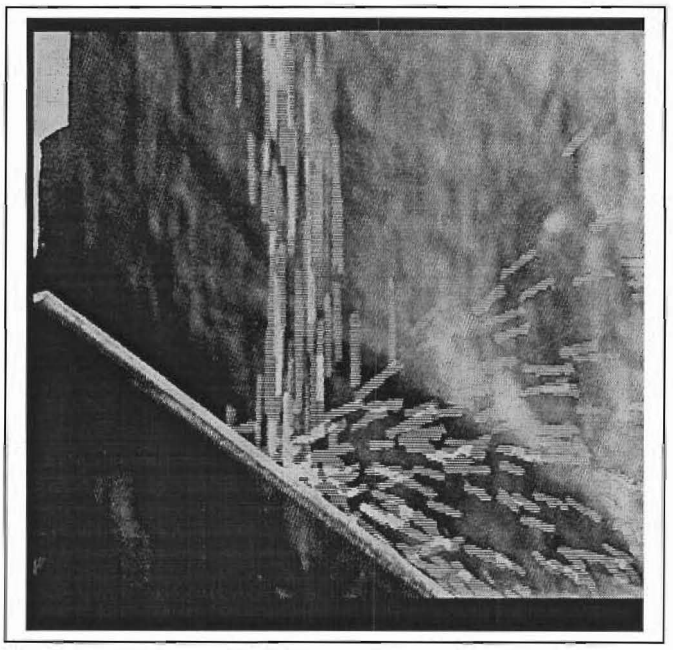

Figure 5.13-1 Silica gel particles bouncing from a mild steel plate inclined at 35° Size range: 850–1000 μm

Using the average values for the angles and velocities the coefficient of restitution between the silica gel and the steel surface is given by:

$$e = \frac{1.13Cos(47)}{2.15Cos(35)} = 0.44 \qquad (5.13\text{-}1)$$

The definition of the coefficient of restitution used here is that of the ratio of the post and pre-collision normal velocity components. The range of values for the reflected angles represents a range of values of coefficient of restitution from 0.03 to 0.61. A corresponding range in particle reflected total velocity is from 0.56 to 1.36 m s^{-1} for the low and high values for the coefficient of restitution respectively.

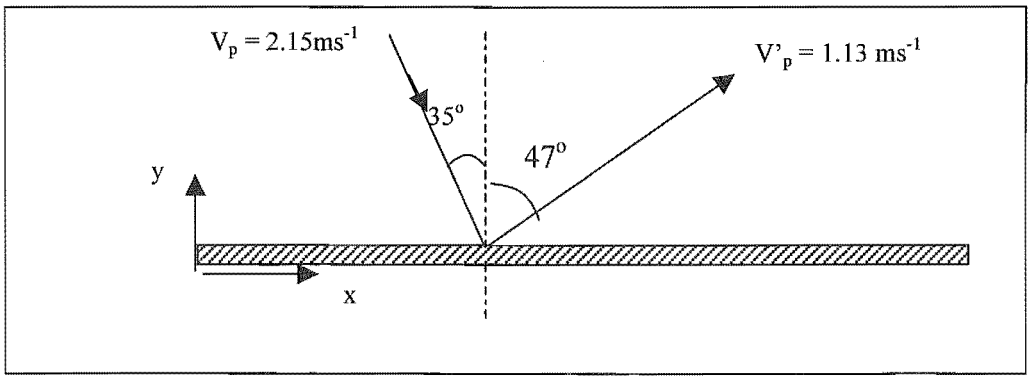

Figure 5.13-2 Bouncing of Silica gel particles from a mild steel surface

The bouncing of silica gel particles of size range 700-850 μm on a mild steel plate inclined at an angle of 30° is shown in Figure 5.13-3. In Figure 5.13-4 sand particles of size range 250-500 μm are shown bouncing from the same steel plate are as well and in Figure 5-13-5 glass beads are shown. Glass beads have a very highly regular spherical shape compared to silica gel but when they bounce from a similar surface they show the same scatter compared to silica gel particles. This would therefore suggest that the scatter in the angle of reflection is more likely to be caused by a surface irregularity on the steel surface or particle. Although the mild steel plate appeared smooth and rust free surface microscopic imperfections are likely to be present.

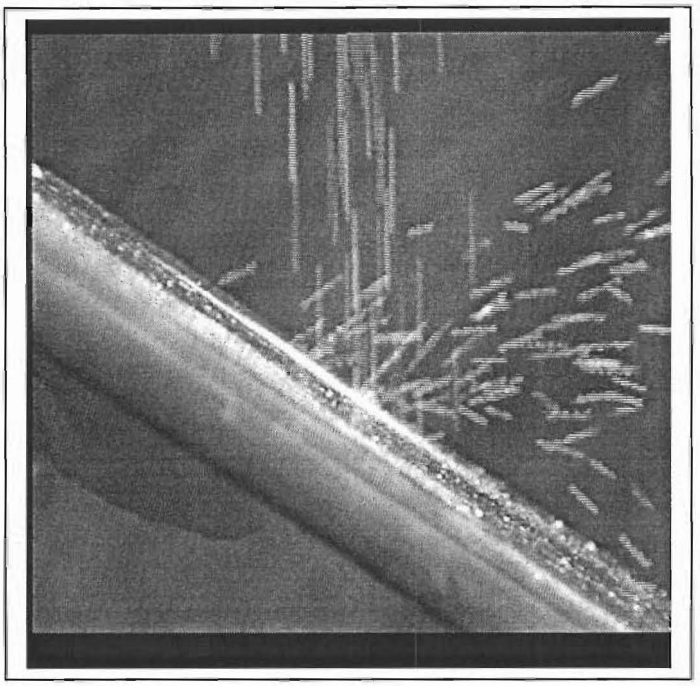

Figure 5.13-3 Silica gel bouncing from a mild steel plate

Size range: 700-850 μm

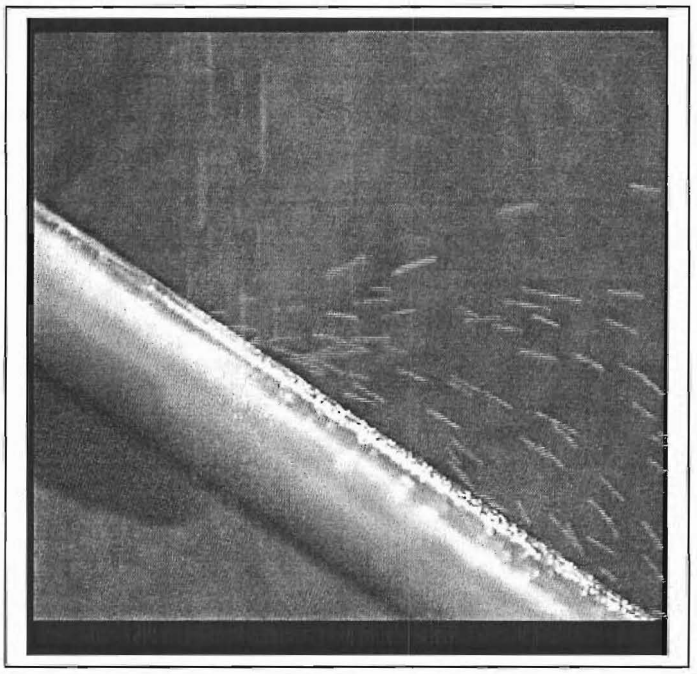

Figure 5.13-4 Sand particles bouncing from mild steel plate inclined at 30°

Size range: 250-500 μm

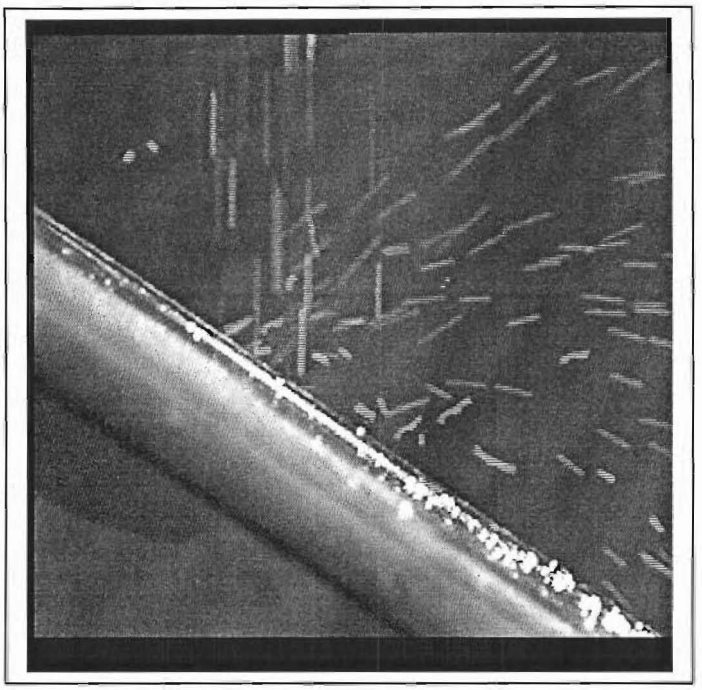

Figure 5.13-5 Glass beads bouncing from mild steel plate
Size: 500 μm

Collisions between glass or silica gel and a mild steel plate are more elastic compared to collisions between a sand particle and the same steel plate. This is shown by the higher post-collision velocity components perpendicular to the plate compared to sand particles that have a very low post-collision velocity component perpendicular to the plate. The coefficient of restitution for sand with a mild steel surface is lower compared to that for silica gel and is about 0.3 compared to 0.7-0.8 for silica gel and glass. This implies the collision of sand with a steel surface is highly inelastic and damped.

The case of particles bouncing on a clear mild steel plate is an ideal one. In reality when particles are travelling in the cyclone a layer of particles can cover the wall and therefore when a particle strikes the wall region it may impact on a particle at the wall. As a simplification this surface layer of particles is a rough surface.

To create this rough surface layer a mild steel plate was coated with a thin layer of glue, and sand particles of size range 250–500 μm were sprinkled to create a monolayer of sand particles. Particles were again dropped from a height of 40 cm as

described above. The highly regular pattern of the reflected paths of silica gel particles when bouncing off from a plain surface as shown in Figure 5.13-1 and Figure 5.13-3 can be compared to the irregular pattern as shown in Figure 5-13-6 for a rough sand coated surface. Figure 5-13-7 shows the bouncing of sand particles on a rough sand coated surface. Comparison of Figure 5-13-7 with Figure 5-13-6 for silica gel shows that for the same surface roughness sand particles bounce off in a more ordered pattern. The highest angle at which the particles reflect from the surface as measured from the steel surface counter clockwise is about 130° for silica gel and 55° for sand. The silica gel collision highlights the possibility of coefficient of restitution greater than one as reported by Matsumoto and Saito (1970).

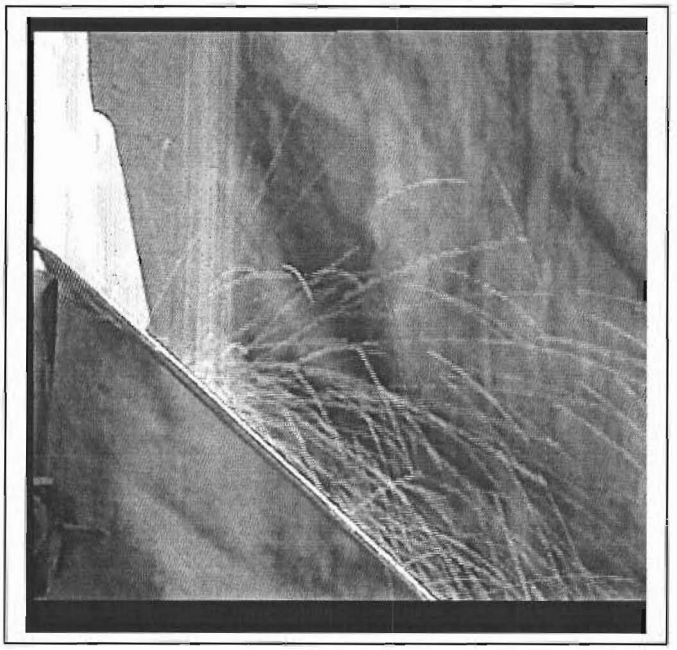

Figure 5.13-6 Silica gel bouncing on sand coated mild steel plate

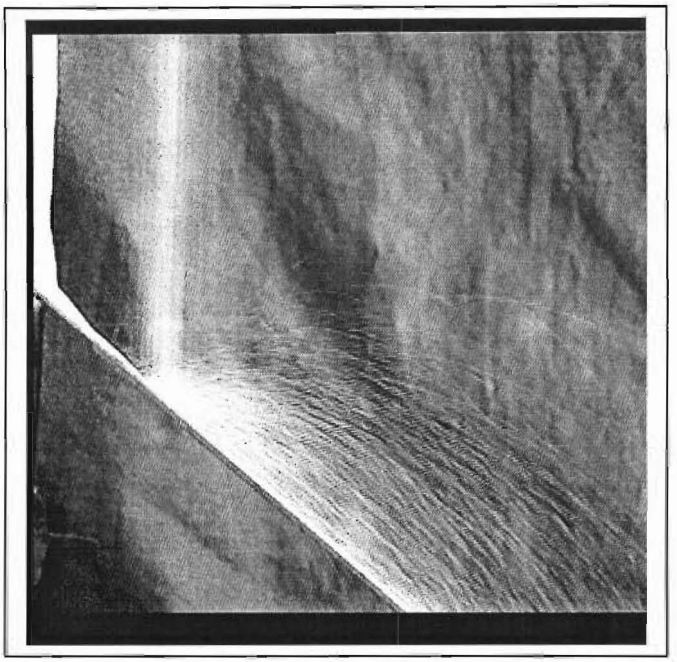

Figure 5.13-7 Sand particles bouncing off from rough sand coated surface
Size range: 250-500 μm

The collisions of these particles with the wall are accompanied by a loss in kinetic energy. This loss in energy is related to the coefficient of restitution and coefficient of friction for the collision process. The coefficient of restitution and coefficient of friction are necessary to describe the flow of particles in the cyclone (§ 6).

Modelling of Particle Flow

6

6.1. Roping Phenomenon along a Wall 6-2
6.3.1. Velocity of rope 6-18

6.2. Sliding Particle Model (SPM) 6-22

6.3. Bouncing Particle Model (BPM) 6-39
6.3.1. Single Particle Approach 6-39
6.3.2. Model Results 6-64
6.3.3. Multiple Particle Approach 6-67

6.1. Roping Phenomenon along a Wall

Roping is described as particle flow in which the particles are concentrated in thin rope-like suspensions. This phenomenon has been observed usually close to the wall in gas-solids suspensions along pipe bends and in cyclones. The other type of flow in which solids are not concentrated into ropes and behave more or less independently of each other will be referred to as the dispersed state. Experimental evidence suggests particles flow in a cyclone by either roping or in a dispersed state. To investigate these roping phenomena six conical sections with the following total included angles 10, 14, 20, 28, 35 and 42° were fabricated. The dimensions and drawings are given in the Appendix 9C. Letters A to F will identify the different cones respectively. Glass windows were fitted on the sides of the conical sections to enable visual observation.

It was observed that there is a change in flow behaviour as the cone angle was increased. Four variables were found to influence this flow behaviour and these variables were particle concentration, particle characteristics, cone angle and airflow. In order to minimise the variable levels one set of observations were made with sand of size range 250-500 μm flowing at 11 g s^{-1} and air flowing at 0.099 m^3 s^{-1}. Under this set of conditions no roping was observed in cyclones A to C, although close to the apex (discharge end) particle concentration increased resulting in formation of some ropes. With cyclones D and E roping appeared in the main conical section. In cyclones A to C, particles that were moving in the conical section were immediately drained into the dust collection hopper when feed was stopped but gas flow continued. However, with cyclones D and E when feed was discontinued the ropes did not drain into the dust collection hopper but moved up about 70 to 100 mm from the apex. This roping persisted without continuous solids feed for run times of up to 10 minutes after which the airflow was stopped. Ranz (1985) observed that when dust feed was stopped abruptly the spiral patterns or ropes persisted briefly on the cone, fading away in a few seconds. The observations mentioned in this study are not at variance with those of Ranz (1985) but emphasise the change in flow pattern with change in the cone geometry. In all the cyclones there was no roping observed in the cylindrical section of the cyclone.

With cyclone F when the solids feed was stopped and the airflow maintained for a period of about 10 minutes, the ropes were also maintained in the main conical section. Later when the airflow was stopped and the solids drained into the dust collection hopper a particle boundary layer remained in the cone. This particle layer marked the original path of the rope. Figure 6-1 shows the existence of a fine layer of particles (white spiral) remaining on the wall for the 42-degree cone.

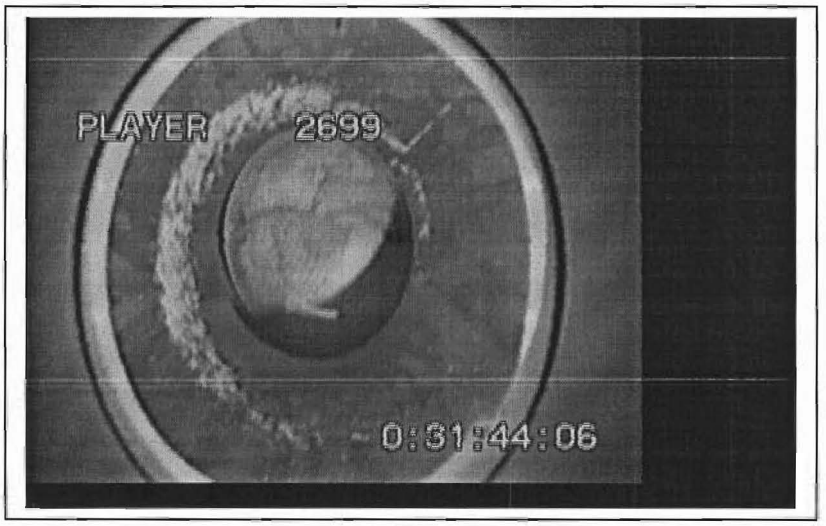

Figure 6-1 Sand particle layer remaining in cyclone F after air flow was stopped

The image was taken from the top of the cyclone looking down into the conical section when the feed and airflow had been stopped. Solids feed to the cyclone had been maintained at a rate of about 11 g s^{-1} of sand particles of size range 250–500 μm. The gas tangential inlet velocity was 20 m s^{-1}. After a continuous run of about 10 minutes both solid and gas flows into the cyclone were stopped. The wall particle layer marks the rope path in the cyclone. At first it was suspected that this particle boundary layer could be attributed to effects of electrostatic forces. If this was the case then the roping phenomena could also be due to electrostatic forces. In order to isolate the effects of electrostatic forces, the cyclone was well earthed and a similar run was repeated. It was observed that after earthing of the cyclone there was no change in the solids flow pattern. The same roping phenomenon was observed with the earthed cyclone. On shutting down the flow to the cyclone the particle layer was still observed. A particular run was also carried out whereby the earthed cyclone was fed with metal filings. Metal particles have a high conductivity

and therefore would prevent any charge build up in the system. The roping pattern was also observed in this case. This evidence therefore suggested that the formation of the particle boundary layer could not be attributed to the effects of electrostatic forces in this particular case. This remainder particle layer was not observed in runs with conical angles of less than 42°. This existence of the particle layer coupled with the fact that the incidence of roping increased with increase in cone angle, would suggest that roping phenomena could be due to the effect of wall friction and higher centrifugal forces.

The coefficient of sliding friction for these sand particles was found by tilting a mild steel plate and recording the angle at which the particles began to slide. The onset of sliding was found at an angle of 20° from the horizontal. The coefficient of sliding friction was therefore determined to be 0.36, from

$$\mu = \tan 20^{o}$$

This figure would suggest that the particle layer remaining on the cyclone wall could not exist purely on the basis of friction alone. The existence of this layer could be attributed to surface imperfections or cohesive molecular forces (van der Waal's) since the particles in the boundary layer are very fine.

As stated before, for a given set of operating conditions the incidence of roping increased with increase in cone angle. With the tangential air inlet velocity at about 20 m s^{-1} no roping was observed in cyclones A to C. Figure 6-2 shows flow of sand particles of size range 250-500 μm in cyclone B at a feed rate of about 11gs^{-1}. It is apparent there is little evidence of roping. The blanket white background on the wall is the sand particles reflecting light. This type of flow is what will be referred to as dispersed flow. A similar photograph is shown in Figure 6-3 for flow in cyclone C.

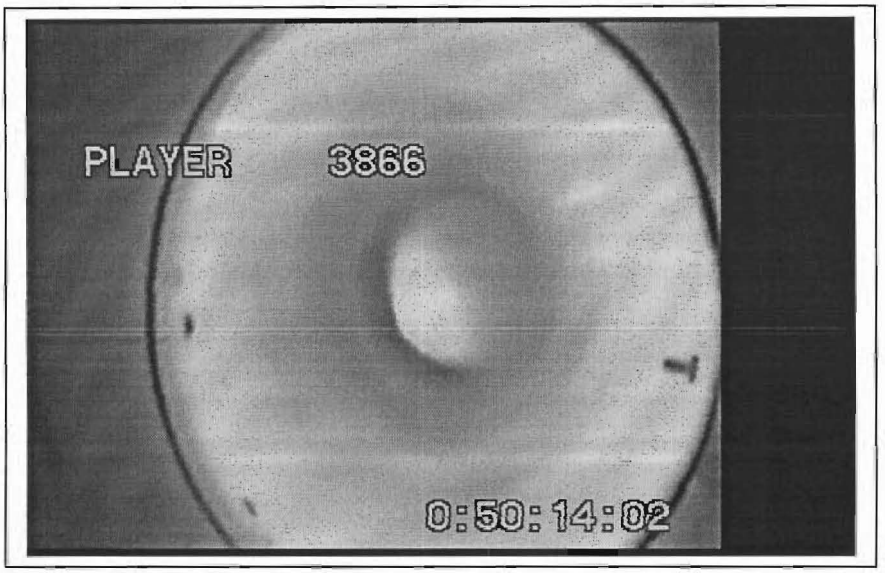

Figure 6-2 Flow of sand particles in cyclone B (cone angle 14°)

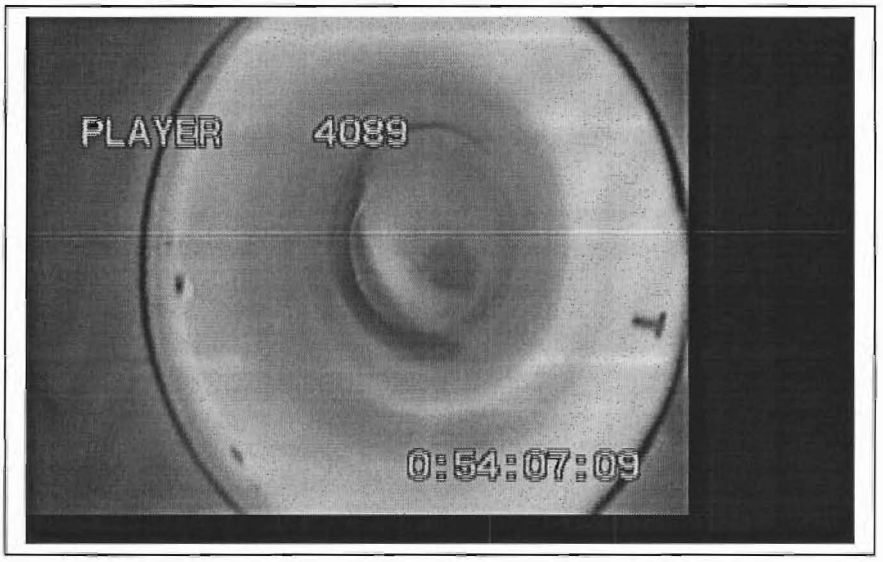

Figure 6-3 Flow of sand particles in cyclone C (cone angle 20°)

As shown in Figure 6-3 there is some evidence of roping in cyclone C especially towards the bottom discharge of the cyclone. Under the same operating conditions the incidence of roping can be more pronounced when the cone angle is increased. Figure 6-4 and Figure 6-5 show very clearly defined ropes in cyclones D and E that have 28° and 36° cone angles respectively. Thus Figures 6-1 to 6-5 progressively show the occurrence of roping when the cone angle is increased while other parameters like air flow, feed rate and particle characteristics are held constant.

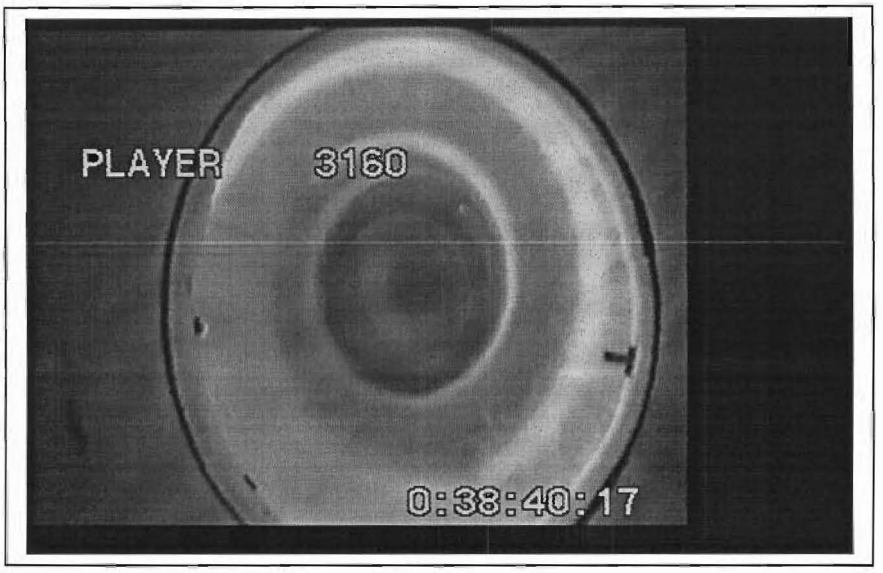

Figure 6-4 Flow of sand particles in cyclone D (cone angle 28°)

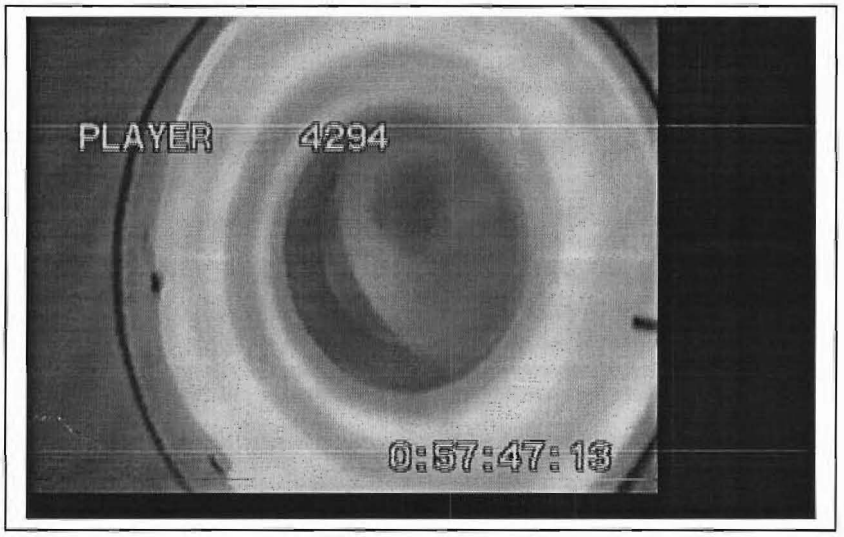

Figure 6-5 Flow of sand particles in cyclone E (cone angle 36°)

Although cyclone B shows no roping under the given conditions it was found that roping could also be triggered by increasing the airflow for the given solids feed rate. While high airflows promoted the onset of roping it was also found that where ropes existed when gas tangential inlet velocity was at 20 m s^{-1}, the ropes were found to disappear when the tangential inlet velocity was dropped to below 10 m s^{-1}. An increase in the centrifugal force would result in both an increase in normal contact force on the wall and an increase in the component of force acting up the

wall. There is therefore an increase in the frictional force acting on the particle. One possibility is that the centrifugal force alters the flow pattern by increasing the particle interaction with the wall. The other is that the particle motion down the wall is opposed by the centrifugal component. If we suppose that with different cones, for a given radius the gas velocity V_g close to the wall remains constant (albeit a small fraction of the former), then the centrifugal force on a particle will be constant. The different cone angles will then alter the components of this acting normal and along the wall. The net result of this increase in the component of the centrifugal force up the wall is that the particle is pushed up the wall or hindered in its travel down the wall. This action may cause an accumulation of particles and result in formation of particle clusters or ropes.

This phenomenon was observed with the 14° cone where no roping occurred at all when the gas inlet velocity was below 10 m s^{-1} but ropes formed in the upper cone when the gas velocity was above 30 m s^{-1}.

A grid was marked on the inside wall in the 36°-angle cone in order to understand this roping behaviour. The following observations were for a non-continuous feed run and therefore were only made on the inventory of solids held in the cyclone after stopping the feed. When air inlet velocity was decreased to values below 10 m s^{-1} ropes were found to disappear and the particles where dispersed on the walls of the cyclone. However when air velocity was increased above 10 m s^{-1} up to 35 m s^{-1} the particles were found to move up against the grid to form a rope. To preclude the possibility of solids elutriation from the bin the bin was emptied whilst the solids were circulating in the cyclone. During this period there was no observed change in flow pattern when the discharge end was at atmospheric pressure. When the bin was reinstalled there was no accumulation of the solids whilst the airflow was maintained. When feed to the cyclone was resumed the length of the rope was rebuilt and observed to stretch to the apex of the cone before discharging into the dust collection hopper. Using the horizontal grid as reference it was also found that the angle the ropes makes with the horizontal decreases to almost zero close to the apex (in 36 degree cone). This can be explained by the increase in the upward

directed component of the centrifugal force parallel to the wall as the radius is decreased.

While the above observations are applicable to sand, the same solids flow behaviour was found not to be applicable to the flow of silica gel. Silica gel showed no tendency for any roping. When the cyclone was operated with sand, a large inventory of solids was retained in the cyclone to the extent of maintaining the rope formation. However with silica gel, when solids feed was stopped all the particles in the conical section were drained into the dust collection hopper.

The density of silica gel is about 1200 kgm^{-3} and is about half that of sand which is approximately 2600 kgm^{-3}. The centrifugal force is given by the following expression

$$F_c = \frac{\pi}{6}\rho_p d_p^{\,3}\frac{V_p^2}{R} \qquad (6\text{-}1\text{-}1)$$

The component of the centrifugal force acting up parallel to the wall is $F_c \sin\alpha$, where α is half the total included angle of the cyclone cone.

For particles with the same velocity the centrifugal force acting on a sand particle would therefore be about twice that acting on a silica gel particle. Therefore the normal component of the centrifugal force and the component of the gravitational force for a sand particle will also be twice that acting on a silica gel particle. Silica gel will also have a relatively shorter response time to the gas drag. The response time is given by the following expression (Stock, 1996)

$$\tau = \frac{\rho_p d_p^{\,2}}{18\mu_g}K_t \qquad (6\text{-}1\text{-}2)$$

where $K_t = f(\mathrm{Re})$ and $K = 1$ for the Stokes regime and Re is the Particle Reynolds number.

The response time of sand is therefore approximately twice that of silica gel for the same particle size and particle velocity.

The properties of sand and silica gel particles are different. Silica gel particles have a higher coefficient of restitution compared with sand (ref. § 5.13). Given their higher coefficient of restitution, the collisions of silica gel particle with a wall will result in higher rebound velocities and lower energy losses compared to sand particles. Sand particles stay closer to the wall and provide an inelastic collision surface for more incoming particles.

The trajectory of a particle is also a function of the ratio C of the centrifugal force component up the wall and the component of aerodynamic gas drag force acting in the opposite direction down the wall, where C is given by

$$C = \frac{4}{3}\frac{V_p^2 \rho_p d_p^2}{C_D \rho_g R(V_g - V_p)(W_g - W_p)} \tan\alpha \qquad (6\text{-}1\text{-}3)$$

where V_g, $V_{p,}$, W_g and W_p are the gas tangential velocity, particle tangential velocity, gas axial velocity and particle axial velocity respectively. α is half the total included angle of cone.

The ratio of the centrifugal force to the drag force up/down the wall can be reduced to the following equation when all other factors except particle density, cone angle and radius are taken as constant

$$C = K\frac{\rho_p \tan\alpha}{R} \qquad (6\text{-}1\text{-}4)$$

where $K = \frac{4}{3}\frac{V_p^2 d_p^2}{C_D \rho_g (V_g - V_p)(W_g - W_p)}$

The ratio C increases with increase in cone angle and decrease in radius R. Equation 6-1-4 is a better representation compared to Equation 6-1-2 as it shows the dependency on the cone angle as well as radius.

Thus while sand particles form well-defined ropes in a 42° cone cyclone, silica gel particles in the same cyclone travel in a dispersed state as shown in Figure 6-6. It is interesting to note that although the particle trajectories are oriented in random directions the average angle of the trajectories is very small.

The inside conical section of cyclone D was covered with a thin layer of glue. Sand particles of size range 250–500 μm were sprinkled over the glued surface to form a rough monolayer of sand particles.

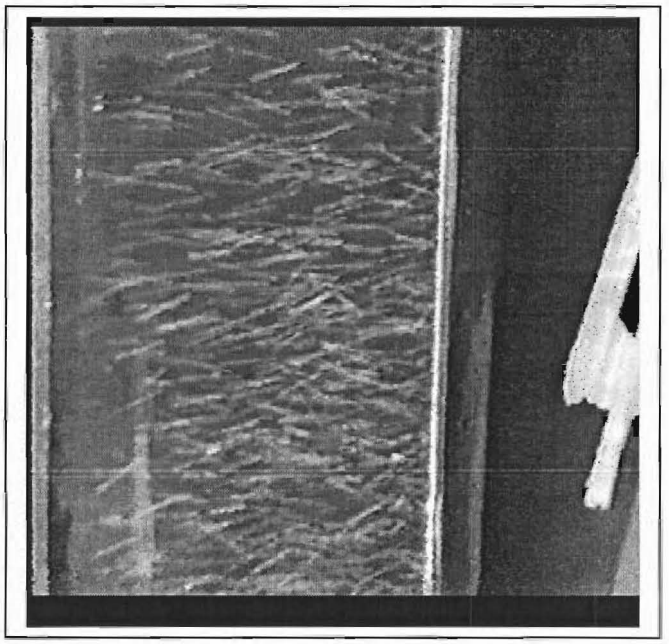

Figure 6-6 Silica gel particles in a 42°-cone cyclone, viewed through a window in the cone wall. Exposure time (1/215)s, Gas inlet velocity 20 ms^{-1}, Scale 1:1
Size range: 250-500 μm

When sand particles of the same size range as the coating material was fed into the cyclone at 9 g s^{-1} no roping was observed. This can be contrasted with the case when roping was observed in the same cyclone before the walls were coated with sand. It appears that the rough sand coated surface did inhibit or rather did not promote the occurrence of roping implying that friction by itself is not the cause of roping in flow of these particles.

Observations of the rope by eye were extremely difficult, as the ropes appeared to be spirals moving up and down. To aid in the observation of the rope a high frame rate JC Lab HSC– 250x2 video camera with an HSR-200s high-speed recording

video recorder capable of recording at speeds of up to 200 frames/s was used. It was found that the rope is not continuous but rather it breaks down as it moves along the wall of the cone, forming a lead and tail. This is contrary to what is reported by Kiselnikov et al. (1971) who found the rope to be continuous. It is not strange therefore to come to this conclusion without probably the aid of a high-speed camera. The discontinuous nature of the rope is chronicled by a series of time coded photographs shown from Figure 6-7 to Figure 6-15 for cyclone D. The time interval between successive frames is 0.017s. Figure 6-7 is taken as the base with time = 0s. The lighter regions show the existence of sand. As time progresses the movement of the sand can be followed. Distinct tails of the rope can be seen in these figures. The rope shown in Figure 6-7 completely discharges into the dustbin after a time of 0.13 s (Figure 6-14). As the first rope completely discharges another one is following its wake (Figure 6-15).

A time plot of concentration of particles at the solids discharge end of the cyclone can also show the intermittent nature of the rope. The particles are collected at the discharge end of the cyclone by a sampling nozzle as described in the experimental section (Chapter 2). Figure 6-16 shows the distribution of particles for cyclones B and E. For cyclone E where ropes occur there is a wide variation in the number of particles collected compared to cyclone B that shows little or no roping where the particle distribution is fairly uniform.

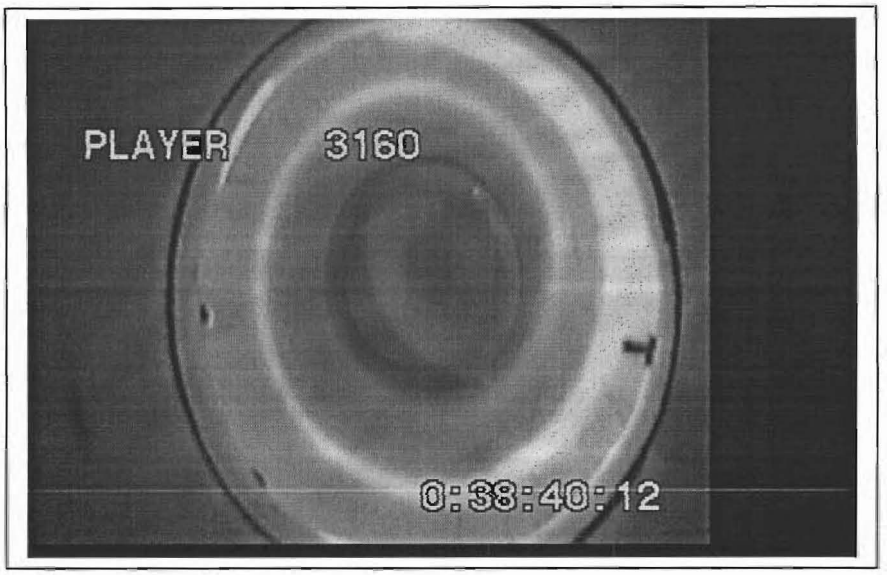

Figure 6-7 Flow of sand in cyclone D; time = 0s

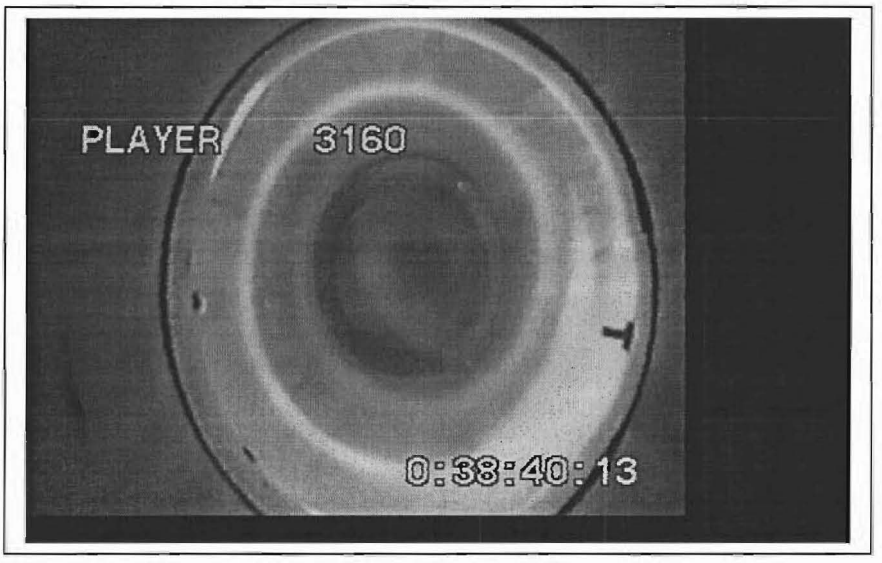

Figure 6-8 Flow of sand in cyclone D; time = 0.02s

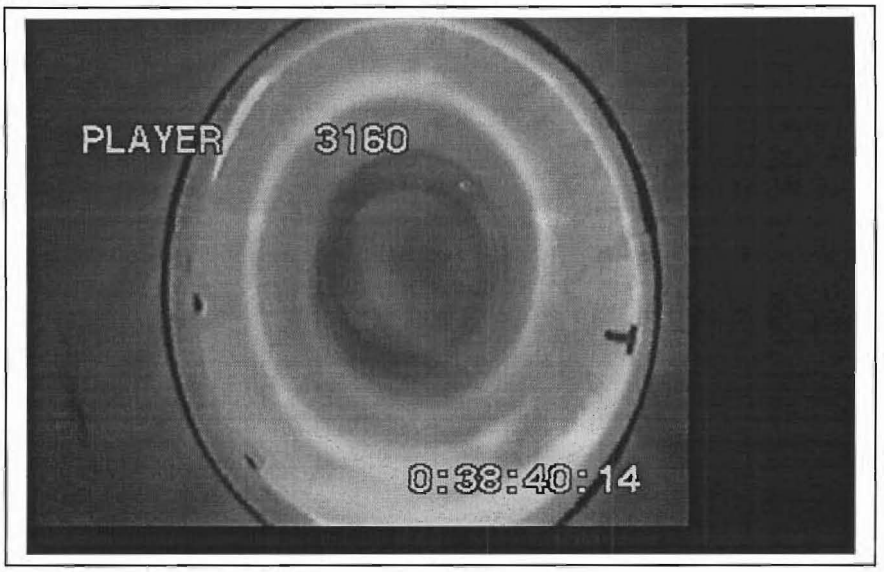

Figure 6-9 Flow of sand particles in cyclone D; time = 0.05s

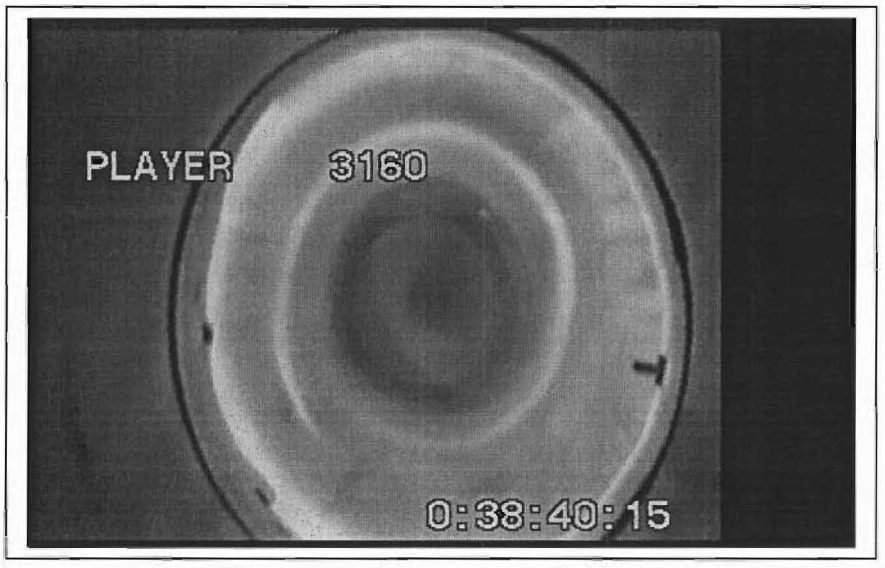

Figure 6-10 Flow of sand particles in cyclone D; time = 0.07s

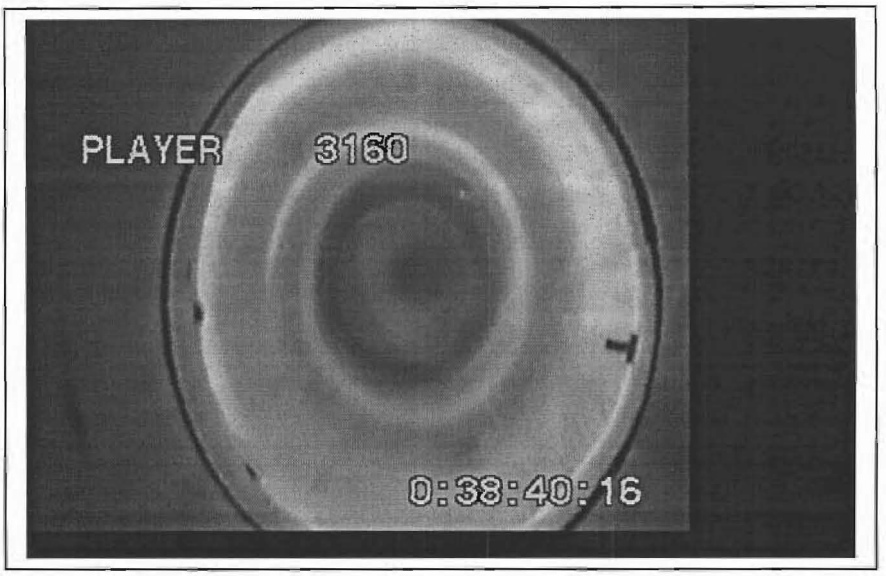

Figure 6-11 Flow of sand particles in cyclone D; time = 0.08s

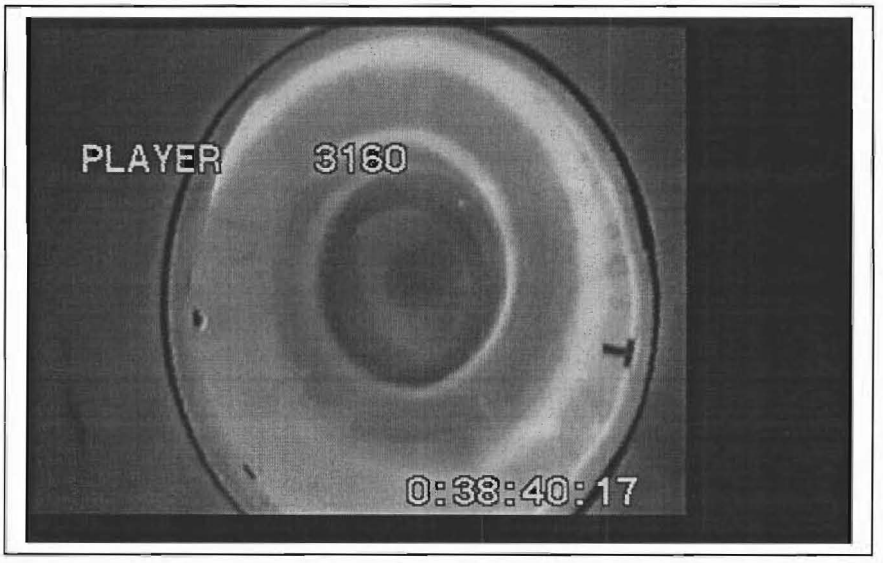

Figure 6-12 Flow of sand particles in cyclone D; time = 0.1s

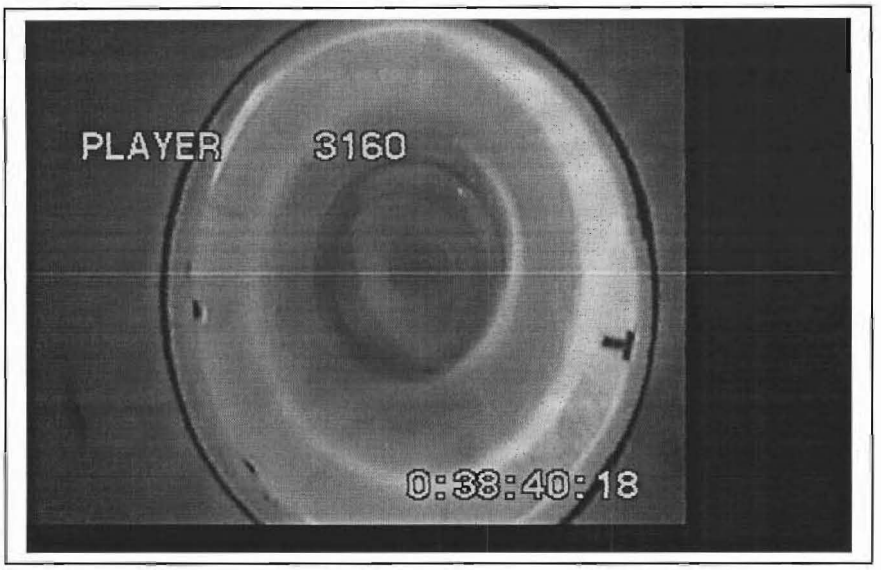

Figure 6-13 Flow of sand particles in cyclone D; time = 0.12s

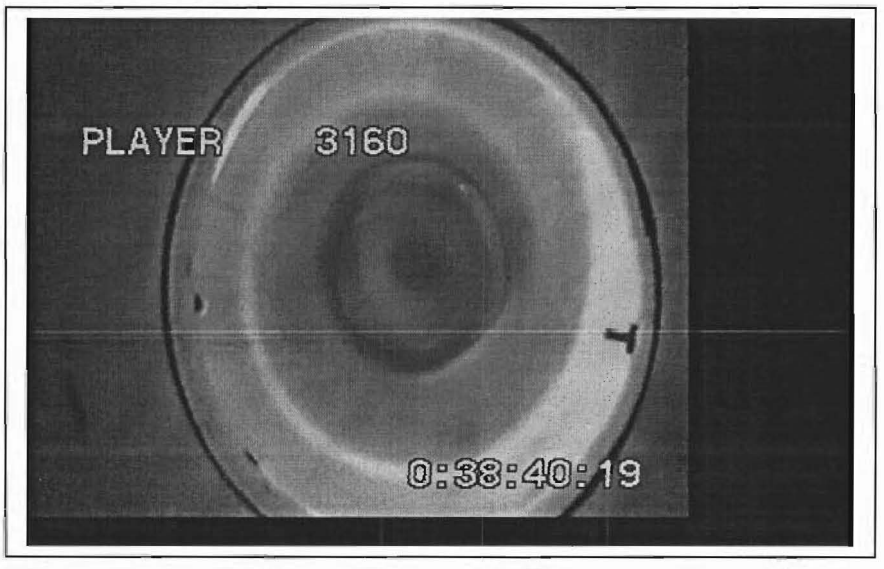

Figure 6-14 Flow of sand particles in cyclone D; time = 0.13s

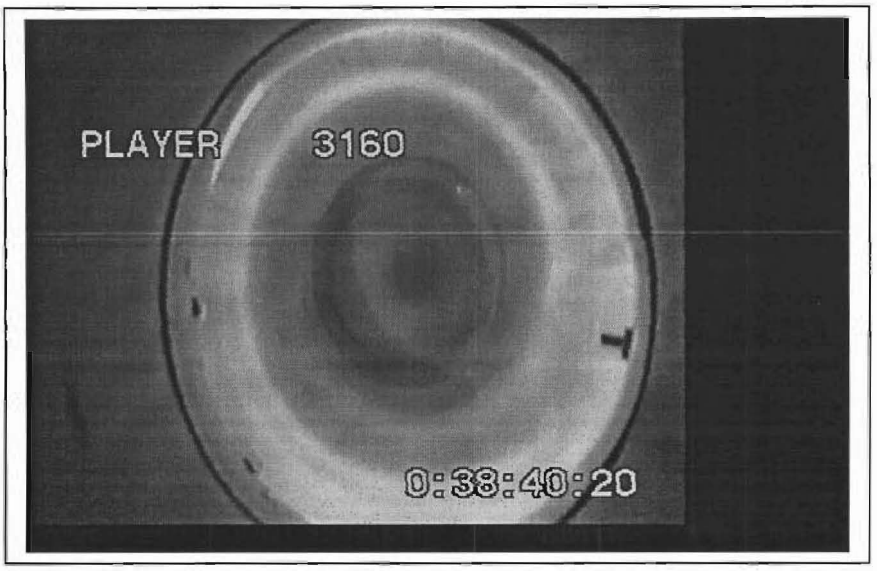

Figure 6-15 Flow of sand particles in cyclone D; time = 0.15s

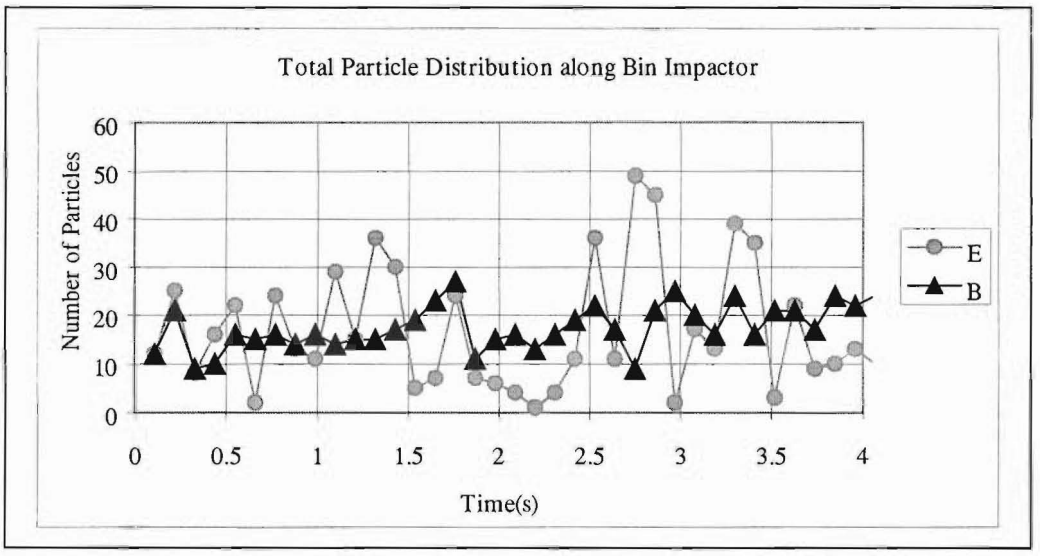

Figure 6-16 Total particle distribution at apex for cyclones B and E

These observations were at a gas inlet velocity of 20 m s^{-1} with sand of size range 250–500 μm and flow rate of about 11 g s^{-1}. For the six different conical sections investigated with a range of total included angle from 10° to 42° the mechanism of

particle travel was found to change from bouncing where the particles were seemingly well dispersed, to flow where the particles formed strands moving along the wall. Particles in the strands maintaining contact with the wall can be treated as sliding and this is the phenomenon of roping as discussed and illustrated (Figures 6-7 to 6-15). For a given gas flow rate an increase in cone angle is also accompanied by an increase in the centrifugal force acting on a particle at a particular radial distance. The 20° cone was found to be transitional for non-roping (ie. dispersed) to roping. Fully developed ropes with diameters of about 15mm were observed with the 36°-angle cone. The non-rope phase can be said to travel in the cyclone by bouncing on the walls as the particles are spread on the walls. This is in contrast to roping where the particles are concentrated in narrow bands with significant inter-particle interactions and particle-wall interactions. However, when the cyclone was fitted with a conical section with an included angle lower than 20° roping was also observed to occur by increasing the gas inlet velocity. This was observed with the 14° cone where no roping occurred when the gas inlet velocity was below 10 ms^{-1}.

It is important to understand these two different mechanisms, as the nature of the flow would impact on heat transfer between wall and particles. If the particles are sliding on the wall there is good heat transfer between the wall and the particle and this situation is obtained in roping travel where a significant proportion of the particles will always be in contact with the wall. However if the particle is repeatedly bouncing on the walls the mechanism of heat transfer will be different as the contacts between the wall and the particle are expected to be of short duration. Although particle-particle interactions also occur it is highly unlikely a significant amount of heat will be exchanged by this mechanism. On the other hand transfer between air and the particles is likely to be higher for cases in which particles travel in a dispersed state as compared to the roping mechanism.

6.3.1. Velocity of rope

Photographs taken with the high-speed camera were used to estimate the total velocity of the rope for a continuous feed of about 9 g s^{-1} at a vertical position about one-third the height of the conical section from the apex (discharge end of cone) in cyclones D to F. It was not possible to obtain the complete velocity flow field because of the limited field of view. Analysis of the high-speed video recordings in the case of cyclone F (42°– cone) showed that particles closer to the wall travelled at lower velocity and particles on the wall had zero velocity. The average velocity of a particle can be assumed to be equal to the velocity of the rope. Figure 6-17 to Figure 6-20 show the pairs of photographs with a time difference of 0.0167s. The rope tail at time = 0s is identified by position A and after time = 0.0167s the new position is identified by B. The distance (L) the rope travels in this time interval is measured and the velocity V is calculated from

$$V = \frac{L}{0.0167} m s^{-1} \qquad (6.1\text{-}5)$$

L is the projected distances of the rope on the wall.

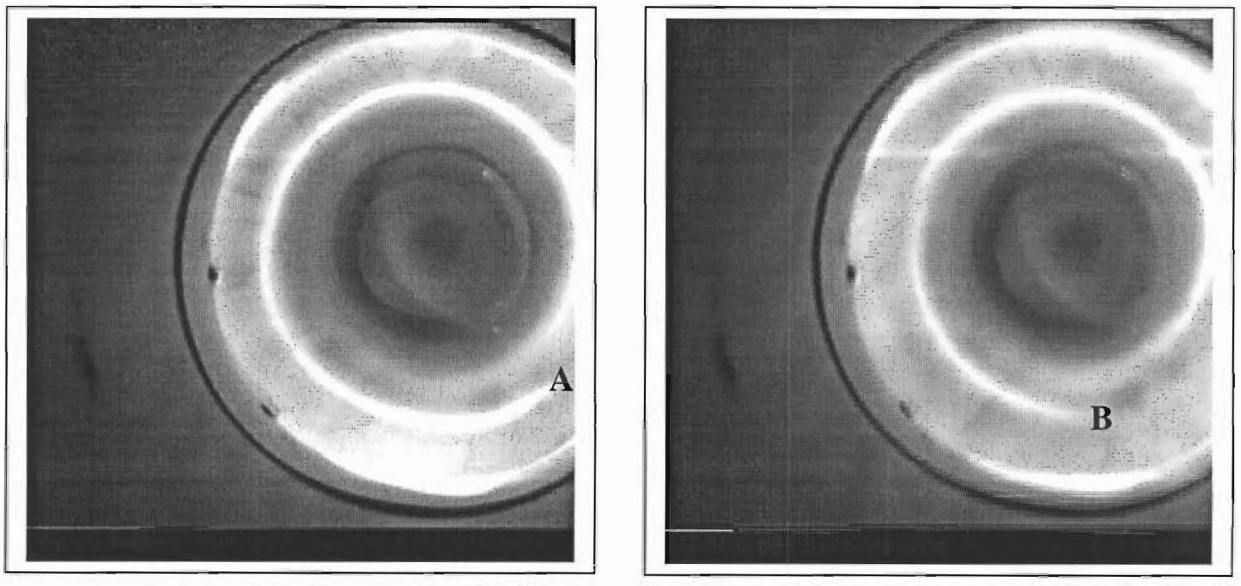

A: time = 0 **B: time = 0.017s**

Figure 6-17 Rope in cyclone D

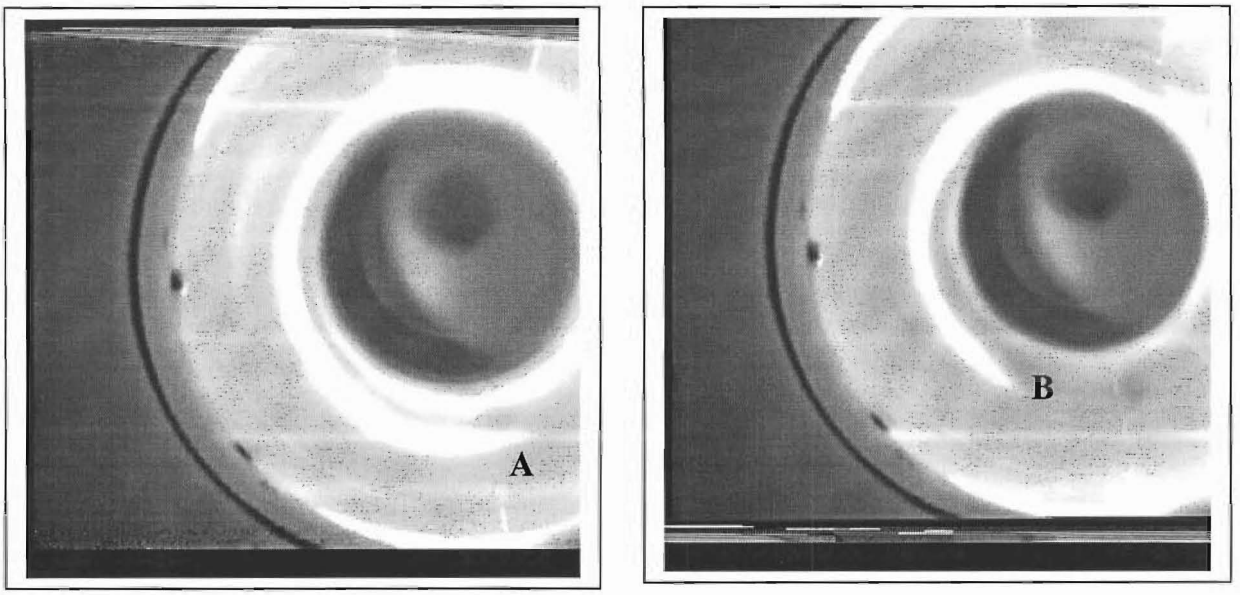

A: time = 0s **B: time = 0.0167s**

Figure 6-18 Rope in cyclone E

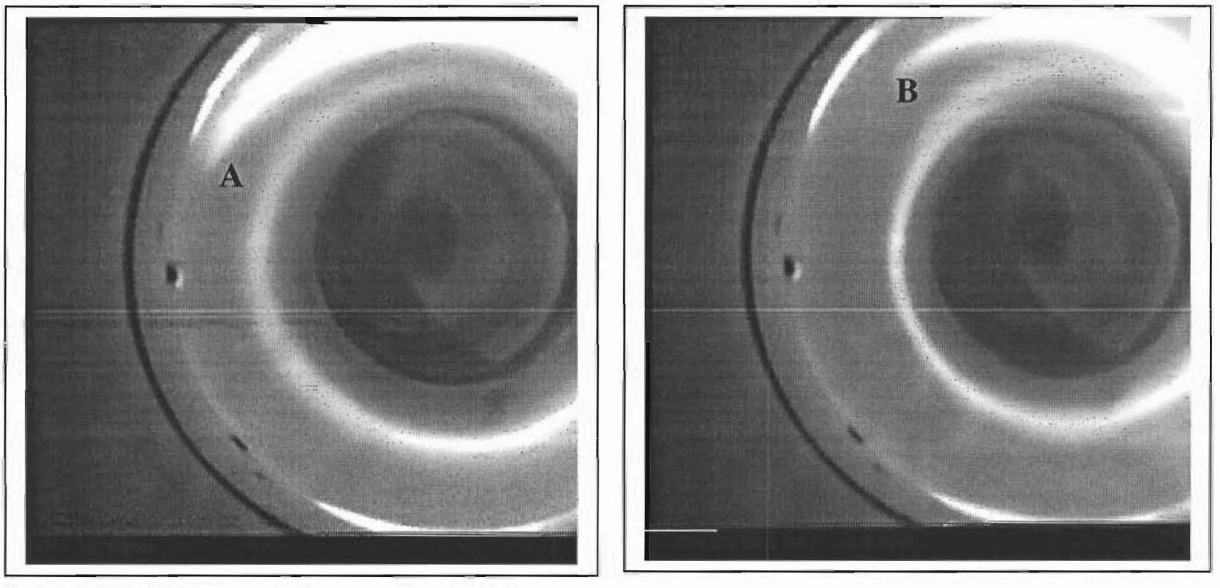

A: time = 0s **B: time = 0.0167s**

Figure 6-19 Rope in cyclone F (sand 250–500-μm)

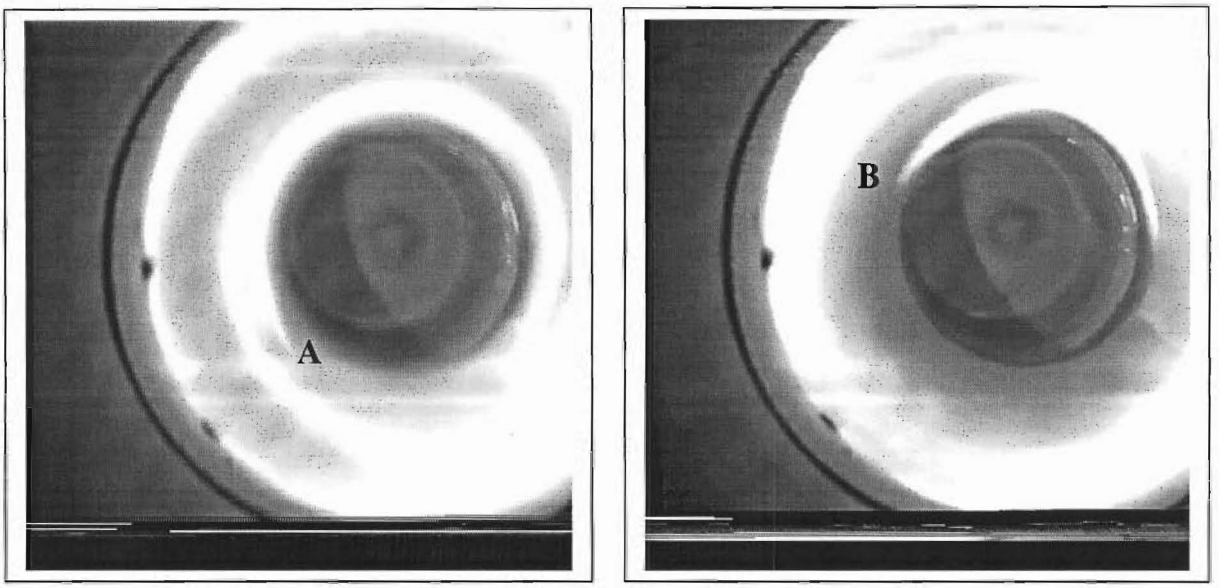

A: time = 0s **B: time = 0.0167s**

Figure 6-20 Rope in cyclone F (sand 150-210-μm)

The *Motion Analysis* tool of the Optimas® (ver. 5) image analysis software evaluated the velocity of the rope. The velocity of the rope was also evaluated manually from Figure 6-17 to Figure 6-20. The results of velocity calculations are shown in Table 6-1.

Table 6-1 Total velocity of sand particles in ropes in different cyclone geometries
Size range: 250–500 μm
Gas tangential inlet velocity = 20 m s^{-1}

Angle of Cone (degrees)	Velocity (ms^{-1})	
	Optimas®	Calculated
20	4.6	-
28	4.2	3.5
36	4.2	3
42	3.2	2.5

The velocity of the sand particles of size range 150–210 μm in the 42 degree cone cyclone under the same conditions as above was 5.1 ms^{-1}. As shown in Table 6.1 as the cone angle is increased there is a corresponding decrease in the particle velocity

in the cyclone. When the cone angle is increased by 50% from 28° to 42° the velocity decreases by approximately 25%. When the average particle size is decreased by almost half from a size range of 250– 500 μm to 150– 210 μm the average particle velocity is increased by the same factor. The angle of the rope with the horizontal is estimated at no more than 5° from the horizontal in the 42-degree cone.

The above velocities for sand particles of size range 250-500 μm are estimated for a rope. The velocities of individual silica gel particles of size range 250-500 μm in a 42° cyclone were measured from Figure 6-6, which showed the streaks of individual particles. An average particle velocity was estimated to be about 2 ms^{-1} and inclined at an average angle of about 7.5° from the horizontal. Figure 6-6 shows wide variation in angle, some moving up, and some moving down resulting in dispersion.

6.2. Sliding Particle Model (SPM)

The work of Lebedev et al. (1979) is a pioneering work on the modelling of particulate flow in a cyclone. In his model Lebedev (1979) considered a particle sliding on the wall of the cyclone. As flow in a cyclone is chaotic in nature any modelling of particulate flow in these systems has to be based on assumptions which can only be postulated through experimental observations. In an earlier paper Kiselnikov et al. (1971) provide an experimentally based concise description of the movement of particles in a cyclone and the forces influencing the behaviour of these particles. The main forces influencing the trajectory of the particles in the cyclone were taken to be the aerodynamic gas drag force F_D, centrifugal force F_c, gravitational force F_g, frictional force F_f and the normal reaction force F_N. In this work, Lebedev et al. did not consider the mutual interactions between particles. Each particle was therefore assumed to behave independently of its neighbours.

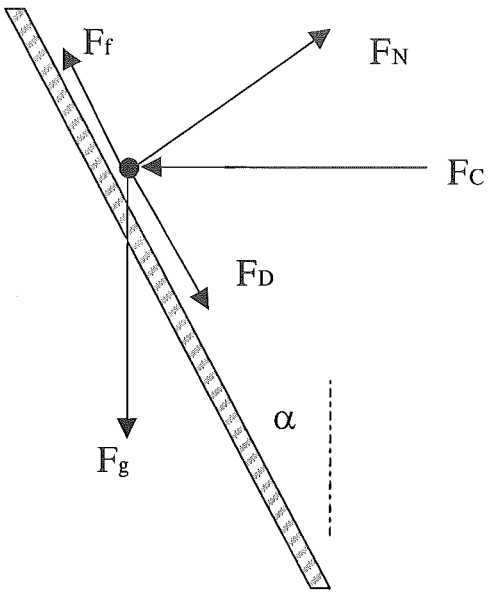

Figure 6-21 Force acting on a particle, as used by Lebedev et al. (1979).

A physical model showing the forces acting on a particle on the wall of the cyclone is given in Figure 6.21. In Figure 6-21, α is the angle the cone makes with the

vertical. In their treatment Lebedev et al. (1979), Lebedev et al. (1987) and Smirnov et al. (1990) also consider the buoyancy force acting on a particle. However, for this work the Archimedes force will be neglected as it constitutes only about 0.1 % of the force of gravity for silica gel which has the lowest density.

Where particles are travelling in a rope a force balance can also be made on an element of the rope as shown in Figure 6-22.

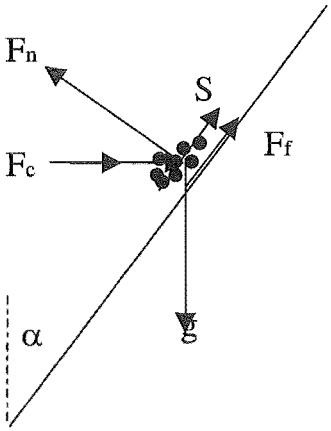

Figure 6-22 Force balance on rope

S is the shear stress due to (a) particles landing from the free stream and (b) gas drag force, F_n is the normal reaction force on the wall of the cyclone cone, F_f is the frictional force, g is the gravitational force and F_c is the centrifugal force.

Under steady state conditions a force balance can be made on the rope as shown in Figure 6-22. If we consider a differential element of the rope of plan area δA and thickness δL, then the volume of this element is $\delta A \delta L$. A force balance can be made on this element. It can be assumed that a dynamic equilibrium also exists due to the simultaneous lift off and deposition of particles on the rope.

The state of equilibrium can be described parallel to the wall along the line of the conical generator by the following equation, for a generalized steady state flow, equating the downward gravity force with the forces acting upwards;

$$\partial A\partial L(1-\varepsilon_g)\rho_p g\cos\alpha = S\delta A + \partial A\partial L(1-\varepsilon_g)\rho_p \frac{V_p^2}{R}\sin\alpha + \mu F_N \partial A\partial L(1-\varepsilon_g)\rho_p$$

(6.2-1)

where ε_g is the voidage, ρ_p is the particle density, and F_N is force per unit mass

The forces in Figure 6.21 can be given by the following expressions *based on unit mass*:

Now if we assume a single particle then $S\delta A = F_D$ (if the impaction of incoming particles is ignored).

Aerodynamic drag force (for a sphere):

$$F_D = \frac{3}{4} C_D \frac{\rho_g}{\rho_p d_p} \mathbf{V}_{rel}^2 \qquad (6.2\text{-}2)$$

C_D is the drag coefficient, d_p is the particle diameter, ρ_p is the particle density and ρ_g is the density of air, V_{rel} is a relative velocity vector quantity and is given by

$\mathbf{V}_{rel} = \mathbf{V} - \mathbf{V}_p$

Gravitational force: $F_g = g$

Centrifugal force: $F_c = \frac{V_p^2}{R}$

Normal reaction force: $F_N = g\sin\alpha + \frac{V_p^2}{R}\cos\alpha$

Frictional force: $F_f = \mu F_N$

The equations of motion can be written in polar cylindrical coordinates

z, r, φ.

In the axial direction:

$$\frac{dW_p}{dt} = g + \frac{3}{4}\frac{\rho_g}{\rho_p d_p}\mathbf{V}_{rel}(W_g - W_p) - F_N\sin\alpha - \mu F_N \frac{W_p}{\|\upsilon_p\|} \qquad (6.2\text{-}3)$$

In the tangential direction

$$\frac{dV_p}{dt} = \frac{3}{4} C_D \frac{\rho_g}{\rho_p d_p} \mathbf{V}_{rel} (V_g - V_p) - \mu F_N \frac{V_p}{\|\upsilon_p\|} \qquad (6.2\text{-}4)$$

In the radial direction

$$\frac{dU_p}{dt} = \frac{V_p^2}{R} + \frac{3}{4} C_D \frac{\rho_g}{\rho_p d_p} \mathbf{V}_{rel} (U_g - U_p) - \mu F_N \frac{U_p}{\|\upsilon_p\|} - F_N \cos\alpha \qquad (6.2\text{-}5)$$

with $W = \frac{dz}{dt}$, $V = R\frac{d\varphi}{dt}$ and $U = \frac{dR}{dt}$

where $\mathbf{V}_{rel} = [(V_g - V_p)^2 + (W_g - W_p)^2 + (U_g - U_p)^2]^{1/2}$,

$$\|\upsilon_p\| = (V_p^2 + W_p^2 + U_p^2)^{1/2}$$

V_g, W_g *and* U_g are the gas velocity components in the tangential, axial and radial directions respectively while V_p, W_p and U_p are the particle velocity components in the tangential, axial and radial directions respectively.

The system of equations was solved numerically and the experimental data was stated to be in good agreement with the mathematical model (Lebedev et al. 1979) although detailed results were not presented.

In their solution Lebedev et al. (1979) did not consider the effect of solid particles on the gas velocity profile. The strong coupling between the particulate and gas phases in cyclone two phase flow is well documented in literature (Yuu et al. 1978; Parida and Chand, 1980). This exchange of energy between the two phases results in a decrease in the tangential velocity of the gas. Smirnov et. al (1990) in their analytical study correct for this exchange in kinetic energy in their calculation of tangential velocity.

Cremasco et al. (1996) using a model based on Lebedev (1979), present a model for the flow of particles in a cyclone reactor. In their model Cremasco et al. (1996) consider the effect of particles on the friction coefficient between the solid particles and gas phases by introduction of the porosity function. The gas friction coefficient on the wall is given by an empirical correlation valid for gas Reynolds numbers greater than 1000. This model assumes that the particle velocity vector is in the same direction as the gas velocity vector. Experimental evidence in this work suggested that the particle flow pattern was a function of the angle of the cone. It is therefore important to incorporate the necessary boundary conditions to take account of this change in flow.

Cremasco et al (1996) also assume, as did Lebedev (1979) that the particles travel on the wall of the cyclone. Silva and Nebra (1994) use the experimental evidence of Ranz (1985) to justify this approach. Ranz (1985) in his study of wall flows in cyclones observed and documented a photograph of the spiral pattern of particles flowing on the wall of the cyclone. Similar observations were made in this study, and several other authors (Lebedev et al. 1971; Yuu et al. 1978; Rajendra and Abrahamson 1994) also report this phenomena. Figure 6-23 shows the spiral patterns otherwise known as ropes.

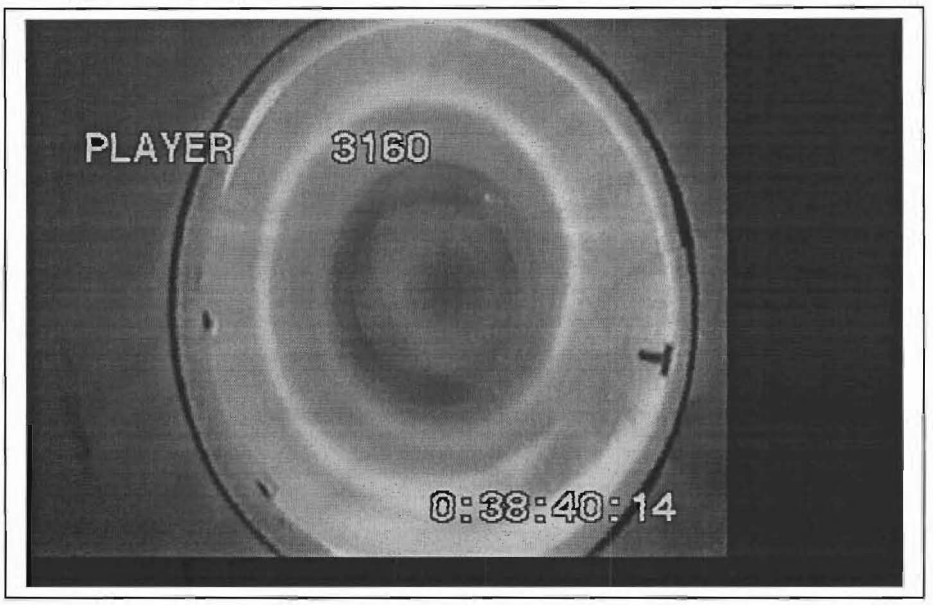

Figure 6-23 Spiral patterns in Cyclone

The photograph in Figure 6-23 was taken from the top of the cyclone as was the case with Ranz (1985) and clearly shows the spiral patterns on the wall of the cyclone. Examination of the photography from a macroscopic point of view will seem to lend credibility to the theory that particles slide on the wall of the cyclone. However closer photographs identifying the individual particles were taken from the bin of the cyclone. The experimental set-up for this facility is shown in Figure 6.24.

These photographs clearly show that at the discharge end of the cone, the majority of particles do not slide on the wall but actually travel by bouncing from the wall when the angle of the cone is less than 20°. Figures 6.25 and 6.26 show the sand and silica particles just before their exit from the cyclone into the dust collection hopper.

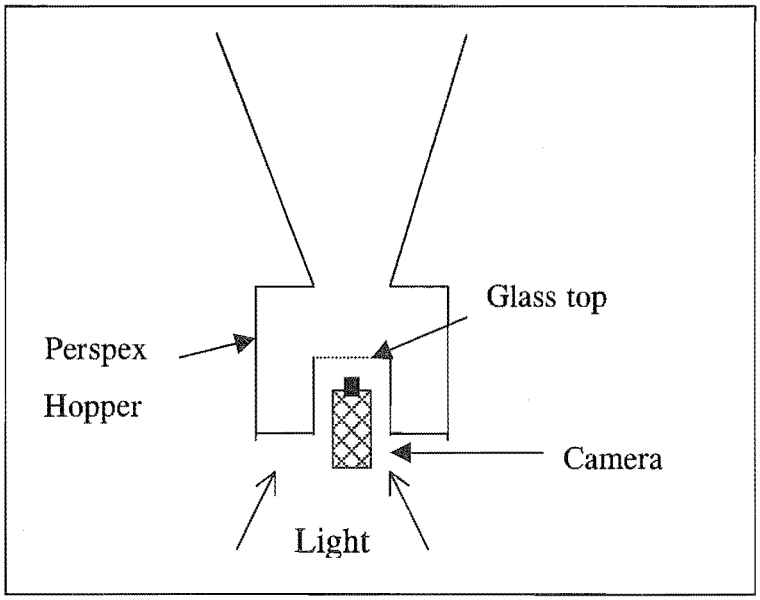

Figure 6-24 Set-up for photographs taken at apex of cyclone

Figure 6-25 shows that for the cyclone with a cone angle of 14°, sand particles of size range 150–210 μm are confined to a radial distance of about 10 mm from the wall boundary. Figure 6-26 shows the result for silica gel where the particles are within a radial distance of about 16 mm from the wall boundary.

This scatter of particles depends on the interaction between the particles and the wall. Silica gel particles are more scattered due to their high bounce when compared to the sand particles.

As the centrifugal force is directly proportional to the density for a given particle size and particle velocity, the centrifugal force acting on a sand particle is about twice that acting on a silica gel particle of similar size. In the presence of a few particles on the wall the particles bounce off from the wall of the cyclone at a large angle.

Observations of particles in the cyclone also where made from the top of the vortex finder through a glass window. The trajectories of silica gel particles, especially in the size range 700–850 μm were observed to cross as far in as the inner vortex of the cyclone. However when the number of particles is increased inter-particle

interactions are expected to influence the angles at which the particles can bounce off from the wall, decrease them and thus influence the particle trajectories. The tangential inlet velocity for the images shown in Figures 6.25 and 6.26 was 20 m s^{-1}. It is expected that as the tangential velocity is further increased, the resultant increase in the centrifugal force will cause particles to stay close to the wall approaching sliding motion. However the practical limit for the gas inlet velocity into cyclones in normal operation is below 20 m s^{-1}.

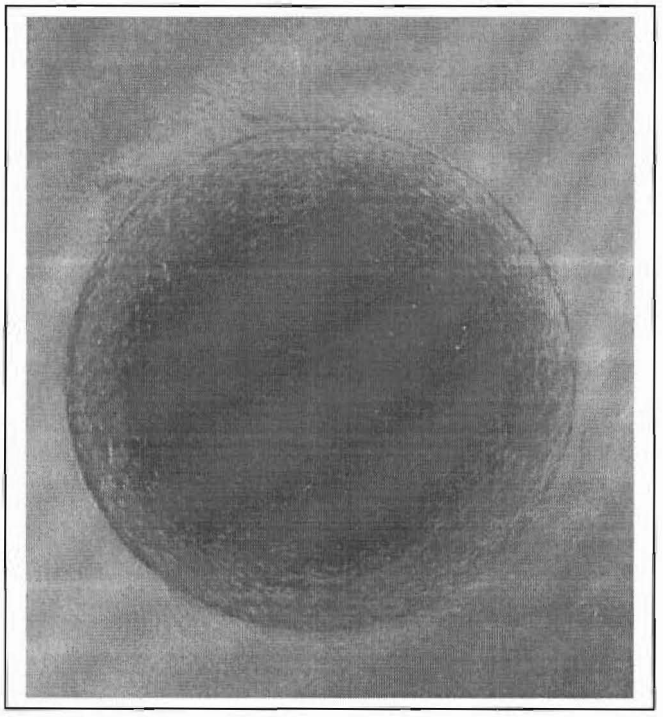

Figure 6-25 Sand particles at the apex of cyclone viewed from the dust collection hopper, for a gas inlet velocity of 20 m s^{-1} and sand loading of 12 g s^{-1}; Cone angle 14°

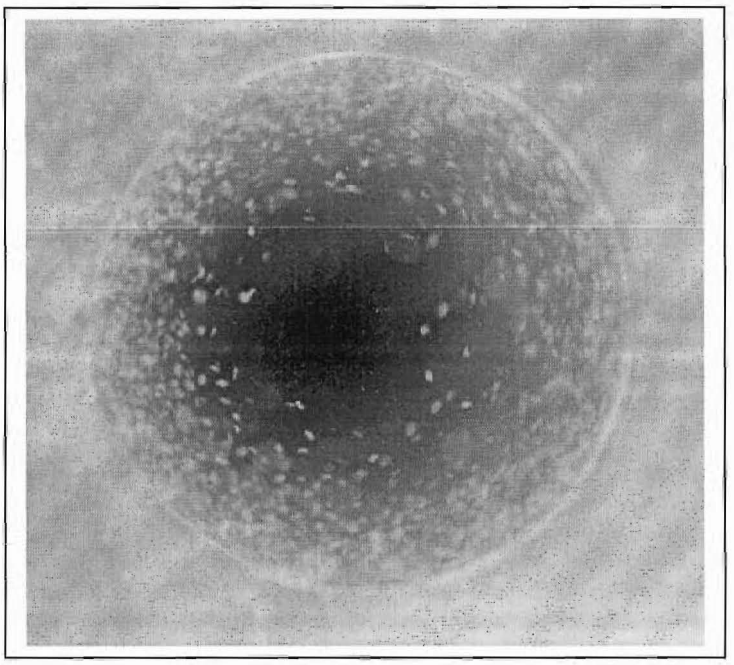

Figure 6-26 Silica gel particles viewed from the dust collection hopper

When particles are acted upon by a centrifugal force there is an opposing drag force due to the radial gas drag. In the radial direction the motion of the particle in free flight after a contact with the wall is governed by the following equation

$$\frac{dU_p}{dt} = \frac{V_p^{\,2}}{R} - \frac{3}{4} C_D \frac{\rho_g}{\rho_p d_p} \mathbf{V}_{rel} \left(U_g - U_p \right)$$

(6.2-6)

While the work of Lebedev (1979) is a milestone in modelling particle flow in a cyclone, the limitation of the model (Lebedev, 1979) is clearly obvious. It has been shown that during passage of particles through a cyclone there is significant mechanical interaction between the particle and the wall. As the particles interact with the wall in the form of bouncing they will have a path and velocity quite different from that of constant contact with the wall. Instead of experiencing constant friction with the wall, they lose kinetic energy at each interaction. This different mode of travel will therefore influence the particle residence time. Therefore any model which attempts to physically represent the actual flow of granular material in the cyclone should consider the phenomenon of particle

bouncing on the walls. There is a need therefore to find a model that will complement the work of Lebedev (1979).

As a preliminary to development of a model that takes account of the bouncing behaviour of particles it was necessary to look at simple cases of the bouncing phenomena itself. To investigate this bouncing phenomenon, simple bouncing tests were performed by dropping the particles on to an inclined steel plate (§ 5-13). Information gained from these simple bouncing tests could also provide answers to trends in experimentally measured particle residence times in the cyclone and supply parameters for a numerical model.

When a stream of sand particles strike a surface they remain close to the surface on reflection. These inelastic collisions between the wall and the sand particles have the effect of maintaining a layer of particles on the wall. Subsequently more particles coming from the free stream have their kinetic energy absorbed by this initial layer resulting in an accumulation of particles. The collision of a particle with a surface randomly composed of similar particles is highly inelastic (White, 1986). The collision with a fixed layer will also be different with a loose layer, as the latter will tend to move after a collision and therefore absorb more energy.

For the particles sliding on the wall, frictional force between particles is significant and should result in a slowing down of the particles. In addition to the mechanical interactions between the particle and wall there is also an alteration of hydrodynamic forces when the particle stays in the wall region (Figure 6-27). Drag force acting on particles in the wall boundary layer is lower compared to that acting on particles in the free stream. Hence particles travelling close to the wall are likely to be travelling slower compared to the dispersed phase.

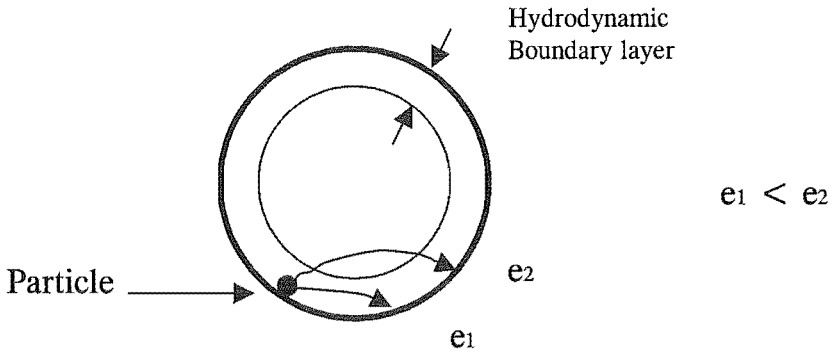

Figure 6-27 Mechanical and hydrodynamic particle and wall interactions for a bouncing particle

White (1986) developed simple empirical expressions for the relationship between the impact and lift-off velocities and angles respectively for the bouncing of sand particles on a surface of like fixed particles. The relationships are

$$V_{LO} = 80\left[1 - \exp\left(-\frac{1}{80}V_{imp}\right)\right] \qquad (6.2\text{-}7)$$

$$\alpha_{LO} = 21.8\alpha_{IMP}^{0.316} \qquad (6.2\text{-}8)$$

where V_{LO} is in cms^{-1} and V_{imp} is in cms^{-1}, α_{IMP} and α_{LO} are in degrees.

The impact and lift-off velocities and angles as defined by White (1986) are shown in Figure 6.28.

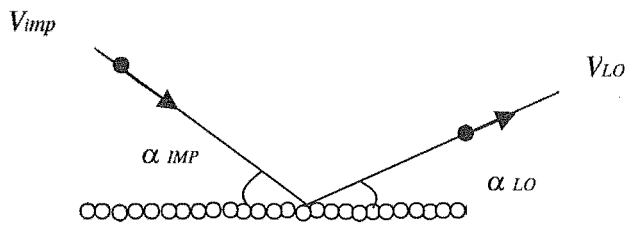

Figure 6-28 Impact and lift-off velocities and angles terminology used by White (1986)

The velocity at impact V_{imp} (ref. § 5.13, Figure 5.13-7) could not be determined from our experiments. However simple calculation was made for free fall from rest 400 mm above neglecting drag force, to give an impact velocity of 2.8 ms^{-1} from $V = \sqrt{2gh}$. The impact angle α_{imp} was measured from Figure 5.13-7 and found to be 50°. Equation 6.2-8 was applied to determine the lift of angle α_{LO} and yielded a value of 75° for the lift off angle. Although Figure 5.13-7 is not very clear a limit can be drawn for the largest angle possible and this is about 60°. For sand particles on a steel surface (Figure 6.13-4) the maximum measured lift off angle is about 50° which can also be compared to the calculated angle from Equation 6.2-8 which yield a value of 75°. There is discrepancy between the correlations of White (1986) for the lift-off angles and velocities and the experimental quantities found here.

The lift-off or reflected velocity and lift-off angle of a particle is dependent on the coefficient of restitution between the particle and wall. The velocity change of the particle in the direction of flow is a function of the coefficient of friction and the velocity change perpendicular to the direction of particle flow. Silica gel particles on account of their high coefficient of restitution will bounce off at a large angle and therefore the momentum change in the direction normal to the impact plane is large. The momentum change in the direction of flow (parallel to plate) is a product of the momentum change in a direction normal to the plate and the coefficient of friction.

The coefficient of friction between silica gel particles and mild steel is lower compared to that between sand particles and mild steel (ref. § 5.13). From the simple bouncing tests as illustrated in Figures 5.13-3 and 5.13-4 it can be deduced that the momentum change perpendicular to the plate is higher for silica gel compared to sand. Therefore the momentum change parallel to the plate will be higher for sand compared to that for silica gel because of the higher coefficient of friction and y-momentum change for sand. Therefore when sand and silica gel particles are travelling in a cyclone, sand particles will lose a larger proportion of their initial energy at each impact. Sand particles are therefore expected to travel at a lower velocity compared to silica gel particles.

Generally the collision of a particle with a surface can be treated by consideration of linear and angular momentum conservation laws as illustrated in Figure 6-29.

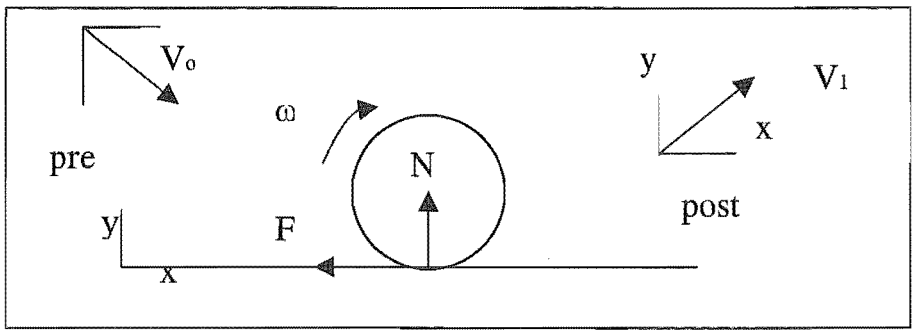

Figure 6-29 Impact of a spherical particle on a plane surface

N and F represent the normal and frictional force respectively and ω is the angular velocity of the particle. If the particle is approaching at a velocity of V_0 then the x and y components are V_{0x} and V_{0y} respectively and the reflected velocity and its components are V_1, V_{1x} and V_{1y} respectively. ω_0 and ω_1 are the angular velocities before and after collision.

Linear momentum change (Crowe et al., 1998) gives

$$m\mathbf{V}_1 - m\mathbf{V}_0 = \int_{t_1}^{t_2} \mathbf{P}\,dt \tag{6.2-9}$$

where **P** is the impulsive force vector, with components F and N

Angular momentum change

$$I\omega_1 - I\omega_0 = \int_{t_1}^{t_2} \mathbf{P}r\,dt \tag{6.2-10}$$

where I is the moment of inertia and r is the radius of a spherical particle. For particles with large values of circularity (see Chapter 5), the existence of a velocity gradient in the gas will also result in a torque acting on the particle causing a spinning action, but that is not considered here.

Assuming there is slip between the contact surfaces, the momentum change in the x direction is given by

$$\Delta V_x = V_{1x} - V_{0x} = \int_{t_0}^{t_1} \frac{F dt}{m} \tag{6.2-11}$$

and the momentum change in the y direction is given by

$$\Delta V_y = V_{1y} - V_{0y} = \int_{t_0}^{t_1} \frac{N dt}{m} \tag{6.2-12}$$

while the change in angular momentum is given by

$$Iw_1 - Iw_0 = \int_{t_0}^{t_1} Fr dt \tag{6.2-13}$$

$$F = \mu N \tag{6.2-14}$$

The coefficient of friction for the collision of silica gel with a mild steel surface can be obtained from Figure 5.13.3 by momentum change considerations. From Equations 6.2-11 to 6.2-12 the relationship between the momentum change in the y direction and the x direction is given by

$$\Delta V_x = -\mu \Delta V_y \tag{6.2-15}$$

where ΔV_y and ΔV_x are the velocity changes per unit mass in the y direction and x direction respectively and μ is the coefficient of friction between the particle and the steel surface.

Table 6-2 Post and pre-collision velocities and momentum consideration for silica gel

V_x^0	V_x^1	ΔV_x	V_y^0	V_y^1	ΔV_y
2.15cos55 =1.23	1.24cos75 = 0.32	1.23-0.32 = 0.91	-2.15sin55 = -1.76	1.24sin75 = 1.20	1.20 - (-1.76) = 2.96

therefore

$$0.91 = 2.96\mu$$

The coefficient of kinetic friction is therefore approximately equal to 0.30.

The coefficient of restitution for silica gel $e = -\frac{1.2}{1.76} = 0.7$

The parameters for glass beads are calculated from Figure 6-30

Table 6-3 Post and pre-collision velocities and momentum consideration for glass

V_x^0	V_x^1	ΔV_x	V_y^0	V_y^1	ΔV_y
2.15cos55 =1.23	1.24cos76 = 0.30	1.23-0.30 = 0.93	-2.15sin55 = -1.76	1.24sin76 = 1.20	1.20 - (-1.76) = 2.96

Therefore from Equation 6-18

$$0.91 = 2.96\mu$$

The coefficient of friction for contact between glass beads and the steel plate is similar to that for silica gel and is equal to 0.31.

The coefficient of restitution for glass beads is also equal to 0.7.

The parameters for sand particles are calculated from Figure 5.13-4.

Table 6-4 Post and pre-collision velocities and momentum consideration for sand

V_x^0	V_x^1	ΔV_x	V_y^0	V_y^1	ΔV_y
2.15cos55 =1.23	0.79cos35 = 0.65	1.23-0.65 = 0.58	-2.15sin55 = -1.76	0.79sin55 = 0.45	0.45 – (-1.76) = 2.21

$$\Delta V_y = 0.45 - (-1.76) = 2.21$$

The coefficient of friction for sand particles and the steel plate is 0.26 and the coefficient of restitution is also equal to 0.26.

The change in velocity when a particle impacts with the mild steel plate represents loss in energy. The loss in energy per unit mass neglecting the rotational component can be expressed by the following relationship

$$\Delta E = \frac{1}{2}\left[\left(V_{xo}{}^2 + V_{yo}{}^2\right) - \left(V_{x1}{}^2 + V_{y1}{}^2\right)\right] \qquad (6.2\text{-}16)$$

For this particular case the silica gel and glass particles on average lose 33 percent of their original kinetic energy on impact compared to sand particles which lose 43 percent. In gas solid suspensions the energy to resuspend the particle is provided by the conveying gas. This loss in energy on collision can be represented by two overall parameters, which are the coefficient of restitution e and coefficient of friction μ for collision between particle and wall.

When the coefficient of restitution, coefficient of friction and the initial velocity components are known the velocity components after the collision are fixed and are given by (from Equation 6.2-15 and the definition of e)

$$V_{x1} = V_{x0} - \mu(1+e)V_{y0} \tag{6.2-17}$$

and

$$V_{y1} = -eV_{y0} \tag{6.2-18}$$

The reflected angle or lift-off angle α_{LO} from the horizontal is given by

$$\alpha_{LO} = \tan^{-1}\left(\frac{V_{y1}}{V_{x1}}\right) \tag{6.2-19}$$

6.3. Bouncing Particle Model (BPM)

6.3.1. Single Particle Approach

A complete description of the system is almost impossible and therefore several assumptions are made as a first approximation to simply the problem. The following assumptions are made:

Particle is spherical.

Absence of particle-particle interactions.

Post collision velocity and angle determined by coefficient of restitution, Coulombic friction and impact velocity.

The particle travels in close proximity to the wall in a near curved path .

The curvature in the trajectory of the particle is a result of the force perpendicular to the direction of particle travel and directed towards the confining wall. If this trajectory is maintained the particle will impact the wall and be reflected and re-entrained by gas in the general direction of gas flow. The force maintaining this particle motion is the gas drag force and this force is in the direction of the free stream velocity. The force acting perpendicular to the direction of travel of particle is the centrifugal force pushing the particle towards the wall and an opposing small opposing radial drag force.

The total gas drag force acting on the particle is given by (not per unit mass)

$$F_D = \frac{1}{2} C_D \rho_g \frac{\pi}{4} d_p{}^2 \mathbf{V}_{rel}{}^2 \qquad (6.3\text{-}1)$$

and the centrifugal force is given by

$$F_c = m_p \frac{V_p^2}{R} \qquad (6.3\text{-}2)$$

The centrifugal and radial drag forces are perpendicular to the axial line of symmetry. A momentum balance per unit mass in the radial direction is:

$$\frac{dU_p}{dt} = \frac{V_p^{\,2}}{R} - \frac{3}{4} C_D \frac{\rho_g}{\rho_p d_p} \|\mathbf{V}_{rel}\| (U_g - U_p) \qquad (6.3\text{-}3)$$

Large and dense particles have a higher radial acceleration and quickly reach the retaining wall boundary.

The drag coefficient C_D used in this work is that given by (Tsuji et al. 1993)

$$C_D = \frac{24}{\mathrm{Re}}\left[1 + 0.15\mathrm{Re}^{0.687}\right] \qquad (6.3\text{-}4)$$

for Re < 1000

Re is the Reynolds number given by

$$\mathrm{Re} = \frac{\rho_g \|\mathbf{V}_{rel}\| d_p}{\mu} \qquad (6.3\text{-}5)$$

d_p is the diameter of the particle.

Initial Conditions at entry into cyclone

The velocity of the particles was measured about 0.30 m upstream of the cyclone in the tangential entrance tube. The distance from this point to where a collision with the wall initially takes place is about 0.35 m for a representative particle on the centre line. The horizontal movement of the particle in this region was assumed governed by the following equation

$$\frac{dV_p}{dt} = \frac{3}{4} \frac{C_D \rho_a}{\rho_p d_p} V_r \left(V_g - V_p\right) \qquad (6.3\text{-}6)$$

where $V_r = \sqrt{(V_g - V_p)^2 + (W_g - W_p)^2 + (U - U_p)^2}$

V and W are velocity components parallel and perpendicular to the axis of entrance tube respectively.

Equation 6.3-6 is solved by the following algorithm (Figure 6.30) to evaluate the final velocity of the particle at initial impact with the cyclone wall.

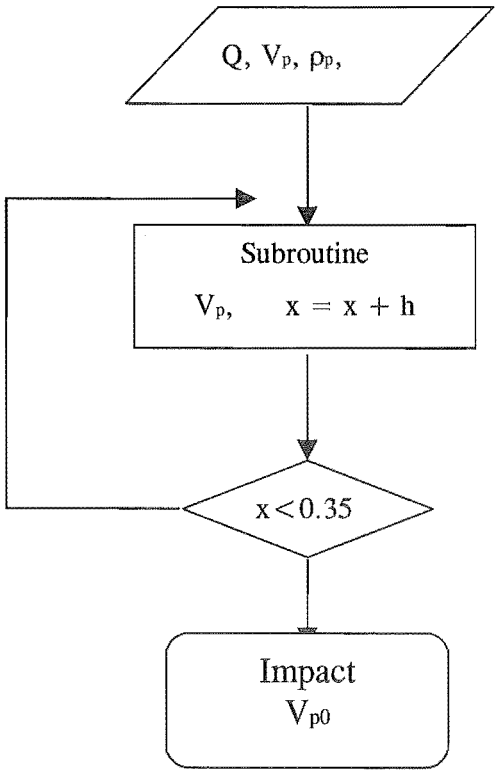

Figure 6-30 Algorithm for calculating particle initial velocity

In Figure 6-30 h is the step size (m) and x is the incremental distance (m). The velocity just before impact with the cyclone wall is V_{p0}.

From the geometry of the cyclone a representative particle at the centre of the tangential entrance tube strikes the wall at an angle of 40 degrees as shown in Figure 6-31.

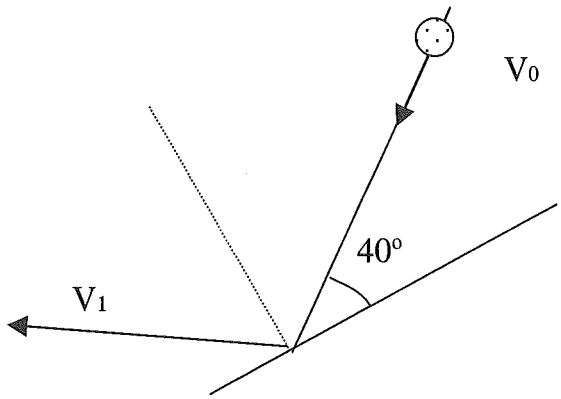

Figure 6-31 Initial impact of particle with wall at entrance

In general after impact with the wall of the cyclone the post collision velocity components normal and along the wall are calculated by the following equations respectively

$$V_{p1} = V_{p0} - f(1+e)U_{p0} \tag{6.3-7}$$

$$U_{p1} = -eU_{p0} \tag{6.3-8}$$

where f is the coefficient of friction and e is the coefficient of restitution and allowing some slip at point of contact.
U_{p0} and U_{p1} are the impact and rebound normal velocity components and V_{p0} and V_{p1} are the impact and rebound tangential velocity components.

It is assumed that during contact with the wall only the mechanical interactions with the wall are considered important. These are of short duration, and significantly larger than the gas particle interaction. The hydrodynamic effect of the gas is considered only after the particle leaves the wall. The next particle-wall collision is then determined by this hydrodynamic interaction.

Equations 6.3-7 and 6.3-8 describe the general case in which the velocity components have been resolved into components perpendicular to the wall and parallel to the wall. In the cylindrical section the radial velocity acts perpendicular

to the wall and is derived from the centrifugal force. The radial velocity thus has no component along the wall. In the conical section however, the particle radial velocity is not perpendicular to the wall. The impact-rebound relationships in the cylindrical and conical sections of the cyclone are thus treated separately, while still using the above two equations.

The following subscripts and nomenclature will be used

b before collision

a after collision

$\perp$ Perpendicular to wall

$=$ parallel to wall

$U_{\perp b}$ particle radial velocity perpendicular to the wall before collision

$U_{\perp a}$ particle radial velocity perpendicular to the wall after collision

W_b particle axial velocity before collision

W_a particle axial velocity after collision

$V_{=b}$ particle velocity parallel to wall before collision

$V_{=a}$ particle velocity parallel to wall after collision

V_b particle tangential velocity before collision

V_a particle tangential velocity after collision

ω_b particle velocity down along wall (along conical generator) before collision

ω_a particle velocity down along the wall (along conical generator) after collision

α half angle of cone (degrees)

θ angle along wall of total particle velocity from the horizontal, measured in the plane of the wall

γ_b impact angle of particle to wall in plane of collision

γ_a lift-off angle of particle from cyclone wall in plane of collision

Impact Relationships:

Cylindrical section

The impact-rebound velocity relationships for a particle in the cylindrical section of the cyclone are shown in Figure 6-32 and Figure 6-33.

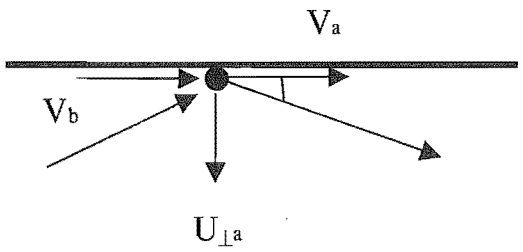

Figure 6-32 Impact-rebound velocity relationships (plan view - i.e. looking from the top down cylinder wall) Using cylindrical coordinates.

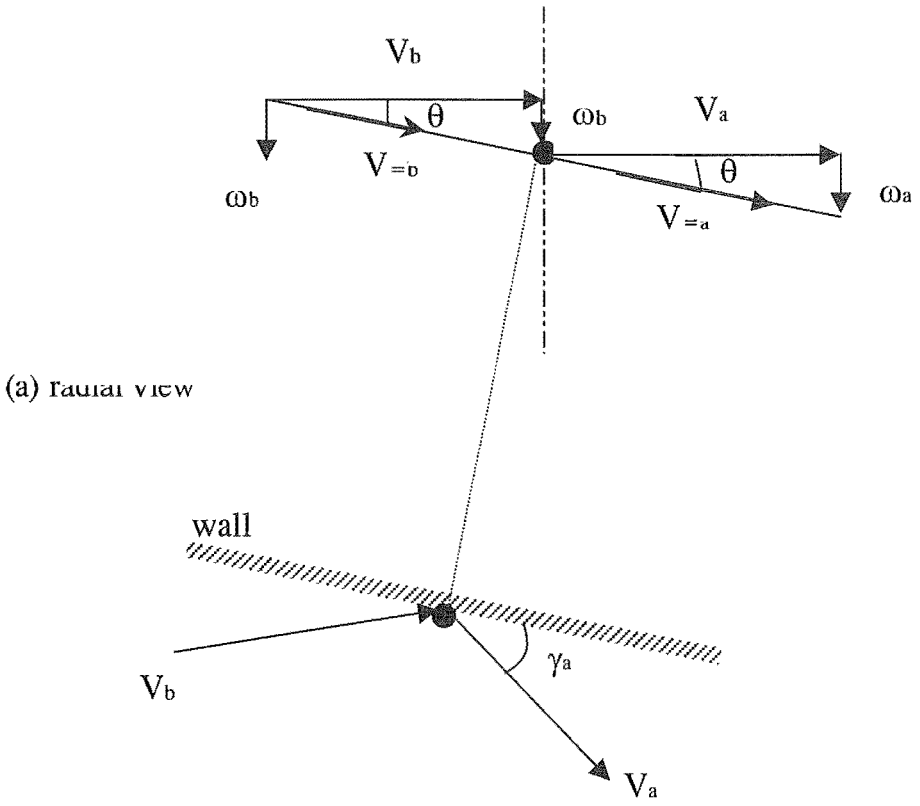

(a) radial view

(b) projected view in plane of collision

Figure 6-33 Impact-rebound velocity components in cylindrical section (a) radial view and (b) projected view . Using also wall related velocities.

Where $V_{=b}$ and $V_{=a}$ are the particles' velocity vectors along the wall before impact and on rebound. It is assumed that the angle of the particle velocity vector to the horizontal before and after impact is the same and equal to θ. The radial velocity

component before and after impact acts towards and away in a direction perpendicular to the plane of the paper. The impact-rebound along the wall velocities are described by the following equations

$$V_{=b} = \sqrt{\omega_b^2 + V_b^2} \tag{6.3-9}$$

In the cylindrical section $W_b = \omega_b$ and $W_a = \omega_a$

The angle of the total velocity from the horizontal θ is given by

$$\theta = \arctan\left(\frac{W_b}{V_b}\right) \tag{6.3-10}$$

The post collision velocity along wall is given by the following equation

$$V_{=a} = V_{=b} - f(1+e)U_{\perp b} \tag{6.3-11}$$

The post collision tangential velocity is given by

$$V_a = V_{=a}\cos\theta \tag{6.3-12}$$

The post collision axial velocity is given by

$$W_a = V_{=a}\sin\theta \tag{6.3-13}$$

The post collision radial velocity is given by Equation 6.3-8, rewritten in the new nomenclature:

$$U_{\perp a} = -eU_{\perp b} \tag{**6.3-14**}$$

Conical section

In the conical section the particle radial velocity component is not perpendicular to the wall. It has components that can be resolved perpendicular and parallel to the wall. In addition the axial velocity component also has a component acting parallel and perpendicularly to the wall. A general diagram is shown in Figure 6-34.

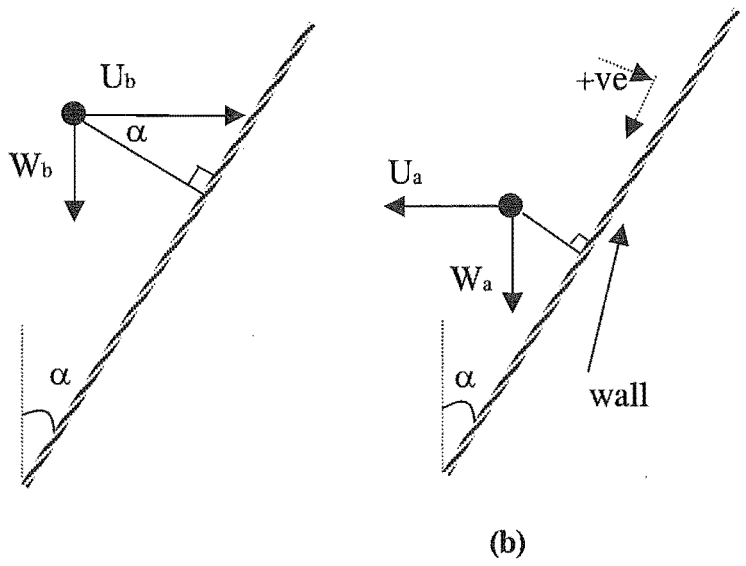

Figure 6-34 Particle axial and radial velocity components in conical section (side view) (a) before collision and (b) after collision

The pre-collision velocity components acting perpendicular to the wall are given by the following equation

$$U_{\perp b} = U_b \cos\alpha + W_b \sin\alpha \tag{6.3-15}$$

The post collision velocity component perpendicular to the wall is

$$U_{\perp a} = -eU_{\perp b} \tag{6.3-16}$$

Pre collision velocity component parallel to the wall along the conical generator, ω_b is given by

$$\omega_b = W_b \cos\alpha - U_b \sin\alpha \tag{6.3-17}$$

The pre-collision ("before") total velocity component parallel to the wall as shown in Figure 6-35 is then given by the following equation

$$V_{=b} = \sqrt{V_b^2 + (W_b \cos\alpha - U_b \sin\alpha)^2} \qquad (6.3\text{-}18)$$

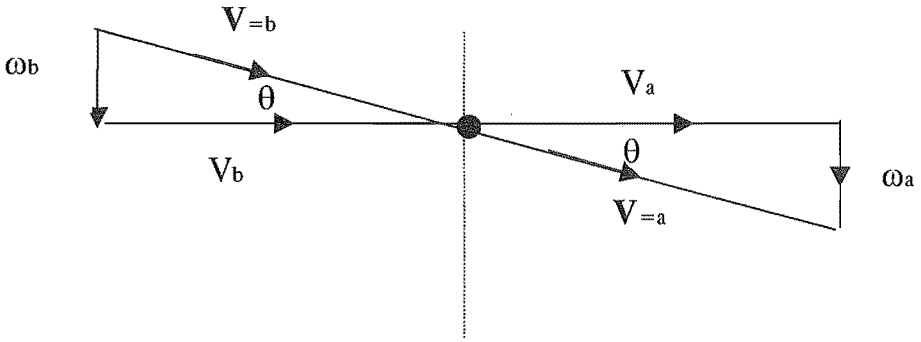

Figure 6-35 Impact and rebound velocities in conical section (looking down on plane ⊥ to cone wall)

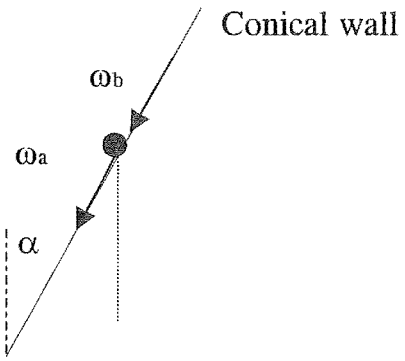

Figure 6-36 Impact and rebound velocities in conical section (side view sectioned along conical generator)

The post-collision total velocity component parallel to the wall is given by

$$V_{=a} = V_{=b} - f(1+e)U_{\perp b} \qquad (6.3\text{-}19)$$

The angle of the total velocity vector from the horizontal θ (measured within the plane of the wall at the impact point) is given by

$$\theta = \arctan\left(\frac{\omega_b}{V_b}\right) = \arctan\left(\frac{W_b \cos\alpha - U_b \sin\alpha}{V_b}\right) \qquad (6.3\text{-}20)$$

After collision, the velocity component down the cone generator parallel to the wall is given by (refer to Figure 6-34 (b))

$$\omega_a = W_a \cos\alpha + U_a \sin\alpha \qquad (6.3\text{-}21)$$

Also, assuming that the angle of the particle total velocity is at the same angle of θ before and after collision, $\frac{\omega_a}{V_a} = \tan\theta$

thus,

$$W_a \cos\alpha + U_a \sin\alpha = V_a \tan\theta \qquad (6.3\text{-}22)$$

Also (refer to Figure 6-35)

$$V_a = V_{=a} \cos\theta \qquad (6.3\text{-}23)$$

Equation 6.3-22 is expressed in terms of W_a

$$W_a = \frac{V_a \tan\theta - U_a \sin\alpha}{\cos\alpha} \qquad (6.3\text{-}24)$$

Substitution for V_{pa} in Equation 6.3-24 from Equation 6.3-23

$$W_a = \frac{V_{=a} \sin\theta - U_a \sin\alpha}{\cos\alpha} \qquad (6.3\text{-}25)$$

The post collision velocity component perpendicular to the wall is given by the following equation (refer to Figure 6-34 (b))

$$U_{\perp a} = W_a \sin\alpha - U_a \cos\alpha \qquad (6.3\text{-}26)$$

Equation 6.3-26 is rearranged, expressed in terms of the particle radial velocity U_a

$$U_{pa} = \frac{W_a \sin\alpha - U_{\perp a}}{\cos\alpha} \qquad (6.3\text{-}27)$$

Substitution for W_a from Equation 6.3-25 and rearranging to find U_a,

$$U_a = -\left|V_{=a} \sin\theta \sin\alpha - U_{\perp a} \cos\alpha\right| \qquad (6.3\text{-}28)$$

The velocity components expressed in Equation 6.3-28 are illustrated in Figure 6-37 (a) and (b) below

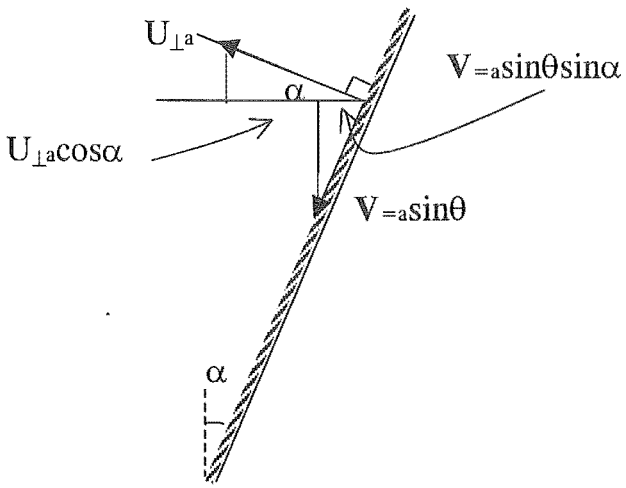

(a) Sectioned through wall in radial plane

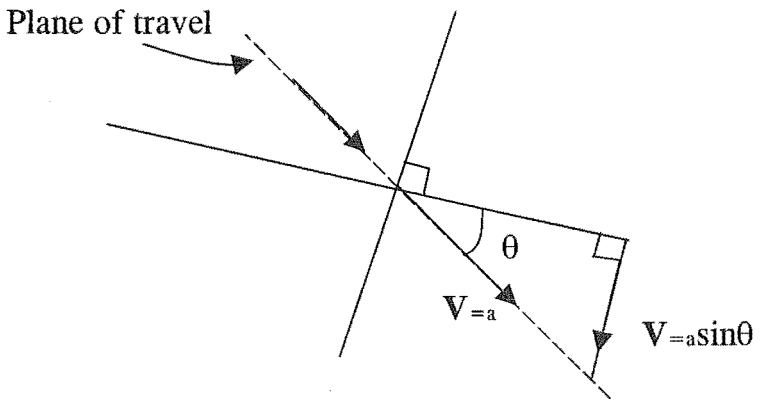

(b) Looking perpendicular to wall at point of collision

Figure 6-37 Diagrammatic representation of velocity components in Equation 6.3-28

Now $V_{=a}$ and $U_{\perp a}$ can be obtained from pre-collision velocities through the collision model equations 6.3-16 and 6.3-19, so that all components of the particle velocity in cylindrical coordinates, U_a and W_a (from rearranging 6.3-26) and V_a from Equation 6.3-23, can be calculated.

Free flight relationships:

A tangential momentum balance on the particle between bounces can be represented by the following equation

$$V_p \frac{dV_p}{dx} = \frac{3}{4} \frac{C_D \rho_g}{\rho_p d_p} \left[\left(V_g - V_p\right)^2 + \left(W_g - W_p\right)^2 + \left(U_g - U_p\right)^2 \right] \qquad (6.3\text{-}29)$$

The radial momentum balance (Equation 6.3-3) can be simplified further by consideration of the fact that for particles where $\rho_p >> \rho_g$ the centrifugal force is much greater than the radial drag force i.e. $F_c >> F_d$. Equation 6.3-3 can then be reduced to the following expression where the radial acceleration of the particle is dominated by the centrifugal force

$$\frac{dU_p}{dt} = \frac{V_p^2}{R} \qquad (6.3\text{-}30)$$

For small time increments Equation 6.3-30 can be expressed as a finite difference equation for radial velocity U_p.

$$\Delta U_p = U_{p1} - U_{p0} = \frac{V_p^2}{R}\Delta t \qquad (6.3\text{-}31)$$

The tangential velocity component V_p is in the direction of particle motion and the radial component U_p is positive radially outwards.

As the particle is transported the radius of the centre of mass of the particle R from the cyclone axis changes. For small time intervals the radial position is expressed by the following equation

$$R_i = R_{i-1} + \Delta R \qquad (6.3\text{-}32)$$

ΔR is evaluated by the following expression

$$\Delta R = U_p \Delta t \qquad (6.3\text{-}33)$$

where Δt is obtained by

$$\Delta t = \frac{h}{V_p} \qquad (6.3\text{-}34)$$

where h is the chosen step size (m) in the tangential direction.

The resultant equation for the evaluation of ΔR is

$$\Delta R = \frac{U_p}{V_p} h \qquad (6.3\text{-}35)$$

Equation 6.3-31 can now be replaced by the following equation

$$U_{pi} = U_{p(i-1)} + \frac{V_{pi}}{R_i} h \qquad (6.3\text{-}36)$$

Equation 6.3-32 is now expressed by the following equation

$$R_i = R_{i-1} + \frac{U_{pi}}{V_{pi}} h \qquad (6.3\text{-}37)$$

Criterion for a particle-wall collision (bounce)

The schematic diagram of the trajectory of a particle is shown in Figure 6-39. The radius of the cyclone is R_c and R is the current radius of the center of mass of the particle from the axis of the cyclone. It is assumed that when a particle-wall collision occurs the particle does not undergo any deformation. When a particle of diameter d_p impacts with the wall the following condition is satisfied

$$R_c - R_i = \frac{d_p}{2} \qquad (6.3\text{-}38)$$

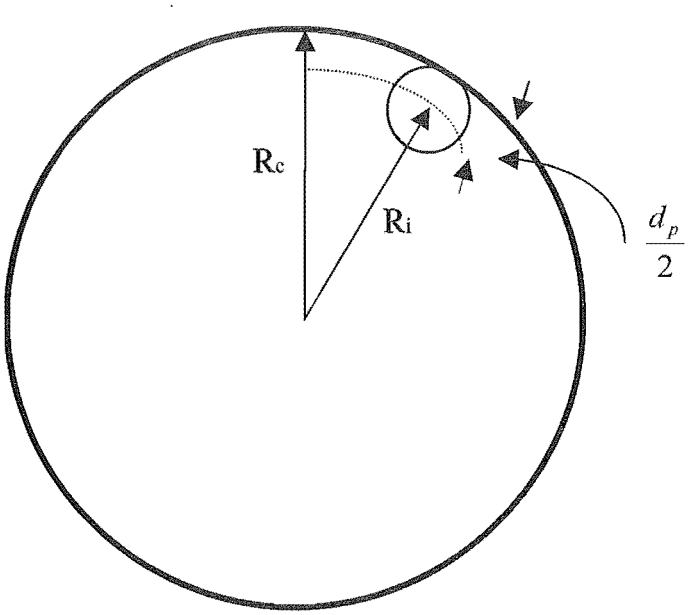

Figure 6-38 Schematic diagram shown bouncing phenomena in cyclone

When the condition in Equation 6.3-38 is satisfied the particle is assumed to have made contact with the wall and post collision velocity components U_{p1}, W_{p1} and V_{p1} are calculated from Equations 6.3-7 and 6.3-8 (via Equations 6.3-28, 6.3-26 and 6.3-23).

No particle collision with the wall will occur in the interval if the following condition is satisfied

$$R_c - R_i > \frac{d_p}{2} \qquad (6.3\text{-}39)$$

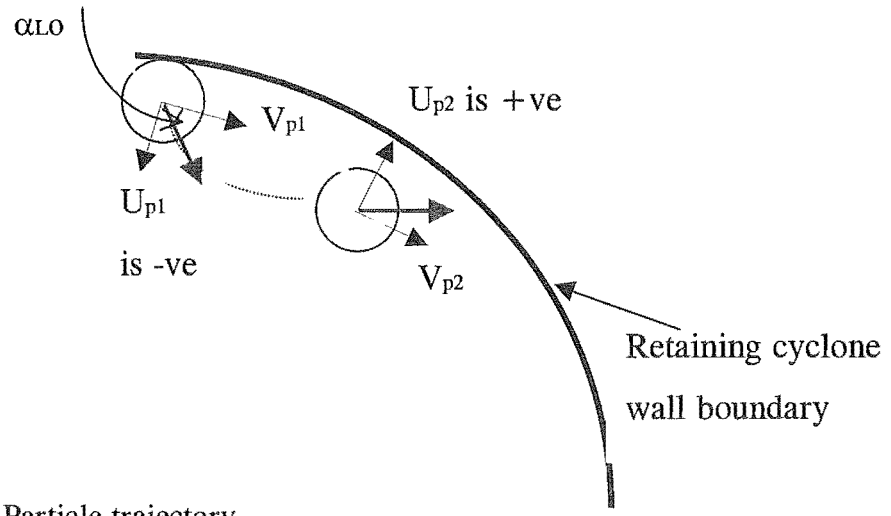

Figure 6-39 Particle trajectory

The particles are thrown to the wall and they rebound with a finite radial velocity away from the wall. As the particle travels, the direction of the radial velocity is changed due to the centrifugal acceleration towards the wall (Equation 6.3-3) and is gradually redirected towards the wall.

After the evaluation of the radial velocity of the particle after rebound, the distance travelled by the particle in a small time interval $\Delta t = \frac{h}{V_p}$ is calculated. h (m) is the chosen step interval in the direction of the tangential velocity and V_p the particle velocity in the tangential direction. If the distance travelled from the wall in the radial direction in the interval after a collision was not greater than $\frac{d_p}{2}$ then the particle does not possess enough momentum to leave the wall and then continues its motion along the wall by sliding.

For the case of sliding on the wall the tangential velocity of the particle is based on the particle tangential momentum equation (Cremasco et al. 1996) and given by the following equation

$$W_p \frac{dV_p}{dz} = \frac{3}{4} C_D \frac{\rho_g}{\rho_p d_p} \|\mathbf{V}_{rel}\| (V_g - V_p) - \mu F_N \frac{V_p}{R_x (V_p^2 + W_p^2)^{0.5}} \qquad (6.3\text{-}40)$$

The tangential momentum balance (Equation 6.3-6) for the particle in free flight in between bounces was solved by the fourth order Runge-Kutta method. When the conditions for particle sliding on the wall (ie. zero particle radial velocity) were satisfied then Equation 6.3-40 was solved. At each interval when the tangential velocity was evaluated the equations for the particle radial and axial velocities were solved simultaneously. The parameters in the model - coefficient of restitution and coefficient of friction were obtained from the simple plate bouncing experiments. At each impact with the wall the absolute value of radial velocity of the particle is reduced by a factor equal to the coefficient of restitution, and the velocity reversed. The particle is resuspended with this new velocity and is accelerated until it impacts again on the wall.

Particle flight after bounce with wall

The angle at which the particle will leave the wall after a collision, is obtained by Equation 6.3-41 after substituting for values of post collision velocities in the radial and total velocity along the wall

$$\lambda_a = \tan^{-1}\left(\frac{-eU_{\perp b}}{V_{=b} - \mu(1+e)U_{\perp b}}\right) \qquad (6.3\text{-}41)$$

Equation 6.3-41 shows that the angle at which a particle will bounce off from the wall is greatly influenced by the coefficient of restitution or the elasticity of the impact. The normal component of the velocity after impact $U_{\perp a}$ is very low for collisions that are highly plastic or where the coefficient of restitution is close to zero. In that case when $U_{\perp a} \rightarrow 0$, then $\lambda_a \rightarrow 0$. Therefore when the particle radial velocity is close to zero then the condition of particle sliding on the wall is

attained. If the number of particles is large enough this may trigger roping. The particle under these circumstances does not possess enough momentum to drift from the wall because of the large influence of the centrifugal force especially in the conical section. The free flight particle momentum equations and the particle-wall collision equations are no longer applicable. Instead the momentum equations (Equations 6.2-3 and Equation 6.2-4) are used.

General motion of particles in cyclone – angle of gas and particles

The gas tangential inlet velocity was calculated by the following equation

$$V_g = \frac{Q}{ab} \tag{6.3-42}$$

where Q is the gas volumetric flow rate and a and b are the rectangular inlet dimensions.

The tangential gas velocity was assumed to be independent of the axial coordinate and a function of only the radial coordinate (Kelsall, 1952; Mothes and Löffler, 1988; ter Linden, 1949). The tangential velocity near the wall does not deviate much from the velocity of the gas in the rectangular inlet duct. Of the three velocity components, V_g, W_g and U_g, the tangential velocity component predominates and is almost equal to the total velocity (ter Linden, 1949). Although the presence of solids is known to affect the gas flow field, as a first approximation this influence was not considered but could be incorporated as a refinement to the model. The bouncing of particles in the cyclone and the effect on collection efficiency by particles bouncing into the inner vortex has long been recognised (Stairmand, 1952). However no quantitative work is reported in literature with regard to this bouncing phenomenon.

The following gas velocities were used close to the wall. The axial velocity of the gas was estimated by the following equation, based on the remaining flow at height

h_x being averaged over the cross sectional area outside an imaginary cylinder extending below the vortex finder.

$$W_g = \frac{Q\left(0.1 + 0.9\left(1 - \frac{h_x}{h_c}\right)\right)}{\pi\left(R_x^2 - R_{ex}^2\right)} \qquad (6.3\text{-}43)$$

where h_x is the incremental axial height from the top to the bottom and h_c is the total height of the cyclone. R_x is the current radius to the wall boundary and R_{ex} is the radius of the gas exit tube. It was assumed the gas recirculation in the dust hopper was 10 per cent.

The gas radial velocity close to the wall is effectively zero. However, as one moves towards R_{ex} the following equation can be used

$$U_g = \frac{Q}{2\pi R_{ex}(h_c - S)} \qquad (6.3\text{-}44)$$

Relevant dimensions used are shown in Figure 6-40 below.

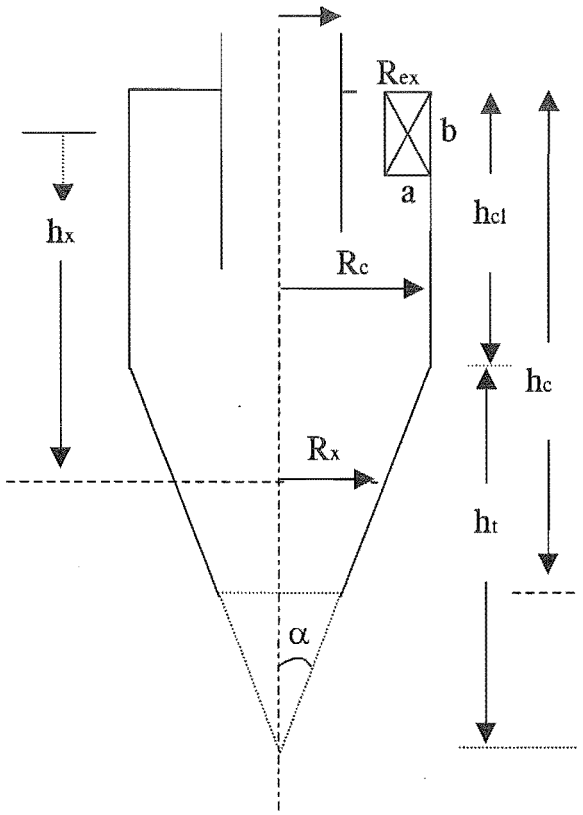

Figure 6-40 Schematic representation of cyclone

Algorithm and Computer Program

An algorithm for the process is shown in Figures 6-41 and 6-42. Figure 6-41 is for the motion of the particle in the barrel of the cyclone and Figure 6-42 is for the motion in the cylindrical part of the cyclone.

The computer program is listed in Appendix 9C. The program was written using Visual Basic (1997 version). The design variables for a given cyclone were initially assigned and also the viscosity of the carrier gas. The programs accepts the following operation variables as input: the gas volumetric flow rate, the entrance velocity of the particle, the diameter of the particle, the density of the particle, the coefficient of restitution for particle wall collision, the coefficient of friction and the step size (0.5 mm). The small step will ensure that changes in properties are small in that interval so that errors in finite difference calculations are small. The velocity components of the particle are calculated and written to a file to enable retrieval and analysis. The program gives as output the particle residence time.

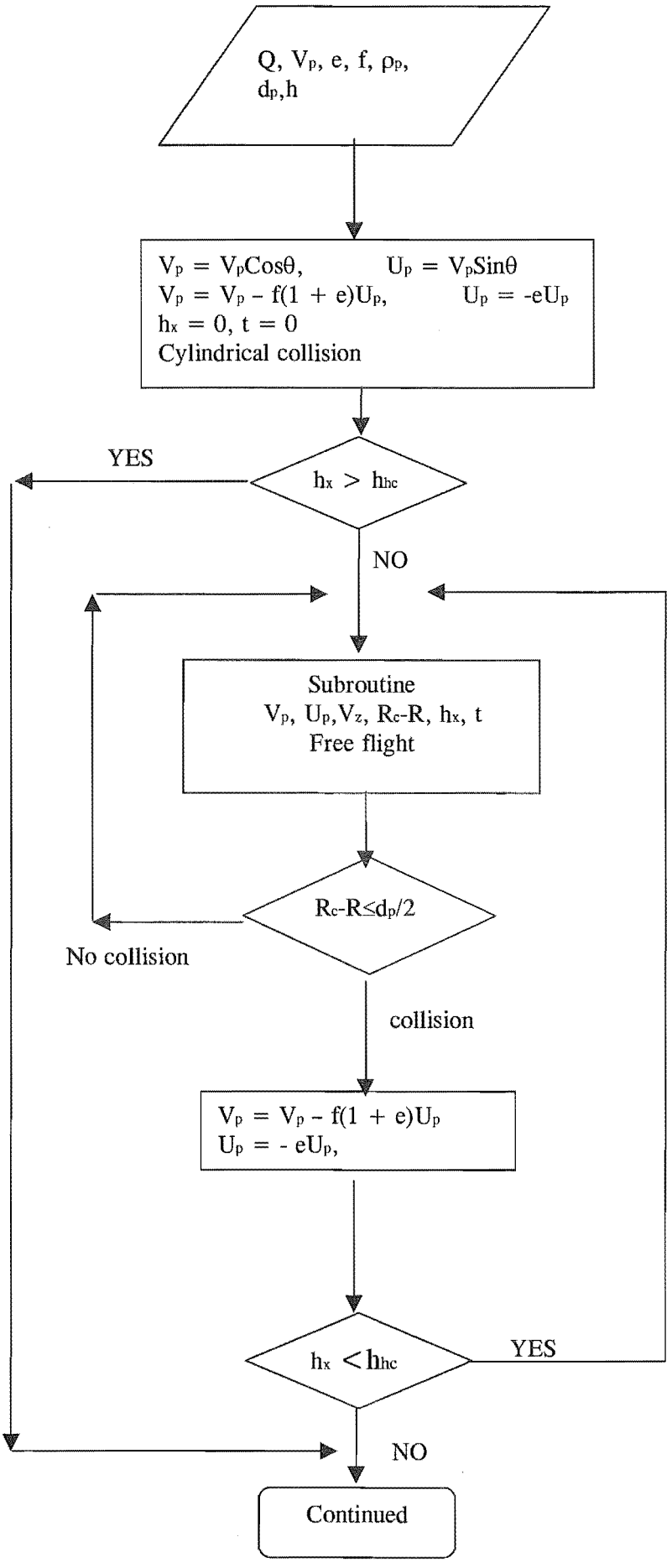

Figure 6-41 Algorithm for the Bouncing Particle Model (a)

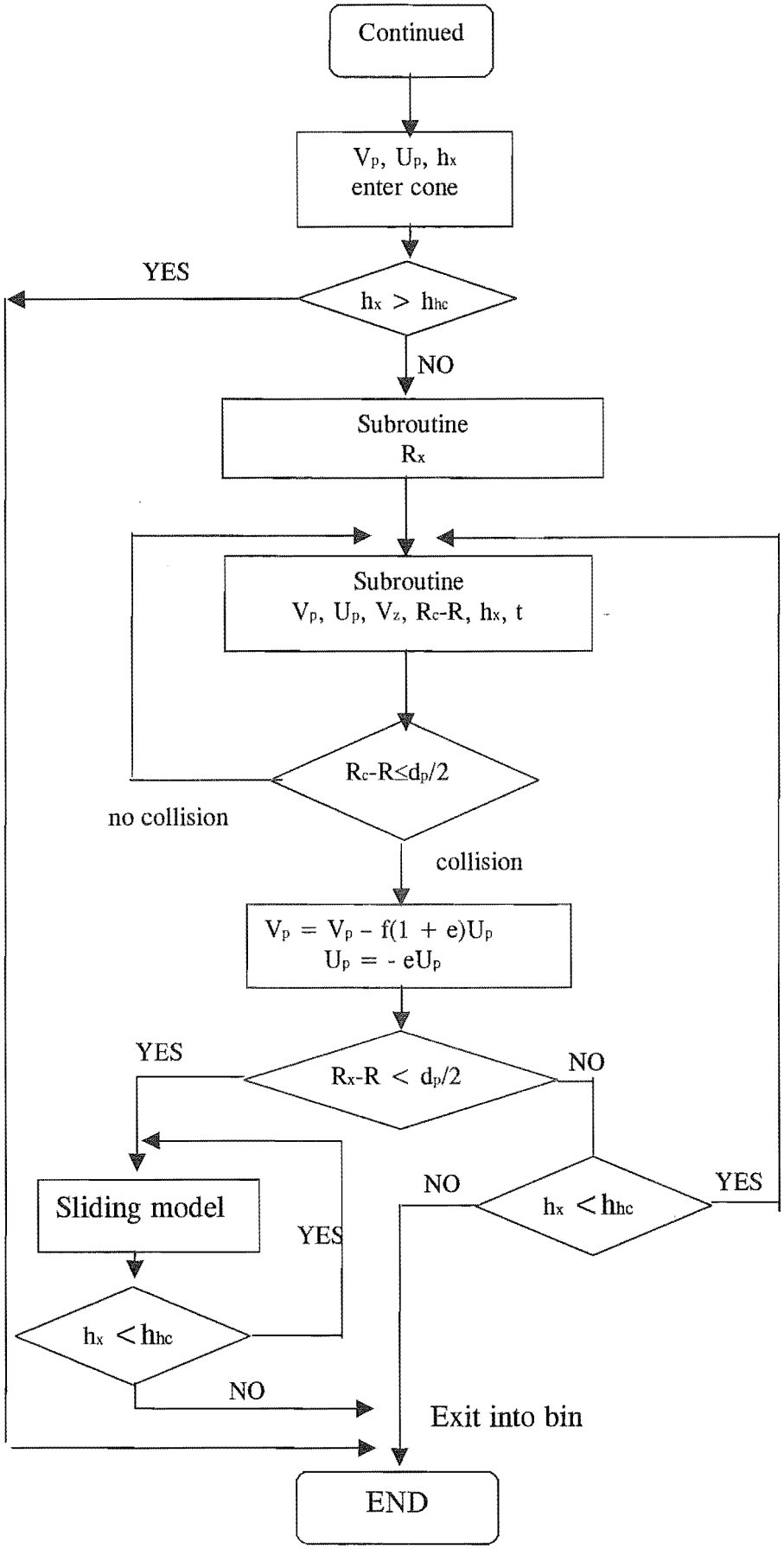

Figure 6-42 Algorithm for the Bouncing Particle Model (b)

Angle of particle total velocity vector

In the following, the single particle model will be used to discuss the motion of particles on the wall, despite the formation of a rope. It was observed experimentally that the angle of the rope was not constant down the axis of the cyclone. The angle was at its maximum in the cylindrical section of the cyclone and gradually decreased to almost zero at the apex of the cyclone. This change in angle was a result of the component of the centrifugal force acting on the particle and directed up along the wall, which increased as the radius decreased down the cone. The increase in the force component up the wall is a function of the included half angle of the cone for a given geometry. When the tangential inlet velocity was increased the angle of the particles with the horizontal decreased and the ropes became more concentric. θ was estimated from observations at between 2.5 and 7° in the conical section for cyclone D when the tangential inlet velocity was 20 m s^{-1}.

At a tangential inlet velocity of 20 m s^{-1} a jet of ink was injected through a hole in the cylindrical section of cyclone B. After stopping the airflow the angle the streak made with the horizontal was measured and found to be about 20°. This is interpreted as the angle of the gas to the horizontal. The track angle of fine aluminium particles in a hydrocyclone was estimated from the work of Kelsall (1952) and estimated at about 17-18°. These measurements were made in a cone with an included angle of 20°.

In the present model the angle of the velocity vector of the particles parallel to the horizontal was calculated by Equation 6.3-10.

Wakelin (1993) measured tangential (V_g) and axial velocity (W_g) components of the gas at different ports in a standard Staimand (1951) high efficiency design cyclone of diameter 750 mm and at a radial distance of 2 mm from the wall. The tangential inlet gas velocity for this data was 15 m s^{-1}. The data was subsequently scaled for a gas tangential inlet velocity of 20 m s^{-1}. From these measurements the angle of the

gas velocity vector was calculated from $\theta = \tan^{-1}(\frac{W_g}{V_g})$. The average values of the angles from measurements at diametrically opposite points on the cyclone are shown as a function of axial height of cyclone in Figure 6-43.

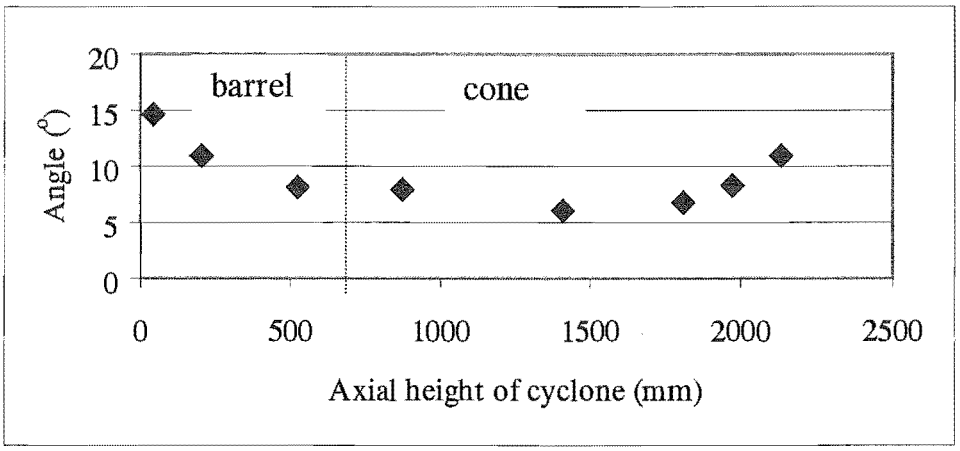

Figure 6-43 Angle of total gas velocity vector at different ports down a Stairmand high efficiency cyclone (Wakelin, 1993)

The angle of the total gas velocity vector from the horizontal decreased with increase in axial distance, from the top of the barrel down to the cone. In the barrel section of the cyclone the tangential velocity component was almost constant while the axial velocity decreased which resulted in a corresponding decrease in the angle. In the conical section the tangential velocity component at the wall was higher compared to that in the barrel section on the wall, this also resulted in a gradual decrease in the angle. However the angle as measured by Wakelin (1993) appears to increase towards the dust exit after the downward trend. The data from Wakelin (1993) was with a dust free environment.

The angle of the gas was also measured in this work in the conical section of the 36-degree cyclone (D) at height of 80 mm from the dust exist (Figure 6-44). The measurements were made without the dust collection hopper fitted which would have made a major difference.

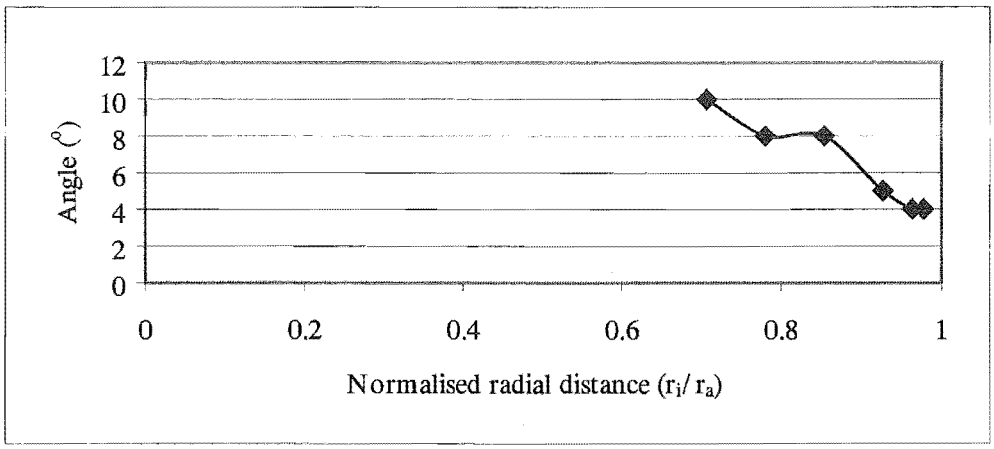

Figure 6-44 Angle of total gas velocity vector as a function of normalised radial distance at height of 80 mm from dust exist - cyclone D.

As the angle of the cone is increased the direction of the net force acting on the particle and the drag force of the gas will act in different directions. The effective force acting on the particle is a resultant of the gas drag force and the centrifugal force component acting up the wall of the cyclone and the gravity component acting down the wall. Evidence of this phenomenon is discussed in Section 6.1 where ropes persisted in the conical section of cyclones D and E when the solids feed to the cyclone was stopped but the air flow maintained. A force diagram showing the net drag force acting on the particle and the gas drag force is shown in Figure 6-45 (a) and (b). F_p is the net drag force acting on the particle and F_D is the gas force. Note that the direction of F_D is close to that of the gas, because V_p is much less than V_g, and not largely different in direction.

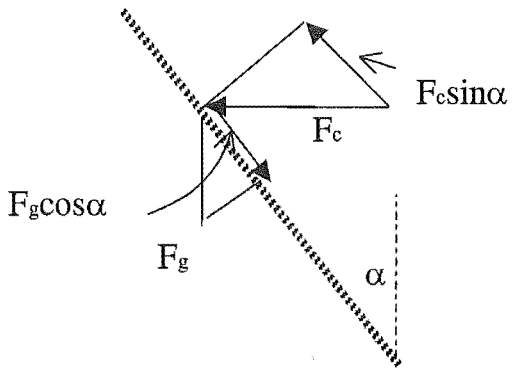

(a) section perpendicular to wall

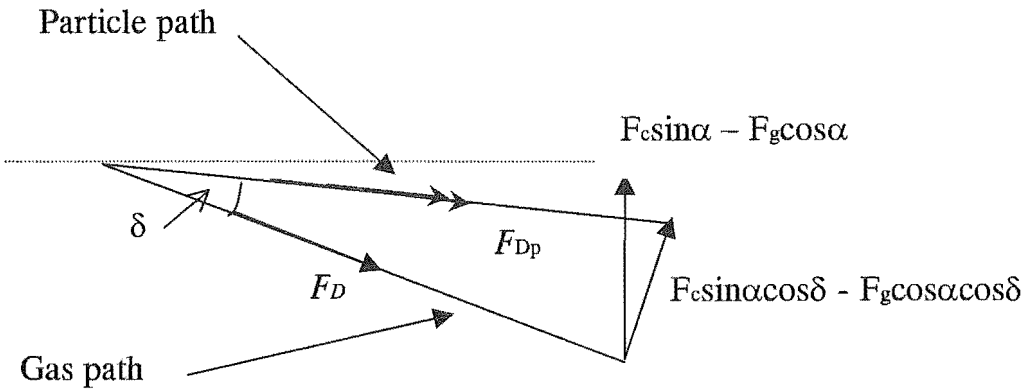

(b) forces in plane of wall at particle position (at steady state, the direction of net force on the particle and the direction of the particle coincide)

Figure 6-45 Force diagrams showing resultant force acting on particle and gas drag

$F_c\sin\alpha$ is the component of the centrifugal force acting up the wall. The influence of the centrifugal force and cone angle on the direction of the net force is shown in Equation 6.3-45. The angle δ (the deviation of the particle from gas path) can be continually adjusted by the following relationship as the particle progresses down the cyclone

$$\tan\delta = \frac{F_c \sin\alpha - F_g \cos\alpha}{F_D} \qquad (6.3\text{-}45)$$

where F_c is the centrifugal force, F_g is the gravitational force and F_D is the gas drag force and α is the total included half angle of the cone.

The influence of the cone angle α on the angle δ in Equation 6.3-45 is very strong. For constant F_c and F_D an increase in the cone half angle from 5 degrees for the 10-degree cyclone (A) to 21degrees for the 42-degree cyclone (cyclone F) will result in an increase of about 300 per cent in magnitude of angle δ. There is therefore a phenomenal increase in slip velocity as the cyclone cone angle is increased.

6.3.2. Model Results

The model was used to predict the mean residence time of single silica gel particles with representative sizes 300 to 500 μm. The average inlet velocity of these particles into the cyclone was 15 m s^{-1}. The gas volumetric flow rate into the cyclone was 0.099 $m^3 s^{-1}$, giving a gas inlet velocity of 20 m s^{-1}. The density of the silica gel particles was 1200 kg m^{-3} and the step size for the iterations used was less than 0.001m. Larger time steps resulted in some instability in the solution. The mean values of the coefficient of restitution and friction (§ 5.13) were used. The coefficient of restitution was also generated using the random number generator in Visual Basic subject to constraints of a maximum value of 0.9 and minimum of 0.1 at each collision with the wall. It was found that there was no significant difference between the two calculated results ($< 0.2\%$).

The residence times from the model were compared with the experimental results (Figure 6-46). The model predicted residence times in Figure 6-46 do not represent change in residence time with change in SGL but rather different particle sizes. Experimentally it was shown that within the range of SGL shown in Figure 6-46 the particle residence time was not sensitive to changes in SGL.

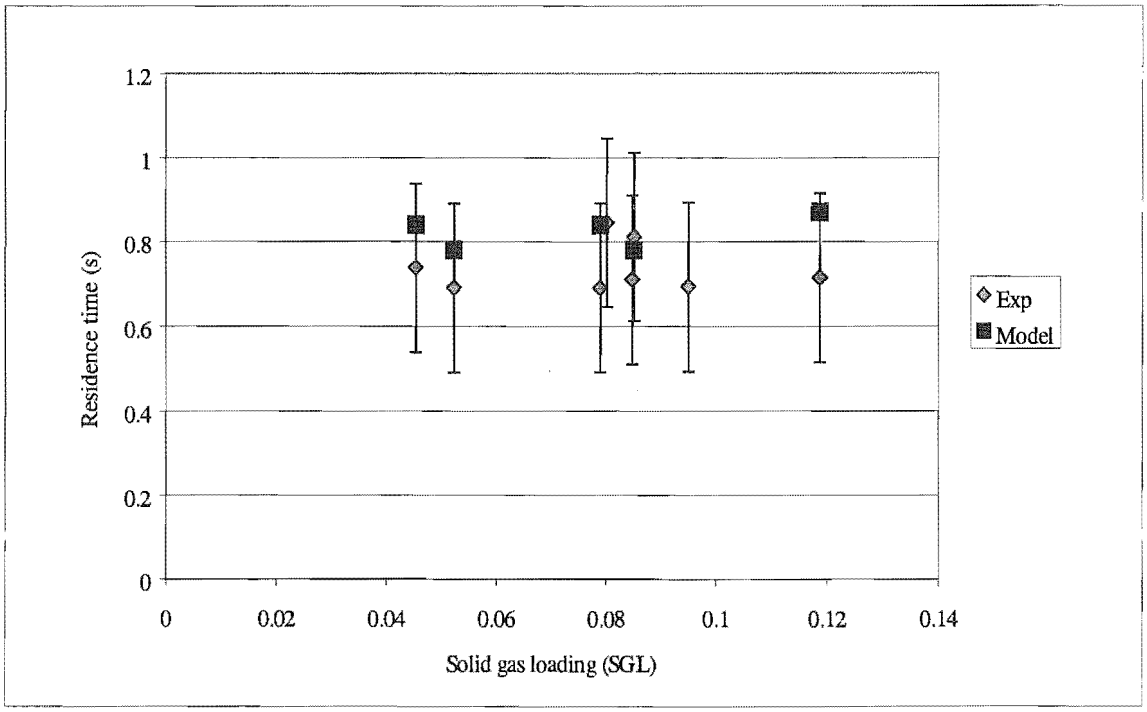

Figure 6-46 Experimental and model predicted residence time for silica gel particles. Cyclone B; particle size range 300-500 μm; Gas inlet velocity 20 m s^{-1}

The model predicted residence times are consistently higher than the experimentally measured values but falls within the bounds of experimental error of 20 per cent (Appendix K).

The variation of mean particle residence time with gas tangential inlet velocity for silica gel particles of size range 699-850 μm is shown in Figure 6-47. For the range of gas tangential velocity the model was used to calculate the residence time of a silica gel particle with a diameter of 750 μm as shown in Figure 6-47.

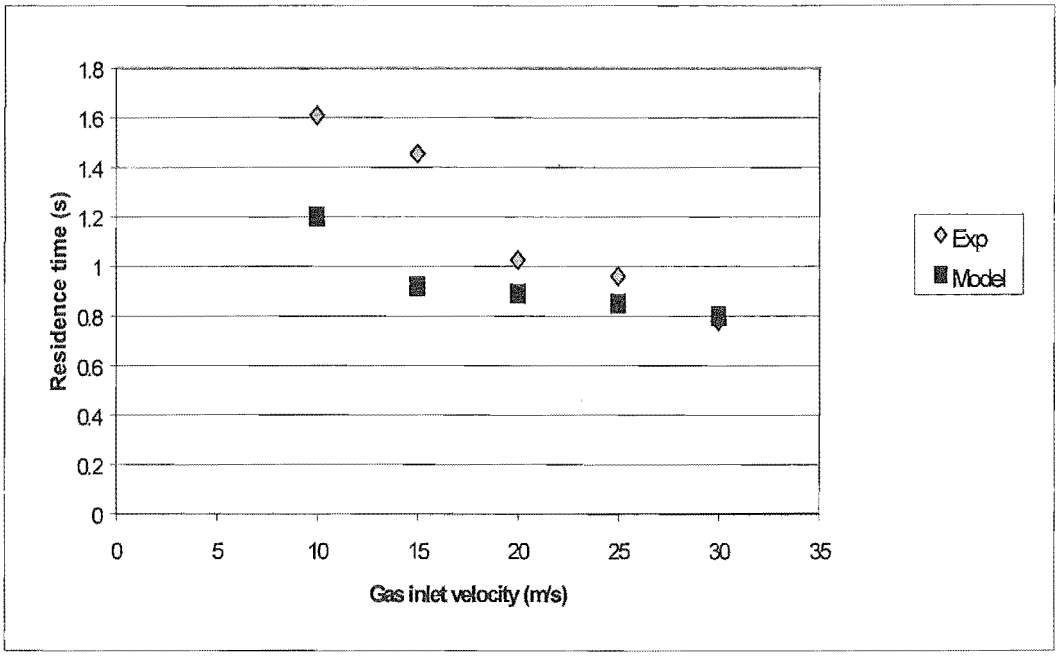

Figure 6-47 Experimental and Model predicted residence time with increase in gas inlet velocity, SGL = 0.08, silica gel particles of size range 699-850 μm

The model-calculated residence times of sand and silica gel in different cyclones are shown in Figure 6-48. The residence time of both sand and silica gel show two distinct trends. The residence time of both materials decreases with increase in the total included angle of the cone reaching a minimum at an angle of about 25 degrees. Thereafter the particle residence time increases. Also shown in Figure 6-48 are the average values of the experimentally measured residence times for sand particles. In Figure 6-48 it was assumed that SGL has no effect on residence time and therefore the values were averaged to give a mean value for each cyclone.

Experimental results indicated an increase in residence time with increase in density. Thus from experimental measurements sand with higher density (2600 kgm^{-3}) had a residence time about twice that of silica gel (1200 kgm^{-3}). These trends reversed in the predictions of Figure 6-48. However, an analogy can be drawn between this minimum in residence shown in Figure 6-48 and the change in flow pattern discussed in § 6.1. It was observed experimentally that as the cone angle was increased there was an early transition (in the conical section) of particle travel from bouncing sliding on the wall.

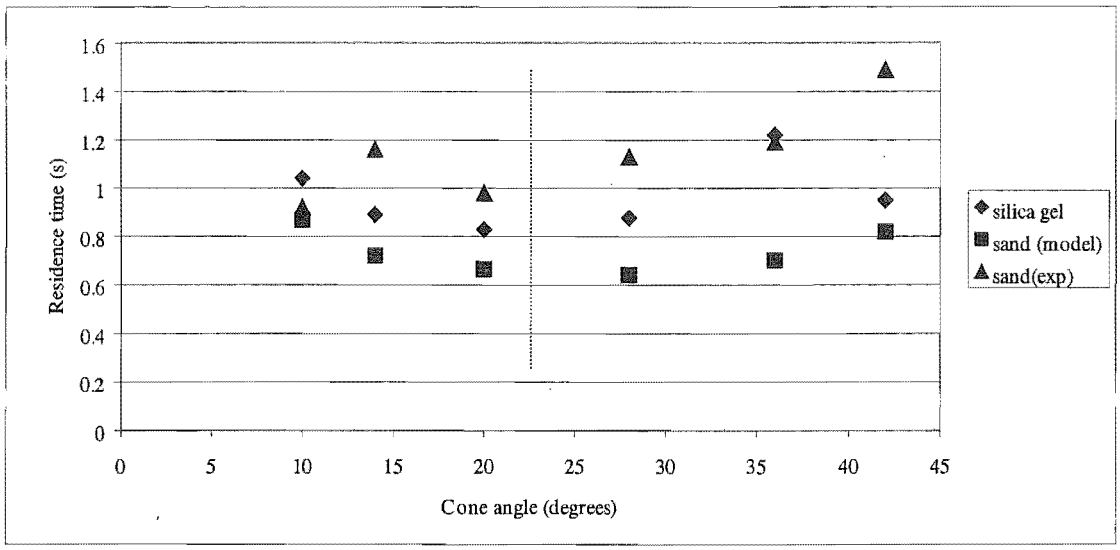

Figure 6-48 Model predicted residence times for sand and silica gel particles particle size range 250-500 μm; gas inlet velocity 20 m s^{-1}

6.3.3. Multiple Particle Approach

The single particle approach is the simplest model in which there is no interaction between particles and the isolated particle is surrounded by gas. When dealing with multiple particles especially near the cyclone wall several additional factors compound the problem. For the case of a single particle the free stream drag F_D is considered. Where F_D is given by

$$F_D = \frac{1}{2} C_D \rho A \left(\boldsymbol{V_g} - \boldsymbol{V_p} \right)^2 \qquad (6.3\text{-}46)$$

When clusters exist, such as occurs in roping, the fluid drag within these interstices is much less compared to the free stream drag. The drag on an individual particle will depend, amongst other things, on the closeness and geometrical arrangement of neighbouring particles for this will determine the local flow pattern (Rowe and Henwood, 1961). Free stream drag force is higher compared to the drag in the

interstices, and because of this, difference in forces shearing motion can result. It is possible discontinuity of ropes as documented in § 6.1 could be the result of this shearing action. This action increases the frequency of particle-particle interactions (Figure 6-47).

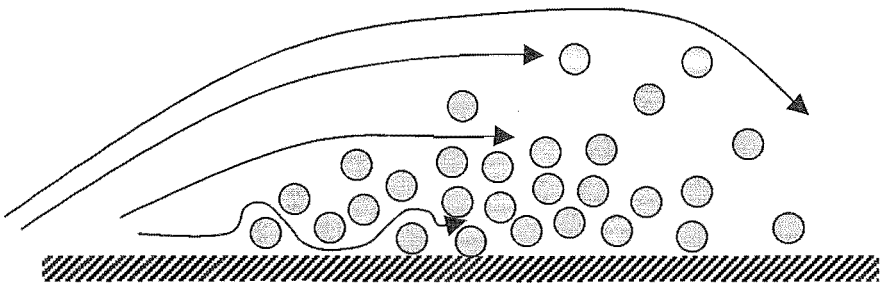

Figure 6-49 Flow regime in multi-particle system

In addition a modified drag coefficient C_{Dm} is used (Hoomans et al., 1996) where

$$C_{Dm} = C_D \varepsilon_g^{-4.7} \tag{6.3-47}$$

where C_D is the drag coefficient for a single particle in a gas with no boundary effects and C_{Dm} is the drag coefficient for a single particle in the presence of other particles with a voidage of ε.

In this treatment it is assumed that the coupling between gas and particles is one way, with the particles having no influence on the gas flow field. It is also assumed that the interactions between particles and wall are only mechanical with the hydrodynamic interactions due to presence of the wall not considered at this stage.

As the voidage is decreased the mean free path of a particle before collision with another particle is decreased. Particles moving faster lose momentum on collision and the slow moving particles gain momentum after a collision. The net result is that the velocity of the particles approaches a mean velocity, which is the velocity at which the assembly is moving.

The frequency of particle-particle interactions is a function of the rate of solids feed into the cyclone $\dot{M}$ and the average maximum distance ΔR attained by particles from the wall after bouncing. In effect these two variables control the void fraction ε_g

$$\varepsilon_g = \frac{Vol_g}{Vol} \tag{6.3-48}$$

where Vol_g is the volume occupied by the gas and Vol is the total volume of interest. The region of interest is the annular volume covering the radial distance ΔR.

The volume fraction occupied by the solids is ε_s

$$\varepsilon_s + \varepsilon_g = 1 \tag{6.3-49}$$

Under steady state conditions the solids mass flow rate is

$$\dot{M} = \rho_p A v \varepsilon_s \tag{6.3-50}$$

where v is the mean particle axial velocity, ρ_p particle density and A is area and is given by

$$A = \pi\left(2R_x\Delta R - \Delta R^2\right) \cong 2\pi R_x \Delta R \tag{6.3-51}$$

For a given solids feed rate into the cyclone the voidage increases with an increase in ΔR because the proportion of particles bouncing higher increases. At a given radius R_x, with a given V_{in}, then V_g will be constant and $\frac{V_g^2}{R_x}$ will be constant. The centrifugal force is fixed. ΔR is a function only of three variables if density of the particle is constant

$$\Delta R = f\left(e, d_p, R_x\right) \tag{6.3-52}$$

where e is the coefficient of restitution.

There is a high probability when ΔR is small that this coefficient of restitution is for the contact of a particle with a wall consisting of a layer of similar particles.
The diameter of particle is an important parameter because for larger particles the inertia is dominant and therefore the maximum value of ΔR for a larger particle is greater than that for a smaller particle (Figure 6-48).

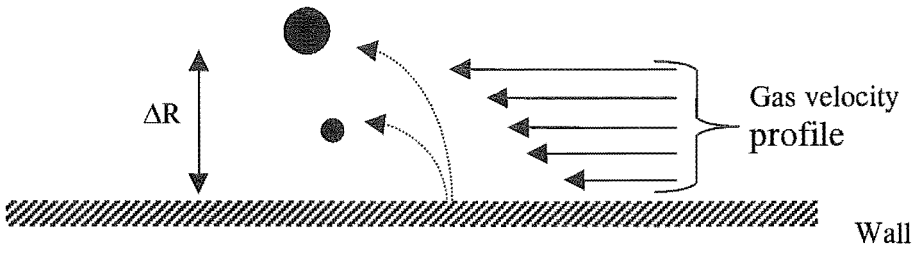

Figure 6-50 Relationship between ΔR and diameter of particle

When a free particle bounces off from a surface the maximum height it will attain is dependent on the coefficient of restitution. However if the particle is surrounded by other particles there is a probability that its path will be impeded by another particle. The probability of impediment is a function of the concentration of the particles. The net result is that the height at which the particle will bounce will be reduced. A collision factor f_p can be introduced to represent the loss in momentum as result of these particle-particle interactions. The effective coefficient of restitution e_p is given by

$$e_p = f_p e \tag{6.3-53}$$

where $f_p < 1$
The collision factor represents the collision of a particle with another particle. The likely result of a particle colliding with another particle is a decrease in ΔR

The total solids volume fraction can be expressed by the following equation

$$\varepsilon_s = \frac{\dot{M}}{\rho_p \pi (2R_x \Delta R)_v} \qquad (6.3\text{-}54)$$

The solids volume fraction increases with a decrease in the R_x with all other factors are held constant. This explains the formation of ropes towards the discharge end of the cyclone.

Discussion

7

7.1. Measurement uncertainties 7-2

7.2. The Imperfect Tracer Technique 7-6

7.3. Axially Dispersed Plug Flow Model 7-7

7.4. Particle Residence Times 7-7
- 7.4.1. Effect of moisture content on residence time 7-7
- 7.4.2. Particle size 7-8
- 7.4.3. Particle density 7-11
- 7.4.4. Solid Gas Loading (SGL) 7-12
- 7.4.5. Gas Inlet Velocity 7-16
- 7.4.6. Particle Inlet Velocity 7-17
- 7.4.7. Cyclone Diameter 7-17
- 7.4.8. Total Height, and Proportion of Cone Height 7-18

7.5. Particle Peclet Numbers 7-20

7.6. Roping 7-24

7.7. Modelling 7-32

7.1. Measurement uncertainties

It is well appreciated that any measurement is associated with some uncertainties. The two most common error sources are systematic (bias) and precision (random) although errors which can be classified as "blunders" are sometimes encountered but will not be considered here.

Central to the moving impactor technique was

(a) the accurate specification of the velocity of the impactors and

(b) collection of representative samples of particles for counting.

The movement of the impactors was monitored on a chart recorder via a potentiometer. The velocity of one of the impactors was determined by timing the time it took the impactor to travel a distance of 181 mm. The velocity of the other impactor was thus matched to the known velocity by adjusting the oil control needle valve and monitoring the movement on the chart recorder. The velocity was checked before and during each run. The uncertainty in the determination of the velocity of the impactors was estimated at 6%. This uncertainty was mainly associated with timing errors.

From the previous set-up of Rajendra (1995) it was noticed that the line pressure to the hydraulic system fluctuated depending on secondary air requirements on the main line. A lot of effort was thus required to readjust the oil needle valves depending on available pressure. To control this a regulator was installed to maintain the driving pressure at 5 bar. Another source of error was friction in the hydraulic ram. Friction decreased the velocity of the ram and was attributed mainly to dust deposits and bends in the shaft. To minimise the effects of friction the hydraulic ram was kept well oiled and straightened when required especially the lower impactor which was not well supported. Leakage of oil through the couplings was detected on a couple of occasions and the problem was immediately fixed and the results of the affected runs discarded. Oil leakage resulted in hydraulic pressure fluctuations and consequently affected impactor velocity.

It was also noticed that during the movement of the hydraulic ram the impactor could have a free displacement of a maximum of 2mm. Allowing for the maximum displacement gave an additional uncertainty in residence time of 0.1 s.

In addition to the uncertainty in the velocity of the impactors in the moving impactor method, another source of error was in the collection and counting of particles to yield concentration time curves. In fact no sophistication in data reduction technique could make up for any shortcomings at this stage and yield a reasonable result. The collection and counting of *well-mixed* sample particles from the flow stream was therefore also of critical importance to the moving impactor method. The particles, the tracer and non-tracer particles should be adequately mixed. This was very important considering that, for example, for the inlet impactor with a 3 mm diameter nozzle the sampling area was about 0.14 per cent of the total area of particle flow and about 0.27 per cent for the bin impactor with silica gel particles. The tail of the concentration curve, with the lowest concentrations had the most uncertainty. To minimize this effect the sampling position was changed to achieve higher numbers and therefore more uniform number distribution of tracer particles in the flow. This need was recognised from the beginning of this study.

To increase the number of particles collected, the impactor was removed from a position part way down the bin wall and positioned at the exit from the cyclone where particle flux was higher. This improved reliability in the number of particles collected, especially for the dispersed non-roping particles. It was unlikely that this arrangement altered the flow pattern of the particles in the cyclone. This was supported by finding no change in the residence time of the particles as a result of the replacement of this probe. The number of particles collected was also controlled by the diameter of the sampling nozzle. For the lowest particle size range of 150-210 μm a 2-mm diameter nozzle was used and the largest nozzle used was 3 mm in diameter. The number of particles that could be collected by the inlet impactor for a given particle size, solids mass flux and sampling nozzle diameter could be estimated from the following calculation. It was assumed that the solids were

distributed uniformly in the entrance duct after leaving the ejector. This assumption was validated by visual observation through a glass window with the aid of a stroboscope.

Solids mass flow rate into cyclone ($\dot{M}$) = 10.5 g s^{-1}

Gas volumetric flow rate = 0.099 $m^3 s^{-1}$

Cross sectional inlet area of cyclone (A_{in}) = 0.045x0.110 = 0.00495 m^2

$$\textit{Solids mass flux} = \frac{\dot{M}}{A_{in}} = \frac{10.5}{0.00495} = 2121.2 \frac{g}{m^2 s}$$

Cross sectional area of a 3 mm sampling nozzle (A_n) = $\frac{\pi}{4}(0.003)^2 = 7.069 \times 10^{-6}$ m^2

Mass of solids collected per second = Mass flux x A_n

= 0.015g s^{-1}

$$\text{Mass of solids collected per mm of impactor (N)} = \frac{\textit{Mass collected per second}}{V_s}$$

Where V_s is the velocity of the shuttle (mm s^{-1})

$$N = \frac{0.015}{22.6}$$

$$= 0.00065634 g/mm$$

For sand particles of mean diameter 350 μm and density 2.6 g/cm^3 the mass of a particle m_p is given by

$$m_p = \frac{\pi}{6} d_p^{\,3} \rho = 0.0000584 g$$

Number of particles per mm of impactor surface =

$$\frac{0.00065634}{0.0000584}/mm \quad = \quad 11 \text{ particles per mm of impactor surface}$$

Total number of particles that could be collected over the entire surface in one cell = 11x2.5 = 28.

The calculated number compares well with the experimental average of 25 per cell for sand particles of size range 250-500 μm particles on the inlet impactor as shown in Figure 5.8-1.

Collection of too few particles introduced errors. The bimodal nature of the curve in Figure 5.8.3 was likely to be caused by an insufficient and unrepresentative number of particles collected. In the time intervals of the tail of the bin response a very low number of particles were counted. The particles sampled in this period appeared to be not travelling in a rope, there was a corresponding decrease in the average number of particles, and therefore the flux was lower compared to that for a rope. For instance, if only two particles are collected, one trace and the other non-tracer, this would give a tracer concentration of 0.5 at that point. The net result would be high weighting for this measurement point, which will give an uncharacteristic high residence time. On the other hand if the number of particles collected is too high resulting in several particle layers this will hinder the counting. However when handled properly the effect on residence time will be minimal compared to the case when not enough particles are collected. The ideal case was to have particles that were monolayered and amenable to counting. Particle flux in the inlet duct was steady and well distributed resulting in a steady number of particles on the inlet impactor. The position of the bin impactor at the cyclone discharge improved the number of particles collected for non-rope particles ie. particles travelling in the dispersed phase.

The major types of errors encountered in this measurement technique are random errors, and could be the cause of scatter in the data. If the residence times of the particles were dependent on the particle size the distribution of particle sizes within an interval would cause some scatter in the results. From Figure 5.9-3 the mean

residence time of silica gel particles in the size interval 210-295 μm ranged from about 0.55 to 0.65 s. In the size interval of 295-500 μm the range was from about 0.65- 0.85 s. For the narrow size ranges used, there is a general scatter in the mean measured particle residence time of about 0.2 s. This scatter cannot solely be attributed to a range in particle sizes, as there are also other sources of error like variation in impactor velocity and error in collection of particles. Although these undesirable random errors could not be totally eliminated the data is nevertheless valuable as significant trends are revealed.

Bias or systematic errors are usually easy to handle when detected. The results for the first 27 runs had to be adjusted to rectify a systematic error. It was found that the alignment of the impactors was offset by about 6.5 mm. This necessitated the adjustment of the residence times by adding 0.28 s to the evaluated result.

7.2. *The Imperfect Tracer Technique*

With the imperfect tracer technique the need to achieve perfect tracer changes was not necessary. However, this technique should be used with care especially when dealing with particulate solids. The radial or axial dispersion of a tracer gas in a gas or liquid stream is much higher compared to solids dispersion within the whole solids stream. Thus where dispersion of the tracer is not sufficient, the sampling of a representative number of particles could therefore pause a challenge.

Nevertheless, results obtained by the imperfect pulse technique were consistent when sufficient and well-mixed particle samples were collected on the impactor. Both pulse and step input changes were used. The introduction of the tracer by the methods illustrated in Figure 2-5 and Figure 2-6 with the aid of a conveyor belt for both pulse and step input meant no flow disturbance was brought about by the introduction of the tracer. This can be compared with that reported by Rajendra (1995) with his technique of blowing a high peak in over a small time. Therefore

the residence times obtained by this method were representative of normal flow conditions and not transient flow regimes.

7.3. Axially Dispersed Plug Flow Model

The axially dispersed plug flow model was found to be a valid representation of the flow of particles in a cyclone. Using this model the mixing process was interpreted as a diffusion phenomena. As explained in Saruchera and Abrahamson (1997) (Appendix 9A) the transfer function method was found not suitable for evaluation of particle Peclet numbers. The residence times and Peclet numbers in this study were thus evaluated by the least squares method using the Solver tool in Excel. This method improved considerably the quality of information obtained from otherwise erratic data. As shown in Figure 5.8-8 there was a very good fit between the model predicted and the experimental curve. The usefulness of the parameters from this fitting technique is solely dependent on the quality of experimental data obtained and how representative it is of the full stream.

7.4. Particle Residence Times

The particle residence times were measured as a function of both operational and design variables. The influences of each of the variables on the particle residence time are discussed separately in the following subsections.

7.4.1. Effect of moisture content on residence time

Ideally cyclones are very effective at removing surface moisture of materials in the drying chamber. The residence times of silica gel particles exposed to highly humid atmospheres (up 80 per cent relative humidity) was found to be within normal bounds of experimental error when compared to that of normal silica gel particles in ambient air. This implied there was no change in trajectories of these

particles as a result of the change in moisture content with the corresponding change in mechanical properties.

7.4.2. Particle size

Solids handling systems usually generate some fines. Moreover, rarely are monosized particulate solids encountered in normal processing streams. The sizes are instead reported in terms of particular size intervals as per cent size passing or retained on a particular screen mesh size. Different particle sizes are usually accompanied by changes in hydrodynamics in the gas solid suspensions. This change in hydrodynamics can give rise to a distribution of residence times of these different particle sizes.

The concentration-time distribution curves for unsieved silica gel particles (the batch obtained from SPS, Harwell, UK) covering a size interval from about 100 μm to 850 μm is shown in Figure 7-1. This can be compared to the distribution for silica gel particles for a size interval of 500-700 μm shown in Figure 7-2.

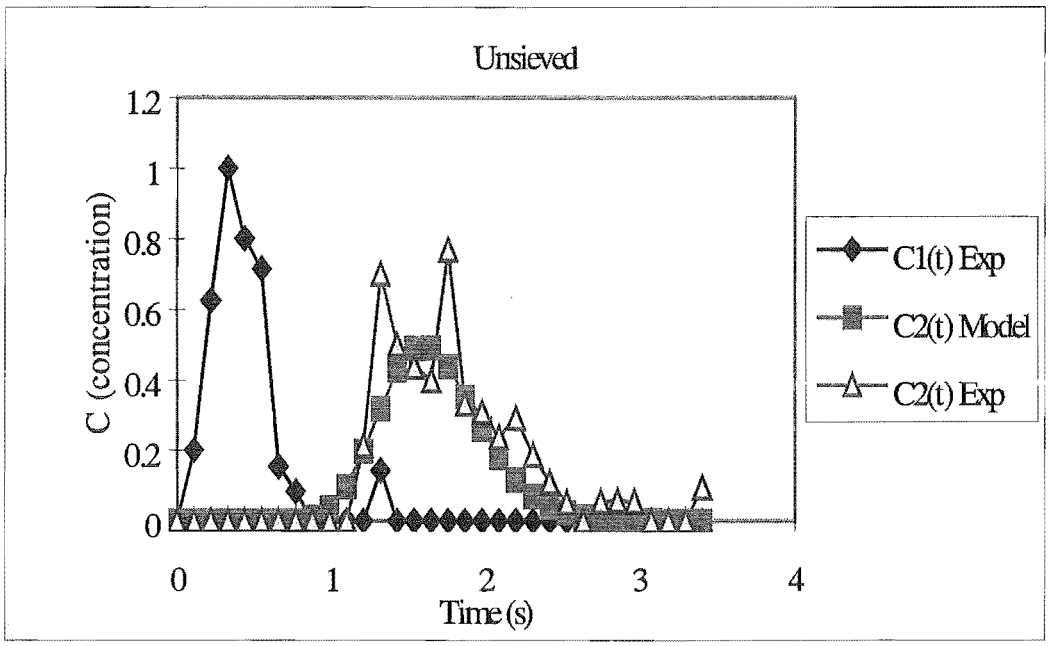

Figure 7-1 Tracer concentration-time curve for unseived silica gel [run 11]

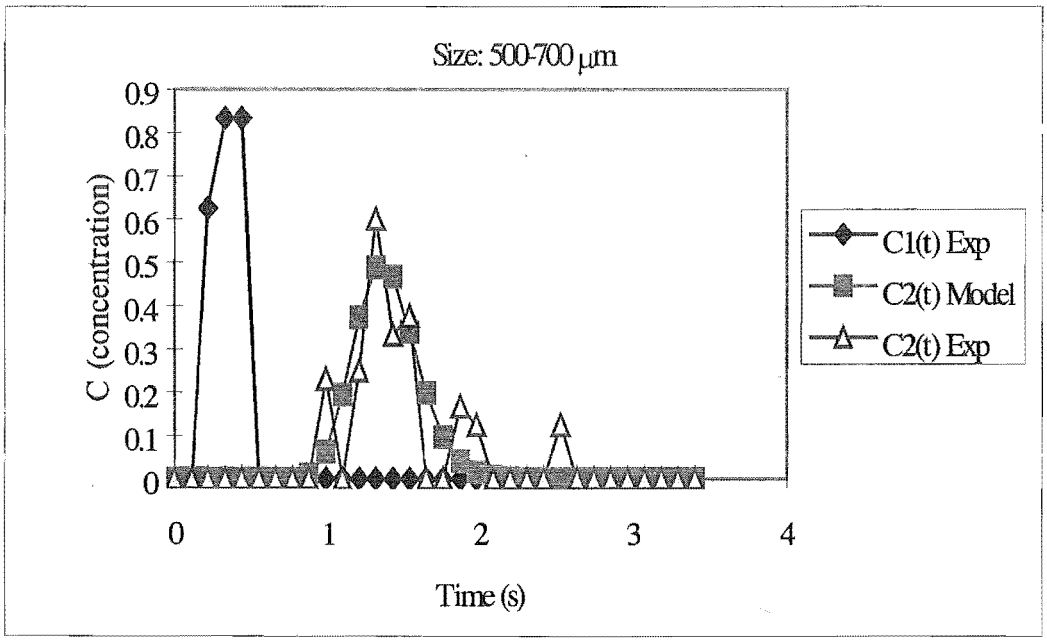

Figure 7-2 Tracer concentration-time curve for silica gel of narrow size interval [run 43]

Comparing Figures 7-1 and 7-2, a wider distribution is obtained from a wide size distribution. The mean particle residence time of unseived silica gel was larger compared to the mean particle residence time of silica gel in a specified narrow size interval. Although a full size distribution of the unsieved particles was not noted these results suggest that there where a smaller proportion of fines.

The experimental results of this study showed clearly that the residence time of particles increased with increase in particle size. The trends are shown in Figure 5.9-3. The significance of these results is that for small particles with high drying rates the exposure time would be limited while larger particles with significantly lower drying would be exposed for longer periods.

The range of particle sizes investigated was 210-295μm, 295-500 μm, 500-700 μm and 700-850 μm. Comparison with literature is complicated by the different experimental and operating conditions resulting in diverse claims. The results of Kang et al. (1989) showed an increase in particle residence time with decrease in particle size at a gas inlet velocity of 6 m s^{-1}, which conflicts with the findings of this experimental study. The results shown in Figure 5.9-3 are for a gas inlet velocity of 20 m s^{-1} in a standard Stairmand cyclone with overall height of 0.845 m (cyclone B) compared to that of Kang et al. with an overall height of 1.50 m. The cyclone of Kang et al. (1989) had a total included cone angle of 18 degrees while cyclone B (this study) had a total included cone angle of 14 degrees. This therefore implies that these results apply to different regions of the ratio of the centrifugal acceleration to gravity ($\frac{V^2/R}{g}$). The mean particles sizes used by Kang et al. were 141μm, 178 μm and 211 μm. The trends shown in Figure 5.9-3 are in agreement with the result of Kemp et al. (1998). If true the trends of larger residence times with decrease in particle size (Kang et al) could pause operational problems for operation of cyclone driers as the fine material will be over exposed.

The particles used by Kang et al. were char particles with density of 1700-kg m^{-3} compared to silica gel with a density of 1200-kg m^{-3}. A possible explanation by Kang et al. is that the small char particles are drawn into the central vortex by a radial gas flow, rise up and are later thrown onto the wall by centrifugal force action. Similar flow behaviour would have been expected of silica gel particles used in this study as they have a lower density than char particles and therefore particle inertia forces will be less significant. Also the low velocities used by Kang et al. would mean that the centrifugal force effect would be much smaller.

7.4.3. Particle density

The experimental results showed an almost two fold increase in particle residence time for a two fold increase in particle density when the particle size range was kept constant (Figure 5.9-4 and Figure 5.9-5). The materials compared were silica gel and sand, which had different densities, 1200 and 2600 kg m^{-3} respectively. As shown in Figures 5.2-1 and 5.2-2, in addition to the differences in density these particles have different shape characteristics with sand particles being more circular compared to silica gel particles which were more angular. The coefficient of restitution of the particles was also different, as determined from bouncing tests (§ 5.13). The average coefficient of restitution for silica gel was about 0.7 compared to that of sand, which had an average of about 0.25. Collisions between silica gel particles and the wall were more elastic and therefore after contact with the wall a silica gel particle leaves the wall boundary layer, moving into the main gas stream where the aerodynamic gas drag force is higher. In contrast sand particles stay closer to the wall in the region of lower drag force because the collisions are relatively more inelastic. The drag force close to the wall region is lower because of the boundary layer effects leading to lower particle velocities. Where the boundary layer is thin a higher density and hence higher centrifugal force will result in higher frictional force with the wall t hereby retarding the particle.

7.4.4. Solid Gas Loading (SGL)

Figure 7-3 shows the region in which there is little change in the particle residence time with increase in SGL and region in which particle residence time decreases with increase in SGL for different cyclones. Cyclones C, D and F have total included cone angles of 20, 28 and 42 degrees respectively. There is a change (decrease) in residence time of about 50 per cent for cyclone D and about 20 per cent for cyclone C when the SGL is increased from about 0.07 to 0.11. Therefore while solids residence time is weakly dependent on SGL (Kemp et al., 1998) for cyclones with cone angles less than 20 degrees this result cannot be extended to large cone angle (> 28 degree) cyclones.

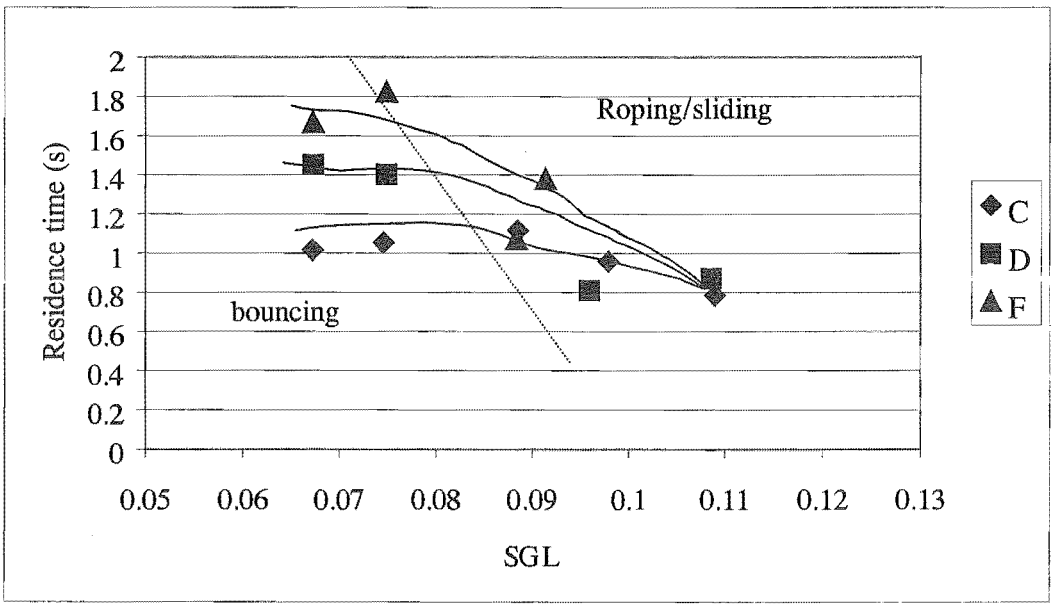

Figure 7-3 Change in residence time with SGL for cyclones C, D and F
Sand particles: size range 250-500 μm

The variation of particle residence time with SGL as shown in Figure 7-3 can be attributed to different flow patterns. The two main flow regions are illustrated in Figure 7-3 and were corroborated by observations of particle flows inside the cyclone. The first region shows little or no change in particle residence time with increase in SGL up to an SGL of about 0.08. However this upper limit of SGL is also a function of the total included cone angle of the cyclone and particle characteristics. In the region where the residence time of the particles shows little

or no dependency on SGL the particles move in a chaotic manner by bouncing repeatedly on the walls of the cyclone with long inter-particle distances. Therefore in this region the mode of transport of particles is predominantly by bouncing. The existence of different flow regimes could account for the diverse claims of trends or particle residence time with SGL reported in literature.

The second region where there is a sharp decrease in residence time with increase in SGL is characterized by roping, where particles form locally high concentration streams flowing on the wall.

The solids flowing in the cyclone obtain their energy from the gas. A light loading of solids would be expected to result in shorter residence times as a lot of energy is available to the solids and they travel with the gas with lower slip velocity. Thus coupling is one way with the solids not affecting the gas flow field. This is on the assumption that particles move along with the gas and that only the gas influences the free flight of the particles. The slight decrease in residence time with increase in solid gas loading (Figure 5.9-3) would point to a possible change in flow pattern. For larger particles the change in residence time with SGL appears to be greater compared with smaller particles. When there is a local high concentration of particles as happens in ropes, it is likely that the particles away from the surface and close to the wall have low velocity. The whole vortex will be slowed down by the presence of these particles. The effect of the reduction of the vortex is a reduction in the tangential velocity. Momentum is transferred from particles impacting on the surface and propagated to particles deep in the layer. Because of the low velocity, the centrifugal force of these particles will therefore be very low. Under these circumstances it is probable that with increase in SGL the effect of gravity will be greater and the particles settle out and slide down the wall, independent of the gas flow. This flow pattern changes when the gas velocity is increased which results in an increase in centrifugal force and its component up the wall.

Therefore for the lower cone angles the bouncing model can be applied where the free flight of the particles is dependent on the gas drag. However, with the higher

cone angles (cyclones C, D and F) wall flows are more significant. The residence time of particles in these cyclones appears to be more sensitive to changes in the SGL (Figure 7-3).

When wall flows are predominant, the flow of the particles can be described by the following relationships.

If the rate of solids flow is give by M (kg/s)

Then

$$M = \rho_p A v(1-\varepsilon_g) \qquad (7\text{-}4\text{-}1)$$

where v is the mean velocity of the rope and ε is the voidage, A is the cross sectional area of the rope (assuming solids travel exclusively in a rope) and ρ_p is the density of the particles.

If L and τ_r are the equivalent trajectory length of the particles in the rope and the mean residence time of the particles travelling in a rope in the cyclone respectively, the mean velocity of the particles travelling in a rope is given by the following equation

$$\upsilon_r = \frac{L}{\tau_r} \qquad (7\text{-}4\text{-}2)$$

From Equation 7-4-1, rearranging in terms of v_r

$$\upsilon_r = \frac{M}{\rho_p A(1-\varepsilon_g)} \qquad (7\text{-}4\text{-}3)$$

Equating Equation 7-4-2 to Equation 7-4-3

$$\tau = \frac{L}{M}\rho_p A(1-\varepsilon_g) \qquad (7\text{-}4\text{-}4)$$

Experimentally it was observed that L decreased with an increase in solids flow rate (M). For a given material and cyclone design the particle density ρ_p in Equation 7-4-4 is a constant.

The relationship between the particle residence time for the rope and the inverse of the solids feed rate is plotted in Figure 7-4. The mass flow rate of the solids is based on an inlet velocity of 20 m s^{-1} and gas density of 1200 kg m^{-3}. In the interval of solids mass flow rates shown in Figure 7-4 there is no change in particle residence time for cyclone C. Figure 7-4 shows that if the mass feed rate is increased the particle residence time is decreased. The slope of the graphs is given by the following equation

$$LA(1-\varepsilon_g) = \text{constant} \qquad (7\text{-}4\text{-}5)$$

for constant ρ_p

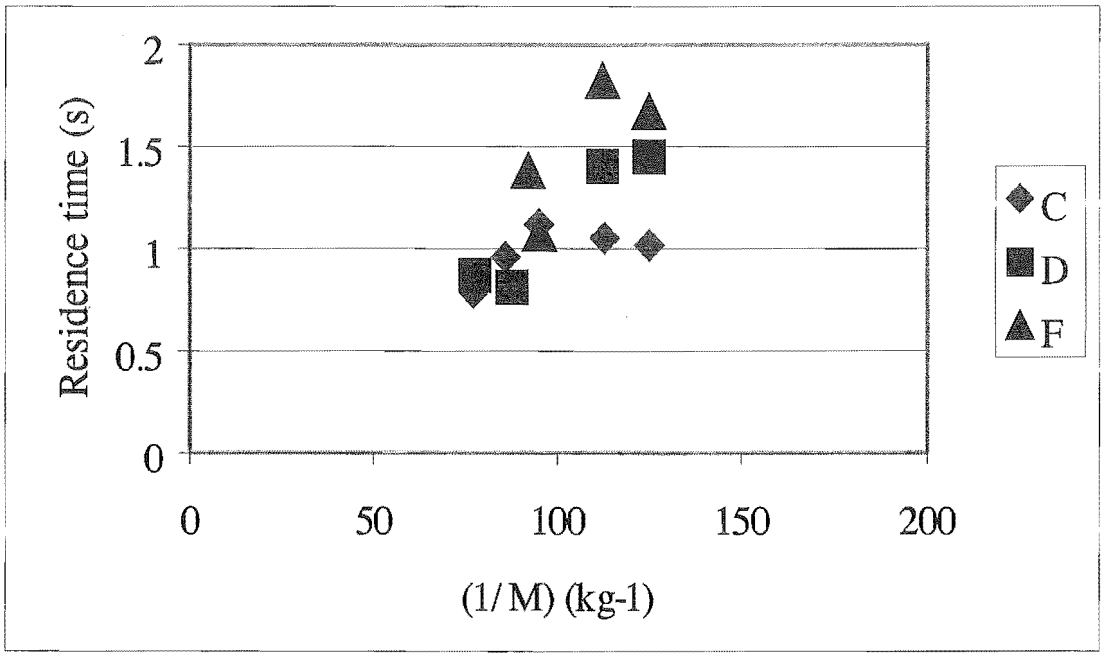

Figure 7-4 Particle residence time as a function of inverse of mass flow rate

Noting that experimentally L decreased with increase in M, then A must increase strongly with M at high angles if ε_g is assumed constant.

For cyclone C the following relationship is valid

$$LA\left(1-\varepsilon_g\right)=1 \qquad (7\text{-}4\text{-}6)$$

The validity of Equation 7-4-6 can probably be extended to cyclone A and B as well, where particles travel independently with no change in particle residence time with increase in SGL.

7.4.5. Gas Inlet Velocity

Over the range of gas inlet velocities of 10 to 30 ms^{-1} the mean residence time of silica gel particles at an SGL of 0.08 in cyclone B decreased with increase in the gas inlet velocity (Figure 5.9-6). Results of Lede et al. (1989) showed an increase in the mean particle residence time with increase in gas inlet velocity, ie. contradicting the trend in this work. The size of particles used by Lede et al. (1989) was about of the same order of magnitude as used here. The discrepancies in the results could possibly lie in different experimental conditions. Lede et al. measured the mean residence time of single particles. As mentioned in the previous subsection (§ 7.4.4), there is a change in flow pattern for few particles with little or no interactions to multi-particle phases where wall particle boundary layers form presenting a highly inelastic collision surface. Kang et al. (1989) also reported an increase in particle residence time with increase in inlet velocity. The solid gas loading for the results reported by Kang et al. (1989) is not specified and therefore makes comparison impractical.

7.4.6. Particle Inlet Velocity

The velocity of particles into the cyclone was controlled by a change in the velocity of gas in the ejector. The results of measurement of mean solids residence time under these conditions are shown in Figure 5.9-9. For two similar particles travelling at velocities of 40 and 10 ms^{-1} respectively the particle Reynolds numbers are 670 and 330 respectively. The particle relaxation times for these particles are 0.14 and 0.22 s respectively corresponding to travel distances of (40)*(0.14) = 0.5 m and (10)*(0.22) = 0.2 m respectively. Therefore the low velocity particle would be almost up to gas velocity at the first impact with the wall whilst the fast moving particle would be above the gas velocity. However, from the results it appears that equilibrium for both particles is attained after only a few bounces and hence no differences in residence times. In practice only minimal acceleration of the solids is necessary in the ejector with the main objective being to reach steady state conveying velocity. Once the particle enters the cyclone steady state conditions with respect to gas flow are attained quickly. The results obtained under these conditions will therefore unlikely deviate from the case when normal ejector feed operating conditions are used. The gas flow rate can be used as a means of controlling particle residence times by varying the drive motor speed.

7.4.7. Cyclone Diameter

The results in this study where obtained with cyclones all with the same barrel diameter. The results of this study were combined with those of SPS for larger cyclone by Kemp et al. (1998). The residence time of the particles was reported to be proportional to cyclone diameter through an empirical correlation (Kemp et al., 1998).

7.4.8. Total Height, and Proportion of Cone Height

The total height ranged from 420 mm to 1020 mm with a constant length of barrel of 230 mm and varying cone lengths. The particle residence time did not increase with increase in total height of the cyclone, but rather increased with increase in cone angle.

The range of ratios of cone height to total height investigated was from 0.45 (cyclone F) to 0.775 (cyclone A). This range of ratios represented a range in the total included cone angle from 42 degrees to 10 degrees. It appeared that there was a perceptible decrease in residence time with increase in SGL, especially for cyclone C, D and cyclone F where runs were performed at different values of SGL (Figure 5.9-11) compared to cyclone B were similar data is also available. The increase in the ratio of cone height to total height by a factor of about 1.7 (cyclone F to A) was not matched by an increase in residence time of the particles. Instead it appeared that within bounds of experimental error of 16% that particles residence time actually increased with a decrease of this ratio. Table 7.1 shows the residence times for different cyclone geometrises.

Table 7-1 Residence times of sand particles in different cyclones
(size range 250-500 μm)

Cyclone	Cone angle (total)	Total Height (m)	Ratio*	Residence Time (s)
A	10	1.02	0.775	0.7-1.2
B	14	0.79	0.709	1-1.3
C	20	0.627	0.633	1
D	28	0.510	0.549	1.4
E	36	0.452	0.491	0.9-1.4
F	42	0.420	0.450	1.3-1.7

* $\text{Ratio} = \frac{\textit{Height of cone}}{\textit{Total Height}}$

Particle residence time was reported to increase monotonically (Kang et al. 1989) with increase in height as the total distance travelled by the particle increased. Kang et al. increased the total height by increasing the height of the barrel. The results in this study cannot be compared to those of Kang et al. (1989) as they kept the cone angle constant. However, when the geometry is kept constant an increase in total height should result in an increase in residence time as reported by Kang et al. and also by Kemp et al. (1998). When the cone angle is not constant there is no increasing relationship between height of cone and mean particle residence time. At a given SGL the particle residence time appeared to increase with increase in cone angle or rather does not decrease with decrease in overall height of the apparatus. This change in the residence time for similar operating conditions can thus be explained by a change in solids flow pattern on the cone surface when the cone angle is increased.

If envelopes (or bands) are to be drawn in Figure 5.9-11 for ranges in residence times with SGL for cyclones B, C, D and F these surface envelopes becomes steeper in moving from cyclone B to F. The rate of decrease of residence times with SGL increases with increase in cone angle. Earlier in this section (§ 7.4) it was pointed out that for a given cyclone geometry when the solids feed rate was increased the degree of particle-particle interactions increased while a wall particle boundary layer formed. This flow pattern appears to be associated with lower particle residence times. It can thus be inferred that for a given geometry the increase in SGL results in a more ordered flow pattern and thus shorter residence times. More discussion on these flow patterns is treated in § 7.6 and § 6.1.

It can be noted that gas residence times in cyclones A to F decreased as shown in Table 5.6-1. Although gas residence time decreased there was no corresponding decrease in particle residence times in these cyclones. The solids therefore appear to be less influenced by the gas flow resulting in large slip velocities. The solids inventory or hold-up and also the residence times increase with decrease in the ratio of cone height to total height.

7.5. Particle Peclet Numbers

Particle Peclet numbers are a measure of the back mixing of the solids in the cyclone. The mechanism of dispersion in particulate systems is by displacement of particles into void spaces in the suspension and is normally associated with shear action. Therefore suspensions with high voidage are characterised by high particle dispersion coefficients and low dispersion coefficients are associated with systems with low voidage.

Effect of Feed Rate on Peclet Number

It is convenient to think in terms of inverse Peclet numbers. High inverse Peclet numbers and therefore high dispersion coefficients were obtained at low feed rates (Figure 5.10-1). The particle Peclet numbers shown in Figure 5.10-1 are for silica gel particles for which no roping was observed. There was a gradual decrease in inverse Peclet number or decrease in solids dispersion when the solids feed rate was increased. At low solids feed rates the void fraction was high and therefore inter-particles distances were also high. The particles had higher dispersion lengths or mean free paths. Particle-wall interactions are then more significant than particle–particle interactions, as the particles bounce off from their collisions with the wall at high angles analogous to the kinetic theory of gases. However as the particle numbers increase the void fraction is reduced and with it the mean free paths of the particles. Particle-particle interactions also become significant where ropes or clusters are formed. Although these interactions increase, the collisions are localised. The mean free path of each particle under these flow conditions is reduced. Instead the masses of particles move as an assemblage with high inter-particle interactions with low dispersion or back mixing as particles push on each other. Therefore the effect of an increase in particle concentration is a decrease in solids dispersion.

Effect of Gas Inlet Velocity on Peclet Number

The effect of an increase in gas inlet velocity on Peclet number of silica gel particles is shown in Figure 5.10-2. The size range of these particles was 700-850 μm and the SGL was 0.08. The inverse Peclet number increased with increase in the gas inlet velocity indicating a very high dispersion of these solids. Higher gas inlet velocities result in higher centrifugal force acceleration and increased particle wall interactions and in some case formation of ropes. However, no roping was observed in the flow of these large silica gel particles. Where ropes are formed there is an expected decrease in particle dispersion within the rope itself as the void fraction in this wall region will be reduced. Rather the dispersion of these large silica gel particles could be attributed to the random trajectory paths of the particles as they bounce on and off the walls.

The silica gel particles under consideration were large and therefore would possess very large momentum. For these large particles, particle inertia is more important so the movement of the particles is less influenced by the gas flow turbulence. The particles were observed to be bouncing randomly in the cyclone, with particle trajectories even crossing the inner vortex. The results of Kang et al. (1989) also show a decrease in the Peclet number with increase in gas inlet velocity. However the particles used by Kang et al. were small and ranged in size from 141-211 μm. In this study the Peclet number of silica gel particles of size range 500-700 μm at an SGL of about 0.08 (10 g/s) was 40 (Figure 5.10-1). From Figure 5.10-2 the Peclet number of silica gel particles of size range 700-850 μm was also about 40. Also a 275 per cent increase in solids feed rate (Figure 5.10-1) resulted in a 900 per cent increase in Peclet number. Kang et al. (1989) did not specify the solids concentration but it appears the solids concentration or void fraction influences the dispersion of solids more than the particle size when the gas inlet velocity is held constant.

Effect of Cone Angle on Peclet Number

Flow in high cone angle cyclones was found to be associated with formation of ropes or clusters. This kind of flow was described as highly ordered flow. When the Peclet number of these cyclones was plotted (Figure 5.10-3) it was found that the highest values of inverse Peclet number or highest dispersion was associated with the cyclone possessing the highest cone angle. The highest particle dispersion coefficient was associated with cyclone F that had a total included cone angle of 42°. Analysis of flow of particles in this cyclone showed that particles formed ropes in this cyclone. Similar observations were made as the angle of the cone was decreased, but to a lesser degree. Although particle-particle interactions are strong for particles within the rope the mean particle distance are also small. Therefore effective dispersion coefficient for particles within the rope is small. On the other hand shear forces acting on the surface of the strand due to the gas drag force are likely to be higher. It has been established that dispersion within the rope itself will be low and therefore the low Peclet numbers obtained for the cyclones in which roping was predominant can be attributed to shear induced dispersion or mixing. The residence time of particles in the high angle cyclone in which roping was predominant was found to be higher. This would imply that the axial velocity of the rope down the wall was low. Therefore a lot of mixing would take place in the lateral direction due to the removal by shear action and subsequent deposition of particles on the surface of the rope as illustrated in Figure 5.12-1. Thus the high dispersion is likely due to be induced by the gas and not as a result of the independent behaviour of the particles.

High-speed video analysis showed that the particles close to the wall were almost stationary. This stationary boundary layer would result in less wear on the cyclone walls. The evidence of this layer was also shown by a stationary boundary layer which remained after feed and air flow to the cyclone had been stopped (Figure 6.1). The void fraction in this particular case is very low and therefore gas drag force in these voids would be very low. The increases in dispersion, hence high inverse Peclet number of these particles can likely be explained by a shear by the

fluid drag and saltation effects. Particles close to the surface could be picked up by gas shear force and deposited a small distance downstream by the saltation effect. The point that the gas sweeps over the particle layer can be supported by experimental observation, which showed that there were dispersed particles bounded by a rope in the direction of gas flow. For the wide angle cyclones when solids feed rate was stopped but airflow continued the particles in the ropes were not swept out but continued to circulate in spite of the continuous airflow.

It is therefore most likely that the dispersion in this case was gas induced as compared to the case where the dispersion was a result of the particle interactions (Figure 5.10-1). Although the Peclet number can be compared at the same SGL in Figure 5.10-3, in actual fact the relative local concentration of the particles increases with increase in cone angle. For the lower cone angle cyclones (eg. Cyclone A) the particles are more influenced by the gas flow and therefore can move along with the gas. As the local particle concentration increases with increase in cone angle the velocity of the particles is decreased. This results in a lowering of centrifugal force and gravity becoming more important. Subsequently there is settling out of solids from the gas forming a boundary layer. This boundary layer wall flow travels at a lower velocity compared to the lean phase particles and this therefore accounts for the increase in the particle residence time.

Effect of Wall Roughness on Peclet Number

The effect of the wall roughness on the dispersion or effective mixing of particles in the cyclone was investigated. Cyclone C with a cone angle of 20 degrees appeared to be the transition from the dispersed flow to flow in which roping was predominant as cone angle was increased. Cyclone C was coated with a monolayer of sand particles with a roughness equivalent to the particle diameter of the sand particles used as feed material. It was observed that the very faint ropes that were observed with a smooth wall cyclone disappeared in the rough sand coated cyclone. Therefore the rough surface disrupted the near ordered flow observed when the

cyclone walls were smooth. The disappearance of these ropes in the rough wall cyclone was accompanied by an increase in dispersion of the solids hence higher inverse Peclet numbers (Figure 5.10-1). Attention can also be drawn to Figures 5.13-3 and 5.13-6 where silica gel particles bounce off from a mild steel plate and sand coated mild steel plate. The effect of the surface roughness causes a lot of scatter of these particles both on the plane sand coated plate and in the sand coated cyclone. Therefore where roping is not desirable it could be destroyed or disrupted by a rough surface wall. Comparison of measured particle residence times in a normal cyclone and sand coated cyclone showed that the differences in the measured residence times were within bounds of experimental error.

7.6. Roping

The flow of particulate material in a cyclone can be described by two phenomena, roping and non-roping (dispersed phase) flow. ter Linden (1949) reported the phenomenon of roping with fine dusts. He observed that even though the dust entering the cyclone was uniformly distributed after entering the cyclone chamber, the dust formed narrow bands. The formation of these strands or ropes appears to be controlled by several parameters. When other conditions are held constant the formation of these ropes requires a threshold of dust concentration at the entry into the cyclone. Ropes are a result of the wall deposition of particles by the action of the centrifugal force, particle concentration and property of coefficient of restitution of the particles. In the present study, the gas inlet velocity was found to be critical to the formation of these ropes. Of the different cyclones tested, when fed with sand at a flow rate of at least 10 g s^{-1} and gas tangential inlet velocity below 10 m s^{-1} no ropes formed in the different cyclones. The ropes could re-appear or disappear when the gas inlet velocity was above or below 10 m s^{-1} respectively. The formation of these ropes appears to be a result of the centrifugal force component acting up the wall against the gravitational force component acting down the wall.

When the gas inlet velocity was increased to about 30 m s^{-1} it was observed that the ropes became more concentric and the angle of the rope to the horizontal also decreased. This is a net result of the increase in the centrifugal force component up

the wall, which would tend to dominate the flow. As shown in Figure 6-6 the angle of streaks of silica gel particles in cyclone F is almost zero in the conical section. This means that the axial velocity of these particles is close to zero. At steady state the discharge of solids is equal to the new feed. Conversely when the velocity was decreased the angle of the rope to the horizontal increased as the rope stretched to the apex with continuous solids feed. The relative movement of the rope is a result of the component of the centrifugal force up on the wall.

The existence of the ropes is a result of the interaction of the particles and the wall. The mechanics of particle and wall interactions was found to be critical to the presence or absence of these ropes. If the solids enter well dispersed, the manner of their bouncing will determine whether they will concentrate sufficiently close to the wall to form a rope. Thus in this instance, property of coefficient of restitution of the particle appears to be the criterion for presence or absence or ropes. Silica gel particles, whose coefficient of restitution was determined to be about 0.7 did not form ropes compared to sand which had a coefficient of restitution of about 0.3. Silica gel particles did not form ropes while ropes were observed with sand for similar conditions. Silica gel particles would move more or less independently by repeated bouncing on the walls. For sand particles accumulation of the particles on the wall would result in strong particle-particle interactions where immediate neighbours influence particles.

The clustering of particles into ropes in the wall region has implications on the flow pattern. Particles with high coefficient of restitution rebounding further from the wall are subjected to the free stream gas aerodynamic drag force. However, for particles in a rope the drag force acting on a particle in the centre of the rope is no longer the free stream drag force and the gas within the interstices is almost stationary. The result of the low drag force acting on the particles within the ropes is a significant decrease in slip velocity between the gas phase and the particles in the ropes. At extremely high solid loadings in the gas the velocity vector of the particles will exceed that of the gas because the gravitational weight of the solids

will be large compared to the component of force acting up the wall when the solids loadings are low. Moreover where fairly thick particle boundary layers exist, the velocity at the bottom of the particle boundary layer would be almost zero. Therefore, for these particles in this layer there is no centrifugal force component and the gravitation force component acts downward with the shear force on adjacent particle layers resisting this downward flow. There will therefore be a change in flow pattern of the solids. At low loadings the centrifugal force field controls the solids flow and at extremely high concentrations gravity becomes more important.

For the higher angle cyclones ropes persisted when the solids feed to the cyclone was stopped. Only additional solids feed into the cyclone could trigger solids discharge from the cyclone. This observation indicates that the sand particles being fed into the rope make physical contact with the ones below, either passing on some axial momentum by collision, or more likely acting by gravity force. This contact from above could explain the sharp decrease in residence time with increases in the SGL in the higher angle cyclones. For cyclones A and B where data on particle residence time with change in SGL was available there was very little change in residence time with increase in SGL (Figures 5.9-3 and 5.9-4). In the absence of roping the particles more or less act independently of each other. In these systems at constant gas flow an increase in the SGL will not affect the flow pattern and therefore particle residence time. The particles act independently of each other and only respond to the gas aerodynamic drag force. The flow pattern changes at the onset of roping.

Once ropes have been formed the solids forming the ropes stay close to the wall albeit with some change in flow patterns, like discontinuity in the ropes. This could explain the bimodal nature shown in Figure 5.8-3. It would appear as though another rope came by, and with its collection of tracer, so the double concentration peaks correspond to separate ropes. It is probable that the discontinuity is brought about by stresses in the solids generated by the gas flow.

Particles travelling in the rope have aggregate properties. Thus although within the rope itself there exists particle velocity distributions, we can describe a mean rope velocity, which is the velocity at which the rope front moves. For these particles in the rope the ratio of effective drag to gravity is much lower compared to that for a single particle. The gravitational weight cannot easily be sustained by the normal gas flow. The rope must therefore be at a higher angle from the horizontal compared to the gas velocity vector (Figure 7-5). The behaviour of the aggregate solids in the rope is analogous to the flow of solids in pneumatic conveying, which is referred to as stratified flow, as illustrated in Figure 7-6.

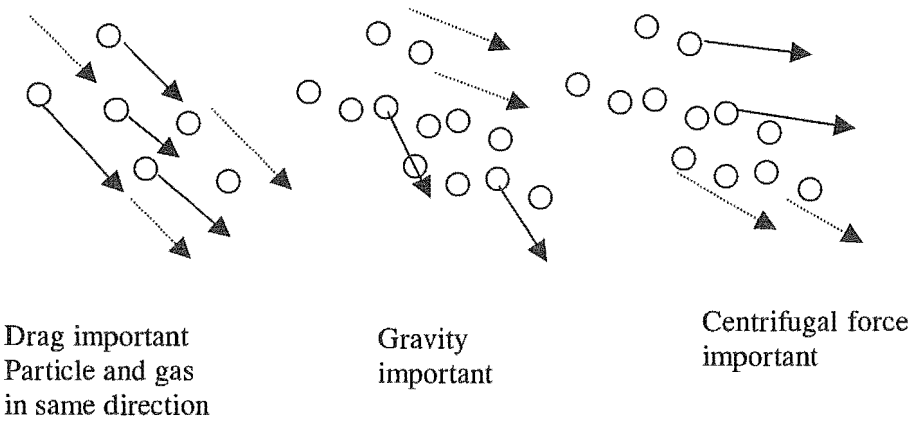

Figure 7-5 Relative importance of drag and gravitational force

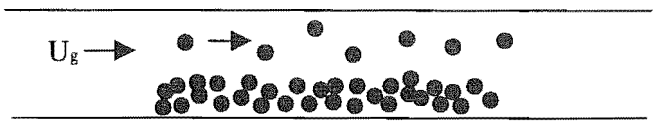

Figure 7-6 Particle deposition in stratified flow

It appears the rope concentration profile as illustrated in Figure 5.12-1 was caused by the gas drag force, which picked up some particles from the surface of the rope and dragged them off. These particles would pick up momentum from the gas phase and therefore travel faster than the particles (but in the direction of the gas

flow) in the rope. When the particles made one complete revolution in their travel they impacted on the slow moving particles and lost their energy. In the process other particles could be ejected and picked up by the gas drag and the process is repeated. Under steady state conditions the rope is therefore self sustaining if it crosses the path of the gas, ie. is at a different angle of travel.

It was suggested in § 7-4 that frictional contact with the wall was necessary for rope formation. As depicted in Figure 5.12-1, the rope is free to move axially down the wall and could also rotate on its axis. However if the wall is rough consisting of a layer of other particles the coefficient of friction is almost equal to the coefficient of static friction μ_s. The movement of the rope is then restrained because the particles in contact with the wall are stationary. A shear force is thus generated between the stationary particles in contact with the wall and adjacent moving particles. This shear force results in a spread of particles, which are subsequently picked up by the gas drag and therefore breaks down any rope approaching a rough surface.

Experimentally it was observed that in cyclones E and F once ropes formed they persisted even with no fresh feed into the cyclone. This existence of the layer of particles in the rope and the rope maintaining a constant angle with the horizontal for given gas flow conditions would imply that the rope is not in line with the gas flow as mentioned above. Therefore where the rope is fully formed, because of its gravitational weight the angle of the rope from the horizontal is likely to be higher compared to that of gas. For particles in the rope the gravitational force is more important compared to the centrifugal force.

In the direction of the gas drag force there is also a dynamic equilibrium about the rope with particles being picked up by the gas and striking on the other side of the rope.

The equilibrium of forces on a rope element could be upset by new feed. During continuous feed the rope extends to the apex and subsequently discharges into bin. When feed is stopped the rope initially becomes unstable, moves up the cone and subsequently establishes the equilibrium discussed above. The weight of the new feed causes a disturbance of this equilibrium of forces, and then causes net downward movement of the rope presumably due to gravitational force and the rope is stretched. When the centrifugal force is increased by an increase in the gas tangential velocity the net force acting up the wall is increased and the rope moves up. The inventory of solids held up on the wall can be reduced by change in geometry of the cone angle. A decrease in the cone angle of the cyclone would result in a smaller component of the centrifugal force acting up along the wall and a higher component of the gravitational force acting down parallel to the wall.

It is probable that the discontinuity in the rope causing a lead and tail could be the result of the shear stress exceeding the strength of the solids deposit resulting in flow. When the rope structure is weakened as a result of this shear, the gas drag force lifts off individual particles.

Discharge patterns of the ropes were observed from the underside of the discharge end of the cyclone through the perspex hopper with the aid of a high-speed camera.

It was observed that the rope had a tangential velocity profile with the faster moving particles associated with the dispersed particles (as shown in Figure 5.12-1) and the slow moving particles with the particles in the rope. The mean velocity of the rope is therefore smaller than the velocity of particles travelling outside of the rope. The discharge of solids from the cyclone is shown photographically in Figure 7-7. The outer white ring is the edge of the part of the perspex hopper. The white cloud on the edge of the inner circle shows a rope discharging. Examination of photographs of a discharging rope showed that a velocity profile of these particles discharging into the bin could be deduced. A rope velocity profile is illustrated schematically in Figures 7-8.

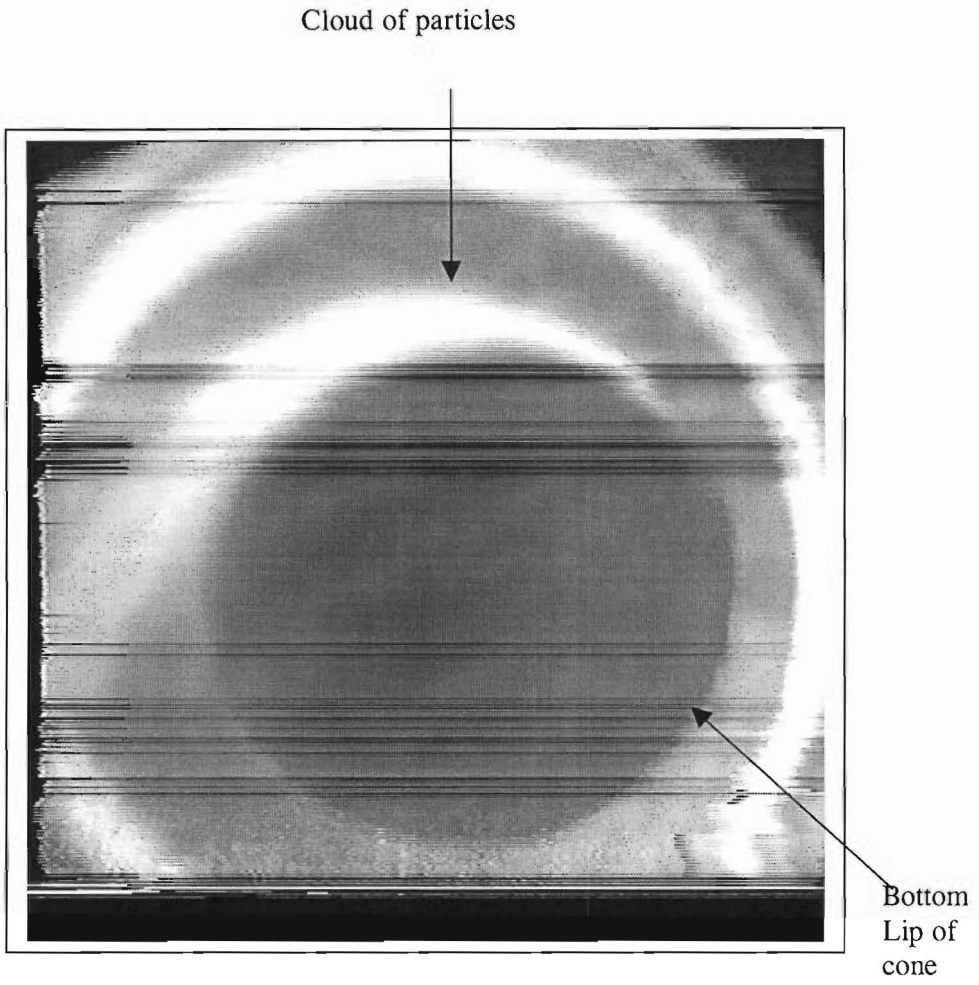

Figure 7-7 Cloud of particles discharging into the bin, viewed from the bin. Cyclone F; Sand 250-500 μm; feed rate 9.85 g s^{-1}

The discontinuity in the flow of particles in the rope was also confirmed by video observations from the bottom of the cyclone. The rope could be characterised by finite discharge times and periods in which there was no discharge of solids. Analysis was made for the discharge of sand particles at a feed rate of 9.85 gs^{-1} in a 36-degree cyclone (cyclone E). Typical times in which the rope was discharging and times for which the rope was not discharging are shown in Table 7-2. The time was evaluated based on the frame rate.

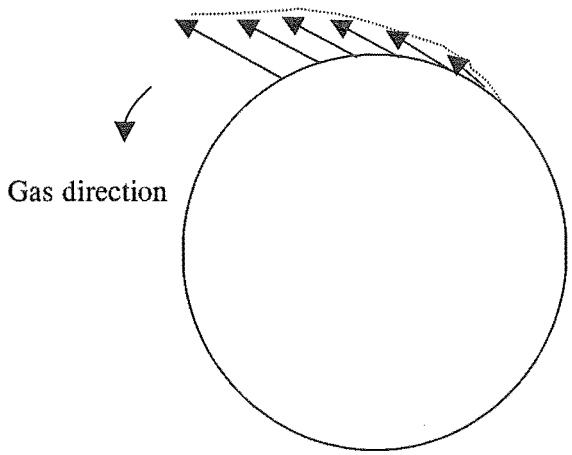

Figure 7-8 Schematic diagram illustrating solids velocity profile in rope at discharge end (projected)

Table 7-2 Periods of rope discharge and no discharge from cyclone E

Discharge/No Discharge	Time (s)
No Discharge	1.1
Discharge	0.2
No Discharge	0.27
Discharge	0.23
No Discharge	0.80
Discharge	0.23
No Discharge	0.03
Discharge	0.1
No Discharge	0.93
Discharge	0.1
No Discharge	0.63

Of the total period for non-rope discharge and rope discharge in Table 7-2 the rope discharged for a period of about 20 per cent of the total and for the rest there was no rope discharge. During the period of discharge of the rope particle mass flux was high. Measurement of particle distributions on the impactor in these cyclones were thus characterised by high particle fluxes and very few or no particles in between. These particle measurement distributions can be compared with the near uniform number distributions for flows not characterised by roping (Figure 6-16). These discharge times of the ropes highlight the transient nature of the flow. The highly transient flow probably marks the boundary for the limit of application of the

moving impactor method, as it is most suitable for flows not characterised by roping.

7.7. Modelling

Observation of particles in the cyclones showed two main mechanisms of transport of particles. For single particles the bouncing of particles was predominant in cyclones with lower included cone angles (< 28 degrees) ie the narrow and long conical sections. Particles in this flow regime did not have a zero radial velocity component as assumed by Lebedev et al. (1979) and later also by Cremasco et al. (1996). Centrifugal force is important for vortex flow in cyclones. The centrifugal acceleration, as given by Equation 7.7-1 was therefore higher where radius was smaller

$$a_c = \frac{V_p^2}{R} \tag{7.7-1}$$

With increase in the total included angle of the cone there was a resultant increase in centrifugal force as the radial distances at the same axial position in the cyclone was smaller. The particle stayed close to the wall maintaining contact and therefore travelled by sliding along the wall. The radial distance was smaller because the increase in cone angle was achieved whilst maintaining the same ratio of the barrel diameter to the bottom discharge diameter. The higher centrifugal forces caused higher particle concentrations and therefore increased particle-particle interactions.

Influence of cone angle on particle residence time

The experimentally measured and model calculated particle residence times in a cyclone with different cone angles are shown in Figures 5.9-11 and 6-46 respectively. The bouncing particle model (BPM) also showed the strong influence

of the cone angle on the particle residence time as revealed by the experimental results (Figure 6-46 and Figure 5.9-11). There was a gradual decrease in experimental residence time as the included angle of the cone was increased from 10 to 20 degrees. This increase in angle corresponded with a decrease in the overall height of the cyclone from 1.02 m to 0.63 m. Further decrease in the overall height of the cyclone accompanied by a corresponding increase in the included cone angle from 28 degrees to 42 degrees resulted in a reversal of the earlier trend of decrease to an increase in the particle residence time. There is therefore no simple relationship between the height of the cyclone with residence time of the particles when the cone angle is not constant.

However the model calculated results for change of residence time with cone angle (Figure 6.46) deviate from the experimental trends of increase in particle residence time with increase in particle type. Here it is mentioned particle type as it was noted that in addition to the density differences silica gel and sand particles also had different shape characteristics. The model predicted a consistently higher residence time for silica gel particles which had a density about half that of sand particles.

Effect of gas inlet velocity

There was good agreement between the model predicted residence times and experimentally measured times for gas inlet velocities over 20 m s^{-1}. However, there was a significant discrepancy between the model prediction of particle residence time with change in gas inlet velocity when the gas inlet velocity was lower than 20 ms^{-1} as shown in Figure 6.45. While the experimental results showed an increase in particle residence when the gas velocity was low, the model predicted result was lower than the experimental values although it also showed an increasing trend.

Effect of particle size

The model predicted an increase in particle residence time with decrease in particle size (Figure 6-44). The increase in residence time with increase in particle type coupled with the increase in residence time with decrease in particles size might suggest that for the model the effect of gravitational force is more important.

A probable explanation for this discrepancy, in addition to the consistently low values given by the model could be the effect of the wall boundary layer, giving a reduced gas velocity in this boundary layer. Wakelin (1992) estimated the boundary layer thickness on the cone from tangential and axial velocity profiles. The boundary layer thickness was approximately 3 mm for a 140 mm diameter cyclone and 15 mm for a 750 mm diameter cyclone. Bohnet et al. (1997) proposed an expression for calculation of the boundary layer thickness on the roof of the cyclone given by the following equation

$$\delta_d(r_i^*) = \delta_d^*(r_i^*) \cdot r_a \cdot \mathrm{Re}_d^{-0.2113} \qquad (7.7\text{-}2)$$

where the Reynolds number is given by $\mathrm{Re}_d = \frac{u_a r_a \rho}{\eta}$, r_a is the radius, η is gas viscosity, ρ is gas density and u_a is gas tangential velocity at the wall (just outside the boundary layer).

We can use the following relationship to estimate the thickness of the boundary layer as a function of radius, from Equation 7.7-3 and the reported figure of 15 mm by Wakelin (1992) for the 375 mm radius cyclone.

$$\delta_d(r_i^*) \approx 15 \cdot \left(\frac{r}{0.375}\right)^{0.789} \qquad (7.7\text{-}3)$$

In the barrel of the cyclone used in this study with a radius of 112.5mm, the boundary layer would be about 5.8 mm as illustrated in Figure 7.8. From the model, in the barrel of the cyclone, silica gel particles bounced to radial distances as high as 20 mm from the wall, which is outside the boundary layer. For a particle outside this boundary layer the velocity would actually be higher. For multi-particles, when a particle bounces off after a collision with the wall, there is a probability that it might collide with another incoming particle and therefore remain in the boundary layer. If this thickness of boundary layer were maintained in the conical section then a particle sliding on the wall would be moving in this boundary layer. When this boundary layer was taken into account in the case of sand which had a higher density and lower coefficient of restitution similar trends as those obtained with silica gel were also found.

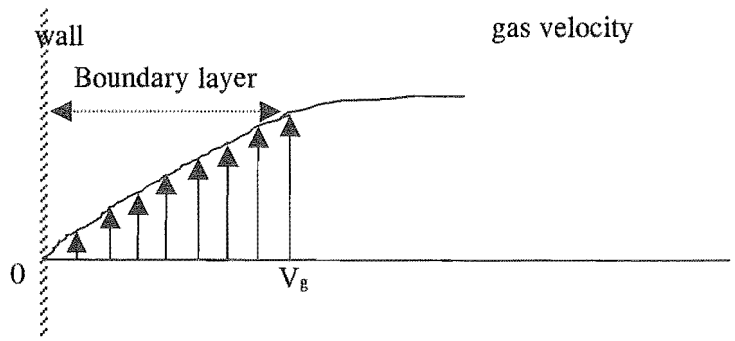

Figure 7-8 Wall boundary layer

In the model, the presence of other particles was represented only by the coefficient of restitution, which was assigned random values. A single particle was assumed in the model. With a single particle, coupling between the gas and particles is one way with the gas supplying momentum to the particle and the particle on the other hand not having any effect on the turbulent structure of the gas phase. It is therefore possible that the higher experimental residence time results were obtained on account of the two way coupling between the gas and the particles. In reality where this two way coupling exists, the result is a reduction in the gas tangential velocity by exchange of energy between gas and particles. This would imply reduction in momentum available to the particles and a corresponding increase in

particle residence time as the particles would be moving slower. This coupling was not accounted for in the model where the gas tangential velocity close to the wall was assumed to be equal to the gas tangential inlet velocity.

At low loadings the presence of particles does not change the velocity field of the conveying gas (Crowe, 1982). When the particle concentration is not high, fluid dynamic force on a suspended particle can be assumed to be the same as that on a single particle without interaction (Tsuji et al., 1982). The model did not account for the interactions between the particles. In multiphase flows the trajectories of a given particle is affected by collision with other particles which is accompanied by a loss in momentum by the faster moving particle and gain for the slow moving particle. Agreement between the model predicted residence times and experimental values at higher gas inlet velocities could be due to change in flow pattern at higher velocities to rope flow part way down in the cone.

At low gas velocity the centrifugal acceleration is lower and therefore there is a low concentration of particles on the wall. Under these conditions when the particles strike on the wall it is likely they impact and rebound with little loss in energy. These particles, because of inertia effects behave almost independently of the gas flow. It is therefore likely that the model accounts for the presence of more particles on the wall by lower coefficient of restitution than there actually is.

Distribution of Particle Residence Times

The distribution of particle residence times could be simulated using the model by considering that for particles entering the cyclone there is a velocity distribution. Different particle sizes and inter-particle collisions cause these velocity differences. These velocity distributions would result in different particle trajectories. For the model, a representative particle was chosen with a mean size and travelling at the centre the pipe. A distribution of residence times could also be obtained if the

different entry positions were considered. In moving across a grid on the entrance tube, along the width of the entrance pipe there would be a range in the impact angle of the particle with the cyclone wall as illustrated in Figure 7-9. Particles close to the wall are also slowed down by collisions with the wall boundary.

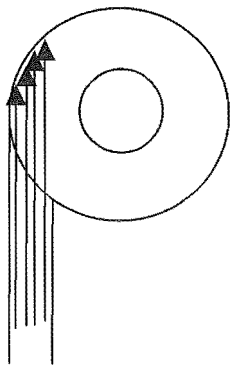

Figure 7-10 Different entrance paths for particles into the cyclone

There is also a distribution in the total height travelled by the particles from 0.78 m for a particle at the base of the entrance tube to 0.89 m for a particle travelling at the roof of the entrance tube.

The angle to the tangent at the point of impact ranges from a very low angle to almost 90 degrees for the particle at the other end of the grid (left to right). Distribution of residence times is also due to the random change in the coefficient of restitution because of different surface properties. However when the random values of the coefficient of restitution were used the predicted mean particle residence time was not sensitive to the changes.

The distribution of particle residence times predicted by the model for a silica gel particle with change in the approach angle of the particle on the first collision with the wall is shown in Figure 7-10. The mean particle diameter was 350 μm and the particle inlet velocity was 15 ms^{-1}. As shown in Figure 7-10 the distribution in particle residence time was not sensitive to the change in the approach angle of the

particle before collision. This implied that the flow of the particles as represented by the model was not influenced by the initial conditions but dominated by the general flow conditions inside the cyclone, especially the drag force and the random change in the coefficient of restitution.

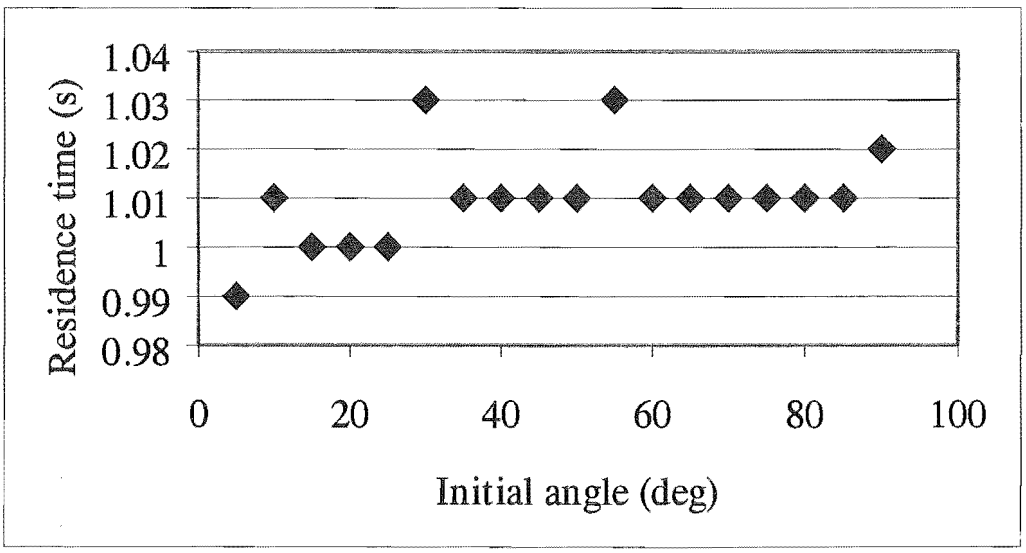

Figure 7-11 Predicted particle residence times with change in approach angle, for the single bouncing particle model

Similarly the variation of particle residence time caused by a distribution of particle inlet velocities was simulated using the model. The residence time of a 350 μm silica gel particle with inlet velocity ranging from 3 to 18 ms^{-1} was predicted using the model and the results are shown in Figure 7-11 below.

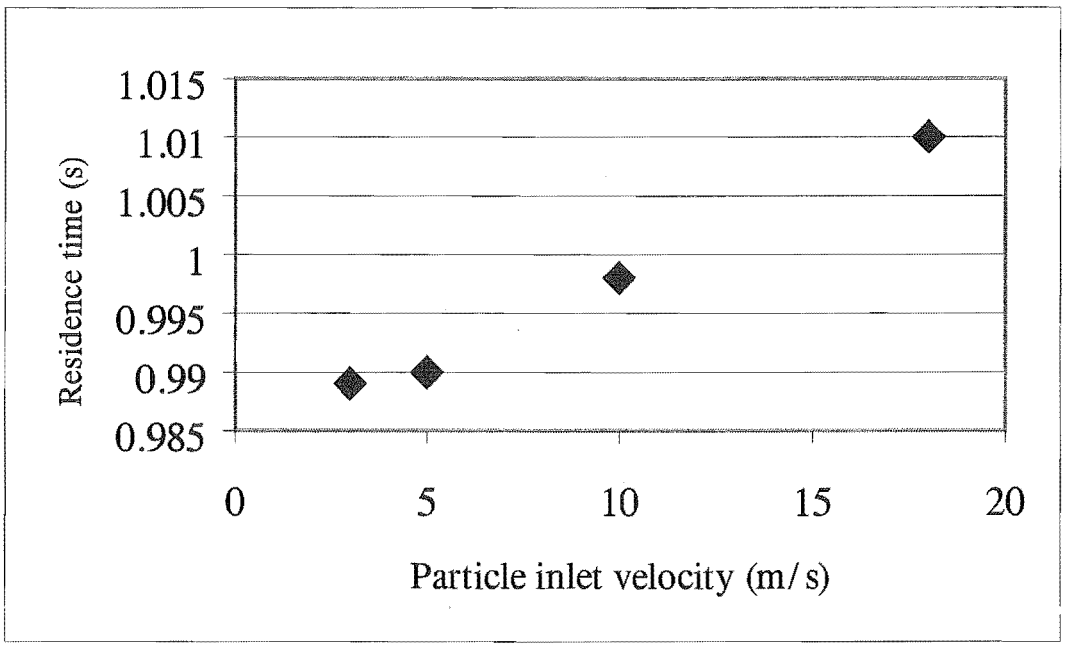

Figure 7-12 Particle residence time with change in particle inlet velocity
Cyclone B; silica gel 350 μm; gas inlet velocity 20 ms^{-1}

As shown in Figure 7-11 the model gave a slight increase in residence time with increase in particle inlet velocity although the differences were small, and not significant compared to experimental error. Examination of the particle radial velocity profiles showed that the particle radial velocity away from the wall increased with increase in the initial particle entrance velocity. Particles entering with low velocity stayed close to the wall and moved in with the gas resulting in slightly shorter residence times. The trend of a slight increase in particle residence time with increase in particle entrance velocity can be contrasted with the slight increase in particle residence time with decrease in gas inlet velocity (Figure 6.5-4).

The model calculations also showed that particle axial velocity in the bottom one third of the cone decreased to almost zero with the result that for a one particle model the particle spends a lot of time spinning in this region. Measurements on

hold-up also showed that there was a minimum inventory of particles in the cyclone (§ 5-5).

The major assumption was that the gas tangential velocity was not affected by the particles and that the tangential velocity close to the wall was equal to the gas inlet velocity.

Limitations and Suggested Improvements of the Model

The model in its present form does not directly account for the presence of other particles in the flow. It was assumed in the model that when other particles were present they were confined to the wall region. Thus no particle-particle collisions outside the wall boundary layer were accounted for. The probability of an inbound particle striking on to other particle was assigned through a randomly generated coefficient of restitution. For very high particle flows the solids cover nearly most of the wall (Trefz and Muschelknautz, 1993). Under those flow conditions it might appear reasonable to assume a constant coefficient of restitution, that with a layer of other particles and not with a plane wall material. However this assumption can be far from the truth as the layer of particles also presence a highly irregular surface for which collision cannot be described by a constant coefficient of restitution. Nevertheless the coefficient of restitution would be low under these circumstances of particle wall flows. Similarly when the randomly generated coefficient of restitution was high the particle would have impacted on a mild steel wall. The collisions of particles in free flight are not accounted for in the model in its present form. Such collisions dominate the flow especially at higher feed rates were particle numbers are large.

The local spin component of the particle momentum was also not taken into consideration in the single particle model. The rotation of particles due to local velocity gradient which is referred to as the Magnus effect has been reported to sometimes affect the linearity of motion of particles (Torobin et al., 1960).

For more accurate results the effect of the particles on the gas tangential velocity has to be taken into consideration in the modelling.

The dynamics of the flow of granular solids in cyclones is very complex. A number of simplifying assumptions were made to simplify the problem whilst retaining the key aspects of the flow based on experimental observations and basic laws of physics. Whilst this theoretical model will not be an exhaustive solution to the flow of particles in the cyclone it will nevertheless serve to highlight important trends based on experimental measurements.

Some of the major assumptions are discussed. A single spherical particle was assumed and therefore there was no correction for the shape factor. Average values of the coefficient of restitution e and the coefficient of friction μ were used and obtained from the simple bouncing experiments. The coefficient of restitution for silica gel was 0.7 and the coefficient of friction 0.3. For sand particles the coefficient of restitution was 0.26 and the coefficient of friction 0.25. Although the average value of the coefficient of restitution for sand is low it ranged up to a high of about 0.7. For both materials the coefficient of restitution did not vary with change in the approach angle of the particle. Molerus (1993) reported a friction coefficient of sand of about 0.4. This difference in value could reflect difference in surface conditions on the steel plate and different properties of the sand used. In reality the coefficient of restitution for irregular particles of the same material is not uniform but covers a range of values. Matsumoto and Saito (1970) reported that when particles bounced on a rough wall the probability of the coefficient of restitution greater than 1 was large ie. $P(e > 1)$. Therefore the presence of other particles and shape characteristics of the incoming particle influences the bouncing characteristics. In practice no unique value of the coefficient of restitution can be assigned because of the random change in the surface brought about by the movement of particles. At first constant values of coefficient of restitution and friction were used. Later a random number generator was used to assign a value to the coefficient of restitution at each collision instant. A rebounding particle can also

collide with an incoming particle. As the concentration of solids is increased and voidage decreases inter-particle distances are reduced restricting the free movement of these particles. The flow properties of these particles are then described better by averaged properties of the assemblage of particles. The Magnus rotational force was neglected but where particles shape is irregular shear forces can cause rotational motion especially where considering course particles.

The experimental observed phenomenon of bouncing of particles was corroborated in this model where particles had non-zero radial velocity values at certain axial distances dependent on the angle of the cone. From the model the radial velocity reduced to zero in the conical section at an axial height dependent on the angle of the cone. The particle radial velocity reduced to zero much earlier in the wide-angle conical sections. However photographic evidence (Figures 6-24 and Figure 6-25) shows that particles still possess non-zero radial velocities as they are not confined to the wall region. A possible explanation for this anomaly between experimental evidence and model behaviour was that the gas tangential velocity used in the wall region was higher than would be the case, given the modulation of the gas velocity by the presence of particles (Parida and Chand, 1980).

This model predicted the experimentally observed trend of decreasing angle of the total particle velocity vector from the horizontal. For the very wide conical sections (cyclone F) the experimental axial velocity was almost zero resulting in an almost zero angle. Zero vertical velocity implies no discharge. Experimentally it was observed that there was no discharge of particles without continuous feed into the cyclone for the wide-angle cyclones (cyclones E and F). Therefore the rate of discharge of particles was proportional to the rate of fresh feed coming in. This flow was close to plug flow.

Conclusion

8

In this study the residence time of granular particles was measured by the stimulus-response technique using an imperfect tracer signal. A band of tracer particles was sandwiched between regular feed particles for pulse input, or changed from tracer to non-tracer particles for step input. The particles, both tracer and non-tracer were fed into the gas stream using a small conveyor belt up stream of the cyclone. The responses at the inlet and outlet were measured by capturing samples of particles onto sticky aluminium impactors by the moving impactor method. The numbers of both tracer and non-tracer particles in each cell on the moving impactors were counted using a travelling microscope with an image grabbing software. Three data reduction methods were used to yield a characteristic mean particle residence time and a particle Peclet number. The data reduction methods used were: moments analysis, Laplace transform and the least squares methods. The least squares method was found to be the most suitable for analysis of this data, especially for evaluation of particle Peclet numbers. The axially dispersed plug flow model was found to valid for representation of flow of these particles in the cyclones tested.

The residence time of silica gel and sand particles in the cyclone was measured as a function of several operating variables and different cyclone designs. The particle size intervals used were 210-295 μm, 250-500 μm, 500-700 μm and 700-850 μm. Particle residence time was found to;

(a) decrease with increase in airflow into the cyclone

(b) increase with increase in density of the particle

(c) increase with increase in particle size

(d) increase with increase in cyclone diameter and length for a given cone geometry

(e) be independent of SGL at low SGL (< 0.08) and decreased with SGL at higher SGL (> 0.08)

(f) be strongly influenced by the total included angle of the cone

Within a range of SGL up to about 0.08 the particle residence time was found to be independent of the SGL and beyond that SGL the particle residence time was found

to decrease monotonically with solids feed into the cyclone. The flow of particles in this lower SGL range was found to be predominantly by bouncing. In this flow regime the interaction between wall and particles by bouncing was predominant. Further increase in solids flow or increase in conical angle changed the flow pattern of the solids in the cyclone, where wall flows become more important. This flow was characterized by the phenomenon of roping, where particle-particle interactions were strong. For this flow, gravity was found to become more important compared to the centrifugal force component and therefore the particles were little affected by the gas flow field. Thus the rate of discharge of the particles in the rope was controlled by the rate of solids feed and not by gas flow. Particle Peclet numbers calculated using the axially dispersed plug flow model were used for interpreting the flow of the particles in the different cyclones.

In order to understand and explain the flow of particles in a cyclone by particle-wall bouncing interactions, the bouncing characteristics of different particles were investigated with different surface properties. The coefficient of restitution and the surface characteristics were found to influence the occurrence or absence or roping in flow of particles. Particles with low coefficient of restitution were found more likely to travel by roping in a cyclone compared to particles with a high coefficient of restitution. Roping was interpreted as a kind of ordered flow and bouncing as chaotic flow. The bouncing of particles on a rough wall consisting of a layer of particles was found to be random and chaotic. Roping in the cyclone was disrupted when the cyclone wall was made rough by coating with a layer of particles.

The phenomenon of roping was studied using a high frame rate camera (up to 200 frames per second) with a high-speed video recorder. The rope was found be discontinuous and discharged intermittently into the bin. A characteristic rope velocity was estimated from these high-frame rate video recordings.

Experimental evidence suggested that the bouncing of particles on cyclone walls was important and should be incorporated in any modelling work on the flow of particles in cyclones.

The residence time of particles in the cyclone was modelled using the bouncing particle model assuming a single particle. This model accounted for the travel of the particle by both bouncing and sliding depending on particle characteristics and cone angle. For all the cyclones, travel of the single particle in the barrel was purely by bouncing. The proportion of the distance travelled by the particle in the cone by the sliding mechanism increased from less than 30 percent for cyclone A to over 90 percent for cyclone E.

The model results agreed with the experimentally observed strong influence of the cone angle on the residence time of particles in the cyclone. In the model, the progression of the single particle down into the bin of the cyclone was also slowed in the conical section by the action of the centrifugal force component acting up the wall. The model predicted results however gave lower residence times of particles with increase in particle size and density compared to the experimental results.

References

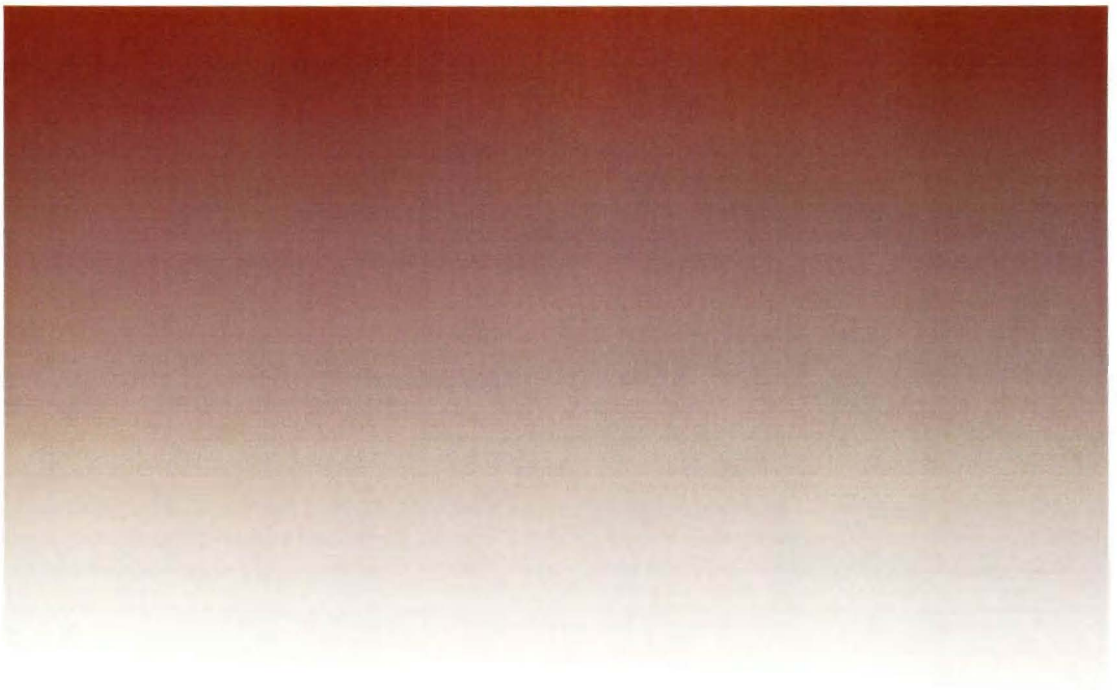

Anderssen, A.S. and White, E.T., "Parameter estimation and the weighted moments method", Chem. Eng. Sci., **26**, pp. 1203-1221, (1971).

Arastoopuor, H. "Pneumatic transport of solids" , Encyclopedia of Fluid Mechanics, Vol **4**, Solids and Gas-Solids Flows, pp 359, (1986).

Aris, R., "Notes on the diffusion-type model for longitudinal mixing in flow", Chem. Eng. Sci. **9**, pp. 266-267, (1959).

Beeckmans, J.M. & Morin, B. "The effect of particulate solids on pressure drop across a cyclone" Powder Technology **52** pp. 227-232, (1987).

Bischoff, K.B., "The general use of inperfect pulse inputs to find characteristics of flow systems", Can. J. of Chem. Eng., **41** (3), p. 129, June (1963).

Bohnet, M., Gottschalk, O., and Morweiser, M., "Modern design of aerocyclones", Advanced Powder Tech., **8**(2), pp. 137-161, (1997)

Bohnet, M., "Cyclone separation of gas solids mixtures", Ger. Chem. Eng., **6**, pp. 211-220 (1983).

Bloor, M.I.G. and Ingham, D.B., "Theoretical investigation of the flow in conical hydrocyclone", Trans. Instn. Chem. Engrs, **51**, pp. 36-41, (1973).

Boysan, F., Ayers, W.H. and Swithenbank, J. "A fundamental mathematical modelling aproach to cyclone design", Instn. Chem. Engrs, **60**, pp. 222-230, (1982).

Cabrejos, F.J., Klinzing, G.E., "Minimum conveying velocity in horizontal pneumatic transport and the pickup and saltation mechanisms of solid particles", Bulk Solids Handling, **14**, pp. 541-550 (1994).

Clements, W.C., "A Note on Determination of the Parameters of the Longitudinal Dispersion Model from Experimental Data", Chem. Eng. Sci., **24**, pp. 957-963, (1969).

Clift, R. and Gauvin,W.H., "Motion of entrained particles in gas streams" , Can. J. Chem. Eng, **49**, pp. 439-448, (1971).

Clift, R., Grace, J.R. and Weber, M.E. "Bubbles, drops and particles", Academic Press, p. 223, (1978).

Cremasco, M.A., Maciel Filho, Nebra, S.A. "A model for the flow of air and course particles in cyclones", International Drying Symposium (IDS'96), August 1996, Vol. A., pp. 291-299, (1996).

Cross, J.A., "Electrostatics: principles, problems and applications", Adam Hilger, (1987).

Crowe, C., Sommerfeld, M., Tsuji, Y. "Multiphase flows with droplets and particles", CRC Press, (1998).

Crowe, C.T. "Review - numerical models for dilute gas-particle flows", J. Fluids Eng., **104**, p. 297-304 (1982).

Cundall, P.A. and Strack, O.D.L. "A discrete numerical model for granular assemblies", Geotechnique, **29**(1), pp. 47-65, (1979).

Danckwerts, P.V., "Continuous flow systems - distribution of residence times", Chem. Eng. Sci., *2*, p. 1, (1953).

Davison, A.C. and Hinkley, D.V. " Bootstrap methods and their application" Cambridge University Press, (1997)

Di Giacinto, M., Sabetta, F. & Piva, R., "Two-way coupling effects in dilute gas-particle flows", J. Fluids Eng. , **104**, pp. 304-312, (1982)

Dieck, R.H., "Measurement uncertainty methods and applications", Instrument Society of America, (1995).

Dietz, P.W. "Collection efficiency of cyclone separators", AIChE Journal, **27**(6) pp 888-892 (1981).

Efron B. and Tibshirani R.J. "An Introduction to the Bootstrap", Chapman & Hall, (1993)

First, M.W., "Fundamental factors in the design of cyclone dust collectors", PhD Thesis, Harvard University, (1950).

Fogler, S.H., "Elements of chemical reaction engineering", Prentice Hall, 2nd Edition, pp. 709-803 (1992).

Gregory, J., "Solid-liquid separation", Ellis Horwood Limited, pp. 66, (1984).

Haider, A., and Levenspiel, O., "Drag coefficient and terminal velocity of spherical and non-spherical particles", Powder Technology, 58, pp. 63-70, (1989)

Hoomans, B.P.B., Kuipers, J.A.M., Briels, W.J., and Van Swaaij, W.P.M., "Discrete particle simulation of bubble and slug formation in a two-dimensional gas-fluidized bed: a hard sphere approach", Chem. Eng. Sci., **51** (1), pp. 99-118, 1996.

Hsieh, K.T. and Rajamani, R.K., "Mathematical model of the hydrocyclone based on physics of fluid flow", AIChE Journal, **37**(5), pp. 735-746, (1991)

Johnson, P.C. and Jackson, R. "Frictional-collisional constitutive relations for granular materials, with application to plane shearing", J. Fluid Mech., **176**, pp. 67-93, (1987).

Kang, S.K, Kwon, T.W and Kim, S.D, "Hydrodynamic characteristics of cyclone reactors", Powder Technology, **58** pp. 211-220 (1989)

Kehinde, A.J., Hudgins, R.R. and Silveston, P.L., "Measurement of axial dispersion in packed beds at low reynolds numbers by imperfect pulse chromatography", Journal of Chem. Eng. of Japan, **16**(6), pp. 476-482 (1983)

Kelsall, D.F., "A study of the motion of solid particles in a hydraulic cyclone", Trans. Instn. Chem. Engrs, 30, pp. 87-104 (1952)

Kemp, I.C., Frankum, D.P., Abrahamson, J., & Saruchera, T., "Solids residence time and drying in cyclones", Drying '98, pp. 581-588, (1998).

Kim, W.S. & Lee, J.W. "Collection efficiency model based on boundary-layer characteristics for cyclones", AIChE Journal, **43**(10), pp. 2446-2455 (1997).

Klinzing, G.E., Marcus, R.D., Rizk, F., and Leung, L.S., "Pneumatic conveying of solids, a theoretical and practical approach", 2nd Edition, Chapman & Hall, p. 61 (1997).

Kiselnikov, V.N., Lebedev, V.Ya., Vialkov, V.V. & Romanov, V.S. "Investigations of the aerodynamics of two-phase streams in cyclone apparatus" Scientific Publications of the Invanovo Chemical Technological Institute, **12** pp. 185-190 (1971) (Russian)

Kuczynski, R., Przekwas, A., and Kucinski, W., "The static electrification of particles in gas-solids pipe flow", Journal of Electrostatics, **10**, pp. 309-314, (1981)

Lebedev, V.Ia., Barulin, E.P., Romanov, V.S. and Mukhin, V.V. "Investigations of the aerodynamics of two-phase streams in cyclone apparatus, Izvestiia, Vys. Uchebnye Zavedeiia, **22**(7), pp. 872-875 (1979) *Russian*

Lebedev. V.Ya, Barulin, E.P., Romanov, V.S. and Kisel'nikov, V.N. "Combined drying of a granulated material in a fluidized-bed apparatus", Translated from Zhurnal Prikladnoi Khimii, **60**(7), pp. 1452-1458 (1987).

Lede, J., Verzaro, B. Antoine and Villermaux, J., "Flash Pyrolysis of Wood in a Cyclone Reactor", Chemical Engineering Science, pp. 309-317 (1986).

Lede, J., Li, H.Z.,and Villermaux, J., (1989) Le Cyclone Réacteur Partie II: Mesure de la Distribution des Temps de Séjour de la Phase Solide-Lois d'Extrapolation, Chemical Engineering Science, **42**, pp. 103-117 (1989)

Lédé, J., Mercadier, J. and Villermaux, J. "Le cyclone, un réacteur de sublimation: application à la sublimation de l'acide isocyanurique", The Chemical Engineering Journal, **62**, pp. 13-21 (1996)

Levenspiel, O. " Chemical reaction engineering", Wiley International Edition, (1972).

Liang-Shih Fan and Chao Zhu, "Principles of gas-solid flows", Cambridge University Press, (1997).

Louge, M.Y., Mastorakos, E. and Jenkins, J.T., "The role of particle collisions in pneumatic transport", J. Fluid Mech., **231**, pp. 345-359, (1991).

Lun, C.K.K., Savage, S.B., Jeffrey, D.J. and Chepurniy, N. "Kinetic theories for granular flow: inelastic particles in Couette flow and slightly inelastic particles in a general flowfield", J. Fluid Mech., **140**, pp. 223-256, (1984).

Matsumoto, S. and Saito, S., "On the mechanism of suspension of particles in horizontal pneumatic conveying: monte carlo simulation based on the irregular bouncing model", J. Chem. Eng. Japan, 3(1), pp. 83-92, (1970)

Matsumoto, S., and Saito, S. " Monte carlo simulation of horizontal pneumatic conveying on the rough wall model", J. Chem. Eng. Japan, **3** (2), pp. 223-230 (1970).

Min, K., "Intensity of particle motion in solid-gas suspension flow", Journal of Applied Physics, **38**(2), pp. 564-567, (1966).

Molerus, O., "Principles of Flow in Disperse Systems", Chapman & Hall, (1993)

Mori, Y., Suganuma, A. & Tanaka, S. "On collection efficiency of gas cyclone in course particle range - an application of model of particle back-mixing by bouncing to a centrifugal air vortex system", J. Chem. Eng. Jap. **1** pp 82-86 (1968).

Mothes, H. & Löffler, F. "Motion and deposition of particles in cyclones", Ger. Chem. Eng. **8**, pp. 223-233 (1985).

Mothes, H. and Löffler, F. "Prediction of particle removal in cyclone separators", International Chemical Engineering, 28(2), pp. 231-240 (1988).

Muschelknautz, E, and Trefz, M., "Extended cyclone theory for gas flows with high solids concentrations", Chem. Eng. Technol. **16**, pp. 153-160, (1993).

Ostergaard, K., and Michelsen, M.L., "On the use of the imperfect tracer pulse method for determination of hold-up and axial mixing", Can. J. Chem. Eng., **47**, pp. 107-112, (1969)

Parida, A. and Chand P. "Turbulent swirl with gas-solid flow in cyclone", Chemical Engineering Science, **35**, pp. 949-954, (1980).

Pasley H.S., and Kemp, I.C., "Experimental studies and modelling of particle motion in cyclones", The 1993 ICHEME Research Event, pp. 495-497, (1993)

Patankar, S.V. "Numerical heat transfer and fluid flow", Hemisphere, NY, p. 197, (1980).

Patterson, P.A., and Munz, R.J., "Gas and particle flow patterns in cyclones at room and elevated temperatures", Can. J. Chem. Eng., 74, pp. 213-221, (1996)

Rajendra, Y.D. & Abrahamson, J. "Particle residence time in return-flow cyclones", CHEMECA '94, Perth, pp 141-148 (1994)

Rajendra, Y.D., "Particle residence time in return-flow cyclones", ME Thesis, University of Canterbury, (1995)
Ranz, W.E. "Wall flows in a cyclone separator: a description of internal phenomena", Aerosol Science and Technology, **4**, pp. 417-432, (1985).

Ranz, W.E., Talandis, G.R, and Gutterman, B., "Mechanics of particle bounce", A.I.Ch.E. Journal, **6** (1), pp. 124-127, (1960).

Rowe, P.N. and Henwood, G.A. "Drag forces in a hydraulic model of a fluidised bed - part 1", Trans. Instn. Chem. Engrs, **39**, pp. 43-54 (1961).

Saruchera, T., and Abrahamson, J. "Residence time of granular particles through a cyclone - analysis using moments, laplace transform and least squares methods", Chemeca 97, Particle Technology, pp. 201-211, (1997).

Schmidt, P., "Unconventional cyclone separators", International Chemical Engineering, **33**(1), pp. 8-17, (1993)

Senior, R.C. and Grace, J.R. "Integrated particle collision and turbulent diffusion model for dilute gas-solid suspensions", Powder Technology, **96**, pp. 48-78, (1998).

Sheppard, C.B. & Lapple, C.E. "Flow pattern and pressure drop in cyclone dust collectors without inlet vane", Ind. Eng. Chem. **32** p. 1246 (1940).

Sheppard, C.B. & Lapple, C.E. "Flow pattern and pressure drop in cyclone dust collectors", Ind. Eng. Chem. **31** p 972-984 (1939).

Shirolkar, J.S., Coimbra C.F.M., and McQuay, Q.M. "Fundamendal aspects of modelling turbulent particle dispersion in dilute flows", Prog. Energy Combust. Sci. **22**, pp. 363-399, (1996).

Silva, M.A., and Nebra, S.A., "Numerical calculations of gas-solid flow in a cyclone", International Drying Symposium (IDS'94), pp. 1319-1326, (1994).

Smirnov, A.S., Lebedev, V.Ya., Barulin, E.P. and Gorlova, N.V. "Mathematical model of flow in the reverse-flow cyclone", Khimiia i Khim. Tekhnologiia, **35**(2), pp. 108-113 (1991) *Russian.*

Smirnov, A.S., Lebedev, V.Ya., Barulin, E.P. and Gorlova, N.V., "Analytical study of the flow in a reverse-flow cyclone", Khimiia i Khim. Tekhnologiia, **35**(8), pp. 84-88 (1991) *Russian*

Soo, L.S. and Tien, C.L., "Effect of the wall on two-phase turbulent motion", Journal of Applied Mechanics, March, pp. 5-14, (1960).

Soo, S.L. "Particulates and continuum – multiphase fluid dynamics", Hemisphere Publishing Corporation, p 330, (1989).
Stairmand, C.J., "The design and performance of cyclone separators", Trans. Instn. Chem. Engrs, **29**, pp. 356-373, (1951).

Stock, D.E., "Particle dispersion in flowing gases – 1994 Freeman Scholar Lecture", Trans. ASME, 118, pp. 4-17, (1996).
Szekely J., and Carr, R., "Heat transfer in a cyclone", Chemical Engineering Science, **21**, pp. 1119-1132, (1966)

ter Linden, A.J. "Investigations into cyclone dust collectors", Inst. Mech. Eng. Proc. **160** p. 233-242 (1949).

Torobin, L.B. and Gauvin, W.H. "Fundamental aspects of solids-gas flow – part iv: the effects of particle rotation, roughness and shape", Can. J. Chem. Eng. **38**, pp. 142-152 (1960a).

Torobin, L.B. and Gauvin, W.H. "Fundamental aspects of solids-gas flow, part v: the effects of fluid turbulence on the particle drag coefficient", Can. J. Chem. Eng. **38**, pp. 189-200, (1960b)

Trefz, M., Muschelknautz, E., "Extended cyclone theory for gas flows with high solids concentrations", Chem. Eng. Technology, **16**, pp. 153-160 (1993).

Tsuji, Y., Kawaguchi, T., and Tanaka, T. "Discrete particle simulation of two-dimensional fluidized bed", Powder Technology, **77**, pp. 79-87 (1993).

Tsuji, Y., Morikawa, Y. & Terashima, K., "Fluid-Dynamic Interaction Between Two Spheres", Int. J. Multiphase Flow, **8** (1), pp. 71-82 (1982)

Tsuji, Y., Tanaka, T. and Yonemura, S. "Cluster patterns in circulating fluidized beds predicted by numerical simulation (discrete particle model versus two-fluid model", Powder Technology, **95**, pp. 254-264, (1998).

Wakelin, R. " Vortex breakdown in dust-collecting return-flow cyclones", PhD Thesis, University of Canterbury, (1993).

Weber, H.E., "The boundary layer inside a conical surface due to swirl", J. App. Mech., **23**, pp. 587-592, (1956).

Wen, C.Y., and Galli, A.F., Fluidization (Edited by Davidson, J.F., , Cliff, R. and Harrison, D), Academic Press, (1985).

Werther, J., and Hirschberg, B., "Solids motion and mixing", Circulating Fluidized Beds, Blackie Academic & Professional, pp. 119-148, (1997).

White, B.R. "Particle dynamics in two-phase flow", Encyclopaedia of Fluid Mechanics Vol 4: Solids and Gas-Solids Flows, pp. 240-282, (1986).

Yuu, S., Jotaki, T., Tomita, Y and Yoshida, K. "The reduction of pressure drop due to dust loading in a conventional cyclone", Chem. Eng. Sci. **33** pp 1573-1580 (1978).

Zhou, L.X., and Soo, S.L., "Gas-solid flow and collection of solids in a cyclone separator", Powder Technology, **63**, pp. 45-53, (1990).

Zhu, C., Liang, S.C. and Fan, L.S. "Particle wake effects on the drag force of an interactive particle", Int. J. Multiphase Flow, **20**, pp. 117-129 (1994).

Appendices

9

Appendix 9A - Chemeca 97 Paper *A-2*

Appendix 9B - International Drying Symposium (IDS'98) *A-16*

Appendix 9C – Visual Basic Program for BPM *A-25*

Appendix 9D – Conical Sections *A-41*

Appendix 9E – Air-Hydraulic Circuit for Moving Shuttles *A-45*

Appendix 9F – Electric Circuit Diagram for Solenoid Controller *A-46*

Appendix 9G – Timing Diagram *A-47*

Appendix 9H - Convolution Theorem *A-48*

Appendix 9I – Experimental Results *A-51*

Appendix 9J – Video Recording of Flow in Cyclone ***A-54***

Appendix 9K – Error Analysis *A-55*

Appendix 9A - *Chemeca 97 Paper*

Residence Time of Granular Particles Through a Cyclone - Analysis Using Moments, Laplace Transform and Least Squares Methods

Thomas Saruchera and John Abrahamson
Department of Chemical and Process Engineering
University of Canterbury, New Zealand

SUMMARY

The residence time of sand particles in a cyclone was measured by the stimulus-response technique and the results analyzed by moments, least squares fitting and Laplace transform in the time domain. All methods proved to be adequate for evaluation of residence time but only the least squares method adequately evaluated Peclet numbers. The axially dispersed plug flow model was found to be valid for representation of flow of these particles through a conventional long cone cyclone. For the particular geometry and conditions studied (Stairmand high efficiency cyclone diameter 225 mm, and gas inlet velocity 20 m s^{-1}), the mean residence time was 1.12 ± 0.16 s and the Peclet number 40.1 ± 12. Using these parameters, the residence time distribution (RTD) of these particles in the cyclone is given.

Keywords: cyclone, residence time, transform, moments, least squares, plug flow, diffusion

INTRODUCTION

Fluid and particle flow in a cyclone is strongly swirling and turbulent. Highly turbulent flows enhance heat and mass transfer rates. Given these very important attributes, cyclone reactors are receiving considerable attention for application in many industrial processes characterized by high heat and mass transfer rates and short reaction times of the order of a few seconds. Examples of these reactions are gas-solid pyrometallurgical processes and drying of granular materials. However, because of the high transfer rates, product degradation can also occur through overexposure, especially when drying heat-sensitive materials. Particle residence times and appropriate kinetic transfer coefficients are required for equipment design and product quality control. The average particle residence time is therefore an important parameter, but also the upper and lower extremes of the residence time are important. Two attempts to measure the distribution of particle residence time are known to the authors (1,2). However, Lede et al. (1) uses single particle methods, and Kang et al. (2) use a narrow collection tube to replace the bin, both giving an artificial condition which cannot strictly be related to industrial practice. This paper reports a measurement of particle residence time distribution under normal bin/cone geometry and solids loading.

The experimental method of measuring particle residence time in a cyclone used in this work was described by Abrahamson and Rajendra (3). They used synchronised travelling sticky impaction surfaces at both the inlet and in the bin of the cyclone, sampling at a point in the suspension flow. The moving impactor surface travels perpendicular to the flow, past a stationary nozzle, exposing succeeding elements (cells) of its surface at succeeding times. Each moving surface (shuttle) was contained in a protecting tube which spanned the duct or bin. Abrahamson and Rajendra (3) used a pulse of tracer (coloured) particles blown into the otherwise steady feed of non-tracer particles. This pulse may have disturbed the regular flow, providing non-representative residence times, so later

efforts have been directed towards introducing tracer signals without disturbing solids flow. Also a vibrating channel was used in the earlier work to feed the solids into the gas flow (via an air ejector). This was found to cause appreciable mixing, making sharp tracer changes at the inlet impossible, so reducing precision in residence times. In this work, a small belt conveyor replaced the vibrating channel, almost eliminating the mixing before the solids reached the inlet sampling point.

Particles found on the impactor surfaces were counted after the experiments, both tracer and non-tracer, and the fraction of tracer particles recorded as a function of distance. In Abrahamson and Rajendra's (3) analysis, a characteristic particle residence time was calculated from the time difference between the peaks of the input and output signals. The objective of the present study is to measure the *distribution* of residence times of granular particles in a cyclone by both the pulse and step response technique. Quantitative methods of analysis are applied for data reduction. The Laplace transform, moment analysis and least squares methods (4) will be considered and the results compared.

Theory

The mean residence time and the Peclet number are evaluated using the moment analysis method. For each measuring point (5,6,7),

$$\mu = \frac{\sum_{i=1}^{N} C_i t_i}{\sum_{i=1}^{N} C_i} \quad \text{.....(1)}$$

$$\text{and } \sigma^2 = \frac{\sum_{i=1}^{N} C_i t_i^2}{\sum_{i=1}^{N} C_i} - \mu^2 \quad \text{.....(2)}$$

The mean residence time and the variance are calculated by the difference between the mean and variance at the two measuring points 1 (inlet) and 2 (bin):

$$\tau = \mu_2 - \mu_1 \quad \text{.....(3)}$$

$$\Delta\sigma^2 = \sigma_2^2 - \sigma_1^2 \quad \text{.....(4)}$$

$$Pe = \frac{2\tau^2}{\Delta\sigma^2}, \text{ for large } Pe \quad \text{.....(5)}$$

Use is also made of Laplace transforms, applied to a likely flow model. The plug flow model with axial dispersion has been used to model many industrial flow systems (8,9,10). The mathematical representation of the plug flow model with axial dispersion, and constant cross-sectional area is based on Fickian type of diffussion (11) and is the following partial differential equation:

$$\tau\frac{\partial c}{\partial t} + \frac{\partial c}{\partial x} - \frac{1}{Pe}\frac{\partial^2 c}{\partial x^2} = 0 \quad \text{.....(6)}$$

The model accounts for hydrodynamic mixing effects represented by an effective dispersion coefficient causing distribution of residence times. Only the solids flow cross-section is relevant, rather than the vessel cross-section. With constant solids flow and velocity, the solids cross-section will be constant. In our case of a cyclone, changes in direction are also found, so the label "axial" for diffusion should rather be "streamline", or in the direction of solids flow.

For a linear system, the relationship between the output and input signal is the transfer function *F(s)*:

$$F(s) = \frac{C_2(s)}{C_1(s)} \quad \text{.....(7)}$$

The transfer function can be derived for the model by taking the Laplace transform of equation (6) with the following boundary conditions

$C = C_1(t)$ at $x = 0, t \geq 0$ and $C = 0,\ 0 < x < \infty$, at $t = 0$.

$$F(s) = \exp\left\{\frac{Pe}{2}\left(1 - \left(1 + \frac{4s\tau}{Pe}\right)^{\frac{1}{2}}\right)\right\} \quad \text{.....(8)}$$

For the experimental traces c_{1i} (input) and c_{2i} (output) at times t_i,

$$F(s) = \frac{\sum_{i=1}^{N} c_{2i}\, e^{-st_i}\Delta t \,/\, \sum_{i=1}^{N} c_{2i}\Delta t}{\sum_{i=1}^{N} c_{1i} e^{-st_i}\Delta t \,/\, \sum_{i=1}^{N} c_{1i}\Delta t} \quad \text{.....(9)}$$

where t_i is the mean time for interval i.
F(s) is computed for arbitrary values of s, where s is the weighting factor.
Equation (8) is algebraically manipulated to obtain:

$$\left(\ln\frac{1}{F(s)}\right)^{-1} = \tau s\left(\ln\left(\frac{1}{F(s)}\right)\right)^{-2} - \frac{1}{Pe} \quad \text{.....(10)}$$

The validity of the model can be checked by graphical technique. Using the experimental F(s), if a plot of $\left(\ln\frac{1}{F(s)}\right)^{-1}$ versus $s\left(\ln\frac{1}{F(s)}\right)^{-2}$ yields a straight line the model is adequate. The slope is τ and the intercept is $-\frac{1}{Pe}$. If equation (8) is inverted by means of the convolution theorem of the Laplace transform, the output tracer fraction $C_2(t)$ can be given by:

$$C_2(t) = \int_0^t C_1(u)\frac{1}{2\sqrt{\pi}}\sqrt{\frac{Pe\,\tau}{(t-u)^3}}\exp\frac{\left[Pe(\tau - t + u)^2\right]}{4(t-u)\tau}du \quad \text{.....(11)}$$

The generalized response to an ideal pulse can be given by solution of equation (6) to give (12):

$$C(\theta) = \frac{1}{2\sqrt{\pi\theta^3/Pe}}\exp\left[-\frac{Pe(1-\theta)^2}{4\theta}\right] \quad \text{.....(12)}$$

where $\theta = \frac{t}{\tau}$

The estimated residence time distribution E(t) is then given by:

$$E(t) = \frac{c_i(t)}{\sum_{i=1}^{N} c_i(t)dt\Delta t} \quad \text{.....(13)}$$

EXPERIMENTAL

The cyclone used is of the Stairmand high efficiency design (13) with a diameter of 225 mm. The experimental set-up is as described by Abrahamson and Rajendra (3) but with some modifications.

In the present set-up the outlet impactor is placed just below the cone, at the discharge from the cone into the bin, instead of further down into the bin against the bin wall. By placing the second impactor just below the cone, the total particle count is increased, thereby minimising signal noise due to short term fluctuations in particle flux. Air was driven through the cyclone by an 8kW rotary lobe Rootes blower at a flow of about 0.099 $m^3 s^{-1}$ (giving a velocity of about 20 m s^{-1} in the rectangular entrance section). A small conveyor belt moving at a linear velocity of 26.6 mm s^{-1} was used to feed the sand into the ejector. Sand was placed with uniform depth onto a 550 mm length of the conveyor belt with a 15 mm band (≈5g) of 100 % tracer (black) particles for the pulse experiments and a sharp transition to 100 % tracer particles for the step change tests. A schematic diagram of the apparatus is shown in Figure 1.

The size range of the sand used was +250 - 500 μm with a density of 2610 kg m^{-3}. The solids feed rate was 9.6 g s^{-1} giving a solids loading of about 97 g m^{-3} (kg solids/kg gas = 0.08) for all the tests. The particle velocity determined by flash photography in the rectangular entrance was about 15 m s^{-1}.

RESULTS

The distributions of particles with time on the inlet and bin impactors for a typical pulse run are shown in Figure 2 and Figure 3 respectively. Figure 4 shows a plot of the fraction of tracer particles to total particles for both the inlet and bin impactors. The fraction of tracer for both inlet and bin impactors for a step change experiment is shown in Figure 5. With the second impactor positioned at the bottom of the cone the average number of particles collected per cell was 25. This can be compared to earlier work by Abrahamson and Rajendra (3) when the second impactor was positioned on the wall of the bin, where the average number of particles collected under otherwise the same conditions was about 4. The conveyor belt feed assembly is capable of achieving uniform feeds and there is absence of particle mixing prior to discharge into the ejector. Thus fairly sharp tracer signals were obtained.

The applicability of the dispersion model to describe particle flow in the cyclone is verified by plotting the relationship in equation (10). The mean residence time and Peclet number are evaluated from the slope and negative reciprocal of the y-ordinate intercept and the result is shown in Figure 6. The mean particle residence times and Peclet numbers are also calculated by moments analysis. Particle residence times and Peclet numbers computed by the transfer function and moments analysis methods are shown in Tables 1 and 2 respectively. The proposed mathematical model as expressed by the response equation (11) was also matched to the experimental data and evaluated. Using the Solver function in the Excel spreadsheet package the sum of squares of the residuals was minimized with respect to the values of the mean residence time and Peclet number. The results of this procedure are tabulated in Table 3. The standard deviations of the residuals are also shown in Table 3. To smooth out the data, especially in the tails where counts were low, the mean fraction of tracer at each time interval (input and output) for the six pulse experimental runs was also calculated. Again by minimizing the sum of squares of residuals the values of the mean residence time and the Peclet number were 1.12 s and 40.1 respectively. Figure 7 shows the result of this procedure.

A summary of averaged mean residence times calculated by transfer function, moments and model fitting methods for both pulse input and step change experiments is given in Table 4. Also included are peak to peak and median to median measurements. The particle residence time distribution (RTD) (ie that for an idealised perfect pulse) using the τ and Pe from averaged inlet and bin traces is given in Figure 8.

It was observed there is a permanent and finite inventory of solids circulating in the cylindrical part of the cyclone when gas flow continues but the feed is stopped. This inventory of solids was collected and weighed after stopping the air flow. It was about 2 g and therefore small but not insignificant compared to the normal inventory during solids feed, of about $F\tau = (9.6)(1.2) = 12$g

DISCUSSION

The numbers of particles measured are those collected in cells or pockets of a constant size on the impactor surface, and these are proportional to the flux of particles flowing past the probes. The variations in particle distribution in Figures 2 and 3 can be ascribed to two different phenomena. Particle flux fluctuations in Figure 2 (entrance) are random, less than 50 % and short term in nature. They derive from fluctuations in feedrate and distribution across the inlet duct. In contrast fluctuations in Figure 3 (bin) are larger (up to 100 %) and show some broader peaks. These must in part derive

from flow variation within the cyclone, and this can be attributed to "roping". Roping is the collection of particles locally onto a path down the cyclone wall, yielding a measured higher particle flux if sampled by the sampling probe. Figure 3 appears to show the occurrence of roping in the time interval of 0.5 s to 0.9 s It is evident there is less scatter on the bin impactor in the absence of a rope. It is notable that the short term peaks have been eliminated in Figure 4 which uses the ratio of tracer particles to total particles.

Duncan's multiple range test (14) was carried out on the mean values of the residence times in Table 4. It was concluded that there is no significant differences among the different methods of analysis for pulse experiments (to 0.05 level), but the transfer function and least squares methods were significantly different from each other for the step experiments (see Table 5). We can therefore conclude that for purposes of calculating mean residence time, the transfer function method, moment and model fitting methods are equivalent for pulse input, but not for step change. Although the moments method is generally regarded as "less robust" (4), however in this case it produced reliable mean residence time results and this appears to be mostly due to the absence of a significant amount of "tailing" of the tracer response. When calculating the transfer function F(s), the range of values of the weighting factor *s* (1,2,3,4 and 5) were judiciously chosen to give the maximum weighting at the peaks of the input and response curves in the case of the pulse experiments and at about 50% change for the step change experiments.

The least squares technique of matching the model to the experimental data gives the smallest ranges of both mean residence times and Peclet numbers. The Peclet numbers calculated range from 24 to 50. This can be compared to the direct transfer function method which gives a range of 14 to 163 and the moments methods with a range of 32 to 120.

The suitability of the axially dispersed plug flow model to model the flow in our cyclone is attested by the linear plot as shown in Figure 6. The fit of the modelled bin trace (equation 11) to the experimental traces was assessed by χ^2 methods. A typical run yielded $\chi^2 = 9.4$ with mean particle number 25 per cell with 23 cells. This did not show significant difference (cf. $\chi^2 = 32$ at 0.05 level). The fit of the averaged traces shown in Figure 7 was even better ($\chi^2 = 2.0$), but this may have been influenced by the tendency to find a Normal distribution on averaging (Central Limit Theorem). In most of the runs, a second minor peak was observed in the tail of the bin trace (see Figure 4). This may be related to the hold-up of 2g in 12g mentioned above. This hold-up indicates some recycle, and longer residence times, which do not fit the plug flow dispersion model. Averaging the trace as in Figure 7 has removed the separate peaks but shows a larger effective diffusion (lower Pe) for the model.

The particle residence time distribution (RTD) curve (Figure 8) shows that approximately 95 % of the particles have a residence time between 0.6 and 1.6 s with a mean of 1.12 s and a Peclet number of 40.1. As the Peclet numbers and residence times have a narrow range the RTD shows little sensitivity within the range of these parameters

The time difference between peaks and at 50% step change (median to median) is similar to the model mean residence time. These methods, relying on specific positions on both inlet and bin traces, are not necessarily equal to the mean, and are more prone to variation.

The moving impactor method is versatile. The experimenter has the ability to control the number of particles/cell by the size of the nozzle. For our configuration with a 9 mm OD tube the maximum particle size conveniently studied was 850 μm with a 3.5mm nozzle. Optimum results for 150 μm particle were obtained with a 2 mm size nozzle. The objective is to obtain a monolayer of particles amenable to counting.

CONCLUSIONS

1 To give a more precise description of dispersion within the cyclone it is advantageous to prevent mixing of tracer particles before reaching the. This was achieved with a belt conveyor feed.

2 Positioning of the sampler in the bin is important. The particle flux at the discharge end of the cone is higher and less variable than further down into the bin, and therefore the positioning of the second impactor at the bottom of the cone improves the quality of data compared with that obtained when placed down in the bin.

3 It can be concluded that tracer is uniformly distributed across the flow (good lateral mixing). When sufficient particles are captured, fluctuations observed in particle flux do not show in tracer fraction plots for the collected particles.

4 The particle flow in the Stairmand high efficiency cyclone is well described by an axially dispersed plug flow model, with parameters mean residence time and Peclet number. Three methods

were used to derive these parameters. It was found that the Laplace transfer function and analysis of moments methods were reliable for calculating residence time, but neither were capable of accurately determining the Peclet number. Both Peclet number and mean residence time can best be determined together by least squares fitting the model response in the time domain to the experimental data points.

5 The residence times for the cyclone studied covered a ratio of about 3 times; from 0.5 to 1.5 of the mean residence time.

LIST OF SYMBOLS USED AND DEFINITIONS

t time (s)

τ mean residence time (s)

μ mean time at each measuring point (s)

σ standard deviation (s)

Pe Peclet number $= \frac{ul}{D}$ where u = area weighted mean velocity, l = distance between measuring points l (m), D is a dispersion coefficient ($m^2\ s^{-1}$)

x dimensionless distance between measuring points, $x = \frac{l'}{l}$

c(t) fraction of tracer particles to total particles

$c_i(s)$ Laplace transform of the tracer fraction

E(t) residence Time Distribution Function

F rate of solid feed $g\ s^{-1}$

χ^2 Chi squared

subscripts

1 first measuring point (inlet)

2 second measuring point (bin)

REFERENCES

1 Lede, J., Li, H.Z.,and Villermaux, J., (1989) Le Cyclone Réacteur Partie II: Mesure de la Distribution des Temps de Séjour de la Phase Solide-Lois d'Extrapolation, Chemical Engineering Science, Vol. 42, 1989, p. 103-117.

2 Kang, S.K., Kwon, T.W., and Kim, S.D., (1989) Hydrodynamic Characteristics of Cyclone Reactors, Powder Technology, Vol. 58, 1989, p. 211-220.

3 Rajendra Y.D., and John Abrahamson, (1994) Particle Residence Time in Return-Flow Cyclones, CHEMECA'94, Perth, Sept. 1994, p141-148

4 Seinfeld, J.H., and Lapidus, L., (1974) Mathematical Methods in Chemical Engineering Volume 3 Process Modeling, Estimation, and Identification, Prentice-Hall, New Jersey, p. 46-115, 359-373.

5 Levenspiel, Octave, (1972) Chemical Reaction Engineering, 2nd Edition, John Wiley & Sons, Singapore, p. 261-265.

6 van der Laan, E.T., (1958) Notes on the Diffusion-type Model for the Longitudinal Mixing of Fluids in Flow, Chemical Engineering Science, Vol. 7, p. 187-191

7 Bischoff, K.B., and Levenspiel, O., (1962) Fluid Dispersion-generalization and Comparison of Mathematical Models - I Generalization of Models, Chemical Engineering Science, Vol. 17, p. 245-255.

8 Ostergaard, K., and Michelsen, M. L., (1969) On the Use of the Imperfect Pulse Method for Determination of Hold-Up and Axial Mixing, Canadian Journal of Chemical Engineering, Vol. 47, April 1969,
p. 107-112.

9 Mixon, F.O., Whitaker, D.R., and Orcutt, J.C., (1967) Axial Dispersion and Heat Transfer in Liquid-Liquid Spray Towers. A.I.Ch.E. Journal, Vol. 13, No.1, Jan. 1967, p. 21-28.

10 Keey, R.B., and Pham, Q.T., (1977) Residence Time Distribution of Air in A Tall-Form Spray Chamber, Chemical Engineering Science, Vol. 32, p. 1219-1226.

11 Levenspiel, O., and Smith, W.K., (1957) Notes on the Diffusion-type Model for the Longitudinal Mixing of Fluids in Flow, Chemical Engineering Science, Vol. 6, p. 227-283.

12 Fogler, Scott, H., (1992) Elements of Chemical Reaction Engineering, 2nd Edition, Prentice Hall, New Jersey, p. 765-772.

13 Stairmand, C.J., (1951) The Design and Performance of Cyclone Separators, Trans. Inst. Chem. Engrs., Vol. 29, p. 356-383.

14 Montgomery, D., (1976) Design and Analysis of Experiments, John Wiley & Sons, New York, p. 48.

Table1: Particle Residence Times Calculated By Transfer Function and Moments Technique (*all runs were done under the same conditions and settings*)

Run #		Transfer Function	Moments
Pulse	77	1.35	1.35
	78	1.13	1.13
	79	1.14	1.14
	80	1.21	1.21
	81	1.28	1.29
	82	1.13	1.13
Step	83	1.29	-
	84	1.31	-
	85	1.12	-
	86	0.99	-

Table 2: Peclet Numbers Calculated by Transfer Function and Moments Technique (*all runs were done under the same conditions and settings*)

Run #		Transfer Function	Moments
Pulse	77	78.74	104.26
	78	28.41	26.43
	79	84.03	69.49
	80	52.91	62.49
	81	163.93	120.86
	82	36.23	31.73
Step	83	14.56	-
	84	128.21	-
	85	47.39	-
	86	63.29	-

Table 3: Peclet Numbers and Mean Residence Times Calculated by Model-Data Fitting (*all runs were done under the same conditions and settings*)

Run		C_2 Residuals Standard Deviation	Peclet Number	Mean Residence Time (s)
Pulse	77	0.0658	38.52	1.09
	78	0.0847	34.72	1.06
	79	0.0762	50.08	1.08
	80	0.0816	36.67	1.20
	81	0.0648	45.33	1.23
	82	0.0670	35.07	1.04
Average		0.0230	40.10	1.12
Step	83	0.0796	29.30	1.26
	84	0.0830	28.16	1.30
	85	0.0803	29.35	1.23
	86	0.0800	23.93	1.30
Average		0.0807	27.69	1.30

Table 4: Statistical Summary of Residence Times Evaluated by Different Methods

Condition	Method	Averaged Mean Residence Time (s)	Standard Deviation (s)
Pulse input	Transfer function	1.21	0.09
"	Moments	1.21	0.09
"	Least squares	1.12	0.08
"	Peak to Peak	1.20	0.12
Step change	Transfer function	1.18	0.01
"	Least squares	1.27	0.03
"	Median-Median	1.21	0.13

Table 5: Duncan's Multirange Test Insignificant Ranges (to 0.05 probability)

1.118	1.176	1.209	1.210	1.270

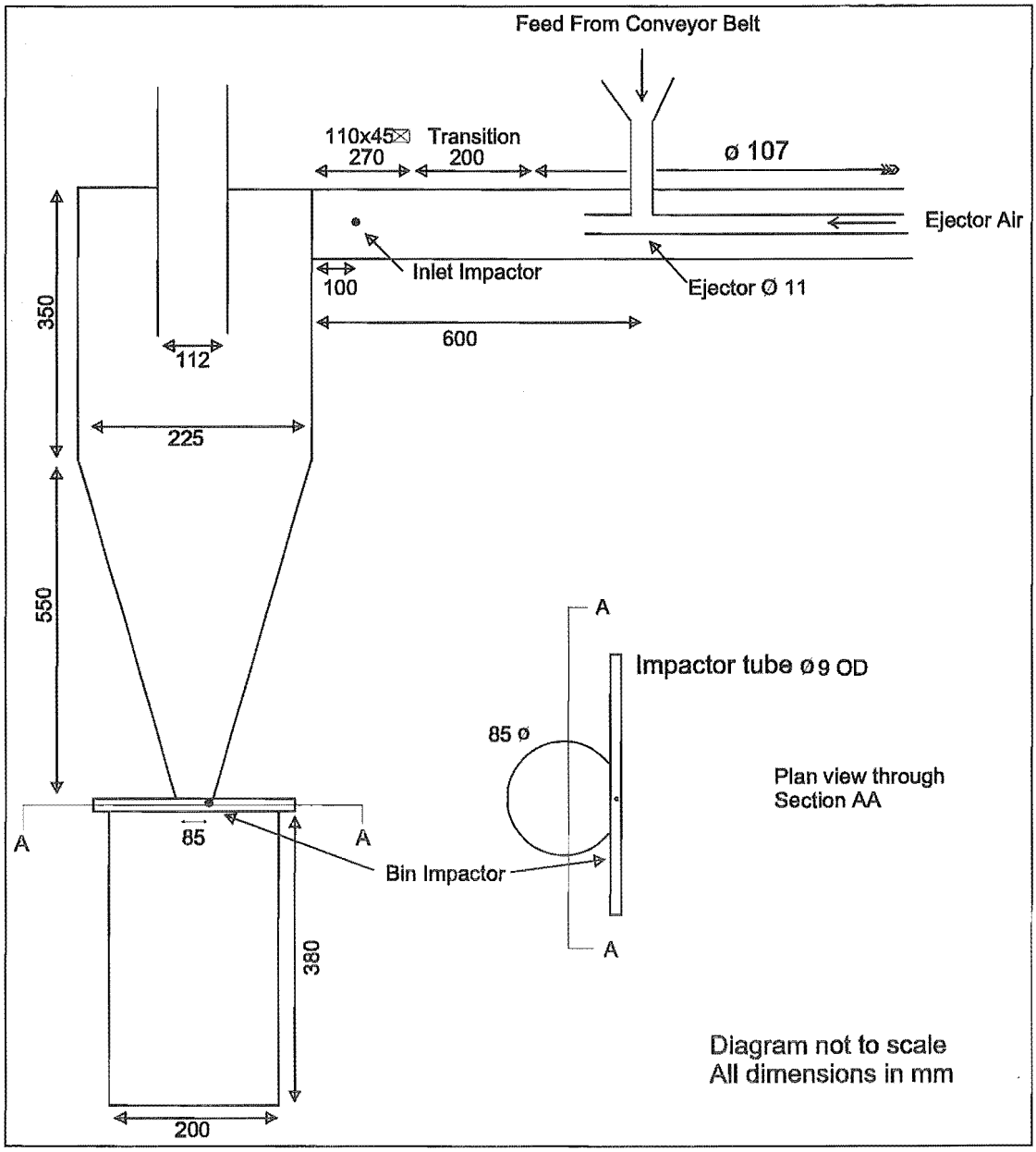

Figure 1: Schematic diagram of Cyclone

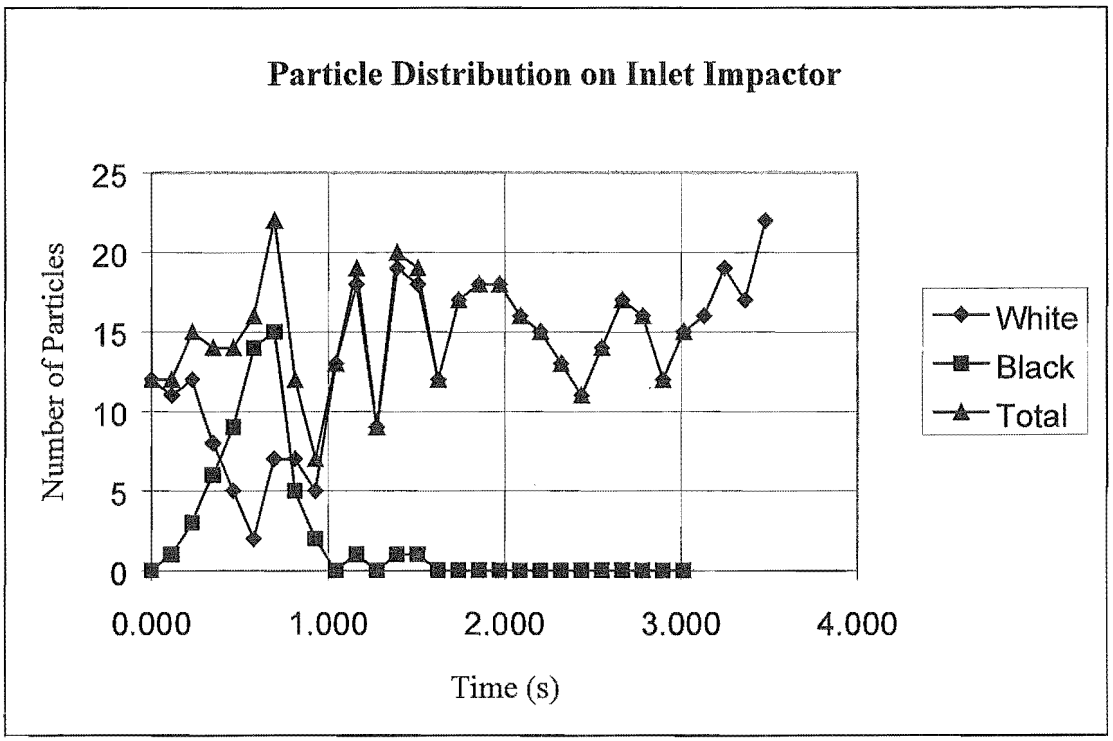

Figure 2: Particle Distribution with Time on Inlet Impactor, Run 79

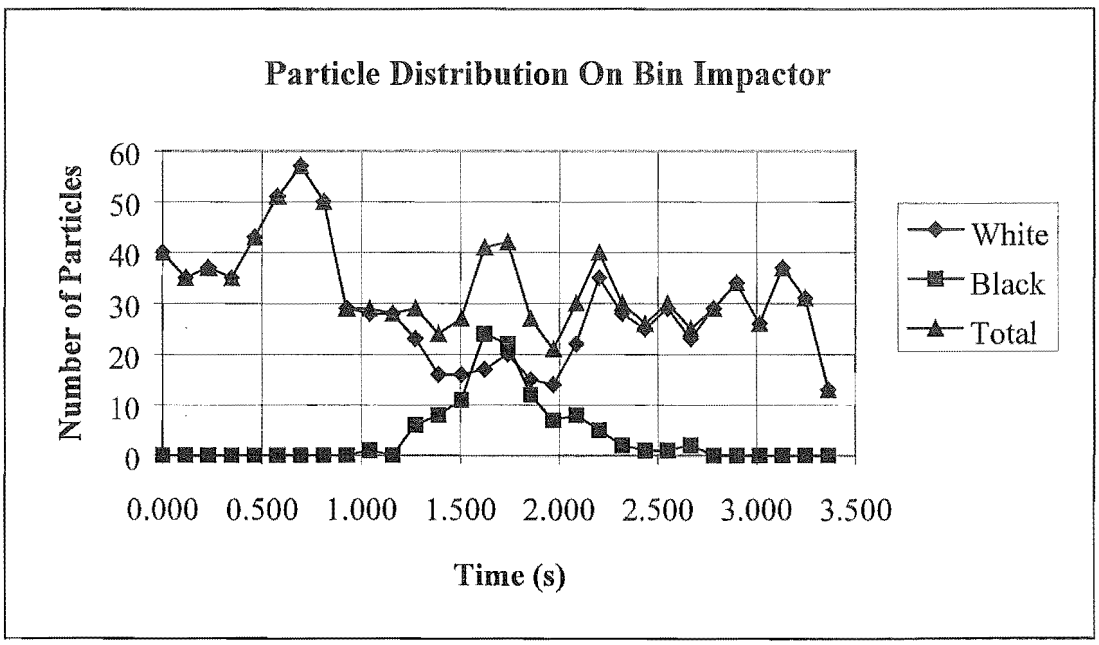

Figure 3: Particle Distribution with Time on Bin Impactor, Run 79

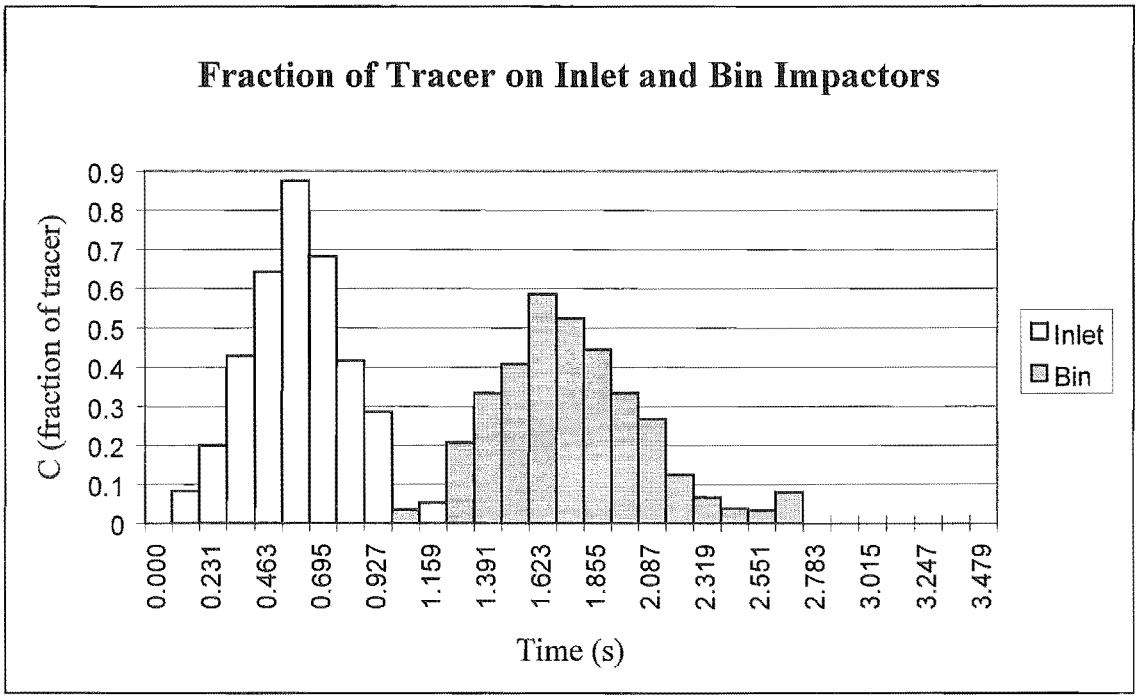

Figure 4: Tracer Fraction on Inlet and Bin Impactors, Run 79

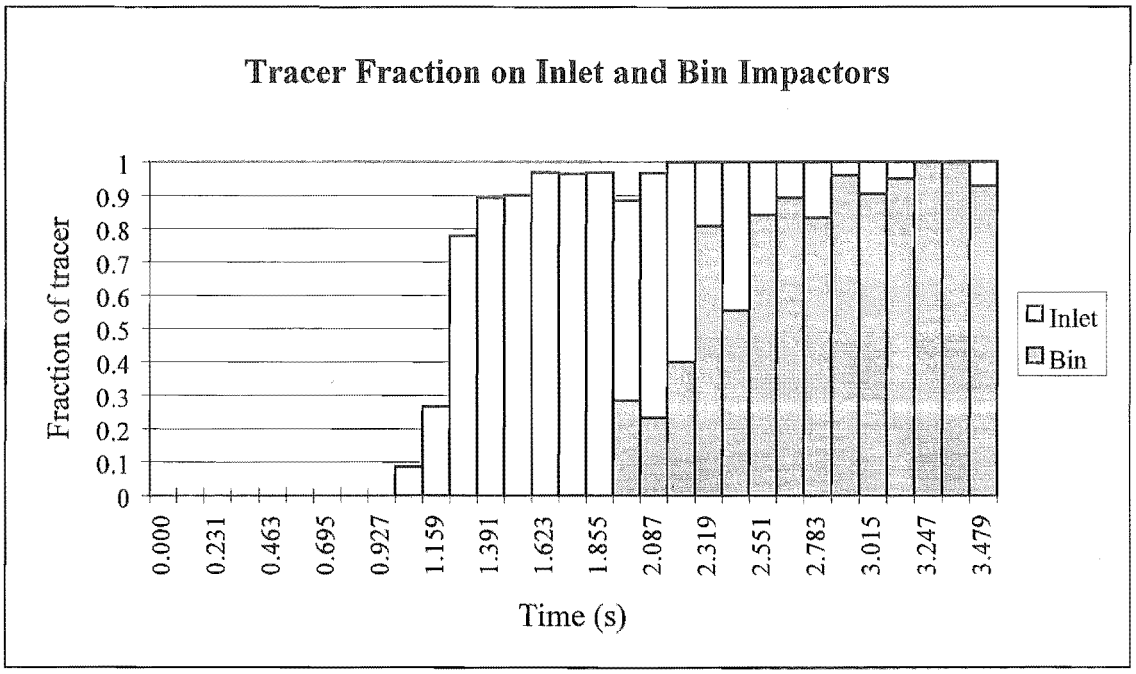

Figure 5: Tracer Fraction on Inlet and Bin Impactors for Step Change Experiments, Run 86

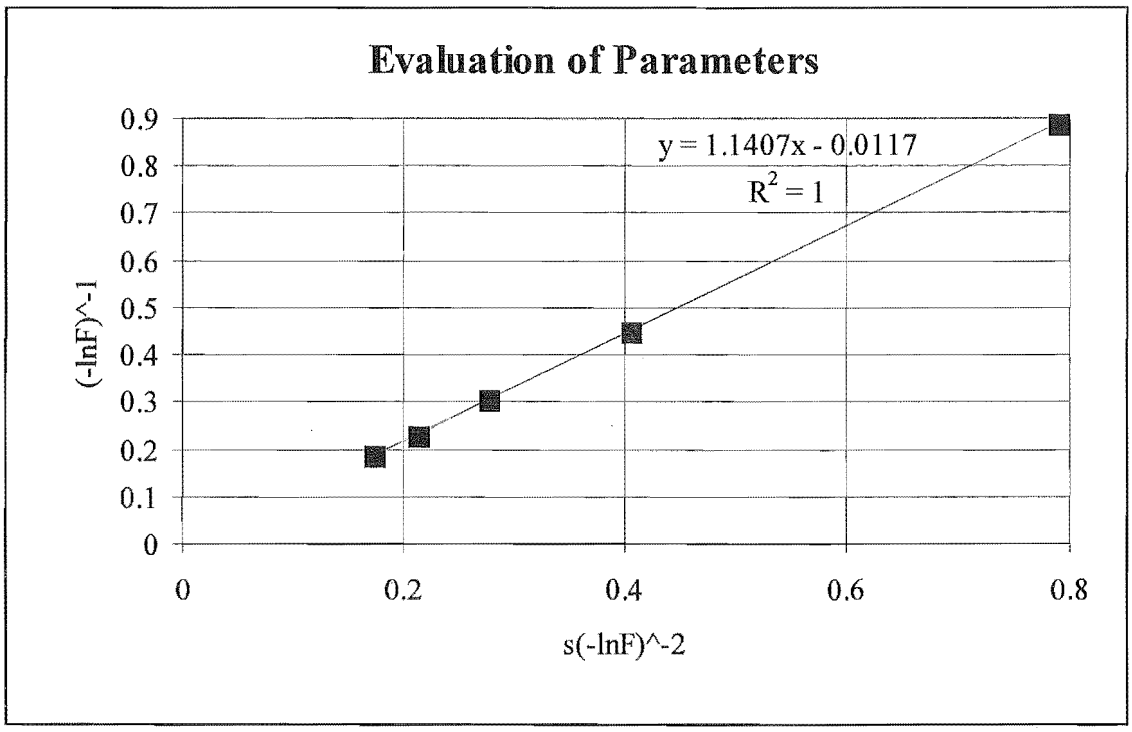

Figure 6: Evaluation of Transfer Function

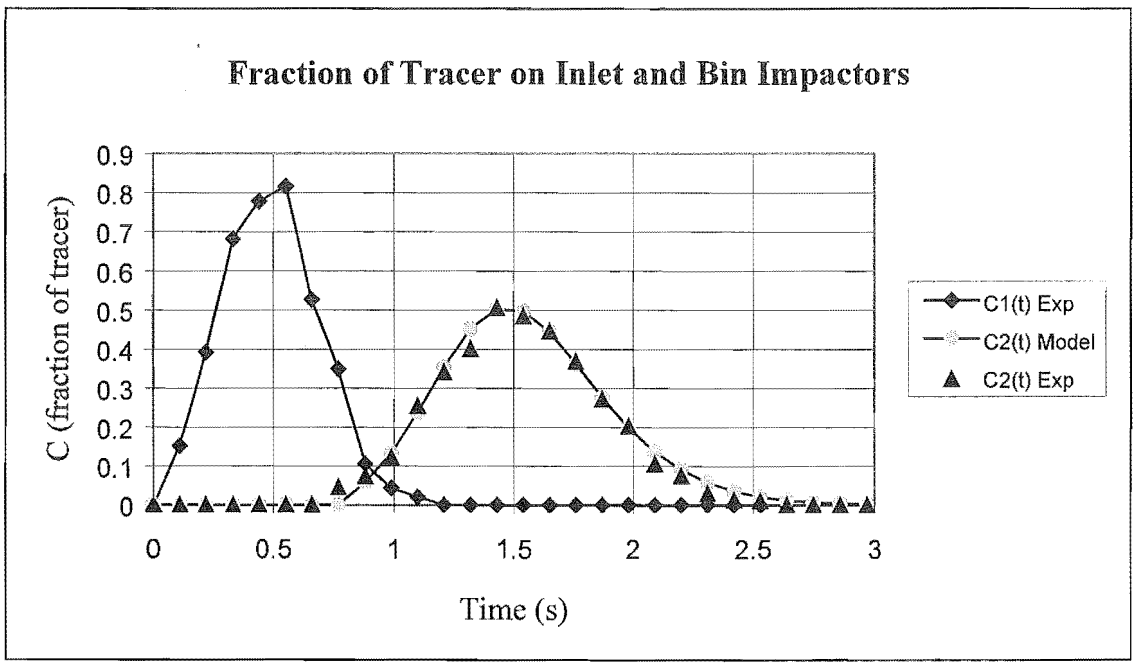

Figure 7: Averaged Experimental Tracer Distributions and Model Fit

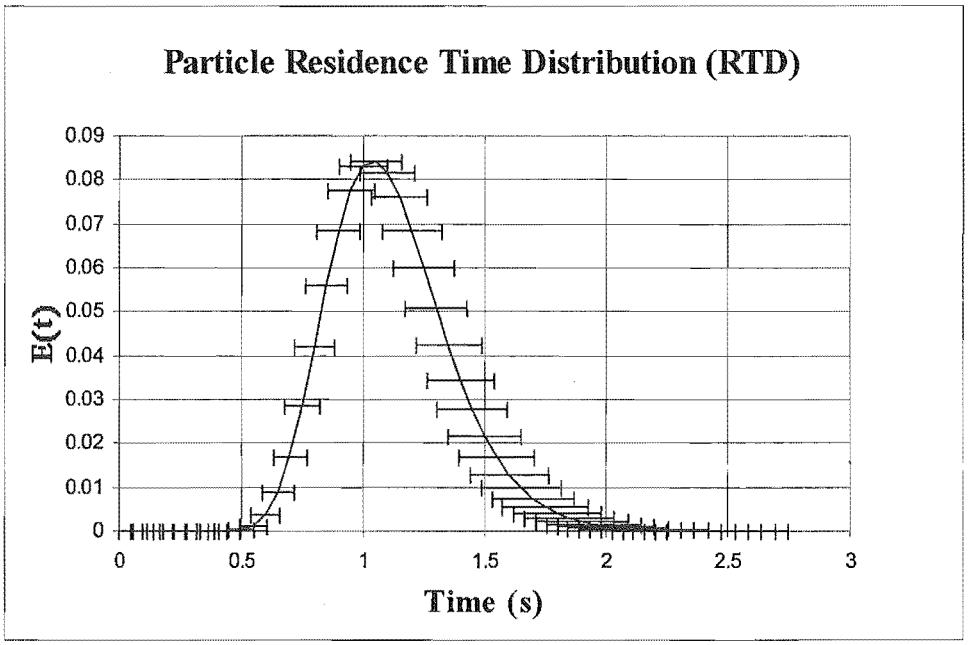

Figure 8: Particle Residence Time Distribution for an Idealised Pulse

Appendix 9B - International Drying Symposium (IDS'98)

SOLIDS RESIDENCE TIME AND DRYING IN CYCLONES

Ian C. Kemp[1] , David P. Frankum[1], John Abrahamson[2] and Thomas Saruchera[2]

1. SPS (Separation Processes Service), AEA Technology plc, 404 Harwell, Didcot, U.K.
2. Department of Chemical and Process Engineering, University of Canterbury, Christchurch, New Zealand

Key Words: experiment, modelling, pneumatic conveying (flash) dryers, design, industrial

ABSTRACT

Significant drying can take place in the cyclone which follows pneumatic conveying and spray dryers. At SPS, solids residence time and drying in cyclones have been measured experimentally and a theoretical model has been developed. Experiments were performed in three industrial-scale cyclones of 225 mm, 350 mm and 450 mm diameter. Residence time was measured by introducing coloured particles into the gas flow and sampling the particles using a novel sticky impactor developed at the University of Canterbury. Variations with gas velocity, solids-gas loading, cyclone diameter, particle diameter and particle density were measured. The residence time depended on particle and cyclone diameter but was surprisingly insensitive to changes in operating conditions. Heat transfer and drying rates were also measured and a qualitative model for the cyclone was developed. Implications for dryer design and performance are discussed. The predicted performance of a flash dryer changes considerably when the overall system including the cyclone is considered, especially when scaling up from pilot plant data or considering the effect of altering gas velocity during operation.

INTRODUCTION

Cyclones are extensively used for gas cleaning and product collection from the exhaust gas from dryers, especially for entrainment-type dryers such as pneumatic conveying (flash) and spray dryers. The effectiveness of fines collection has been extensively studied. The additional residence time of the solids (believed to be of the order of 2-5 seconds) is also significant, especially for a flash dryer where duct residence time is of the order of 1 second; it can allow some internal moisture to be removed. However, solids residence time and the drying attained in cyclones has been little studied in the past.

The practical effect of the cyclone was demonstrated in a troubleshooting study performed by SPS on a pneumatic conveying dryer. In this plant, the cyclone had been removed due to blockage problems and replaced by a bag filter. The exit moisture content immediately rose from 0.3% to 1% due to the loss of the residence time in the cyclone. This could not be overcome by changing dryer operating conditions and eventually a second-stage dryer had to be installed.
In the study of particle transport through a cyclone, the main mechanisms to consider are particle motion, heat transfer and internal mass transfer and drying rates. Each of these has to be considered separately, both in experiments and in the theoretical model. A similar breakdown was used in the extensive set of SPS experiments on pneumatic conveying dryers which led to a complete theoretical model for design, performance and scale-up (Kemp et al, 1994).

EXPERIMENTAL STUDY OF SOLIDS RESIDENCE TIME

Earlier work

Initially, qualitative flow visualisation studies were performed using a small glass-walled cyclone. It could be seen that the particles stayed close to the wall throughout. If the solids feed is turned off, there is a minimum inventory of solids which stay in the cyclone and do not emerge as long as gas flow is maintained. However, the studies showed that, with a continuous solids flow, this material was continuously swept out and replaced, and there was no "dead zone" of particles. The studies also confirmed the observations of Abrahamson (1981) that for high gas velocities and solids concentration, "roping" occurs, where streams of particles cluster together and travel quickly through the cyclone, giving reduced solids residence times.

Residence times have also been previously recorded in a 450mm diameter cyclone, using high-speed cine photography, as reported by Pasley and Kemp (1993). The technique was labour intensive, such that only a few runs were completed. Video was tried as an alternative, but the picture resolution was too poor to distinguish the tracer particles. The trends indicated that the residence time increased with the gas velocity, particle density and particle diameter, whereas it decreased for an increased solids-gas loading.

Experimental method

The main set of experiments for particle motion, heat transfer and drying were all performed in a 350 mm diameter cyclone belonging to the SPS Gas Cleaning Section. The cyclone dimensions and the associated flowsheet are shown in Figure 1.

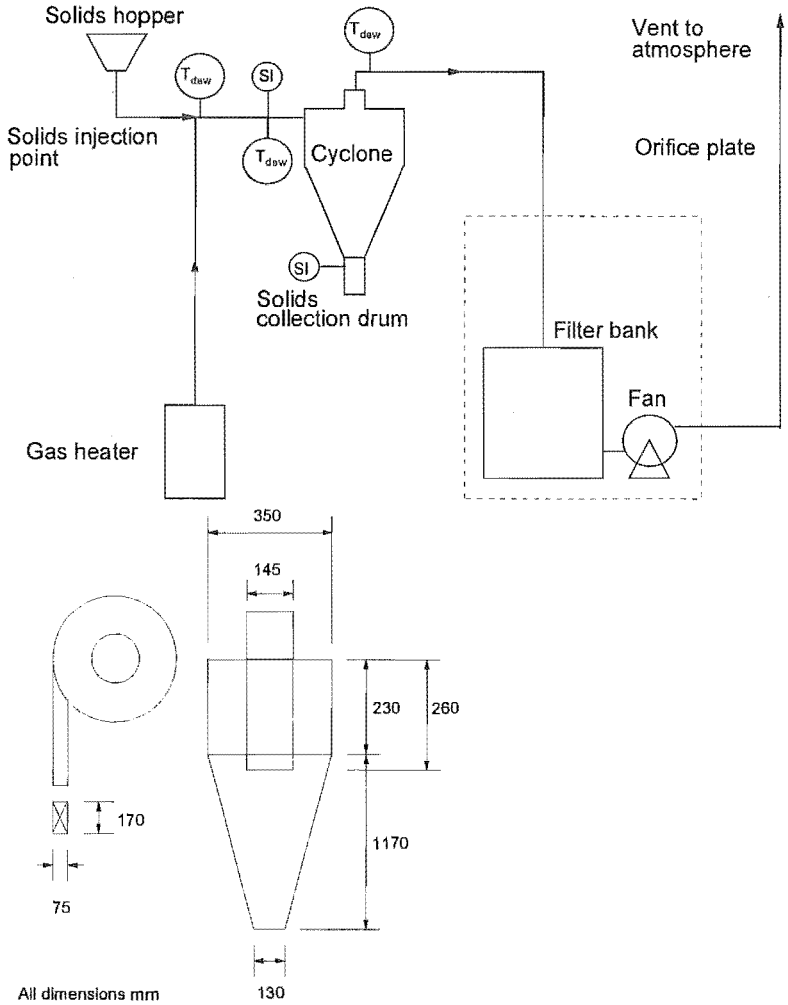

Figure 1. Arrangement of experimental apparatus and geometry of cyclone

Early studies showed that one of the most difficult problems was to find a way of determining particle residence time without affecting the flow through the cyclone. Tracer methods seemed the most natural answer, but two further problems arise; getting the tracer into the flow of solids without disturbing it, and detecting the tracer at the beginning and end of the cyclone.

For the first problem, using a solids injector altered the solids-gas loading, disturbed the local flow patterns in the cyclone and gave unrepresentative results. Injecting particles into an empty cyclone was also unsuccessful, as the cyclone had to "load up" to its minimum solids inventory and the particles never emerged at all! (They could be heard circulating inside the cyclone). Various methods involving mass-flow hoppers with localised layers of coloured solids were tried, but backmixing was always too great. In the end, a simple belt feeder was found to be best. On the belt were arranged a set of white particles to load up the cyclone, a block of coloured particles to act as tracer, and a further set of white particles. This was found to give a sharp pulse of tracer at the entrance to the cyclone, and the distribution of coloured particles at the exit showed how much backmixing took place at the beginning and end of the tracer pulse. On entering the duct, the solids are accelerated by a small paddle wheel to quickly approach the velocity of the gas. The arrangement is shown in Figure 2 (left-hand side).

For detection, bombarding particles with ultra-violet light to make them fluoresce was considered, but it was found that the effect did not last long enough for the particles to be detected at the end of the cyclone. As mentioned above, photographic methods were tried, but failed to give sufficient resolution. The eventual solution was to use the "sticky impactor" developed by John Abrahamson and co-workers at the University of Canterbury, New Zealand (Rajendra and Abrahamson 1994) and illustrated in Figure 2 (right-hand side).

The impactor consists of a brass tube with a small hole in one side enclosing a "U" shaped aluminium channel (shuttle) divided into a series of small compartments. The entrance hole is mounted facing the gas stream. A hydraulic actuator moves the impactor shuttle through the tube and past the entrance hole, and a potentiometer is used to record the speed of the shuttle, from which the time may be calculated. Solid particles pass through the hole and are captured by the shuttle which is covered in petroleum jelly. The shuttle is then removed and the number of both white and coloured particles in each segment is counted using a travelling microscope. Using two Sticky Impactors, one placed before the cyclone and one in the collection bin, the difference in the particle distribution trace allows the residence time to be determined.

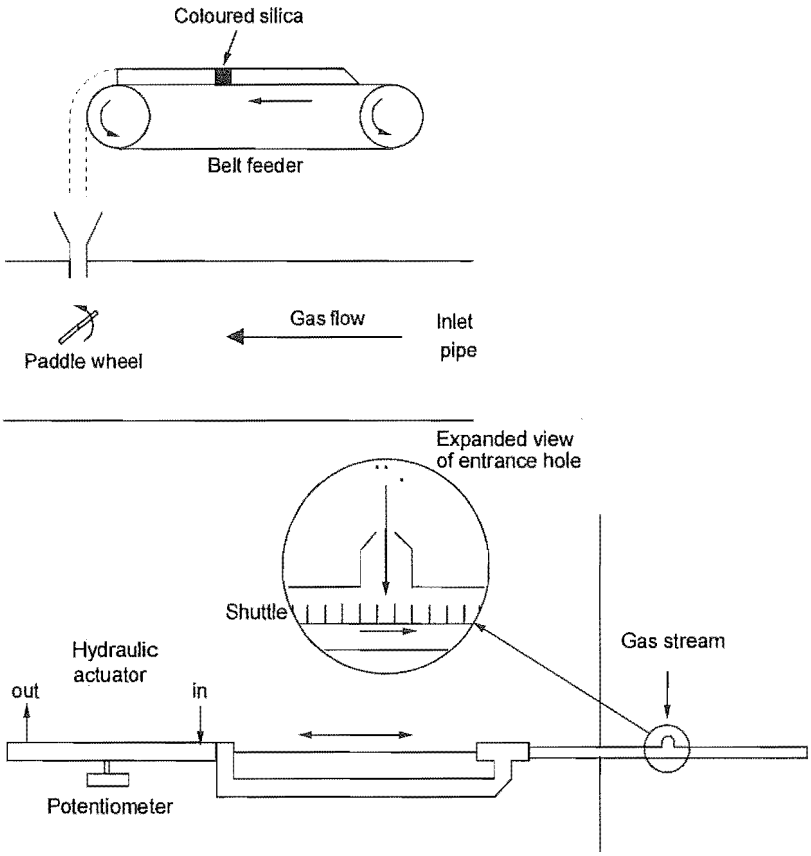

Figure 2. Solids feed arrangement and travelling impactor design for residence time tests

Figure3 shows a typical set of results from an impactor; the total number of particles collected in each slot is shown on the left and the proportion of black particles is on the right. It can be seen that the objective, of introducing a sharp trace but maintaining a steady flow, had been achieved. The difference between the times when the tracer passed the inlet and outlet gave the solids residence time in the cyclone.

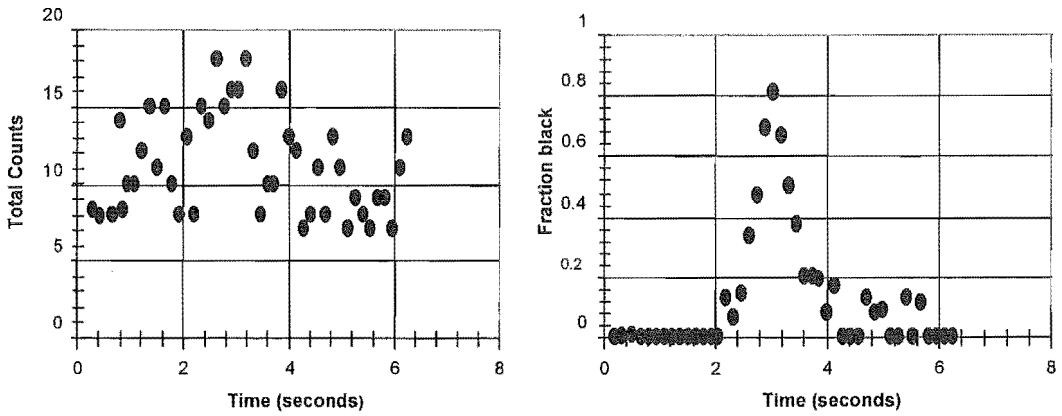

Figure 3. Results from sticky impactor for typical run

Since the outlet pulse is more diffuse than the inlet, two different methods could be proposed to define the solids residence time: peak-to-peak and integrating the distribution using the formula $\tau = \int Ctdt / \int Cdt$.

The integration method was used to generate the results reported below. Analysis methods are covered in more detail by Saruchera and Abrahamson (1997).

EXPERIMENTAL RESULTS FOR SOLIDS RESIDENCE TIME

Initial experiments with 200-1000 μm silica gel gave the surprising result that there appeared to be no dependence of residence time on gas velocity or solids-gas loading (SGL). With a tighter size range of 200-425 μm, a slight fall in residence time with gas velocity was apparent (Figure 4, left-hand side). Note also that the residence times for a solids-gas loading of 0.05 are slightly greater than those for both lower (0.025) and higher (0.1) values. It is difficult to account for this peak, although it could be due to the onset of roping. However, the effect of both gas velocity and solids-gas loading appears to be very weak.

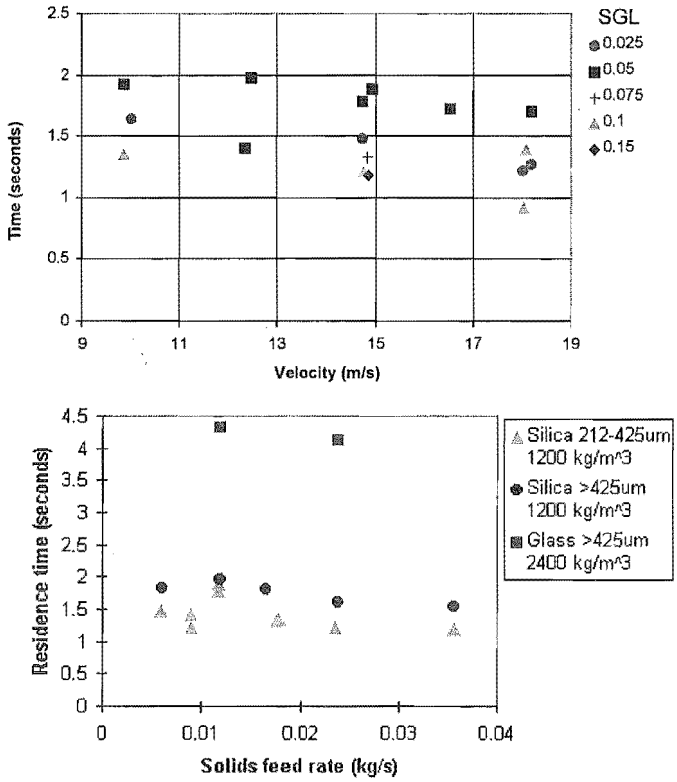

Figure 3. Observed variations of solids residence time with gas velocity and material in 350 mm cyclone

The right-hand part of Figure 4 shows the effect of material properties. Increasing particle size caused a slight increase in residence time, but doubling particle density roughly doubled residence time. The most likely explanation is that for the same solids-gas loading, the particles are clustered closer to the wall and wall friction effects are therefore comparatively greater. The effect might be less at higher solids flowrates.

Comparison with earlier experiments performed at SPS on the 450mm cyclone and Canterbury on two 225 mm units showed a sharp increase in solids residence time with cyclone diameter D, approximately proportional to D^2. Silica gel was used in all the experiments; size distributions were not identical but mean particle diameter was generally 300-350 μm. Since three of the cyclones were of similar geometry (cone angles 10-11^0), the dependence could actually be on DL, where L is cyclone height. For the Stairmand High Efficiency cyclone, the higher cone angle (14.7^0) gives a gentler slope and recent measurements at Canterbury show that this outweighs the shorter length and increases the residence time, but a higher inlet velocity was used and this could reduce it; the net effect is small. The results were:

Canterbury, 225 mm diameter Stairmand HE cyclone	Residence time 0.8 - 1.25 seconds
Canterbury, 225 mm diameter cyclone, cone angle 10^0	Residence time 0.7 - 1.2 seconds
SPS, 350 mm diameter cyclone, cone angle 10.7^0	Residence time 1.4 - 2.4 seconds
SPS, 450 mm diameter cyclone	Residence time 2.5 - 5.0 seconds

Overall, the main factors affecting solids residence time appear to be the cyclone geometry and particle properties. Little change can be made by varying the operating conditions (gas and solids flowrates).

INTERPRETATION AND COMPARISON OF RESIDENCE TIME RESULTS

It is interesting to compare the results from this study with those previously published in the literature:

Table 1. Effects of changes in parameters on solids residence time observed by different workers

Effect of increasing:	Observed effect on solids residence time τ				
	Lede et al. 1989	Kang et al. 1989	Silva and Nebra, 1990	Pasley and Kemp, 1993	This work
Solids-gas loading (SGL)	-	Decrease	Decrease	Decrease	Small decrease
Gas velocity or flowrate	Increase	Increase	Increase	Increase	Small decrease
Particle diameter	Decrease	Decrease	Decrease	Increase	Small increase
Particle density	-	-	-	Large increase	Large increase
Cyclone diameter	-	-	-	-	Large increase

Some of the differences in Table 1 can be explained by the different particle sizes used; the three earlier studies used smaller particles (below 100 micron) for which roping is likely to occur at lower velocities and the smallest particles may become entrained in the recirculating gas stream. Pasley and Kemp used three different particle sizes in the range 0.1-0.8 mm. The sticky impactor technique is also likely to give more detailed and accurate results than many of the techniques previously used. It has been suggested that the dependence on gas velocity may change above about 15 m/s.

The following correlation for solids residence time correlation is an approximate best fit to the new results;

$$\tau = 0.06 d_P^{0.3} \rho_P D L U_G^{-0.3}$$

This gives a calculated residence time τ of 1.5 seconds for 300 μm silica gel particles of density ρ_P=1200 kg/m^3 in the 350 mm diameter, 1400 mm high cyclone at an inlet gas velocity U_G of 15 m/s. There is no guarantee that this correlation can be extrapolated to significantly different situations; for example, other workers' results suggest that a completely different trend applies for particle diameters below 100 micron.
Also it does not allow for changes in geometry, particularly cone angle.

EXPERIMENTAL RESULTS FOR HEAT TRANSFER AND DRYING

For these experiments, the apparatus was modified by installing a propane gas burner to heat the inlet air to the cyclone and substituting a screw feeder capable of much higher solids flowrates than the belt.

Firstly, an attempt was made to investigate heat transfer by entraining dry particles in the hot gas stream. Only five runs were made as it was difficult to get a high enough solids flowrate to give a significant reduction in gas temperature. The results were reasonably consistent, but inconclusive.

Drying experiments were then performed with small (212-425μm) and large (425-1000μm) silica gel using a feed moisture content of 25% dry basis. The inlet and outlet gas temperatures were recorded, and initial and final moisture contents were measured by oven test. Some drying unavoidably took place between the solids feedpoint and the entry to the cyclone; it was not possible to sample the local moisture content at the cyclone entry, but the local gas temperature was recorded. The results were:

Table 2. Conditions and results for drying experiments

Parameter / Run No.	1 (base case)	2	3	4	5	6
Particle size range	Small	Small	Small	Small	Small	Large
Inlet gas temperature T_{GI}	150°C	150°C	150°C	120°C	200°C	150°C
Inlet gas velocity U_{GI}	15m/s	10m/s	10m/s	15m/s	15m/s	15m/s
Solids-gas loading SGL	0.05 kg/kg	0.05	0.1	0.05	0.05	0.05
ΔT across cyclone	26.0°C	25.1°C	35.8°C	20.1°C	36.1°C	19.5°C
ΔT from feedpoint to exit	37.0°C	33.6°C	46.5°C	28.7°C	52.7°C	34.0°C
ΔX from feedpoint to exit	0.177 kg/kg	0.171	0.135	0.117	0.198	0.116

The results can be interpreted as follows:

(a) Increasing gas velocity seems to give little or no increase in specific drying rate ($-dX/dt$) if the same solids-gas loading is maintained (comparing runs 1 and 2). If gas flow is increased without increasing solids flowrate, then drying does seem to increase, due to a heat balance effect; gas temperature stays higher and so do temperature driving forces.
(b) If solids-gas loading is increased, there is a significant fall in drying due to a heat balance effect - gas temperature falls faster and temperature driving forces decrease (Runs 2 and 3).
(c) Increasing gas inlet temperature increases drying rates. The effect seemed to be more marked at moderate temperature than at high ones (comparing runs 4 and 5 with the base case 1); possibly there is a threshold temperature at which drying is fast enough to remove all the reasonably accessible moisture. The only effect on solids residence time should be a weak secondary effect due to changes in gas density.
(d) Particle size has a weak effect on residence time but a strong one on drying (Runs 1 and 6), especially at high drying rates. The dominant effect seems to be the slower moisture movement from the centre of large particles.
(e) The effect of particle density was not measured but the increased residence time would be expected to give increased drying. A weak effect could also arise from the change in surface-to-mass ratio.

THE OVERALL SYSTEM: PNEUMATIC CONVEYING DRYER AND CYCLONE

Table 3 shows how changes in operating conditions affect the residence time and drying rate in a pneumatic conveying dryer (vertical duct) and a cyclone. In some cases, the change in drying in the cyclone opposes that in the pneumatic conveying dryer.

Table 3. Effect of changing design and operating parameters on drying duct and cyclone

	Pneumatic conveying dryer		Cyclone	
Parameter altered	Residence time	Drying (ΔX)	Residence time	Drying (ΔX)
Increase in diameter D	Falls slightly	Falls moderately	Increases greatly	Increases greatly
Increase in SGL	Increases slightly	Falls	Falls slightly	Falls
Increase in temperature T_{GI}	Falls slightly	Increases	Unchanged	Increases
Increase in gas velocity U_G	Falls	Usually falls	Falls slightly	Increases

The interactions can be quite complex. For example, in the pneumatic conveying dryer, increasing the solids-gas loading increases the evaporation load, alters the heat balance and reduces the outlet gas temperature; this gives a slight increase in the gas density and reduction in the gas velocity, which in turn reduces the particle velocity slightly and increases the solids residence time. The overall drying, in terms of moisture content reduction ΔX, falls because of the change in heat balance, which reduces the temperature driving forces in the latter part of the dryer and the cyclone. The effects of increasing solids-gas loading on the dryer and the cyclone are additive; the same is true for changes in gas temperature. However there are two important cases where the trends in the dryer duct and the cyclone are conflicting:

(a) An increase in solids throughput requires a corresponding increase in gas mass flow rate to maintain the heat balance. The cross-sectional area of the main drying duct will have to increase, and it has been found that this decreases wall friction and reduces residence time for a given length of duct (Kemp and Oakley 1997). However, the cyclone diameter generally has to be increased to keep

pressure drop down to an acceptable level, and the solids residence time will rise sharply. Alternatively, if multiple cyclones in parallel are used, there will be less increase in residence time and ΔX compared with enlarging a single cyclone. These results have very important implications for scale-up from pilot plants to full-scale dryers, in determining the drying which will take place in the overall system.

(b) An increase in gas velocity improves driving forces but increases the particle velocity, cutting down the solids residence time in the main drying duct. Simulation has shown that the latter effect usually outweighs the former, so that increasing gas flow actually worsens the drying in the main duct (Kemp and Oakley 1997). However, the driving forces in the cyclone will increase and so more drying can occur there to compensate. This effect will be reinforced if the effect observed by other workers, that higher gas velocities increase solids residence time in the cyclone for small particles, is correct. This has important implications when attempting to change dryer operating conditions for debottlenecking purposes. Obviously, better drying rates can also be achieved by lowering inlet moisture or increasing inlet gas temperature, but these have usually been pushed to their limit already.

CONCLUSIONS

The travelling impactor was a successful method for measuring solids residence time. The results were surprising in that residence time appears to be much more sensitive to solids properties and cyclone dimensions than to operating conditions. Increasing cyclone diameter, particle density or particle diameter gives an increase in residence time for the 300 or 500 μm silica gel used in these tests.

Drying rates were also successfully measured, and the results generally match those that would be expected from consideration of the heat balance and the solids residence time. Specific drying rates increase as gas inlet temperature and velocity increase, and as particle size and solids-gas loading fall.

The new findings on dryer residence time and evaporation rate in the cyclone cause significant changes to the predicted performance of a pneumatic conveying dryer when the overall system including the cyclone is considered. The greatest changes occur when considering scale-up from pilot-plant data (in design mode) or the effect of altering gas velocity during operation (in performance calculations).

SPS are now developing a theoretical model for the residence time and drying rates, based on the experiments and similar to the existing SPS incremental model for pneumatic conveying dryers (Kemp and Oakley 1997). The results will be incorporated into the DRYCON software package.

ACKNOWLEDGEMENTS

The work was carried out for SPS (Separation Processes Service) with 50% funding from the UK Department of Trade and Industry. The authors wish to thank Eva Richter, Manish Bharati, Humphrey Pasley and Alister Hood for their major contributions to the experimental work, and the SPS Drying Panel for their useful comments and constructive suggestions in the periodic reviews of results.

NOTATION

C	fraction of coloured particles	-
d_P	particle diameter	m
D	cyclone diameter	m
L	cyclone length/height	m
SGL	solids-gas loading	kg/kg
t	time	s
T	temperature	^{0}C
U	velocity	m/s
X	moisture content	kg/kg
Δ	difference operator	
ρ_P	particle density	kg/m^3
τ	solids residence time	s

Subscripts

G	for gas
I	at inlet conditions

LITERATURE CITED

Abrahamson, J., 1981, Progress in Filtration and Separation 2 (ed. R.J. Wakeman), p.1.

Kang, S.K., Kwon, T.W., Kim, S.D., 1989, Powder Technology, 58, p. 211.

Kemp, I.C., Bahu, R.E. and Pasley, H.S., 1994, Model development and experimental studies of vertical pneumatic conveying dryers, Drying Technology, (12), 6, pp. 1323-1340.

Kemp, I.C. and Oakley, D.E., 1997, Simulation and scale-up of pneumatic conveying and cascading rotary dryers, Drying Technology, (15), 6-8, pp. 1699-1710. (Selected papers from IDS'96, Krakow)

Lede, J., Li, H.Z., Soulignac, F., and Villermaux, J., 1989, Chem.Eng.J., 42, p 103.

Pasley, H.S. and Kemp, I.C., 1993, Experimental studies and modelling of particle motion in cyclones, IChemE Research Event, Birmingham, pp. 495-497.

Rajendra, Y.D. and Abrahamson, J., 1994, Particle residence time in return-flow cyclones. Chemeca '94, Perth, Australia, Sept. 1994, p 141-148.

Saruchera, T. and Abrahamson, J., 1997, Residence time of granular particles through a cyclone - analysis using moments, Laplace transform and least squares methods. Proceedings of Chemeca 97, Rotorua, New Zealand, pp. 201-213.

Silva, M.A. and Nebra, S.A., 1990, Drying in cyclones - an experimental study, CHISA '90 paper E3.38.

Appendix 9C — Visual Basic Program for BPM

```
' Bouncing Particle Model (BPM)
' Program calculates particle velocity components and evaluates the particle
'residence time in the cyclone
'Using Runge Kutta Algorithm

Option Explicit
Dim x As Single, x0 As Single
Dim e As Single ' coefficient of restitution
Dim f As Single ' coefficient of friction
Dim p_diameter As Double '(m)
Dim Q As Single '(m3/s)
Dim Rep As Double 'particle Reynolds number
Dim CD As Double  'Drag coefficient
Dim p_density As Single  '(kg/m3)
Dim hx As Double 'incremental height of cyclone from top to bottom
Dim ht As Double 'total height of cyclone
Dim h As Double ' step size (m)
Dim Rx As Double ' current radius in conical section
Dim R As Single '(m)  Radius  R = Rc -dp/2
Dim delta_R As Double 'radial distance from wall to particle centre of mass
Dim Vp, V0 As Double ' particle tangential velocity
Dim U0, Up As Double  ' particle radial velocity
Dim Vz As Double  ' particle axial velocity
Dim tp As Double   ' particle residence time
Dim Vg As Double  ' gas entrance velocity (m/s)
Dim Ug As Double  'gas radial velocity (m/s)
Dim Wp, Wg As Double  ' particle axial velocity (m/s)
Dim Upw, U0w, Vpw, V0w, Beta As Single
Dim Fn As Double 'Particle normal force
Dim Ff As Double 'Frictional force
```

```
Dim k0, k1, k2, k3, k4 As Double
Const PI As Single = 3.141592654
Const Alpha As Double = 1 'angle of particle velocity vector from horizontal
Const Angle As Double = 7 'cone half angle(degrees)
Const hc As Double = 0.73  'height of cyclone(m)
Const hcl As Double = 0.23 ' height of cylinder (m)
Const Rc As Double = 0.1125 ' radius of cylindrical section of cyclone (m)
Const Rex As Double = 0.0425 ' radius at apex (exit) (m)
Const viscosity As Double = 0.000018  'gas viscosity (Pas)
Const a As Double = 0.11  ' rectangular entrance height (m)
Const b As Double = 0.045  ' rectangular entrance width (m)

'Procedure for calculatating tangential velocity
Sub Tangential(Vp, Wg, Wp, Ug, Up, h, k0)
Dim Rep As Double, W As Single, t As Single
Dim CD As Double
Vg = Q / (a * b) 'gas tangential inlet velocity
Rep = 1.2 * ((Vg - Vp) ^ 2 + (Wg - Wp) ^ 2 + (-Ug - Up) ^ 2) ^ 0.5 *
p_diameter / viscosity 'Particle Reynolds number

CD = (24 / Rep) * (1 + 0.15 * Rep ^ 0.687)  'Drag coefficient

k0 = h * (1 / Vp) * 0.75 * CD * 1.2 * ((Vg - Vp) ^ 2 + (Wg - Wp) ^ 2 + (Ug -
Up) ^ 2) ^ 0.5 * (Vg - Vp) * (1 / (p_density * p_diameter))

Exit Sub
End Sub

'Fourth Order Runge Kutta Algorithm

Public Sub RungeKutta()
Dim k0 As Single, x0 As Single, V0 As Single, s As Single

Dim n As Integer, h As Single
Dim k As Integer
```

```
Open "c:\thomas\bounce.xls" For Output As #1  'output file
Open "c:\thomas\delta_R.xls" For Output As #2 'output file

Q = InputBox("Please enter gas volumetric flow rate m3/s")
Vp = InputBox("Please enter initial particle velocity - m/s")
p_diameter = InputBox("Please enter particle diameter/m")
p_density = InputBox("Please enter particle density")
e = InputBox("Please enter coefficient of restitution")
f = InputBox("Please enter coefficient of friction")
h = InputBox("Please enter step size") 'step size 5 mm in tangential direction

'When delta_R < p_diameter particle collides with wall
'post collision velocities found using coefficients of
'of restitution and friction (e and f)
'Particle at centre of entrance tube assumed to initially
'strike cyclone wall at angle 40 deg for this particular entrance geometry

Write #1, "height", "tangential velocity", "radial velocity", "axial velocity"
Write #2, "height", "radial distance"

'initial particle axial velocity
Wp = Vp * Tan(Alpha * PI / 180)  'initial angle of particle to horizontal close to
zero

'radial velocity perpendicular and towards wall
U0 = Vp * Sin(PI * 40 / 180) 'pre-collision particle radial velocity

V0 = Vp * Cos(PI * 40 / 180) ' pre-collision particle tangential velocity
'radial velocity perpendicular and away from wall
Up = -e * U0    ' post-collision particle radial velocity

Vp = V0 - f * (1 + e) * U0  'post-collision particle tangential velocity
hx = 0
tp = 0
```

```
Write #1, hx, Vp, Up, Wp

R = Rc - (p_diameter / 2)

'0.083 is distance from centre of entrance tube to end of vortex finder
Wg = Q / (PI * (Rc ^ 2 - Rex ^ 2))  'gas axial velocity

Call Radial1(Q, hcl, Ug)

Cylinder:

Do Until hx > hcl
   x0 = 0
   Do
      x = x0

      Call Tangential(Vp, Wg, Wp, Ug, Up, h, k0)

      k1 = k0

      x = x0 + 0.5 * h
      Vp = V0 + 0.5 * k1

      Call Tangential(Vp, Wg, Wp, Ug, Up, h, k0)

      k2 = k0

      Vp = V0 + 0.5 * k2

      Call Tangential(Vp, Wg, Wp, Ug, Up, h, k0)

      k3 = k0

      x = x0 + h
```

```
Vp = V0 + k3

Call Tangential(Vp, Wg, Wp, Ug, Up, h, k0)

k4 = k0

x0 = x0 + h
V0 = V0 + (k1 + 2 * k2 + 2 * k3 + k4) / 6

Rep = 1.2 * ((Vg - V0) ^ 2 + (-Ug - Up) ^ 2 + (Wg - Wp) ^ 2) ^ 0.5 *
p_diameter / viscosity 'particle Reynolds Number

CD = (24 / Rep) * (1 + 0.15 * Rep ^ 0.687)

Up = Up + h * V0 / Rc - 0.75 * CD * 1.2 * ((Vg - V0) ^ 2 + (Wg - Wp) ^
2 + (-Ug - Up) ^ 2) ^ 0.5 * (-Ug - U0) * h / (V0 * p_diameter * p_density)

R = R + h * Up / V0

delta_R = Rc - R

Vp = V0

Wp = Wp + 9.8 * h / V0 + 0.75 * CD * 1.2 * ((Vg - V0) ^ 2 + (Wg - Wp)
^ 2 + (-Ug - Up) ^ 2) ^ 0.5 * (Wg - Wp) * h / (p_diameter * p_density * V0)
'Call RK_Axial(hx, Wp, Vp, Ug, Up, h, Angle)

hx = hx + h * (Wp / Vp)  ' axial height
'Debug.Print hx, Wp

tp = tp + h / Vp  ' particle residence time



Write #2, hx, delta_R
Write #1, hx, Vp, Up, Wp
```

```
Loop While delta_R > p_diameter / 2

'Approach velocity paralle to wall

Beta = Atn(Wp / Vp)

Randomize

e = (0.1 + Rnd)

'Total particle velocity parallel to wall

V0w = (Vp ^ 2 + Wp ^ 2) ^ 0.5

Vpw = V0w - f * (1 + e) * Up 'post collision total velocity
Up = -e * Up

R = Rc - (p_diameter / 2)

' Post collision particle axial velocity
Wp = Vpw * Sin(Beta)

'Post collision particle tangential velocitt

V0 = Vpw * Cos(Beta)


    If hx > 0.083 Then ' '0.083 is distance from centre of entrance tube to end of
vortex finder
    Wg = Q * (0.1 + 0.9 * (1 - ((hx - 0.083) / (hc - 0.083)))) / (PI * (Rc ^ 2 -
Rex ^ 2)) 'gas axial velocity

    Else
    Wg = Q / (PI * (Rc ^ 2 - Rex ^ 2))
    End If
```

```
Loop

'transition from cylinder to conical section

Call Conical(hx, Rx, Rc)

  R = Rx - (p_diameter / 2)
  Vp = V0
  Debug.Print hx, tp
Do Until hx > hc  'calculate until h > height of cyclone


    x0 = 0

    Do

    x = x0

    Call Tangential(Vp, Wg, Wp, Ug, Up, h, k0)

    k1 = k0

    x = x0 + 0.5 * h
    Vp = V0 + 0.5 * k1

    Call Tangential(Vp, Wg, Wp, Ug, Up, h, k0)

    k2 = k0

    Vp = V0 + 0.5 * k2

    Call Tangential(Vp, Wg, Wp, Ug, Up, h, k0)

    k3 = k0
```

```
x = x0 + h
Vp = V0 + k3

Call Tangential(Vp, Wg, Wp, Ug, Up, h, k0)

k4 = k0

x0 = x0 + h
V0 = V0 + (k1 + 2 * k2 + 2 * k3 + k4) / 6

Call Radial2(Q, hcl, Ug)

Rep = 1.2 * (Vg - V0) * p_diameter / viscosity  'particle Reynolds Number

CD = (24 / Rep) * (1 + 0.15 * Rep ^ 0.687)

Up = Up + h * V0 / Rx - 0.75 * CD * 1.2 * ((Vg - V0) ^ 2 + (Wg - Wp) ^
2 + (-Ug - Up) ^ 2) ^ 0.5 * (-Ug - Up) * h / (V0 * p_diameter * p_density)

R = R + h * Up / V0

delta_R = Rx - R

Vp = V0


Wp = Wp + 9.8 * h / Vp + 0.75 * CD * 1.2 * ((Vg - V0) ^ 2 + (Wg - Wp)
^ 2 + (-Ug - Up) ^ 2) ^ 0.5 * (Wg - Wp) * h / (p_diameter * p_density * V0)

'Call RK_Axial(hx, Wp, Vp, Ug, Up, h, Angle)

hx = hx + h * (Wp / Vp) 'axial height

'Debug.Print hx, Vp, Wp, Up
```

```
'If hx < hcl And Wp < 0 Then GoTo Cylinder

tp = tp + h / Vp  'particle residence time

Debug.Print hx, tp, Wp

If delta_R < 0 Then
   delta_R = p_diameter / 2
End If

Write #2, hx, delta_R
Write #1, hx, Vp, Up, Wp

Call Conical(hx, Rx, Rc)

Wg = Q * (0.1 + 0.9 * (1 - ((hx - 0.083) / (hc - 0.083)))) / (PI * (Rc ^ 2 - Rex ^ 2)) 'gas axial velocity


Loop While delta_R > p_diameter / 2

'Particle approach velocity perpendicular to the wall
U0w = Up * Cos(Angle * PI / 180) + Wp * Sin(Angle * PI / 180)

'Rebound perpendicular velocity away from the wall
Upw = -e * U0w

'Approach velocity parallel to the wall
V0w = ((Wp * Cos(Angle * PI / 180) - Up * Sin(Angle * PI / 180)) ^ 2 + Vp ^ 2) ^ 0.5

'Angle for approach velocity relative horizontal
Beta = Atn((Wp * Cos(Angle * PI / 180) - Up * Sin(Angle * PI / 180)) / Vp)
```

```
'Rebound velocity parallel to the wall
Vpw = V0w - f * (1 + e) * U0w

'Post collision radial velocity

Up = -Vpw * Sin(Beta) * Sin(Angle * PI / 180) + Upw * Cos(Angle * PI /
180)

'Post collision axial velocity
Wp = (Up * Sin(Angle * PI / 180) + Vpw * Sin(Beta)) / Cos(Angle * PI /
180)

'Post collision tangential velocity
Vp = Vpw * Cos(Beta)


R = R + h * Up / Vp

delta_R = Rx - R
If delta_R < p_diameter / 2 Then
GoTo Sliding
End If

V0 = Vp
' Debug.Print Wp
R = Rx - (p_diameter / 2) ' contact with wall
Call Conical(hx, Rx, Rc)

Loop

Sliding:

Do Until hx > hc  'calculate until h > height of cyclone

Fn = 9.8 * Sin(Angle * PI / 180) + Vp ^ 2 * Cos(Angle * PI / 180) / Rx
```

```
Wg = Q * (0.1 + 0.9 * (1 - ((hx - 0.083) / (hc - 0.083)))) / (PI * (Rc ^ 2 - Rex ^ 2)) 'gas axial velocity

Rep = 1.2 * ((Vg - Vp) ^ 2 + (Wg - Wp) ^ 2) ^ 0.5 * p_diameter / viscosity 'particle Reynolds Number

CD = (24 / Rep) * (1 + 0.15 * Rep ^ 0.687)

Wp = Wp + 9.8 * h / Vp + 0.75 * CD * 1.2 * ((Vg - Vp) ^ 2 + (Wg - Wp) ^ 2 + (-Ug - Up) ^ 2) ^ 0.5 * (Wg - Wp) * h / (p_diameter * p_density * Vp) - Fn * Sin(Angle * PI / 180) * h / Vp - f * Fn * Wp * h / ((Vp ^ 2 + Wp ^ 2) ^ 0.5 * Vp)

hx = hx + h * (Wp / Vp) 'axial height
tp = tp + h / Vp

    x0 = 0
    x = x0
    V0 = Vp
    Call Wall_Tangential(Vp, Wg, Wp, Ug, Up, Rx, h, k0)

    k1 = k0

    x = x0 + 0.5 * h
    Vp = V0 + 0.5 * k1

    Call Wall_Tangential(Vp, Wg, Wp, Ug, Up, Rx, h, k0)

    k2 = k0

    Vp = V0 + 0.5 * k2

    Call Wall_Tangential(Vp, Wg, Wp, Ug, Up, Rx, h, k0)

    k3 = k0

    x = x0 + h
```

```
        Vp = V0 + k3

        Call Wall_Tangential(Vp, Wg, Wp, Ug, Up, Rx, h, k0)

        k4 = k0

        x0 = x0 + h
        Vp = V0 + (k1 + 2 * k2 + 2 * k3 + k4) / 6


    Write #1, hx, Vp, Up, Wp

Call Conical(hx, Rx, Rc)
   Debug.Print hx, tp, Wp
Loop
Debug.Print "residence time ="; tp
Close #1
Close #2
End Sub

Public Sub Conical(hx, Rx, Rc)
Dim Re As Double, t As Single
Dim Theta As Double

Theta = Angle  ' half angle of cone
Theta = Theta * PI / 180

ht = Rc * Tan(PI / 2 - Theta) 'total height of cone

Rx = (ht - (hx - hcl)) / Tan(PI / 2 - Theta) 'current radius

Exit Sub
End Sub
```

```
Sub Axial(hx, Wp, Vp, Ug, Up, h, Angle, z)

Dim Rep As Double, Wg As Single, t As Single
Dim CD As Double


ht = Rc * Tan(PI / 2 - (Angle * PI / 180)) 'total height of cone to vertex
Vg = Q / (a * b)

If hx > 0.083 Then

Wg = Q * (0.1 + 0.9 * (1 - ((hx - 0.083) / hc))) / (PI * (Rc ^ 2 - Rex ^ 2))

Else
Wg = Q / (PI * (Rc ^ 2 - Rex ^ 2))
End If

Rep = 1.2 * ((Vg - Vp) ^ 2 + (Wg - Wp) ^ 2) ^ 0.5 * p_diameter / viscosity

CD = 24 / Rep * (1 + 0.15 * Rep ^ 0.687)

z = h * 1.2 * 0.75 * CD * ((Vg - Vp) ^ 2 + (Wg - Wp) ^ 2 + (-Ug - Up) ^ 2) ^
0.5 * (Wg - Wp) / (p_diameter * p_density) + h * 9.8

If hx > hcl Then

t = hx - hcl

Wg = Q * ((0.1 + 0.9) * (1 - (hx - 0.083) / hc)) / (PI * ((ht - t) * Tan((Angle * PI
/ 180))) ^ 2 - Rex ^ 2)

Rep = 1.2 * ((Vg - Vp) ^ 2 + (Wg - Wp) ^ 2) ^ 0.5 * p_diameter / viscosity

CD = 24 / Rep * (1 + 0.15 * Rep ^ 0.687)
```

```
z = h * 1.2 * 0.75 * CD * ((Vg - Vp) ^ 2 + (Wg - Wp) ^ 2 + (-Ug - Up) ^ 2) ^
0.5 * (Wg - Wp) / (p_diameter * p_density) + h * 9.8    ' - (h / Wp) * (Vp ^ 2 *
Cos((Angle * PI / 180)) * Sin((Angle * PI / 180)) / ((ht - t) * Tan(Angle * PI /
180)) - (h / Wp) * 9.8 * Sin(Angle * PI / 180) * Sin(Angle * PI / 180) - f * h * 9.8
* Sin(Angle * PI / 180) / (Vp ^ 2 + Wp ^ 2) ^ 0.5 - f * h * Vp ^ 2 * Cos(Angle *
PI / 180) / ((ht - t) * Tan((Angle * PI / 180))) * (Vp ^ 2 + Wp ^ 2) ^ 0.5)

End If

Exit Sub
End Sub

Public Sub RK_Axial(hx, Wp, Vp, Ug, Up, h, Angle) ' calculate particle axial
velocity
Dim z As Single, t0 As Single, Wp0 As Single

t0 = 0
Wp0 = Wp

Call Axial(hx, Wp, Vp, Ug, Up, h, Angle, z)

k1 = z

t0 = t0 + 0.5 * h
Wp = Wp0 + 0.5 * k1

Call Axial(hx, Wp, Vp, Ug, Up, h, Angle, z)

k2 = z

Wp = Wp0 + 0.5 * k2

Call Axial(hx, Wp, Vp, Ug, Up, h, Angle, z)

k3 = z
```

```
t0 = t0 + h
Wp = Wp0 + k3

Call Axial(hx, Wp, Vp, Ug, Up, h, Angle, z)



k4 = z

t0 = t0 + h
Wp = Wp0 + (k1 + 2 * k2 + 2 * k3 + k4) / 6

Exit Sub
End Sub

Public Sub Radial1(Q, hcl, Ug)
Dim R As Single
'Procedure to calculate average gas radial velocity in the cylindrical section
R = 0.055 ' radius of vortex finder
Ug = Q / (2 * PI * R * hcl)

End Sub

Public Sub Radial2(Q, Rex, Ug)
'Procedure to calculate average gas radial velocity in conical section

Ug = Q / (2 * PI * Rex * 0.7 * (hc - hcl))

End Sub

Public Sub Wall_Tangential(Vp, Wg, Wp, Ug, Up, Rx, h, k0)

Dim Rep As Double
Dim CD As Double
```

```
Up = 0  'particle radial velocity  is zero
Fn = 9.8 * Sin(Angle * PI / 180) + Vp ^ 2 * Cos(Angle * PI / 180) / Rx
Vg = Q / (a * b) 'gas tangential inlet velocity

Rep = 1.2 * ((Vg - Vp) ^ 2 + (Wg - Wp) ^ 2 + (-Ug - Up) ^ 2) ^ 0.5 *
p_diameter / viscosity 'Particle Reynolds number

CD = (24 / Rep) * (1 + 0.15 * Rep ^ 0.687)  'Drag coefficient

k0 = h * (1 / Wp) * 0.75 * CD * 1.2 * ((Vg - Vp) ^ 2 + (Wg - Wp) ^ 2 + (Ug -
Up) ^ 2) ^ 0.5 * (Vg - Vp) * (1 / (p_density * p_diameter)) - f * Fn * h * Vp / (Rx
* Wp * (Vp ^ 2 + Wp ^ 2) ^ 0.5)

Exit Sub
End Sub
```

Appendix 9D *– Conical Sections*

CYCLONE CONICAL SECTION C

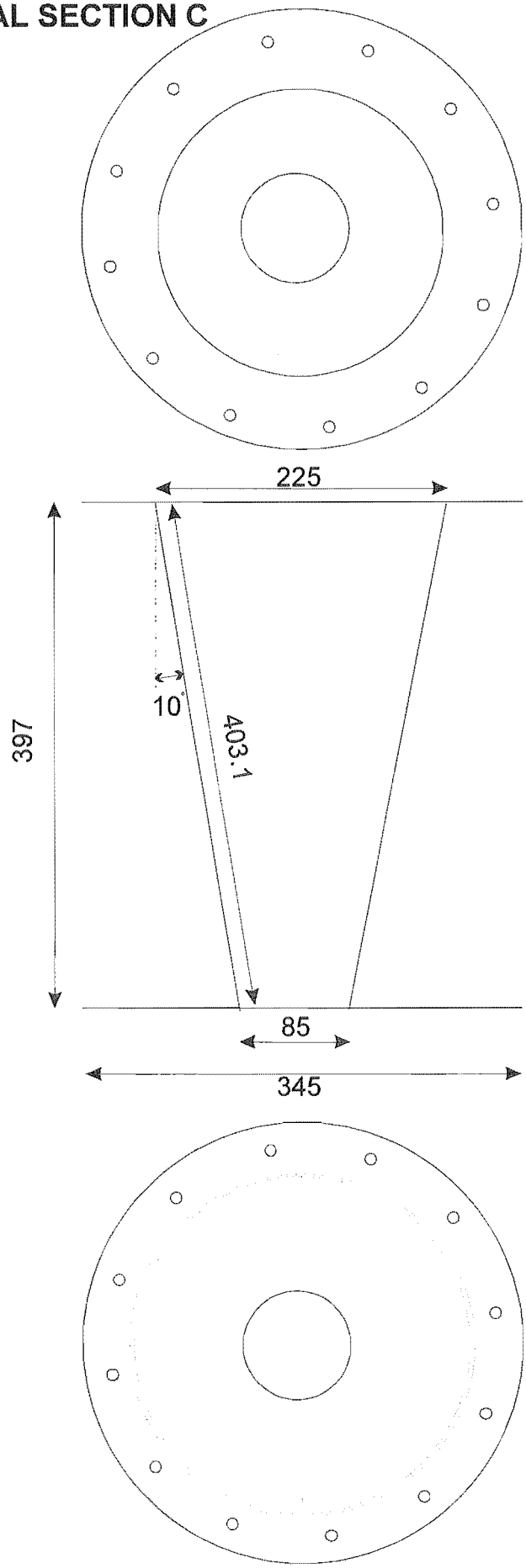

DIMENSIONS IN MM
Material: 6mm Gauge Mild Steel

CYCLONE CONICAL SECTION D

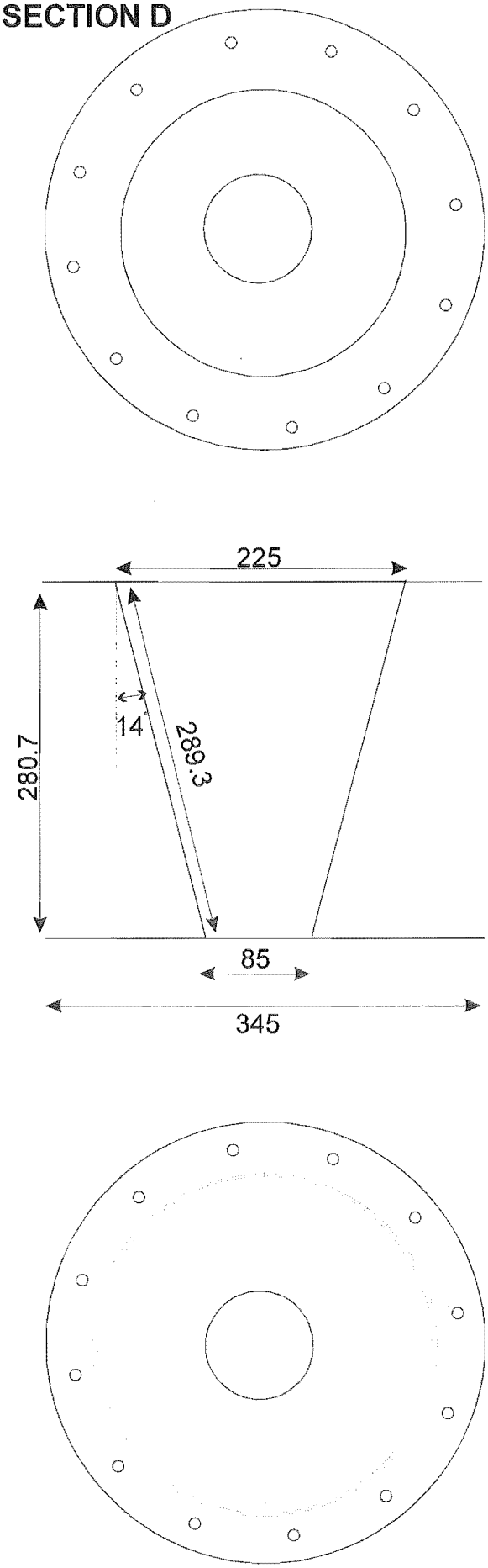

DIMENSIONS IN MM
Material: 6mm Gauge Mild Steel

CYCLONE CONICAL SECTION E

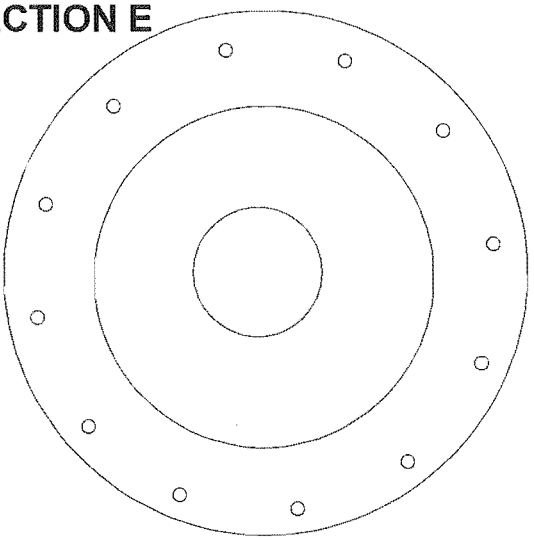

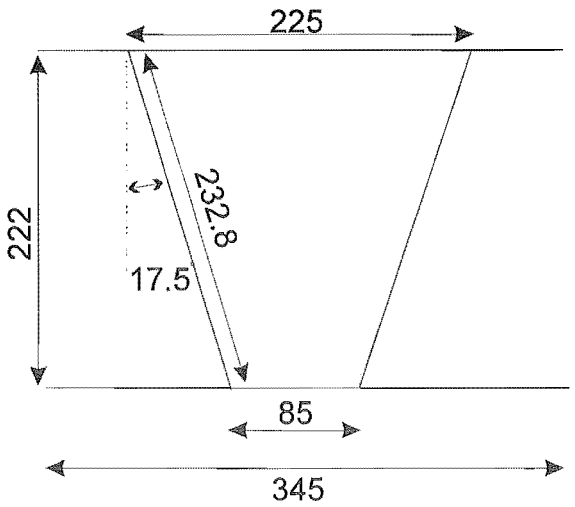

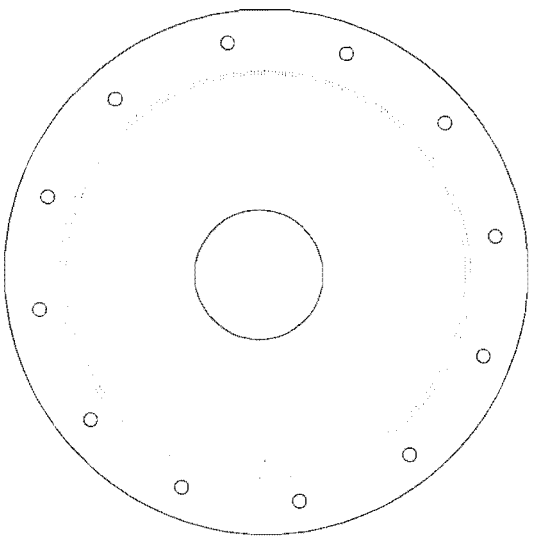

DIMENSIONS IN MM
Material: 6mm Gauge Mild Steel

Appendix 9E – Air-Hydraulic Circuit for Moving Shuttles

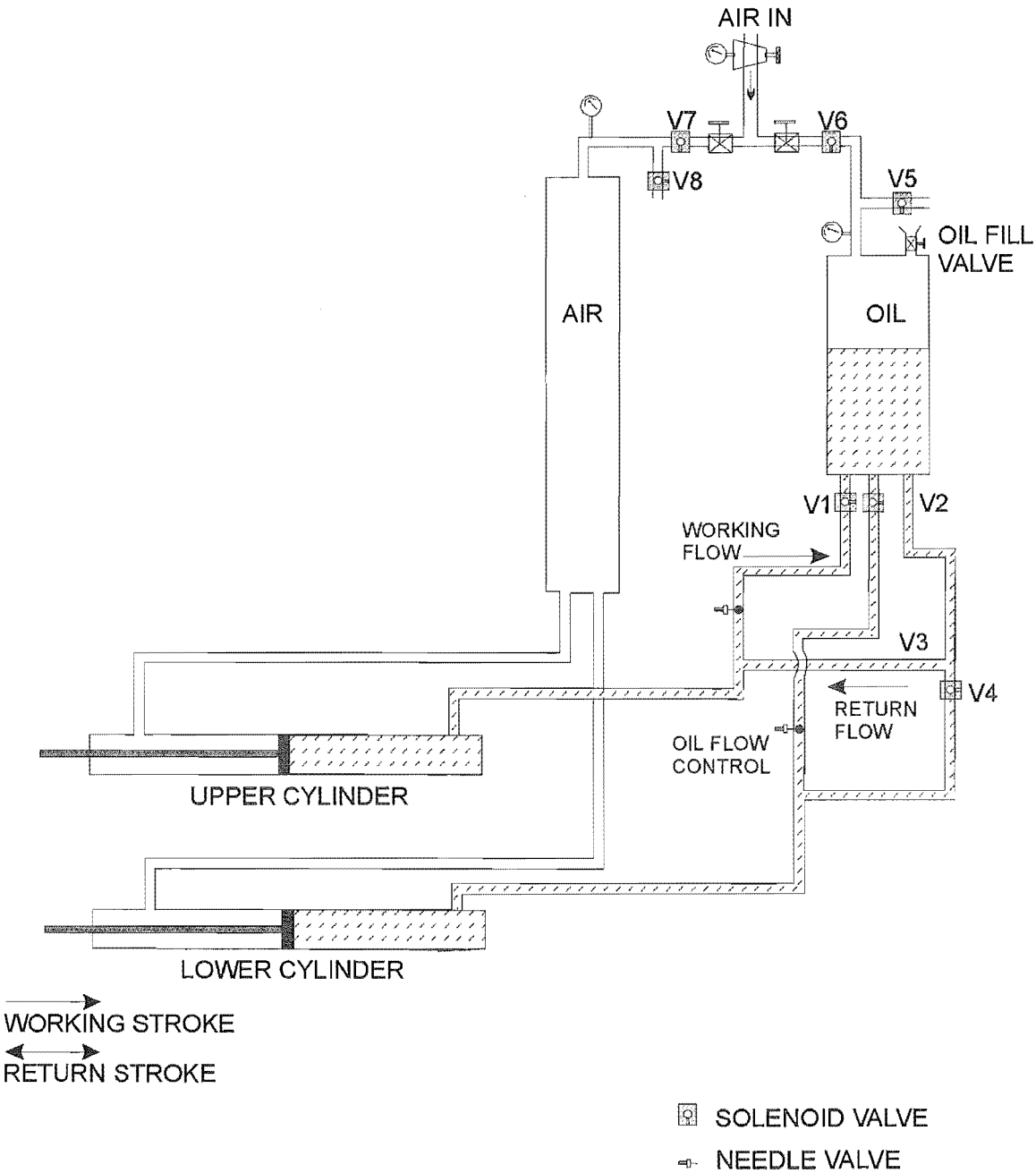

Appendix 9F *– Electric Circuit Diagram for Solenoid Controller*

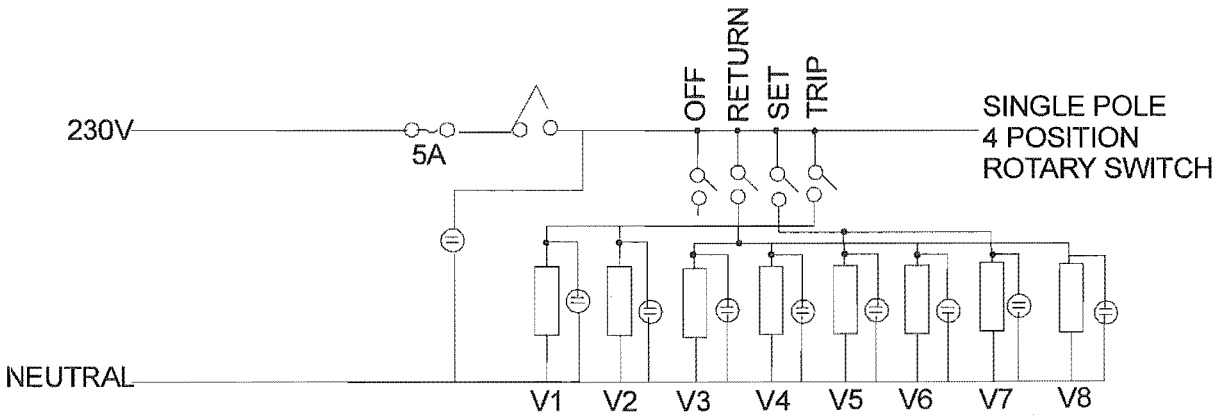

SOLENOID CONTROLLER

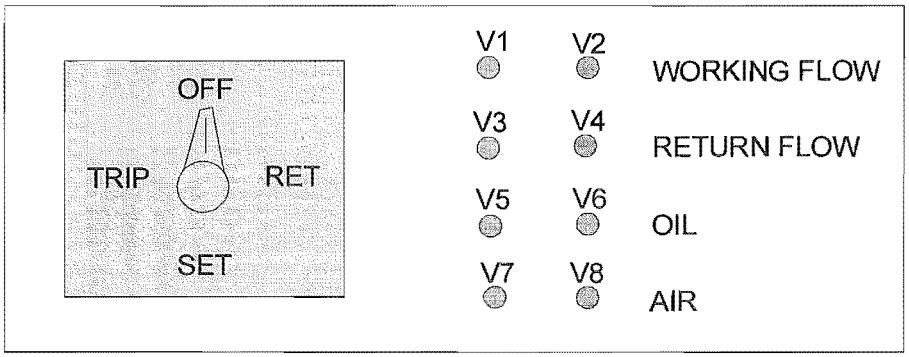

FRONT PANEL

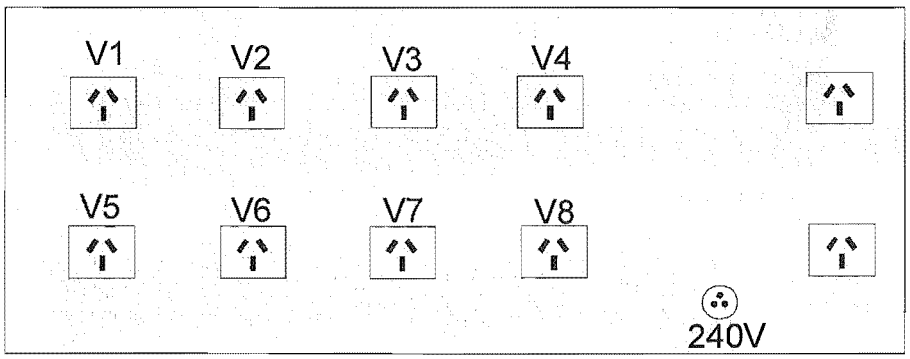

REAR PANEL

Appendix 9G – Timing Diagram

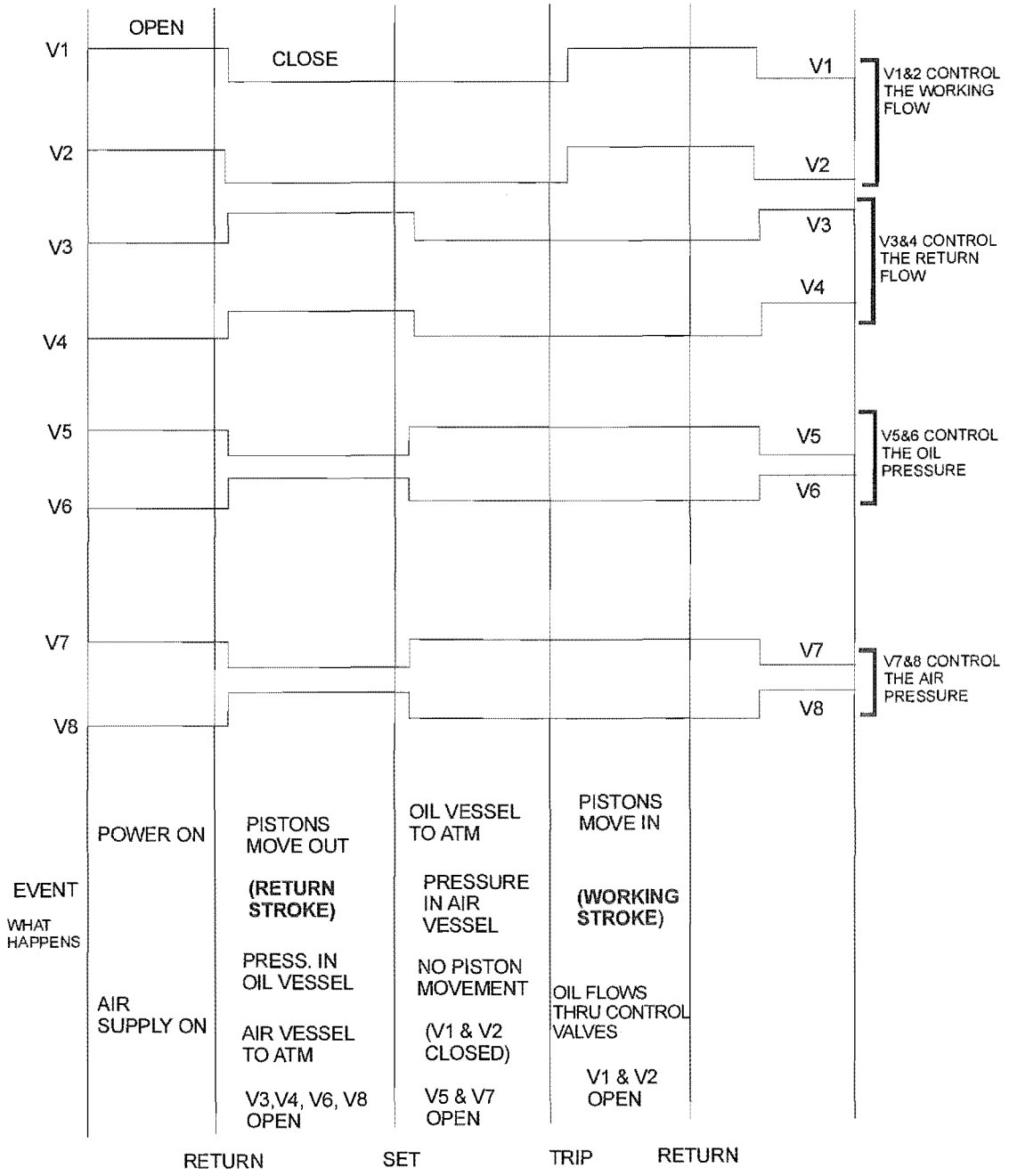

Appendix 9H - Convolution Theorem

The governing equation is

$$\tau\frac{\partial C}{\partial t}+\frac{\partial C}{\partial z}-\frac{1}{Pe}\frac{\partial^2 C}{\partial z^2}=0$$

Laplace transformation of the above equation yields

$$F(s)=\frac{C_2(s)}{C_1(s)}=\exp\left(\frac{Pe}{2}\left(1-\left(1+\frac{4s\tau}{Pe}\right)^{1/2}\right)\right)$$

Where F(s) is the transfer function

Let k $=\frac{4\tau}{Pe}$ and $a=\frac{Pe}{2}$

$$C_2(s)=C_1(s)\exp\left[a\left(1-(1+ks)^{1/2}\right)\right]$$

$$=C_1(s)\exp(a)\exp\left[a(1+ks)^{1/2}\right]$$

Numerical Convolution of above equation

(1) If $F(s)=e^{-a\sqrt{s}}$ where A > 0

then inverse $f(t)=\frac{a}{2\sqrt{\pi t^3}}e^{-\frac{a^2}{4t}}$

(2) Shift Theorem

$$L\left[e^{at}f(t)\right]=F(s-a)$$

(3) $L\left[f\left(\frac{t}{k}\right)\right] = kF(ks)$

since $\int_0^\infty e^{-st} f(\frac{t}{k})dt$

let u = $\frac{t}{k}$, and $du = \frac{dt}{k}$

the subst.

$$= \int_0^\infty e^{-(sk)u} f(u)kdu$$

$$= k\int e^{-(ks)u} f(u)du = kF(ks)$$

Using (2) and (3)

$F(1 + ks) = e^{-a\sqrt{1+ks}}$ has inverse

$$\frac{e^{-t}}{k} f\left(t/k\right) = \frac{e^{-\frac{t}{k}}}{k} \frac{a}{2\sqrt{\pi\left(t/k\right)^3}} e^{-a^2/4(\frac{t}{k})}$$

$$= \frac{a}{2\sqrt{\pi}} \sqrt{\frac{k}{t^3}} e^{-\frac{(a^2k+4t^2)}{4t}}$$

substitution for a and k

from (1) and by the Convolution Theorem

$$L^{-1}\{f(s)g(s)\} = \int_0^t F(u)G(t-u)du$$

Therefore the output tracer concentration is given by the following equation

$$C_2(t) = \int_0^t C_1(u) \frac{1}{2\sqrt{\pi}} \sqrt{\frac{Pe\tau}{(t-u)}} e^{\frac{Pe}{2}} e^{-\frac{Pe}{4\tau}\left(t-u+\frac{\tau^2}{t-u}\right)} du$$

where u is a dummy time variable.

Appendix 9I – Experimental Results

Run	Date	Solids Flowrate	Size range	Material	Air velocity	SGL	Cyclone	Time	Peclet Number
		g/s	µm		m/s			s	
21	2/09/96	9.7	500-700	Sand	20	0.0816	B	0.658	12.74
22	2/09/96	9.7	500-700	Sand	20	0.0816	B	0.67	54.07
23	1/10/96	6.83	500-700	Silica gel	15	0.0767	B	1.061	63.14
24	1/10/96	6.83	500-700	Silica gel	15	0.0767	B	1.199	24.38
25	1/10/96	11.2	500-700	Silica gel	15	0.1257	B	0.93	74.8
26	1/10/96	11.2	500-700	Silica gel	15	0.1257	B	0.883	47.75
27	9/10/96	4.5	500-700	Silica gel	20	0.0379	B	1.07	6.91
28	9/10/96	4.5	500-700	Silica gel	20	0.0379	B	1.025	8.82
29	10/10/96	12.54	500-700	Silica gel	20	0.1056	B	0.819	11.99
30	10/10/96	12.54	500-700	Silica gel	20	0.1056	B	0.943	14.15
31	15/10/96	12.54	500-700	Silica gel	20	0.1056	B	0.942	13.88
32	15/10/96	12.54	500-700	Silica gel	20	0.1056	B	0.77	34.53
33	16/10/96	12.54	500-700	Silica gel	20	0.1056	B	0.869	42.58
34	17/10/96	12.54	500-700	Silica gel	20	0.1056	B	0.955	-
35	17/10/96	8.475	500-700	Silica gel	20	0.0713	B	1.172	10.34
36	17/10/96	8.475	500-700	Silica gel	20	0.0713	B	1.01	18.06
37	18/10/96	10	500-700	Silica gel	20	0.0842	B	1.096	39.06
				Silica gel					
39	18/10/96	5.72	500-700	Silica gel	20	0.0481	B	1.136	68.72
40	19/10/96	5.72	500-700	Silica gel	20	0.0481	B	1.296	12.99
41	21/10/96	14.7	500-700	Silica gel	20	0.1237	B	1.32	97.97
42	23/10/97	14.7	500-700	Silica gel	20	0.1237	B	0.893	37
43	23/10/96	10.15	500-700	Silica gel	20	0.0854	B	1.052	62.46
44	24/10/96	9.38	295-500	Silica gel	20	0.079	B	0.691	26.24
45	24/10/96	5.39	295-500	Silica gel	20	0.0454	B	0.738	16.23
46	24/10/96	6.2125	295-500	silica gel	20	0.0523	B	0.69	14.04
47	24/10/96	14.1	295-500	silica gel	20	0.1187	B	0.714	32.01
48	24/10/96	11.28	295-500	silica gel	20	0.0949	B	0.693	12.35
49	4/11/96	9.63	295-500	silica gel	20	0.0811	B	0.875	39.67
50	4/11/96	10.07	295-500	silica gel	20	0.0848	B	0.71	33.5
51	5/11/96	9.52	295-500	silica gel	20	0.0801	B	0.845	22.1
52	5/11/96	10.11	295-500	silica gel	20	0.0851	B	0.812	88.75
53	13/11/96	4.64	699-850	silica gel	10	0.0781	B	1.609	79.4
54	13/11/96	6.54	699-850	silica gel	15	0.0734	B	1.455	84.71
55	13/11/96	9.04	699-850	silica gel	20	0.0761	B	1.026	36.16
56	13/11/96	11.04	699-850	silica gel	25	0.0743	B	0.96	20.3
57	9/01/97	11.575	295-500	sand	20	0.0974	B	1.296	161.96
58	9/01/97	10.737	295-500	sand	20	0.0904	B	1.197	101.87
59	9/01/97	7.97	295-500	sand	20	0.0671	B	0.909	74.61
60				sand		#DIV/0!			
61	20/01/97	8.3365	210-295	silica gel	20	0.0702	B	0.611	62.56
62	20/01/97	6.8618	210-295	silica gel	20	0.0578	B	0.641	42.73
63	20/01/97	7.8059	210-295	silica gel	20	0.0657	B	0.53	58.93

Run	Date	Solids Flowrate	Size range	Material	Air velocity	SGL	Cyclone	Time	Peclet Number
		g/s	µm		m/s			s	
64	27/01/97	5.6474	295-500	silica gel	20	0.0475	B	0.954	64.39
65	27/01/97	6.5212	295-500	silica gel	20	0.0549	B	0.905	146.35
66	27/01/97	7.5936	295-500	silica gel	20	0.0639	B	0.769	62.86
67	28/01/97	10.657	295-500	silica gel	20	0.0897	B	0.713	117.18
68	28/01/97	7.5234	295-500	silica gel	20	0.0633	B	0.962	64.54
69	28/01/97	6.3658	295-500	silica gel	20	0.0536	B	0.472	10.42
71	29/01/97	8.0921	699-850	silica gel	20	0.0681	B	0.78	77.07
72	29/01/97	8.0921	699-850	silica gel	20	0.0681	B	1.105	59.03
73	29/01/97	8.6218	699-850	silica gel	20	0.0726	B	0.945	14.06
74	29/01/97	8.6218	699-850	silica gel	20	0.0726	B	1.094	38.47
77	20/03/97	9.5739	250-500	sand	20	0.0806	B	1.312	55.86
78	20/03/97	9.5739	250-500	sand	20	0.0806	B	1.062	33.97
79									
80	25/03/97	9.5739	250-500	sand	20	0.0806	B	1.2	36.14
81	25/03/97	9.5739	250-500	sand	20	0.0806	B	1.232	45.83
82	25/03/97	9.5739	250-500	sand	20	0.0806	B	1.152	42.46
83	26/03/97	9.5739	250-501	sand	20	0.0806	B	1.286	14.56
84	26/03/97	9.5739	250-502	sand	20	0.0806	B	1.311	128.21
85	26/03/97	9.5739	250-503	sand	20	0.0806	B	1.119	47.39
86	26/03/97	9.5739	250-504	sand	20	0.0806	B	0.99	63.29
87	24/05/97	9.6	250-500	sand	20	0.0808	A	0.707	22.17
88	24/05/97	9.6	250-500	sand	20	0.0808	A	0.796	50.55
89	26/05/97	9.6	250-500	sand	20	0.0808	A	0.933	55.38
90	26/05/97	9.6	250-500	sand	20	0.0808	A	0.974	77.98
91	26/05/97	9.6	250-500	sand	20	0.0808	A	1.192	93
92	10/06/97	9.6	250-500	sand	20	0.0808	E	1.087	29.19
93	11/06/97	9.6	250-500	sand	20	0.0808	E	1.269	32.17
94	11/06/97	10.08	250-500	sand	20	0.0848	E	1.327	19.14
95	11/06/97	10.04	250-500	sand	20	0.0845	E	1.231	28.57
96	16/06/97	10.04	250-500	sand	20	0.0845	E	0.949	25.54
97	16/06/97	10.04	250-500	sand	20	0.0845	E	1.144	31.29
98	16/06/97	10.04	250-500	sand	20	0.0845	E	1.288	26.95
104	8/01/98	8.861	250-500	sand	20	0.0746	C	1.051	53.41
105	8/01/98	11.633	250-500	sand	20	0.0979	C	0.957	37.44
106	8/01/98	12.9446	250-500	sand	20	0.109	C	0.783	55.37
107	8/01/98	7.992	250-500	sand	20	0.0673	C	1.015	27.69
108	8/01/98	10.5169	250-500	sand	20	0.0885	C	1.116	54.358
109	20/01/98	10.5	250-500	sand	20	0.0884	F	1.071	2.675
110	20/01/98	10.857	250-500	sand	20	0.0914	F	1.379	9.12
111	20/198	8.9	250-500	sand	20	0.0749	F	1.821	4.353
112	20/01/98	8	250-500	sand	20	0.0673	F	1.668	4.589
113	21/01/98	8	250-500	sand	20	0.0673	D	1.449	15.7
114	21/01/98	8.9	250-500	sand	20	0.0749	D	1.402	19.11
115	21/01/98	11.4	250-500	sand	20	0.096	D	0.81	7.55
116	21/01/98	12.9	250-500	sand	20	0.1086	D	0.869	21.51
117	21/01/98	12.9	250-500	sand	20	0.1086	D	0.996	16.01
118	21/01/98	10.5	250-500	sand	20	0.0884	D	1.178	7.27

Run	Date	Solids Flowrate	Size range	Material	Air velocity	SGL	Cyclone	Time	Peclet Number
		g/s	µm		m/s			s	
119	28/01/98	11.4	250-500	sand	20	0.096	C	0.961	21.15
120	28/01/98	12.9	250-500	sand	20	0.1086	C	0.65	12.6
121	28/01/98	8.9	250-500	sand	20	0.0749	C	1.178	14.76
122	11/02/98	8.9	250-500	sand	20	0.0749	D	1.168	5.34
123	11/02/98	11.4	250-500	sand	20	0.096	D	1.28	6.97
124	11/02/98	12.9	250-500	sand	20	0.1086	D	1.312	5.287
125	11/02/98	12.9	250-500	sand	35	0.062	D	0.54	16.56
125 b	13/02/98	15.5	699-850	silica gel	30	0.087	B	0.78	30.1
126	21/02/98	8.04	212-425	silica gel	15	0.0902	A	1.245	165.14
127	21/02/98	10.04	212-425	silica gel	15	0.1127	A	1.068	57.88
128	21/02/98	11.33	212-425	silica gel	15	0.1272	A	0.811	55.31
129	21/02/98	12.44	212-425	silica gel	15	0.1396	A	1.05	82.9
130	21/02/98	13.63	212-425	silica gel	15	0.153	A	1.08	156.2
131	21/02/98	11.33	212-425	silica gel	15	0.1272	A	0.89	85.78
132	23/02/98	25.16	212-425	silica gel	15	0.2824	A	1.03	153.6
133	23/02/98	11.33	250-500	silica gel	25	0.0763	A	0.81	23
134	23/02/98	12.44	250-500	silica gel	25	0.0838	A	0.71	24.4
135	24/02/98	8.04	250-500	silica gel	25	0.0541	A	0.74	42.03
136	24/02/98	10.04	250-500	silica gel	25	0.0676	A	0.82	23
137	24/02/98	21.3	250-500	silica gel	25	0.1434	A	0.77	63.2
138	25/02/98	8.04	250-500	silica gel	25	0.0541	A	0.87	23.9
139	25/02/98	17.12	250-500	silica gel	25	0.1153	A	0.79	15.8

Appendix 9J – *Video Recording of Flow in Cyclone*

Available in Department of Chemical and Process Engineering, University of Canterbury

Appendix 9K – Error Analysis

In this section errors due to the inherent variability of the process will be compared with errors due to the curve fitting method and sampling errors.

(a)Replication Errors

Let $\bar{x}$ be the sample mean

Confidence limits for true value of a quantity =

$$\overline{x} \pm ts_{\bar{x}}$$

where $s_{\bar{x}} = \frac{s}{\sqrt{n}}$

where $\sigma_{pop} \approx s = \left(\frac{\sum (x_i - \bar{x})}{n-1} \right)$

Where t is from statistical tables and depends on number of data points (degrees of freedom) and degree of confidence required.

Assume population is normally distributed

5 replicate measurements of particle Peclet number and mean residence time for sand particles of size range 250-500 μm in cyclone B with a gas inlet velocity of 20 m s^{-1}.

Run	Peclet Number	Mean Residence Time (s)
87	22.17	0.707
88	50.55	0.796
89	55.38	0.933
90	78	0.974
91	93	1.192

Mean $\bar{t}$ = 0.92

Standard deviation s = 0.19

Standard error in mean $s_{\bar{x}}$ = 0.083

For the 90 % confidence interval

Degrees of freedom $\nu =$ 4

From *t* table

$t_4(0.95) = 2.13$

Therefore confidence interval (90%) is

$0.9204 \pm 2.13 \times 0.083 = 0.92 \pm 0.18$

Mean Peclet number = 60

Standard deviation = 27.178

Standard error in mean = 12

Confidence interval (90%) for Peclet Number = 60 ± 26

(b) Curve Fitting errors - Bootstrapping Methods (Efron and Tibshirani, 1993)

The bootstrap method was introduced in 1979 and is based on the method of resampling from a given data set to calculate the standard error in a statistical variable. Using this procedure the sampling variations of statistical estimates is obtained.

Let $\mathbf{x} = (x_1, x_2, x_3, \ldots\ldots, x_n)$ be a population sample of size *n*

A bootstrap sample $\mathbf{x}^b$ is derived from **x** such that

$\mathbf{x}^b = (x_1^b, x_2^b, x_3^b, \ldots\ldots, x_{n-1}^b)$ where $\mathbf{x}^b$ is a random sample of size *n-1*

x_i^b are randomly chosen with replacement from **x**

For example where x has 20 data points, for each bootstrap sample x^b 19 data points are selected. With this data set the mean residence time and Peclet number are calculated. Repeat samples x^b result in "replications" of mean residence time and Peclet number.

For different experimental runs there is variability in the mean residence time or the Peclet number introduced due to

1. random physical process variation
2. curve fitting method
3. sampling error

2 and 3 above are described by variation among bootstrap replications.

By applying the bootstrap method i.e. re-sampling the data for a particular experimental run, the random physical process variations are held constant. The parameters are then evaluated and the procedure repeated with another re-sampled data set.

Sand Particles

Run 91

Size range: 250-500 μm in cyclone B with a gas inlet velocity of 20 m s^{-1}

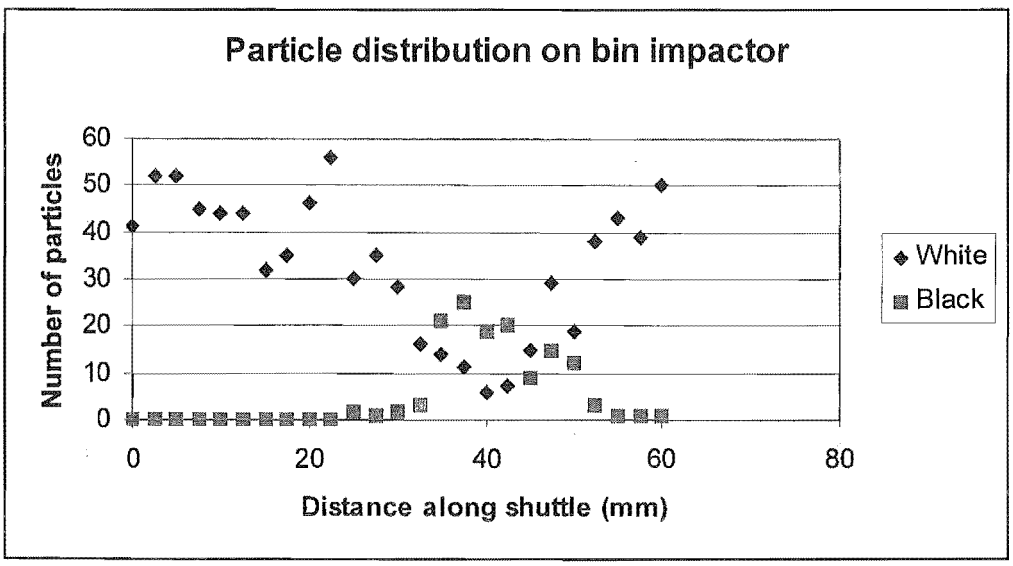

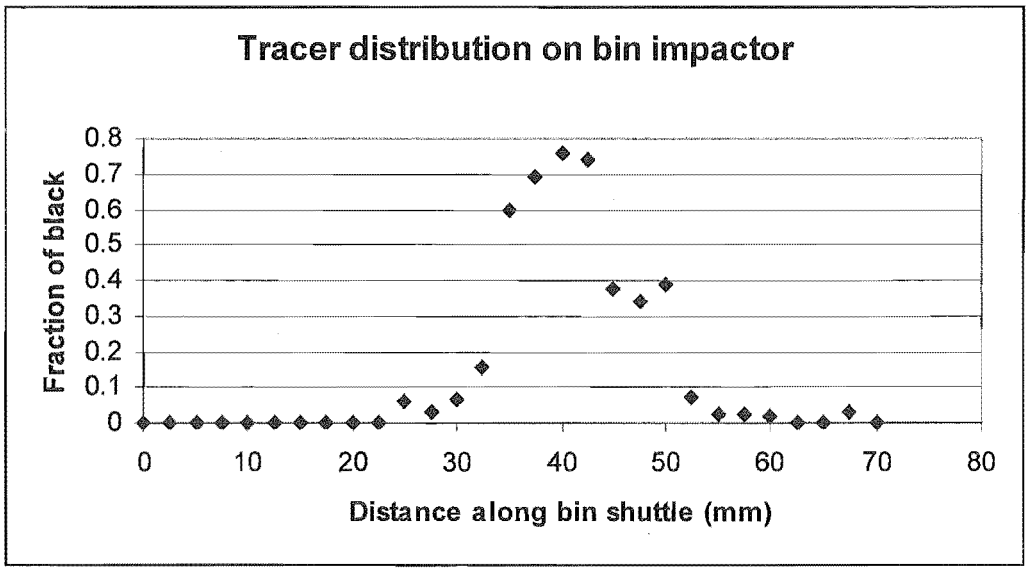

Peclet Number and Mean Residence Time Calculated from 15 Bootstrap Samples

Peclet Number (Pe)	Mean time (s)
93.53	1.1924
94.10	1.1926
97.77	1.1947
102.11	1.2041
97.33	1.2553
56.15	1.2743
33.82	1.2466
38.54	1.1829
84.13	1.1587
132.83	1.1572
142.08	1.1662
98.35	1.1887
94.01	1.1917
93.56	1.1921
93.19	1.1923

Mean residence time = 1.20 s

Standard deviation = 0.034

Standard error = 0.0088

Confidence interval (90%) = 1.20 ± 0.02 s

Similarly

Mean Peclet number = 90.1

Standard deviation = 29.2

Standard error = 7.5

Confidence interval (90%) = 90 ± 13

Sand particles

Run 96

Size range: 250-500 μm in cyclone E with a gas inlet velocity of 20 m s^{-1}.

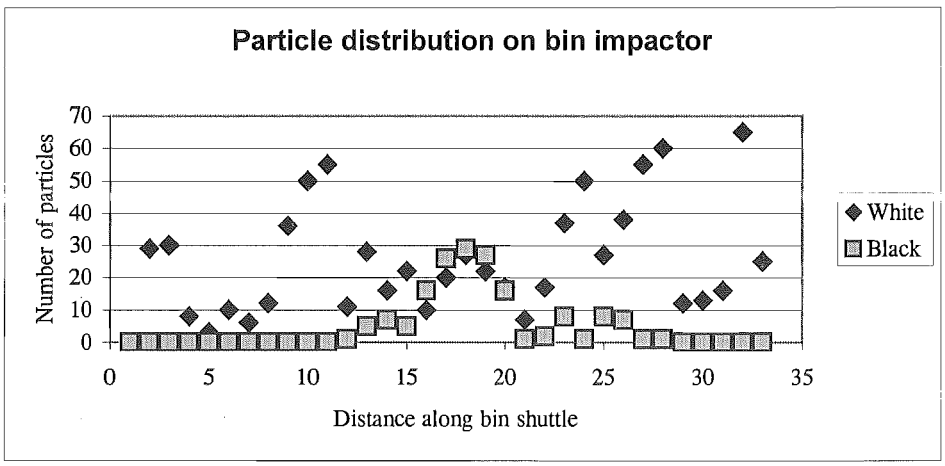

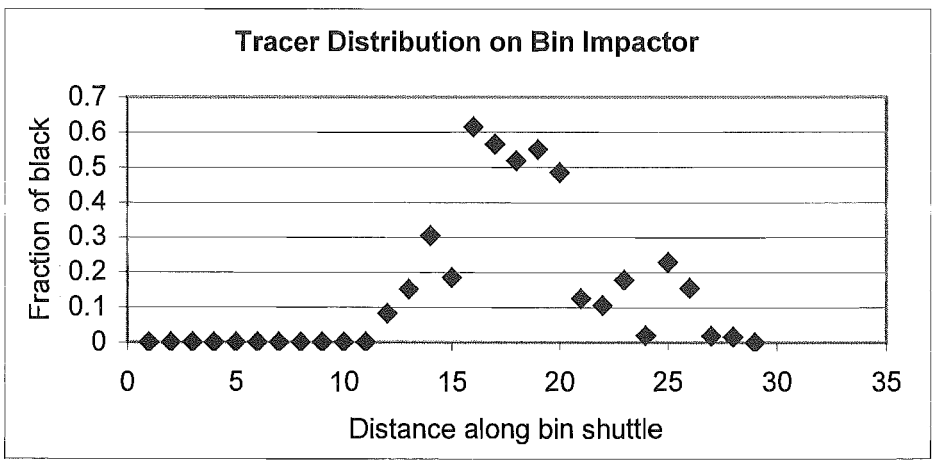

The fraction black is then Bootstrap sampled.

Peclet Number and Mean Residence Time Calculated from 18 Bootstrap Samples

Peclet Number (Pe)	Mean time (s)
32.39	1.0544
33.73	1.056
35.98	1.0615
39.9	1.0812
33.78	1.176
23.03	1.1577
15	1.1066
14.54	1.1066
14.34	1.0561
15.98	1.0084
25.44	1.0382
33.31	1.0408
34.94	1.0362
37.78	1.0799
32.88	1.0527
36.77	1.0431
34.5	1.049
32.56	1.0539

Mean residence time = 1.07 s

Standard deviation = 0.0427

Standard error = 0.0101

Confidence interval = 1.07 $\pm$ 0.02 s

Similarly,

Mean Peclet number = 29

Standard deviation = 8.78

Standard error = 2.07

Confidence interval = 29 $\pm$ 4

Silica gel particles

Run 53

Size range: 699-850 mm in cyclone B with gas inlet velocity of 20 ms^{-1}

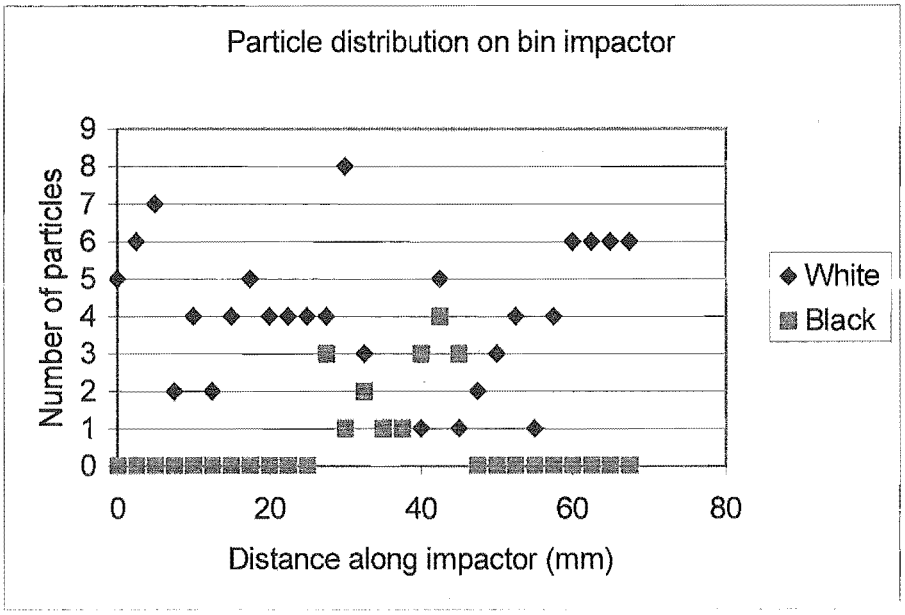

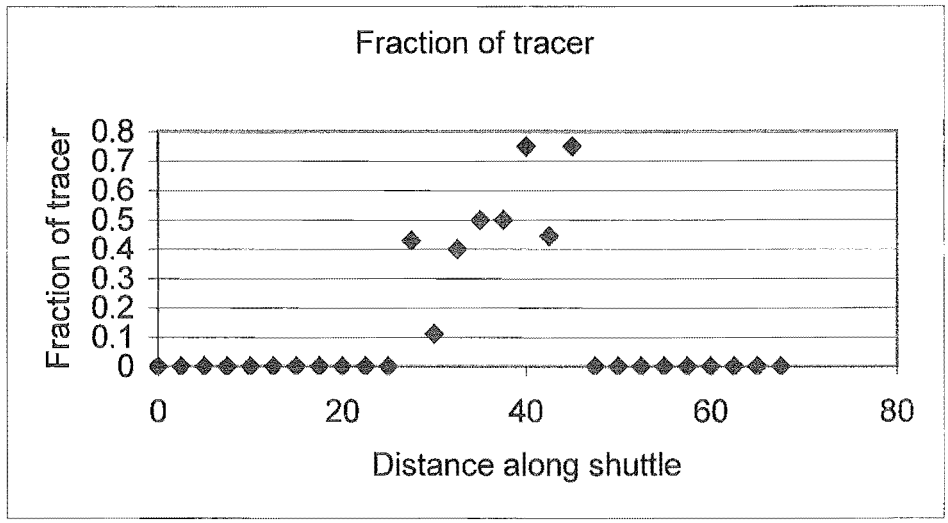

Peclet Number and Mean Rresidence Time Calculated from 9 Bootstrap Samples

Peclet Number (Pe)	Mean time (s)
49.48	1.2851
76.27	1.3099
53.85	1.2978
53.21	1.3350
34.72	1.3428
26.08	1.3218
188.37	1.3056
31.63	1.2597
37.80	1.2132

Mean residence time = 1.30 s

Standard deviation = 0.040

Standard error = 0.013

Confidence interval (90%) = 1.30 ± 0.02

Similarly

Mean Peclet number = 42

Standard deviation = 17.63

Standard error = 5.88

Confidence interval (90%) = 42 ± 11

Silica gel particles

Run 126

Size range: 250-500 μm in cyclone A with a gas inlet velocity of 15 m s^{-1}.

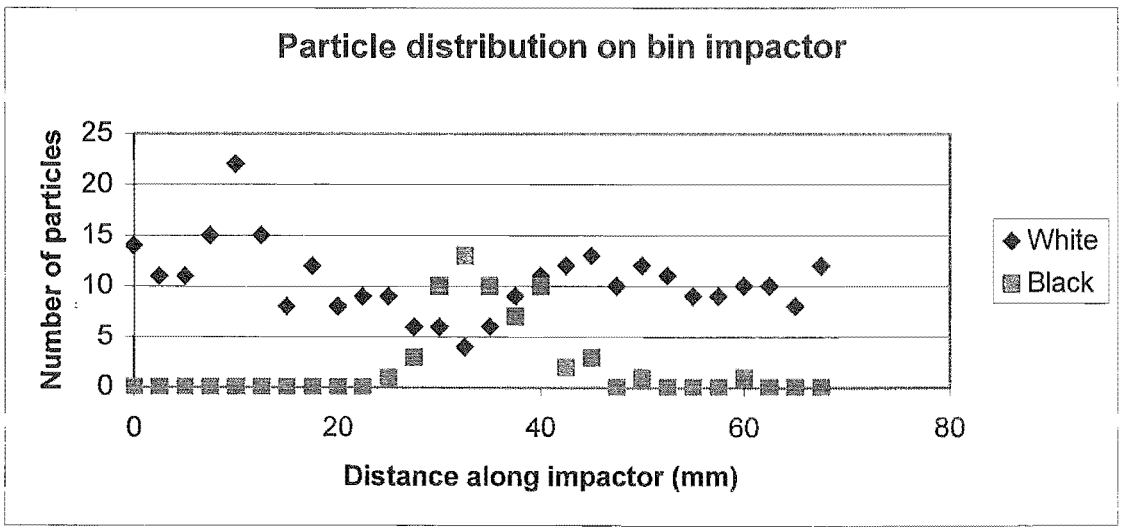

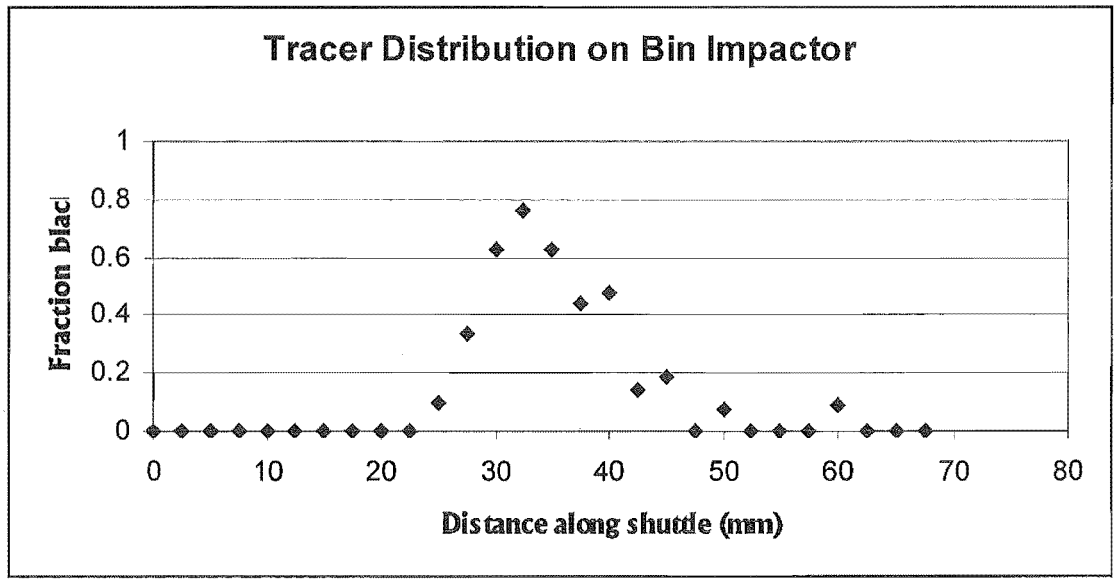

Peclet Number and Mean Residence Time Calculated from Bootstrap 17 Samples

Peclet Number (Pe)	Mean time (s)
19.08	1.4177
16.56	1.3705
12.03	1.3794
23.12	1.2886
22.21	1.2692
25.03	1.2455
30.00	1.2230
26.95	1.2879
28.40	1.2736
27.87	1.2803
27.55	1.2836
27.27	1.2856
26.95	1.2879
28.51	1.2931
29.67	1.3031
31.62	1.3370
26.57	1.3264

Mean residence time = 1.30 s

Standard deviation = 0.049

Standard error = 0.012

Confidence interval (90%) = 1.30 ± 0.02 s

Mean Peclet number = 25

Standard deviation = 5.18

Standard error = 1.26

Confidence interval (90%) = 25 ± 2

F-Test Two-Sample for Variances of Mean residence time (from Bootstrap)

	250-500μm	*699-850 μm*
Mean	1.30	1.30
Variance	0.0024326	0.001619
Observations	17	9
df	16	8
F	1.5025	
P(F<=f) one-tail	0.2858	
F Critical one-tail	3.2016	

No significant difference in mean residence times ($\alpha = 0.05$)

F-Test Two-Sample for Variances of Peclet Number (from Bootstrap

	250-500μm	*699-850μm*
Mean	25.26	42.38
Variance	26.8226	310.6471
Observations	17	9
Df	16	8
F		11.58
P(F<=f) one-tail		2.4E-05
F Critical one-tail		2.59

There is a significant difference in Peclet numbers for different particle sizes

(c) Time Resolution

Estimated shuttle velocity

$$\text{Velocity} \quad v = \frac{s}{t}$$

Where s is measured total distance travelled by shuttle in *t* seconds

$$S = 181 \pm 0.5 \text{ mm}$$

Measured time

$$t = 8 \pm 1 \text{ s}$$

$$e_v = \sqrt{\left(\frac{\partial v}{\partial s}\right)^2 e_s^2 + \left(\frac{\partial v}{\partial t}\right)^2 e_t^2}$$

Where *e* is error in a given quantity

$$\frac{\partial v}{\partial s} = \frac{1}{t} = \frac{1}{8} = 0.125$$

$$\frac{\partial v}{\partial t} = -\frac{s}{t^2} = -\frac{181}{8^2} = -2.828$$

$$e_v = \sqrt{(0.125)^2 (0.5)^2 + (-2.828)^2 (1)^2}$$

$$= 2.87$$

Velocity of shuttle $= 22.6 \pm 2.9 \text{ mm s}^{-1}$

Time

$$\text{time} \quad t = \frac{d}{v}$$

where d is the length to each segment

$$e_t = \sqrt{\left(\frac{\partial t}{\partial v}\right)^2 e_v^2 + \left(\frac{\partial t}{\partial d}\right)^2 e_d^2}$$

$$\frac{\partial t}{\partial v} = -\frac{d}{v^2}$$

$$\frac{\partial t}{\partial d} = \frac{1}{v}$$

$$e_t = \sqrt{\left(\frac{-2.5}{22.6^2}\right)^2 (2.9)^2 + \left(\frac{1}{22.6}\right)^2 (0.5)^2}$$

$$= 0.03 \text{ s}$$

$$\left(e_t^2\right)_{rel} = \left(e_t^2\right)_{out} + \left(e_t^2\right)_{in}$$

where $(e_t)_{rel}$ is the relative error in time

Therefore maximum uncertainty in cell resolution = 0.04 s

Sum of Variances

The variance for the replications can be expressed as the sum of variances due to the physical process, bootstrap and time

$$s^2_{replication} = s^2_{variation} + s^2_{bootstrap} + s^2_{trel}$$

where $S^2_{replication}$ is variance for the replication measurements

$S^2_{variation}$ is the variance due to random physical process errors

$S^2_{Bootstrap}$ is the variance due to curve fitting

$S^2_{t\ rel}$ is the variance due to time resolution in each cell.

Using the variance from replications in Part (a) and the variance for the bootstrap of Run 91

$s^2_{replications} = 0.034453$

df = 4

$s^2_{bootstrap} + s^2_{t\,rel} = 0.001157 + 0.0016$

$= 0.002757$

df = 14

$s^2_{variation} = 0.034453 - 0.002757$

$= 0.031696$

F test

$H_o \quad S^2_{variation} = S^2_{Bootstrap} + S^2_{t\,rel}$

$F_{0.05}(4,15) = 3.06$

For replications and process variation

$$F(4,15) = \frac{0.031696}{0.002757}$$

$= 11.5$

It therefore can be concluded that the major source of error is attributed to variation in the random physical process errors and not to sampling or curve fitting errors.